Inhibitor of differentiation 3 has distinct cell-specific regulatory roles in vascular disease

Victoria Noel Osinski
Wauwatosa, Wisconsin

B.S. in Biochemistry, University of Wisconsin-Madison, 2014

A Dissertation presented to the Graduate Faculty
of the University of Virginia in Candidacy for the Degree of
Doctor of Philosophy

Department of Pathology

University of Virginia
May, 2020

Abstract

Rationale: Cardiovascular disease (CVD) is the leading cause of death worldwide. While advances in CVD therapeutics have been made, there remain unmet needs for better approaches to prevent and treat various forms of CVD such as coronary atherosclerosis and peripheral artery disease (PAD). The McNamara lab has identified the helix-loop-helix transcription factor Inhibitor of differentiation 3 (Id3) as a regulator of atherosclerosis development in both mice and humans. In my studies, I sought to identify cell type-specific roles for Id3 in regulating atherosclerosis development and adaptive neovascularization in the setting of skeletal muscle ischemia as a model of PAD. I hypothesized that Id3 expression in endothelial cells (ECs) and macrophages plays a protective role during atherosclerosis development and B cell-specific Id3 expression promotes angiogenesis during skeletal muscle ischemia to restore blood flow to distal limbs.

Approach: To address these questions, a number of cell-specific transgenic murine models were utilized and generated. B cell-, macrophage-, and EC-specific Id3 knockout lines were used to investigate whether Id3 in these respective cell types regulated vascular density and perfusion during hind limb ischemia (HLI). Macrophage- and EC-specific Id3 knockout lines were used to investigate whether Id3 inhibited progression of plaque development of the aorta in hyperlipidemic mice (a model of atherosclerosis). Additional assays including, but not limited to, flow cytometry, ELISA, immunofluorescence, and cell culture were applied to quantify cell populations, Ig production, plaque size and characteristics, and EC proliferation where relevant.

Results: HLI experiments reveal that B cell-specific Id3 KO, but not macrophage- or EC-specific Id3 KO, have reduced blood flow during HLI. These results correlate with increased presence of B-1b numbers and IgM levels both within ischemic skeletal muscle as well as globally. Preliminary atherosclerosis experiments suggest that EC-specific Id3 KO, but not macrophage-specific Id3 KO mice, have increased atherosclerosis development compared to WT littermates. Macrophage-specific Id3 KO mice demonstrate increased B cell numbers in aortic perivascular adipose tissue (PVAT).

Conclusion: These studies are the first to investigate EC-, macrophage-, and B cell-specific roles of Id3 in atherosclerosis and a murine model of PAD. EC-specific Id3 is atheroprotective, implicating a new molecular mediator through which ECs regulate lesion formation in the setting of hyperlipidemia. B cell-specific Id3 promotes blood flow recovery during ischemia, implicating a potential novel cell type (B cells) in neovascular adaptation to ischemia during PAD. These findings reveal novel cellular mechanisms regulating vascular disease progression and potential new therapeutic targets.

Dedication and Acknowledgements

First, to my doctorate mentor, **Coleen McNamara**: I am extremely grateful for your guidance and mentorship over the last five years. Thank you for teaching me how to be a better scientist, for your patience, for your life lessons, and for being a wonderful role model. This was a long road and I think I'm ending it the best I could be because of your mentorship.

To my committee, **Drs. Janet Cross**, **Gary Owens**, **Shayn Peirce-Cottler**, **Thurl Harris**, **John Luckey**, and **Norbert Leitinger**: thank you for the immense amount of patience, guidance, insights, and confidence you provided me throughout this process.

To my program director, **Janet Cross**, thank you for the help and guidance throughout graduate school. You instilled a sense of calm and confidence in me that was essential in completing these studies. I am extremely grateful that faculty like you exist and can affect the lives of so many graduate students in a positive way.

To the rest of the lab (past and present): **Jim Garmey**, **Chantel McSkimming**, **Melissa Marshall** – thank you for the endless hours of help and support, and for countless laughs and life stories. **Aditi Upadhye** – my lab buddy, thank you for being a role model, supportive peer, and great friend. **Prasad Srikakulapu**, **Hema Kothari**, **Anh Nguyen**, **Claire Bucholz, Rende Xu**, **Jeff Sturek** – my senior science experts, thank you for all of the science and life advice. You all are brilliant researchers who I feel lucky to call role models and lab mates. **Jen Kaplan** and **Heather Perry** – thank you for your early scientific and graduate school guidance. I learned a lot from you about science and life and I'm grateful for your support early on. **Chris Henderson**, **Oom Pattarabanjird**, **Fabrizio Drago** – thank you for the friendship, support, and immense brain power the three of you bring to the lab. It's been a treat working with you. **Stephie Kohlberg** and **Angelina Misiou** – my Dusseldorf buddies, it was wonderful to work with you in lab and make new international friends. **Julia Hartman, Andrea Zhou,** and **Carl Buchol –** thank you for all of your hard work on the AZ project! We could not have accomplished that without you. **Jason Li and Elias Ayoub** – thank you for all your hard work during the 2019 Summer. **Antony Haider** – thank you for all your hard work and contributions to the HLI and athero studies.

To members of the UVA-AstraZeneca collaboration team (**Jeremie Boucher**, **Kim Kelly**, **Sasha Klibanov**, **Gavin O'Mahony**, **Dustin Bauknight**, **Shiva Sai**, **Matt Harms**, **Tobias Kroon**, and **Julien Dimastromatteo**): thank you for all the wisdom, teamwork, and the opportunity to work on such a wonderful collaborative project.

To **Brian Annex** and members of his laboratory: thank you for the extensive training in the murine model of hind limb ischemia and information about peripheral artery disease and angiogenesis in general. In particular, thank you **John Lye**, **Vijay Ganta**, and **Stephanie McDonnell** for all of your experimental guidance.

I must acknowledge and thank the multiple cores and facilities that played an essential role in completion of this body of work: the Flow Cytomery Core, the Advanced Microscopy Core, and the MR5 Vivarium. Thank you for your services, knowledge, patience, and support.

I would also like to recognize members and P.I.s from the following collaborating laboratories who shared reagents, equipment, and knowledge: **Brian Annex lab**, **Gary Owens lab**, **Zhen Yan lab**, **Shayn Peirce-Cottler lab**, **Mete Civelek lab**, **Kim Kelly lab**, **Rich Price lab**, **Swapnil Sonkusare lab**, and **Mark Kester lab**.

To my **friends near and far**: thank you for all of the adventure. The sense of community I have felt before and during graduate school is strong and I have all of you to thank for that.

To my family: **Mom and Dad** – thank you for life, for endless love and support while teaching me to be independent and self-sufficient, for all of the experiences growing up, and for being incredible role models to whom I look up to everyday. **Cassie and Sam** – thank you for your love, companionship, and support. You are incredible, bright, motivated young women who are going to impact the world for the better. **Zach** – thank you for your patience, your love, for making me laugh and teaching me about life, and for keeping me going during graduate school. To the **rest of my family** – thank you for your love and support, and for bringing extra joy and life lessons into my existence. **Kris**, **Brice**, **Cassie**, **Sam**, **Zach**, **Dorothy**, **Nancy**, **Dave**, **Pat**, **Wendy**, **Bill**, **Tracy**, **Rob**, **Cam**, **Julia**, **Brooke**, **Morgan**, **Anna**, **Jessa**, **and Emalie** – I love you all and dedicate this work to you.

“Alone, we can do so little; together, we can do so much”
– Helen Keller

Table of Contents

List of Figures

Chapter 1

Chapter 2

Chapter 3

Chapter 4

Chapter 5

Chapter 6

None.

Appendix 1

Appendix 2

List of Tables

List of Abbreviations

Abbreviations	Definition
αSMA	Alpha-Smooth muscle actin
ANDI	Adaptive neovascularization during ischemia
AKT	Protein kinase B
ApoE	Apolipoprotein E
ATLO	Artery tertiary lymphoid organ
BAFF	B-cell activating factor
BCA	Brachiocephalic artery
CCL2	C-C Motif Chemokine Ligand 2, Monocyte chemoattractant protein 1
CCR2	C-C chemokine receptor type 2
CD31	Cluster of Differentiation 31, Pecam-1
CD68	Cluster of Differentiation 68; Scavenger Receptor Class D, Member 1
CLI	Critical limb ischemia
CVD	Cardiovascular disease
CXCR4	C-X-C chemokine receptor type 4
CXCL12	C-X-C motif chemokine 12, Stromal cell-derived factor 1
CyTOF	Cytometry by time of flight
DAMP	Damage-associated molecular pattern
EC	Endothelial cells
ECM	Extracellular matrix
ELISA	Enzyme-linked immunosorbent assay
eNOS	Endothelial nitric oxide synthase
FACS	Fluorescence-activated cell sorting
FcγR	Fc-gamma receptor
GWAS	Genome-wide association study/ies
H&E	Hemotoxylin & Eosinophin
HDL	High-density lipoprotein
HFD	High-fat diet
HIF	Hypoxia-inducible factor
HLI	Hind limb ischemia
HMGB1	High mobility group box 1

I	Ischemic
IC	Intermittant claudication
ICAM1	Intercellular Adhesion Molecule 1
Id3	Inhibitor of Differentiation 3
Id3105A	Id3 SNP rs11574 major allele expressing an alanine at amino acid 105
Id3105T	Id3 SNP rs11574 minor allele expressing a threonine at amino acid 105
IF	Immunofluorescence
IHC	Immunohistochemistry
IL-1β	Interleukin-1 beta
Ig	Immunoglobulin
LDLR	Low density lipoprotein receptor
LDPI	Laser Doppler perfusion imaging
MBV	Microvascular blood volume
MFI	Mean fluorescence intensity
MMP	Matrix metallopeptidase
NI	Non-ischemic
NFκB	Nuclear factor kappa-light-chain-enhancer of activated B cells
oxPAPC	Oxidized 1-palmitoyl-2-arachidonoyl-sn-glycero-3-phosphocholine
$P2Y_2R$	P2Y purinoceptor 2
PAD	Peripheral artery disease
Pcsk9	Proprotein convertase subtilisin/kexin type 9
PRR	Pattern recognition receptor
PVAT	Perivascular adipose tissue
qRT-PCR	Quantitative Reverse Transcription Polymerase Chain Reaction
RAGE	Receptor for advance glycation end products receptor
TG	Triglyceride
TGFβ	Transforming growth factor β
TLR	Toll-like receptor
VV	Vasa vasorum
VCAM-1	Vascular cell adhesion protein 1
VSMC	Vascular smooth muscle cell
WD	Western diet

Chapter 1: Introduction

I. Cardiovascular disease

Cardiovascular disease (CVD) is the leading cause of death worldwide[1]. The AHA reports that CVD was the leading cause of death in 2016 (**Figure 1.1A**) with approximately 850,000 deaths in the U.S. attributed to CVD. Heron reported that 1 in 4 individuals in the U.S. died of CVD in 2017[2]. While the medical field has made great progress in developing therapies to treat various forms of CVD, a need to identify novel effective therapies still exists. Since the rate of death due to CVD reached its lowest point in 2010, the number of CVD-related deaths has risen (**Figure 1.1B**)[1]. New therapies such as the lipid-lowering PCKS9 inhibitors[3, 4] and anti-inflammatory IL-1β inhibitors[5] demonstrate therapeutic efficacy in some studies, however, not all patients responded positively to these treatments[6]. Thus, an increased understanding of mechanisms driving development of and adaptation to CVD will aid in continued therapeutic and diagnostic advances.

Figure 1.1.

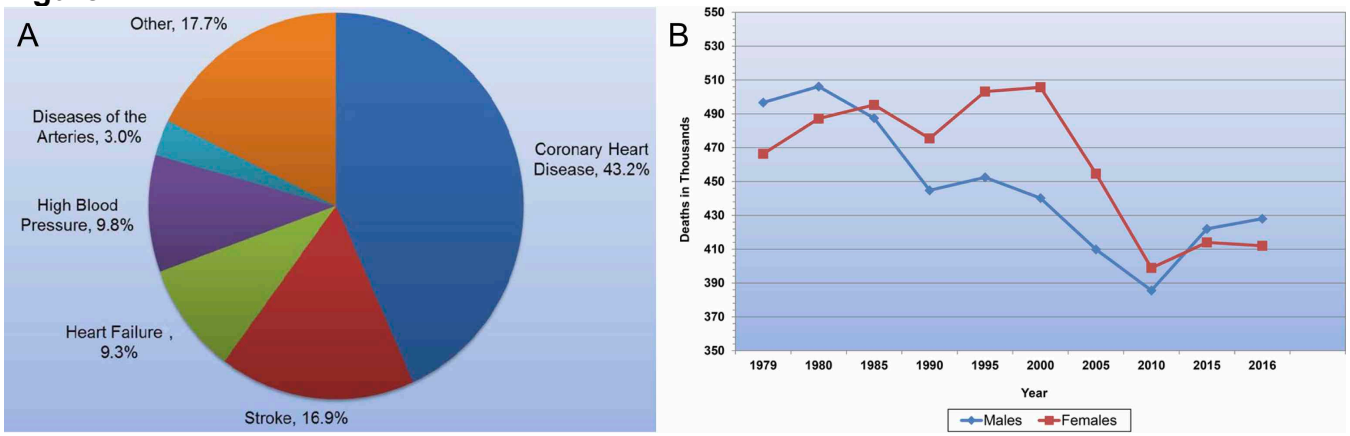

Figure 1.1. CVD prevalence and trends in the United States.
(A) In 2016, CVD was the leading cause of death in the U.S. (Chart 13-4). (B) While the prevalence of CVD had been decreasing from 2000 until 2010, it has been on the rise again since then (Chart 13-6). Both figures are from "Heart Disease and Stroke Statistics—2019 Update: A Report From the American Heart Association"[1].

Specific CVDs such as atherosclerosis and peripheral artery disease (PAD) are multi-factorial diseases mediated by genetics, diet, lifestyle habits such as smoking and physical activity, and co-morbidities such as diabetes and kidney disease. GWAS have identified a number of genetic mutations that correlate with CVD and follow-up studies demonstrate potential causation in some instances. However, these studies utilize genomic information from

samples of heterogeneous populations with differential effects on CVD pathogenesis. Thus, cell-type specific studies of potential CVD-regulators are important for improving our understanding of mechanisms regulating CVD. My studies are centered on understanding the cell-specific roles that transcription factor Inhibitor of differentiation 3 (Id3) in CVD, more specifically in atherosclerosis and peripheral artery disease (PAD). The overarching hypothesis of this work is that Id3 regulates development of atherosclerosis and adaptive neovascularization during ischemia (ANDI) through cell-specific mechanisms. Throughout this work, I will address specific questions that better elucidate the varied and cell-specific roles Id3 plays in regulating vascular disease.

II. Atherosclerosis

One form of cardiovascular disease is atherosclerosis, which is the formation of lipid-laden lesions that reduce or occlude blood flow in major coronary and peripheral arteries[7]. Over time, these plaques may grow larger and unstable due to the advancement of necrosis, a lack of or reduction in a protective collagen-containing fibrous cap, or an influx of pro-inflammatory immune cells[8, 9]. This instability can lead to plaque rupture, inducing thrombosis, and more severe outcomes such as myocardial infarction or stroke. It is estimated that approximately 805,000 myocardial infarctions, or heart attacks, occur each year in the U.S[10]. Many different vascular and immune cells contribute to the development of atherosclerotic lesions including endothelial cells (ECs), vascular smooth muscle cells (VSMCs), macrophages, and B cells. Lesions develop between the intimal (EC-rich) and medial (VSMC-rich) space where their expansion will begin to occlude the lumen. While some immune cells, such as macrophages, are recruited to this intima-medial space, many are found in the adventitia surrounding the plaque-burdened artery[10]. Each of the mentioned cell types play distinct roles during atherogenesis that vary from physically surrounding the lesion, to secreting athero-regulatory factors.

Endothelial cells

Initial steps in the development of atherosclerosis involve the endothelium. Areas of disturbed flow, such as those at branch points and along the curvature of the aortic arch are more prone to lesion development due to mechanical signals that reduce EC barrier function and promote

an inflammatory state[11, 12]. EC barrier function is reduced permitting increased retention of lipids in the sub-endothelial space of the vascular wall where atherosclerotic lesions eventually develop[12]. ECs in areas of disturbed flow also express increased levels of pro-inflammatory molecules such as VCAM-1 and ICAM1[11, 13], which bind to immune cells in circulation and recruit them into the vascular wall as well (**Figure 1.2**). Over time, this accumulation of lipid and immune cells leads to development of small lesions known as fatty streaks, followed by larger and larger lesions that are eventually classified as plaques. These plaques contain lipid, necrotic cells, and immune cells including monocyte-derived macrophages and T cells[8, 14-16].

In addition to the endothelium of the aorta, there is another vascular bed with athero-regulatory functions: the vasa vasorum (VV). These are smaller arteries that run alongside the aorta and provide perfusion of oxygen and nutrients to the thick walls of major arteries (**Figure 1.2**). Under conditions of atherosclerosis, the VV will undergo sprouting of a network of capillaries that perfuse the adventitia via inflammatory and hypoxic signals. This angiogenesis facilitates further transport of immune cells, lipid, nutrients, and cytokines to the growing lesion[17].

Vascular smooth muscle cells

Vascular smooth muscle cells (VSMCs) also play an important role in lesion development. Lipid and inflammatory signals activate VSMCs to proliferate and produce extracellular matrix (ECM) products that aid in stabilizing the outer layers, or cap, of the lesion[18]. A lack of VSMC activation or VSMC dysfunction may prevent these stabilization steps increasing the likelihood of plaque rupture and thrombosis. Recent studies have also demonstrated that chronic stages of atherosclerosis prompt various cell types to adapt non-traditional phenotypes, such as VSMCs adopting phagocyte-like phenotypes[19] or ECs taking on a fibroblastic phenotype[20]. This process may serve to accommodate high lipid levels in the plaque and provide adaptive functions to stabilize the plaques.

Macrophages

Macrophages are professional phagocytes that take up lipid and necrotic cells within the lesion. One study found that accumulation of macrophages was a characteristic of human plaques following MI[9], but research beyond this study demonstrates that macrophages are a

common characteristic of stable and unstable plaques in both mice and humans. While macrophages play useful roles in scavenging lipids and debris within plaques, they are also considered to be atherogenic due to the signals they secrete in this environment. Macrophages are classified as foam cells when they have phagocytosed and are storing high levels of lipid[21]. This hyperlipidemic state modifies signaling within macrophages, leading to secretion of pro-inflammatory cytokines, immune cell-recruiting chemokines, and ECM-degrading proteases[9, 14, 15]. Overall, macrophages are a prevalent cell type in lesions that influences atherosclerosis development.

B cells

B cells are recruited to the surrounding PVAT during atherosclerosis development where they secrete a variety of cytokines and atherogenic IgG or atheroprotective IgM, depending on the B cell subset[22, 23]. These atheroprotective IgM prevent atherosclerosis, at least in part, by binding to oxidized lipids in the lesion and inhibiting uptake by macrophages. This then reduces foam cell formation and secretion of pro-inflammatory cytokines (**Figure 1.2**). B-1 cells are derived from the fetal liver and persist through self-renewal during adulthood[24, 25]. Characterized as $CD19^{+}B220^{low}$ lymphocytes, they are the major source of IgM production – in particular natural, poly-specific IgM[26]. Studies are underway to identify the human equivalent of this subset[27-29]. B-1 cells can be further subdivided into $CD5^{+}$ B-1a and $CD5^{-}$ B-1b cells. B-1b cells secrete higher levels of IgM *in vivo* than B-1a cells[30] and recent unpublished sequencing studies from the McNamara lab demonstrate that each subset secretes a unique repertoire of IgM antibodies. B-2 cells are the major source of IgG and also produce antigen-specific IgM. B-2 cells are derived from progenitor populations within the bone marrow[25]. Studies revealed that B cells are not typically localized within atherosclerotic plaques, but do reside in the PVAT in areas of atherosclerosis in artery tertiary lymphoid structures (ATLOs) (**Figure 1.2**). The full impact of these cells is still under investigation. Further, antibodies are found in abundance within atherosclerotic plaques, but the original source of these immunoglobulins remains unclear. It is thought that they may reach the plaque via the vasa vasorum[22, 23].

Figure 1.2.

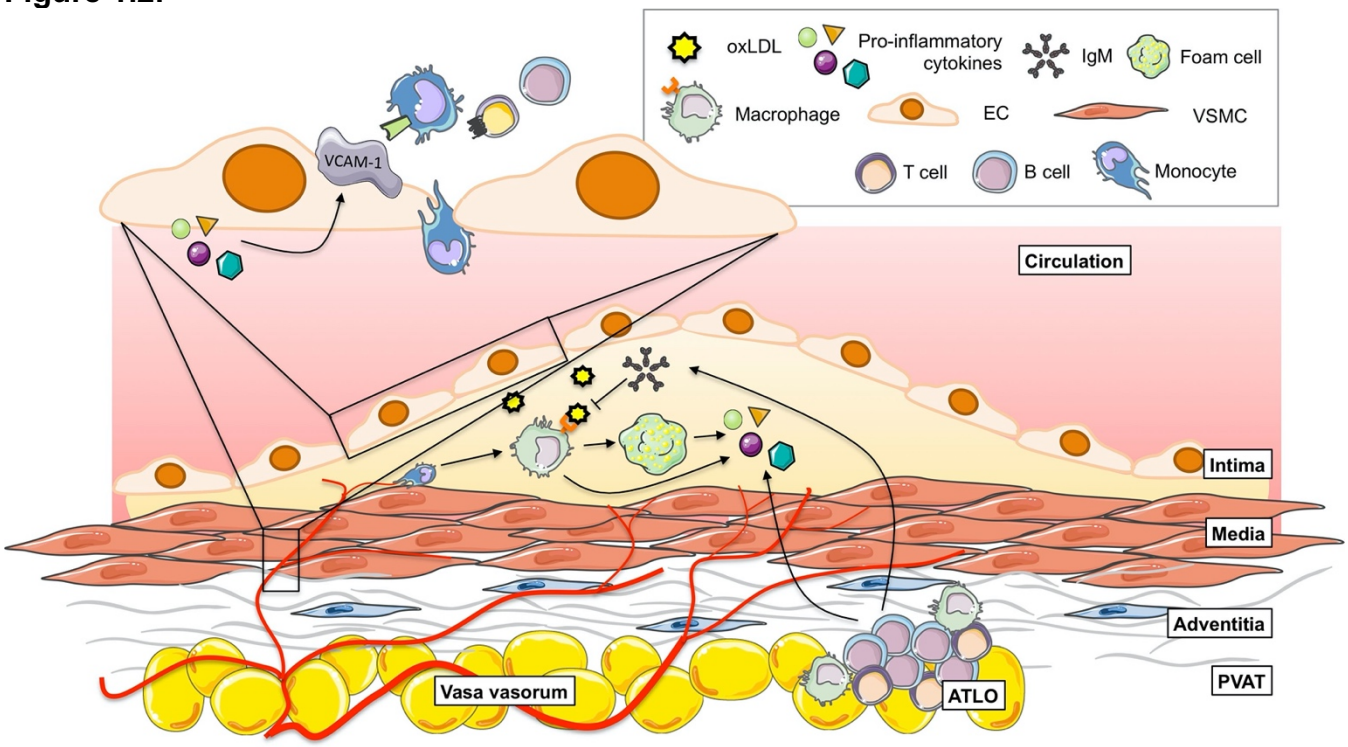

Figure 1.2. Schematic of atherosclerosis development.
Diagram demonstrating the roles that macrophages, B cells, ECs, and VSMCs play during atherogenesis.

III. Peripheral artery disease (PAD)

Peripheral artery disease is another form of CVD that is particularly prevalent in aging and diabetic populations[1]. It is a disease characterized by reduced blood flow to peripheral tissues, such as the legs, as a result of arterial occlusions predominantly due to atherosclerosis[7]. This disease is further classified depending on symptoms and severity. Patients who experience pain in the limbs during activity are classified as PAD with intermittent claudication (IC), while patients with chronic pain in the limbs or tissue necrosis resulting in gangrene or limb amputation are classified as PAD with critical limb ischemia (CLI)[7, 31, 32]. Patients with comparable atherosclerotic blockages demonstrate varying degrees of symptoms ranging from no pain to CLI. The varying outcomes of this disease are due to a multitude of factors that include the capacity for their distal tissue to adapt to ischemia and prompt angiogenic and arteriogenic processes to increase perfusion[33, 34]. Studies presented in this work are in part focused on the mechanisms regulating adaptive neovascularization during ischemia (ANDI). The ischemia that induces ANDI is usually caused by atherogenic processes that induce

blockages in the major arteries of the lower limbs. Affecting around 25% of the aged population in the U.S., very few effective therapies for PAD exist for these patients[1]. More research into the mechanisms driving ANDI will increase our understanding of the disease and how patients adapt to arterial blockages in the lower limbs, and our ability to develop therapies.

Characterizing skeletal muscle ischemia

PAD induces ischemia in distal limb tissue, which can manifest in a variety of co-morbidities including pain and necrosis. Ischemia is defined as a restricted blood flow to a tissue, which results in reduced oxygen levels. This lowered oxygen level induces a variety of cellular responses that include cell activation, cell death, and secretion of chemotactic and pro-inflammatory signals[35-39]. Low oxygen is detected intracellularly by the hypoxia-inducible factors (HIFs): HIF1α, HIF-1β, and HIF-2. HIF promotes expression of genes that promote inflammation, angiogenesis, cell senescence, cell proliferation, and cell death[40, 41]. Much of this is dependent on the magnitude and duration of hypoxic stimuli. In the setting of tissue injury and ischemia, stressed and dying cells also express and release molecular signals that are abnormal to tissue settings at homeostasis[42, 43]. These molecules are known as damage-associated molecular patterns (DAMPs) and they bind to a series of pattern recognition receptors (PRRs) including toll-like receptors (TLRs) and the RAGE receptor. TLRs regulate expression of various anti- and pro-angiogenic signaling including of VEGFA, sVEGFR1, and VEGFR2[44, 45]. Each TLR has a unique effect in ECs and on angiogenesis. The RAGE receptor has been shown to promote endothelial permeability via β-catenin and VE Cadherin activity[46].

Hypoxia promotes angiogenesis

In general, the presence of low oxygen tension leads to stabilization of HIF transcription factors in the cytoplasm. HIF-1α in particular, has been shown to then translocate to the nucleus where it promotes gene expression of many pro-angiogenic genes including VEGFA, VEGFR2, PIGF, angiopoietin-1 and -2, PDGFβ, CXCL12, sphingosine-1-phosphate receptors, and CXCR4, MMP2, and MMP9[40, 41] (**Figure 1.3**). Many of these signals are conserved amongst other diseases and injury conditions that induce angiogenesis.

VEGFA promotes activation of ECs, which releases them from quiescence in a stable vessel[47, 48]. During activation, ECs will extend filipodia for migration and signaling purposes,

produce enzymes to degrade the surrounding ECM, and loosen EC-EC junctions to permit cell motility[47, 49, 50]. The first ECs will migrate away from the existing vessel to begin formation of a neovessel. These cells, referred to as tip cells, upregulate CXCR4, VEGFR2, and endoglin to promote migration toward chemokine gradients originating from the source of hypoxia[51, 52] (**Figure 1.3**). Endoglin also promotes ECM breakdown as part of this process[53]. ECs distal to the tip cell take on a stalk cell phenotype, regulated by Notch/DLL4 signals[52, 54, 55]. These cells downregulate migration and filipodia forming functions. Instead, stalk ECs proliferate and express PDGFβ to recruit pericytes, which stabilize the neovessels. These final, resolving steps are important for establishing a stable vessel. This in part explains why VEGFA treatments for PAD have been ineffective at regenerating vessels in limb ischemia: ECs must be exposed to lower VEGFA levels or be less responsive to VEGFA in order to stabilize new vessels[56]. While other signals and processes also play roles in this highly complicated and temporally orchestrated process, this provides a general summary sufficient for the scope of this work.

Immune system's role in PAD

Inflammation has an established role in PAD[57]. Ridker *et al.* found that subjects with higher levels of hsCRP had increased likelihood of developing PAD independent of traditional risk factors[58]. In a longitudinal study, Liang *et al.* identified rheumatoid arthritis as a predictor of PAD further suggesting that inflammation is potentially influencing angiogenic responses during PAD[59]. Further work, however, is needed to discern between the affects inflammation has on atherosclerosis in the major arteries of the lower limb and ANDI in human patients. Murine models demonstrate that HIF-1α-induction of chemokine expression recruits in monocytes and other bone marrow-derived cells that promote angiogenesis[41, 60]. Indeed, both the CXCR4/CXCL12 and CCR2/CCL2 signaling axes have been implicated in regulating angiogenesis in ischemic muscle[60]. Additionally, Klotzsche-von Ameln *et al*. demonstrate that Del-1 KO mice have increased immune cell recruitment and neovascularization during hind limb ischemia. Del-1, the developmental endothelial locus-1, is a glycoprotein that endogenously inhibits leukocyte adhesion. In Del-1 KO mice, blocking β2-integrin leukocyte infiltration attenuated cell recruitment and angiogenesis in ischemic muscle demonstrating a potential role for recruited inflammatory cells in ischemic angiogenesis[61]. In addition to studies

surveying broad, circulating markers of inflammation, a number of studies have identified specific roles for innate immune signals, macrophages, and T cells in hind limb ischemia. These mechanisms as well as additional cellular mediators of angiogenesis that will be expanded on below are represented diagrammatically in **Figure 1.3**.

Pro-angiogenic inflammatory signals

The cytokines secreted by immune cells in HLI bind to endothelium and induce NFκB-regulated gene expression. In ECs, NFκB promotes expression of VEGFA, IL-8, and other pro-angiogenic signals[62, 63] to promote tubule formation, proliferation and migration, and *in vivo* angiogenesis[35, 64]. These signaling axes demonstrate one mechanism by which inflammation regulates angiogenesis. PRR signaling also regulates angiogenesis with mixed effects depending on the receptor and cell type. Global loss of TLR2 in mice results in reduced blood flow during hind limb ischemia, while global TLR4 and TLR9 KO mice have the opposite phenotype[65, 66]. Iwata *et al.* further support that TLR2 promotes recovery during HLI. The study showed that extracellular BCL2, a DAMP upregulated during ischemia, promotes TLR2-MyD88 signaling, which reduced apoptosis[67]. This study, however, does not investigate cell-specific TLR2 signaling activities, so it remains unclear how much of the effects are driven by EC apoptosis rather than apoptosis in other cell types. Finally, an additional study suggests a role for the inflammasome downstream of PRR signaling. Caspase-1 activation in ECs inhibits cell survival and angiogenesis at least in part via downregulation of VEGFR2[68].

Immune cell subsets in HLI

Monocytes and macrophages have well-established roles in responding to and promoting angiogenesis and arteriogenesis during ischemia in skeletal muscle. CCL2 is necessary to recruit and retain monocytes from the bone marrow to sites of ischemia[69]. Krishnasamy *et al*. demonstrate that monocytes differentiate into macrophages in the ischemic muscle[70]. Once there, monocytes and monocyte-derived macrophages promote angiogenesis in the following ways: 1.) expressing VEGF, bFGF, PDGF, TNFα, and IFNγ, 2.) providing physical support to vascular structures, and 3.) degrading ECM around neovessels to promote growth[60]. Interestingly, Coppacia *et al.* demonstrate that inflammatory monocytes promote angiogenesis more effectively than non-inflammatory monocytes[69]. Additionally, Hellingman *et al*. show that

monocytes pre-stimulated with secreted factors from T cells more effectively promote angiogenesis[71]. This demonstrates the importance of intercellular interactions in regulating angiogenesis.

T cells also regulate perfusion responses during ischemia independently of macrophages. Generally, Th2 and Th17 T cells secrete factors that support EC sprouting and *in vivo* angiogenesis in HLI while Th1 T cells promote vascular regression[72]. $CD8^+$ T cells are recruited to ischemic skeletal muscle where they have pro-arteriogenic effects[73]. Conflicting results are reported regarding Treg-mediated effects on neovascularization during perfusion: some studies demonstrate addition of Tregs augments blood flow during HLI, while others report they attenuate blood flow[73-75]. Recently, Kwee *et al*. demonstrated that antigen-primed T cells implanted into ischemic skeletal muscle promote increased flow during the course of HLI[76]. Del1 KO mice with increased ischemic neovascularization had increased B and T cell lymphocyte numbers in skeletal muscle at day 14 of HLI, but no changes in monocyte or macrophage numbers. This suggests a role for B and/or T cells in promoting angiogenesis, however, the study did not separately quantify these populations to determine individual B- or T-cell influences on angiogenesis[61].

Otherwise, very little research has gone into understanding the potential role that B cells might play during HLI and angiogenesis. Findings from my studies introduce a novel role for B cells in angiogenesis during hind limb ischemia. Before reporting these findings, a review of known roles of B cells in angiogenesis will improve our understanding of the mechanisms in my studies.

Figure 1.3.

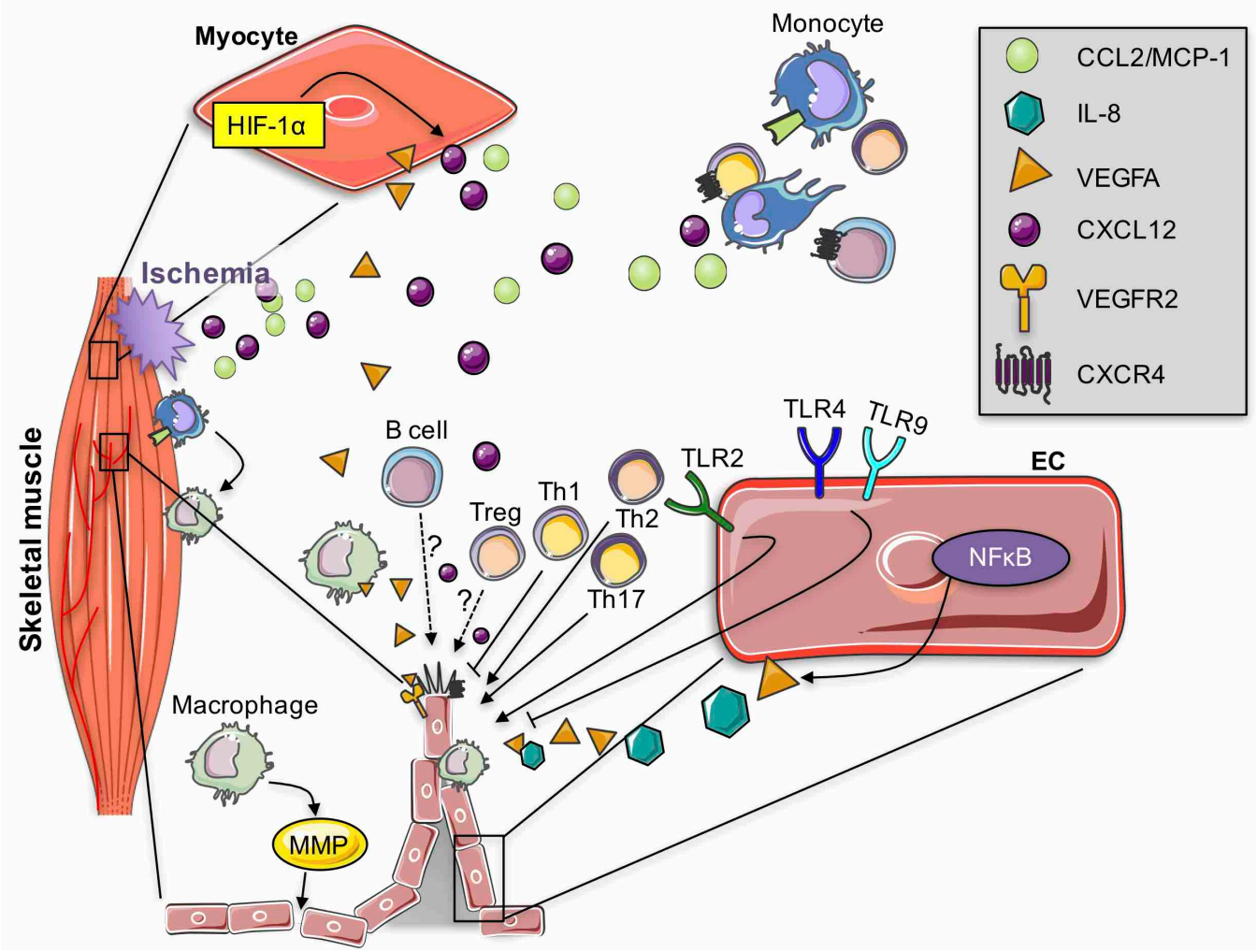

Figure 1.3. Processes driving neovascularization during hind limb ischemia. Hypoxia induces stable expression of HIF-1α, which in turn promotes expression of pro-angiogenic genes including VEGFA and CXCL12 to recruit in immune cells and promote EC sprouting. Inflammatory signaling within ECs also regulates angiogenesis via NFκB and DAMP-PRR signaling.

IV. Immune mechanisms in atherosclerosis and angiogenesis

As briefly overviewed above, the immune system plays an important and varied role in regulating atherosclerosis and angiogenesis. In this section, I will focus on two major processes relevant to the body of work I performed during my PhD training: 1. The emerging role B cells play in angiogenesis, and 2. The role endothelial-immune cell interactions play during atherosclerosis.

Immune cells in angiogenesis

Inflammation has a well-established role in regulating angiogenesis in multiple disease contexts. The innate and adaptive immune systems each regulate angiogenesis in unique ways. While cell types such as macrophages have well-established roles in tumor, ischemic, and wound healing angiogenesis[77-79], the roles of other cell types such as dendritic cells, and innate lymphoid cells in angiogenesis are less understood. Albini *et al*. have reviewed the role of innate immune cells in tumor angiogenesis highlighting that macrophages, neutrophils, natural killer cells, innate lymphoid cells, myeloid-derived suppressor, dendritic cells, mast cells, γδT cells play angio-regulatory roles during tumor growth[77]. Adaptive immune cells also regulate angiogenesis through multiple mechanisms. The roles T cells play in regulating angiogenesis are subset-specific and have been studied in multiple disease settings. Broadly, T cells have the capacity to produce VEGFA and other angio-regulatory cytokines[80]. Cytotoxic $CD4^+$ and $CD8^+$ T cells have been shown to be anti-angiogenic while Tregs and Th2 and Th17 T cells are pro-angiogenic in the setting of ischemia[72, 81-84]. The role that B cells and B cell-derived antibodies have in regulating angiogenesis, however, is slightly more complex and context-dependent (**Figure 1.4**).

B cells in angiogenesis

<u>B cells produce pro-angiogenic signals</u>

Like many other cell types, B cells are capable of expressing and secreting various signals that regulate angiogenesis. B cells can secrete pro-angiogenic signals such as VEGFA in response to multiple stimuli including IL-33[85], BAFF[86], and hypoxia[87]. B-1b cells specifically express VEGFA in response to IL-33, a signal that is released by necrotic cells[85]. B cells can also induce expression of VEGFA by MSCs through direct cell-cell interactions[88]. Overexpression of MYC in a human B cell line has also been shown to induce VEGF protein production[89]. B cells

also express matrix metallopeptidases (MMPs) such as MMP9 and MMP7, which play important roles in angiogenesis[90-92]. While one study demonstrated BAFF-stimulated B cells promote lymphangiogenesis in lymph nodes[86], more studies are required to further demonstrate that B cell production of pro-angiogenic molecules has a significant effect on pathogenic angiogenesis.

One study more directly demonstrates that B cells can secrete pro-angiogenic signals. Yang *et al*. demonstrate that *Stat3* expression in B cells promotes angiogenesis during tumor growth through secretion of VEGFA[93]. *Stat3* knockout B cells administered with tumor cells inhibited tumor growth and vascular density while *Stat3* competent B cells did not, relative to PBS controls. Further *in vitro* assays demonstrate that *Stat3* in B cells promotes endothelial tubule formation in a VEGFA-dependent manner. The study did not subset B cells, so it remains unclear what subset(s) is the source of VEGFA in this model.

B cells, including immature B cells, promote angiogenesis

B cell-deficient models have demonstrated a pro-angiogenic role for B cells in tumor and wound healing models. Using the HPV16 epithelial tumor model, B cell-deficient JH knockout mice demonstrate attenuated tumor growth, vascular density, and expression of MMP9 and VEGF[94]. JH knockout mice were generated via targeted deletion of the JH gene segments, which inhibits assembly of the immunoglobulin heavy chain (H)[95]. This knockout revealed that absence of the H chain prevents development of most B cells. Additionally, using a wound healing model, splenectomized mice demonstrated slower wound healing than sham-treated mice or splenectomized mice administered B cells[96]. Administration of B cells, but not T cells, to mice that did not undergo splenectomy demonstrate faster wound healing and increased $CD31^{+}$ staining within the wound compared to PBS controls[97]. Furthermore, global CD19 knockout mice demonstrate slower wound healing than wild type mice[98]. CD19 knockout mice have B cells and the study demonstrated that CD19 has an important functional role on B cells. In the study, hyaluronan stimulated B cells to express IL-6, IL-10, and TGF-β via TLR4 agonism in a CD19-dependent manner. Finally, Fagiani *et al*. identified a population of pro-angiogenic $CD45^{dim}VEGFR1^{+}CD31^{low}$ cells that displayed many characteristics of immature B cells[99]. These cells are upregulated in circulation during tumor growth and promote angiogenesis *in vitro*.

IgG and FcγR in neovascularization

Studies have demonstrated conflicting roles for IgG binding to FcγR in regulating angiogenesis. First, IgG is deposited at the site of injury during wound healing and perivascularly in ischemic skeletal muscle[100]. FcγR knockout mice demonstrate attenuated tumor growth and vascular density in an epithelial cancer model. Andreu *et al*. demonstrated that FcγR stimulation of mast cells promotes EC proliferation in a VEGFR2-dependent manner[94]. Additionally, FcγR knockout mice demonstrate altered vasodilatory responses to high-fat feeding suggesting that hyperlipidemic-induced changes in endothelial function are at least in part due to FcγR signaling[101].

Conversely, multiple studies have demonstrated that administration of exogenous IgG attenuates neovascularization via FcγR in multiple models including corneal injury[100], tumor growth[100, 102], and hind limb ischemia[100, 103]. Indeed, administration of the Fab region of an anti-VEGFA IgG, Ranivizumab, did not inhibit angiogenesis during hind limb ischemia or corneal injury as effectively as Bevacizumab, which is an anti-VEGFA antibody consisting of the Fab and Fc regions. Furthermore, inhibition of Fc receptors in conjunction with Bevacizumab no longer attenuated angiogenesis compared to Bevacizumab administration alone. Justiniano *et al*. demonstrated that activation of FcγR1 and IgG administration stimulates secretion of soluble-VEGFR1 by monocytes, which inhibited tubule formation *in vitro*[104]. This in total demonstrates that FcγR stimulation by IgG has anti-angiogenic effects in part due to secretion of soluble-VEGFR1 by monocytes.

These studies demonstrate that loss of FcγR expression attenuate neovascularization, but agonism of the FcγR also attenuates neovascularization. Why the results from FcγR KO studies differ from exogenous FcγR stimulation remains unclear. It is possible that FcγR KO results in compensatory expression of other Fc receptors, which may influence angiogenic outcomes. Alternatively, there are multiple isoforms of FcγR and each of these binds to different forms of IgG at different binding affinities[105]. Additionally, each FcγR family member has unique downstream signals that either stimulate or inhibit activation in cells[106]. Different forms of IgG binding to specific FcγR may have differential effects on angiogenesis.

Role for IgM in angiogenesis?

Evidence is emerging to suggest IgM may regulate angiogenesis, but studies directly addressing this question have not been published. IgM is deposited at the site of ischemia in multiple models including hind limb, cardiac, and intestinal ischemia[107-111]. IgM deficiency protects against acute ischemia/reperfusion injury[111, 112], but these models have not been applied to chronic ischemia during which angiogenesis occurs. Furthermore, IgM deposition induces complement deposition and genetic knockout of complement components in this model demonstrated that complement influences I/R injury severity[113, 114]. Finally, genetic knockout of the IgM receptor FcμR both globally and in *Lysm*-expessing myeloid cells results in attenuated tumor growth[115]. This study did not quantify vascular density, so the degree to which neovascularization contributed to the phenotype is unclear. When considered together, this evidence plus the established role for IgG-FcγR signaling in angiogenesis suggests that IgM may regulate pathogenic angiogenesis. Further studies are required to prove this definitively.

Figure 1.4.

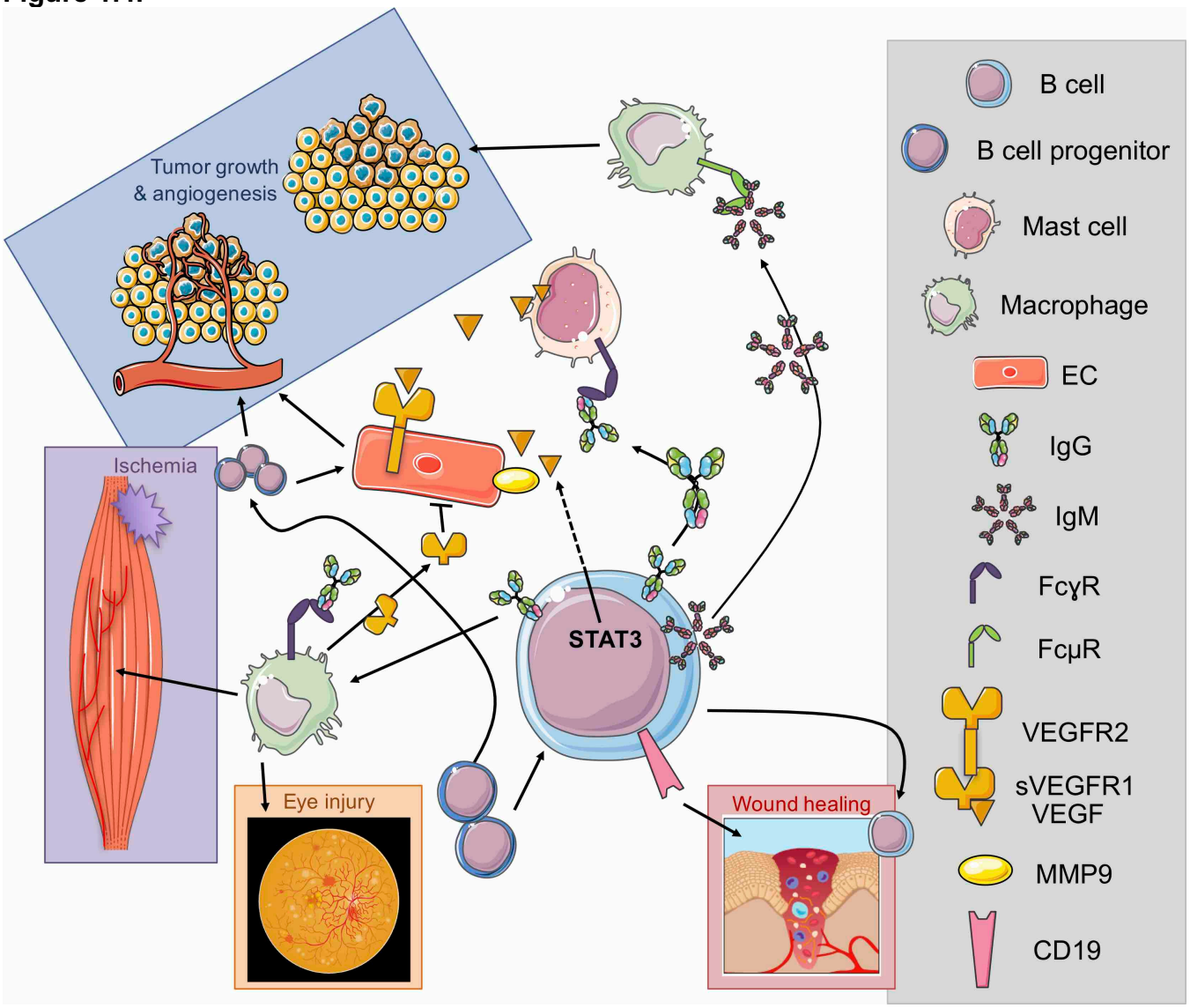

Figure 1.4. Potential mechanisms whereby B cells regulate angiogenesis.
B cells promote angiogenesis in wound healing and tumor growth. IgG produced by B cells binds to FcγR on macrophages and mast cells, which produce angio-regulatory factors and influence angiogenesis in ischemia, tumor growth, and eye injury. FcγR KO models attenuate angiogenesis, while exogenous delivery of IgG to activate FcγR can also attenuate angiogenesis.

Endothelial-immune cell interactions during atherosclerosis

Development of atherosclerotic lesions is in part due to recruitment of immune cell populations through the endothelium. There are multiple families of adhesions molecules with established roles in atherogenesis. Selectins expressed on ECs and leukocytes participate in rolling and initial adhesion. The immunoglobulin superfamily consists of many proteins involved in adhesion and cell recognition. Integrin proteins coordinate extracellular binding of signals and cells to intracellular signaling responses. Integrins also co-signal with members of the immunoglobulin superfamily, such as VCAM-1 and ICAM1[116].

Atherogenic stimuli induce ECs to upregulate expression of these adhesion molecules[13]. P- and E-selectins bind to carbohydrate ligands on leukocytes at the initial tethering and rolling steps. To stabilize binding interactions, VLA-4 and LFA-1 on leukocytes bind to VCAM-1 and ICAM1, respectively. This, coupled with a breakdown of a tight EC barrier through downregulation of tight gap junctions, permits extravasation of leukocytes to the sub-endothelial/intima region. ICAM1 and PECAM-1 mediate this process in conjunction with a chemokine gradient to draw the cells away from the lumen[116, 117].

In these studies, VCAM-1 is of particular interest to us. It is upregulated in regions of disturbed flow, where atherosclerotic lesions also form[11]. Furthermore, it has been shown to be regulated by PKCβ and NF-κB in ECs[118]. In human coronary arteries, a positive correlation between leukocyte number and the level of VCAM-1 expression on neovessels around plaques was observed[119]. This suggests two key mechanistic considerations: 1.) that VCAM-1 expression does indeed participate in recruitment of leukocytes to growing lesions, and 2.) that it is VCAM-1 expression on small neovessels, potentially the vasa vasorum, that correlate with increased immune cell presence, not VCAM-1 expression on arterial ECs. Studies from the McNamara lab mirror these findings in mice where VCAM-1 expression was abundant in the intima and increased VCAM-1 expression correlated with increased macrophage and T cell content[120].

V. Inhibitor of differentiation 3 in CVD

Inhibitor of differentiation 3 (Id3) is a helix-loop-helix transcription factor broadly expressed in mice and humans. Id3 is activated and upregulated by many different stimuli including growth factors, lipids, redox species, and inflammatory stimuli[121-126]. It regulates

cellular proliferation, differentiation, and activation in response to these signals and this influences pathogenesis of multiple diseases and vascular processes including angiogenesis[127, 128] and atherosclerosis[30, 120, 129]. Global loss of Id3 in mice ($Id3^{GKO}$) manifests in multiple phenotypes. On an atherogenic background, such as $Apoe^{-/-}$ or $Ldlr^{-/-}$, Id3 knockout mice develop more atherosclerosis than wild type (WT) controls[120, 129]. $Id3^{GKO}$ mice develop larger lesions containing increased macrophage numbers and VCAM-1 expression, and demonstrate augmented B cell recruitment to the aorta[120, 129]. In the setting of obesity, Id3 promotes increases in microvascular blood volume and proliferation of adipocyte progenitor cells to support expansion of adipose tissue. In my studies, I present the first evidence that Id3 also promotes blood flow recovery during ischemia.

ID3 is also relevant in human CVD. The lab previously identified a single nucleotide polymorphism (SNP) rs11574 that exists in the coding region of the human *ID3* gene. Expression of the minor allele results in placement of a threonine instead of an alanine at amino acid 105[130]. Expression of the minor allele of SNP rs11574 (Id3105T) attenuates interactions with binding partner E12 and significantly correlates with increased indices of coronary artery disease including intima-media thickness[130] and coronary artery calcium[131].

The findings regarding Id3's role in CVD (atherosclerosis and angiogenesis) in $Id3^{GKO}$ mice are compelling. However, given its broad cell-type expression, much is left to understand about the cell-specific roles it plays during CVD pathogenesis. Using an Id3-GFP reporter mouse (**Appendix 1, Figure A1.1A**), we found that Id3 promoter activation was present at the greatest percentage in ECs and T cells (**Appendix 1, Figure A1.1D**). Additionally, Id3 promoter activation was highest per cell in EC and MSC populations (**Appendix 1, Figure A1.1E**). These data and findings from the McNamara lab and others regarding Id3's role in angiogenesis[127, 128, 132, 133] demonstrated compelling rationale for investigating the EC-specific role for Id3 in both angiogenesis and atherosclerosis. The role of macrophage-specific Id3 had also never been investigated in atherosclerosis. Findings from Lipinski *et al.* and Doran *et al.* demonstrated an increase in macrophage populations in atherosclerotic lesions of $Id3^{GKO}$ mice and provided rationale to investigate this question further. Finally, the role of B cells in angiogenesis is a relatively unexplored area of research, thus pursuit of the B cell-specific role of Id3 in angiogenesis provided a novel set of questions and outcomes. In Chapters 3 and 4, I report my findings on the EC-, macrophage-, and B cell-specific roles of Id3 in angiogenesis

during hind limb ischemia and the EC- and macrophage-specific roles of Id3 in atherosclerosis development, respectively.

Chapter 2: Materials and Methods

I. Reagents

Prepared Buffers and Media

AKC lysis buffer: 0.15 M NH4Cl + 0.01 M KHCO3 + 0.1 mM EDTA in ddH_2O

FACS buffer: 0.05% NaN3 + 1% BSA in PBS

Sort buffer: 1% BSA in PBS

Digestion buffer for skeletal muscle and lungs: 1 mg/mL collagenase type I in FACS buffer or DMEM

Digestion buffer for PVAT: 200 U/mL collagenase type XI + 60 U/mL DNase I + 125 U/mL hyaluronidase type I + 500 U/mL collagenase type I + 20 mM HEPES in PBS

Peritoneal lavage media: 5% HI-FBS + 1x Pen/strep in DMEM

Sort collection buffer: 20% HI-FBS + 1 mM HEPES + 1x NEAA + 100 μM NA-pyruvate + 40 μg/ml Gentamycin + 55μM β-mercaptoethanol in RPMI

TLR9 agonist treatment media: 10% HI-FBS + 1 mM HEPES + 1x NEAA + 100 μM NA-pyruvate + 40 μg/ml Gentamycin + 55μM β-mercaptoethanol + 100 nM CpG ODN 1668 in RPMI

EC growth media: 5% HI-FBS + 1x Anti-anti in EC growth media (Cell Applications, 211-500)

EC starvation media (Cell Applications, 209-250)

Antibodies

Table 2.1. Flow cytometry antibodies

Antigen	Clone	Vendor
Alpha-SMA	1A4	Sigma-Aldrich
B220	RA3-2B2	eBioscience
CD3	145-2C11	eBioscience
CD4	GK1.5	Biolegend
CD5	53-7.3	Invitrogen
CD8	53-6.7	BD Biosciences
CD11b	M1/70	BD Biosciences
CD11c	N418	eBioscience
CD19	Id3	eBioscience
CD23	B3B4	eBioscience
CD31	390	eBioscience
CD34	MEC14.7	Biolegend
CD45	30-F11	BD Biosciences
CD115	AFS98	eBioscience
CD184/CXCR4	2B11	eBioscience
CD185/CXCR5	SPRCL5	Invitrogen
CD206	C068C2	Biolegend
CD326/EPCAM	Caa7-9G8	Miltenyi
F4/80	BM8	Biolegend
IgM	R6-60.2	BD Biosciences
Live/Dead	-	Invitrogen
Ly6C	HK1.4	Biolegend
Ly6G	1A8	Biolgend
VCAM-1	429	Biolegend

Table 2.2. Antibodies used for immunofluorescence

Tissue	Antigen	Clone	Dilution	Vendor
Skeletal muscle	CD31	SZ31	1:250	Dianova
Skeletal muscle	Alpha-SMA	1A4	1:500	Sigma-Aldrich
Skeletal muscle	IgM	-	1:100	SouthernBiotech
Aortic root, BCA	VCAM-1	EPR5047	1:250	Abcam
Aortic root	CD68	FA-11	1:250	Biolegend

Table 2.3. SouthernBiotech antibodies used for ELISA

Antibody	Purpose	Catalog Number
Mouse IgM-UNLB	Standard	0101-01
GaM IgM, UNLB	Capture	1020-01
GaM IgM, AP-conj	Detection	1020-04
Mouse IgG-UNLB	Standard	0107-01
GaM IgG, UNLB	Capture	1030-01
GaM IgG, AP-conj	Detection	1030-04
Mouse IgG1-UNLB	Standard	0102-01
GaM IgG1, UNLB	Capture	1070-01
GaM IgG1, AP-conj	Detection	1070-04
Mouse IgG2a-UNLB	Capture	1080-01
GaM IgG2a, AP-conj	Detection	1080-04
Mouse IgG2b-UNLB	Standard	0104-01
GaM IgG2b, UNLB	Capture	1090-01
GaM IgG2b, AP-conj	Detection	1090-04
Mouse IgG2c-UNLB	Standard	0122-01
GaM IgG2c, UNLB	Capture	1079-01
GaM IgG2c, AP-conj	Detection	1078-04
Mouse IgG3-UNLB	Standard	0105-01
GaM IgG3, UNLB	Capture	1100-01
GaM IgG3, AP-conj	Detection	1100-04

II. Murine models of cardiovascular disease

Knockout mice on a C57Bl/6 background were generated and housed at the University of Virginia. All animal experiments performed in this study were approved by the Institutional Animal Care and Use Committee of the University of Virginia.

Genetic knockout models

Five transgenic knockout lines were maintained and utilized in these studies: Id3 global knockout (KO) and wild type (WT) littermates ($Id3^{GWT}$ and $Id3^{GKO}$, respectively), Id3 B cell-specific KO and WT littermates ($Id3^{fl/fl}CD19^{cre/+}$ ($Id3^{BKO}$) and $Id3^{fl/fl}CD19^{+/+}$ ($Id3^{BWT}$)), Id3 myeloid-specific KO and WT littermates ($Id3^{fl/fl}Lysm^{cre/+}$ ($Id3^{MKO}$) and $Id3^{fl/fl}Lysm^{+/+}$ ($Id3^{MWT}$)), Id3 endothelial cell-specific conditional KO and WT littermates ($Id3^{fl/fl}$Cdh5-$CreER^{T2}$ ($Id3^{ECKO}$) and $Id3^{+/+}$Cdh5-$CreER^{T2}$ ($Id3^{ECWT}$)), and secreted IgM-deficient mice and WT littermates ($sIgM^{-/-}$ and $sIgM^{+/+}$). To induce Id3 KO in the conditional knockout line, $Id3^{ECKO}$ and $Id3^{ECWT}$ mice were administered 1 mg of tamoxifen via intraperitoneal injection per day for ten days over the

course of two weeks. Tamoxifen was resuspended in peanut oil at a concentration of 10 mg/mL and filter-sterlized prior to administration. Two weeks were allocated for tamoxifen wash-out following the final injection and prior to the start of any treatments or studies.

Model of coronary atherosclerosis

To induce development of atherosclerosis, mice were treated with one dose of a plasmid containing mutated protein mPcks9-D377Y (Addgene, 58376) packaged in AAV8 (Vigene) (**Figure 2.1A**). $1x10^{11}$ viral genomes were administered via tail vein injection. The following day, mice were placed on a western diet (Envigo TD #88137, 42% fat from cholesterol) to induce hyperipidemia. Following 1-2 weeks of western diet feeding, blood was obtained by orbital bleed to measure plasma levels of cholesterol and validate induction of hyperlipidemia. To quantify atherosclerosis burden, mice were fed western diet for 12 weeks (**Figure 2.1B**).

Figure 2.1.

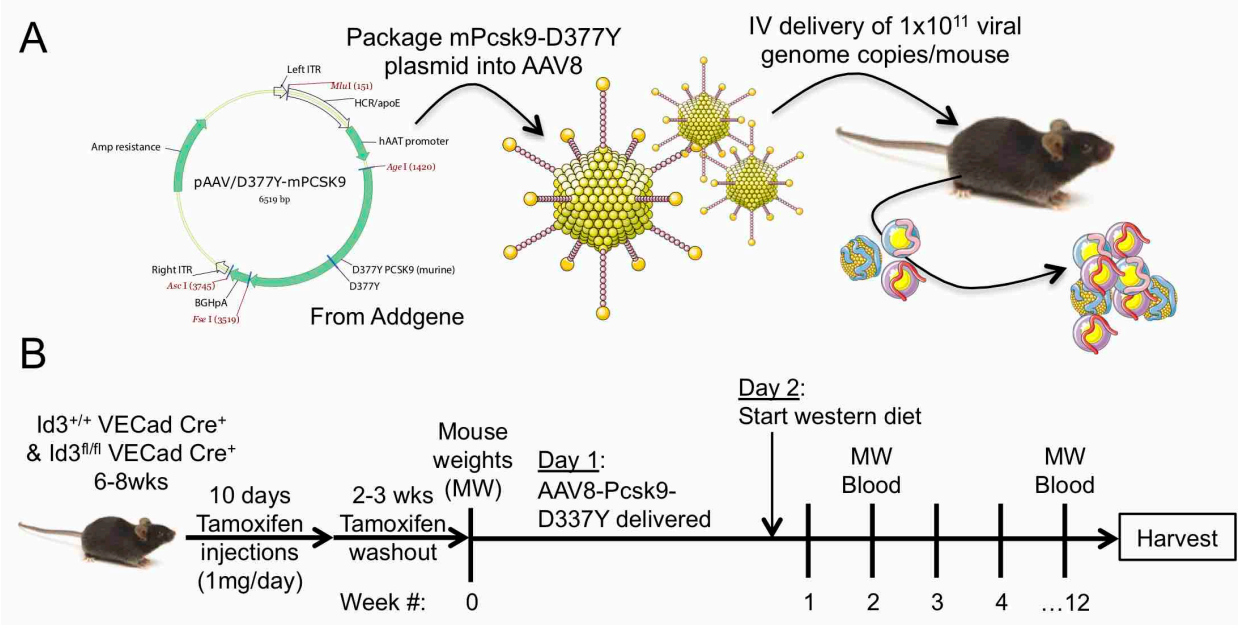

Figure 2.1. Description of Pcsk9-AAV generation and atherosclerosis induction. **(A)** mPcsk9-D337Y plasmid was purchased from Addgene and amplified by Maxi-prep. Plasmid was then sent to Vigene to package in AAV8. $1x10^{11}$ viral genomes were administered via tail vein injection to each mouse to begin induction of atherosclerosis. **(B)** Prior to AAV administration, mice were administered 1 mg of tamoxifen in peanut oil via intraperitoneal injection once per day for 10 days over the course of two weeks. Following 2-3 weeks of tamoxifen washout, mice were administered mPcsk9-D377Y-AAV8. One day following the injection, mice were given a western diet that lasted for the remainder of the experiment. Additionally, blood was drawn after approximately 2 weeks of diet to validate increased circulating lipid levels.

Model of Peripheral artery disease / hind limb ischemia (HLI)

To induce hind limb ischemia, the femoral artery of each mouse was ligated and resected (**Figure 2.2**). Briefly, mice were anesthetized with ketamine/xylazine and placed on a heating pad to maintain a proper body temperature. An incision was made on the underside of the mouse's left leg near the hip crease and adipose tissue and fatia was separated to access to the femoral artery. The femoral artery was ligated immediately rostral to the internal iliac artery bifurcation and then a section of the femoral artery distal to this point was resected. Smaller bifurcations between the internal iliac bifurcation and the epigastric bifurcation were cauterized to prevent bleeding and the femoral artery was carefully separated from the femoral vein and the local skeletal muscle. The femoral artery was cauterized immediately caudal to the epigastric bifurcation to prevent bleeding and end the resection. The incision was closed using staples. Mice were administered buprenorphine every twelve hours for the next 48 hours and water containing antibiotics and acetominophine for the next 7 days to manage pain.

To quantify blood flow in each limb, mice were anesthetized with ketamine/xylazine or isofluorane and placed under a PeriScan PIM-II blood perfusion monitor (laser Doppler scanner) (Perimed, Inc. North Royalton, OH). Images were taken in triplicate. Regions of interest (ROIs) were traced around the ischemic and non-ischemic foot of each mouse to quantify perfusion intensity. Perfusion of the ischemic foot was normalized to the non-ischemic foot for each mouse. Perfusion was quantified at multiple time points including 1, 3, 7, 14, 21, and 28 days post-femoral artery ligation and resection.

Figure 2.2.

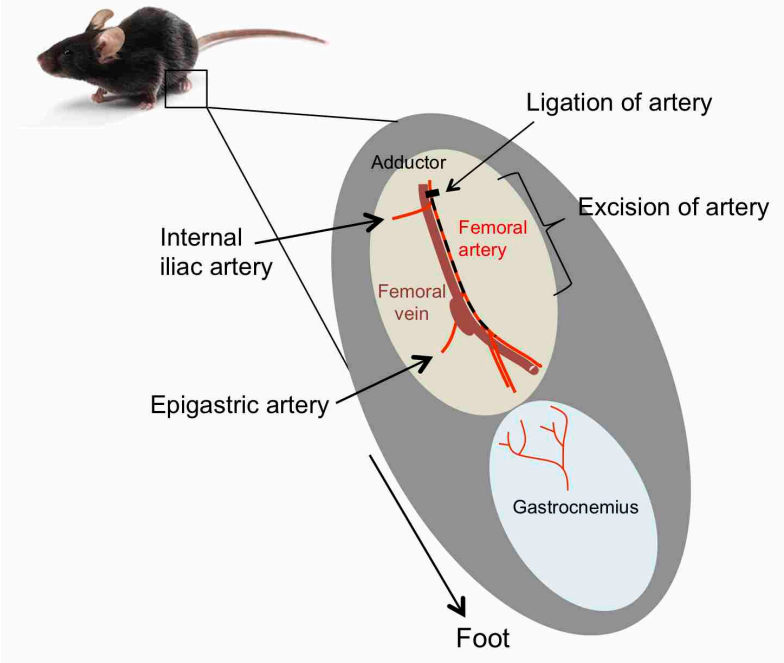

Figure 2.2. Schematic of HLI procedure.
Briefly, the femoral artery was ligated immediately rostral to the internal iliac artery bifurcation and then a section of the femoral artery was resected until immediately past the epigastric artery bifurcation. Ischemia developed distal to the resection in tissues including the gastrocnemius, tibialis anterior, and the foot.

III. Tissue processing

In general, mice were euthanized by CO_2 overdose. Blood was harvested via cardiac puncture and stored in 10 µL of 0.5 M EDTA to prevent coagulation. Mice were perfused through the left ventricle (after cutting the right atrium) with 10 mL PBS supplemented with 0.5 mM EDTA followed by 5–10 mL of PBS before harvesting all other tissues. Inguinal lymph nodes were removed before harvesting the inguinal (subcutaneous) adipose tissue. All tissues harvested for RNA extraction were flash frozen in liquid nitrogen and stored at -80°C.

Aorta and Brachiocephalic artery (BCA)

For en face preparation and BCA isolation, aorta and BCAs were cleaned of PVAT. The BCA was extracted from above the subclavean-carotid bifurcation to the aortic bifurcation and fixed in 4% PFA overnight. The aorta was extracted from the mouse from the aortic arch to the iliac bifurcation, and then fixed in 4% paraformaldehyde. After at least 24 hours, aortas were

opened longitudinally from the aortic arch to the iliac bifurcation and pinned to expose the lumen side of the aorta. BCAs were stored in 70% ethanol and paraffin embedded.
For analysis of the aortic root, whole hearts include the aortic root were fixed in 4% PFA at 4°C, rotating, for 24-48 hours.

Blood

For flow cytometry analysis of cell populations, 100 µL of blood was treated with AKC lysis buffer for 5 minutes, rotating. Lysis was quenched with FACS buffer and cells were spun down. Pellets were resuspended in FACS buffer to be stained for flow cytometry.
To isolate plasma, blood samples were spun down at 5,000 g for 5 minutes at room temperature. Plasma was then transferred into a fresh tube and stored at -20°C.

Bone marrow

Following perfusion, rear femurs and tibias were harvested and excess muscle and tissue removed. The ends of each bone were cut away to access the marrow. Using 5 mL of PBS per bone, each bone was flushed using a syringe. Cell suspensions were spun and treated with AKC lysis buffer to lyse remaining red blood cells. Cells were then washed with FACS buffer to be stained for flow cytometry.

Lungs

Lungs (all lobes) were placed in digestion buffer, minced, and incubated at 37°C, shaking, for ~45 minutes. Digested tissue was then passed through a 19-gauge needle ten times to create a single-cell suspension. The suspension was then passed through a 70 µm filter, washed with FACS buffer, and pelleted. Cells were treated with AKC lysis buffer to lyse remaining red blood cells. Cells were then stained for live cell sorting.

Peritoneal cavity lavage

Peritoneal cells were collected by peritoneal lavage. Lavages were spun down and treated with AKC lysis buffer to lyse remaining red blood cells as needed. Cells were then washed with FACS buffer to be stained for flow cytometry or sort buffer for live cell sorting.

PVAT

PVAT was placed in digestion buffer, minced, and incubated at 37°C, shaking, for ~45 minutes. Digested tissue was then pipetted up and down to create a single-cell suspension, passed through a 70 μm filter, washed with FACS buffer, and pelleted. Cells were treated with AKC lysis buffer to lyse remaining red blood cells as needed. Cells were then stained for flow cytometry.

Skeletal muscle

For flow cytometry analysis of cell populations, gastrocnemius muscles were placed in digestion buffer, minced, and incubated at 37°C, shaking, for ~45 minutes. Digested tissue was then pipetted up and down to create a single-cell suspension, passed through a 70 μm filter, washed with FACS buffer, and pelleted. Cells were treated with AKC lysis buffer to lyse remaining red blood cells as needed. Cells were then stained for flow cytometry.
For who tissue analysis, gastrocs were fixed in 4% PFA at 4°C, rotating, for 24-48 hours.

Spleen

Spleens were mashed through a 70 μm filter and washed with 10 mL of FACS buffer, then spun down. Cell pellets were resuspended in 5 mL of AKC lysis buffer and incubated for 5 minutes before being quenched with 5 mL of FACS buffer. Cells were then spun down and aliquoted to use 1/50th of each sample for flow cytometry.

IV. Flow cytometry and live cell sorting

All cells were stained with fluorophore-conjugated antibodies against cell surface proteins (**Table 2.1**) in FACS buffer or Brilliant Violet Stain Buffer (BD, if more than one Brilliant Violet fluorophore was used at one time) for 25 minutes at 4°C then washed with FACS buffer. For cell population analysis, cells were then stained with Live/Dead (Fisher) in PBS for 30 minutes at 4°C then washed with FACS buffer. Cells were then fixed with 2% PFA for 7–10 minutes at room temperature and washed with FACS buffer. Finally, cells were resuspended in FACS buffer and stored at 4°C until analyzed. Cells were run on the Attune (Thermofisher) and compensated and analyzed in FCS Express. For live cell sorting, cells were stained with DAPI

prior to sorting on the Influx or FACSAria Fusion (BD Biosciences). Cells were sorted into RPMI media enriched with 20% FBS.

V. Cell culture

Cell lines

Human umbilical vein endothelial cells were ordered from Lonza (C2519A) and cultured in EC growth media. Cells were passaged using TrypLE Express (Gibco, 12605-010). Experiments were conducted with cells passaged 2 to 5 times.

Tubule formation

Prior to passing cells, 75 uL of growth factor-reduced Matrigel (Corning) was pipeted into each well of a 96-well plate (as needed). The Matrigel was left to polymerize at 37°C for 30 to 60 minutes. HUVECs were then passaged and 15,000 HUVECs were placed in each well at a final volume of 100 uL. Cells were cultured in EC starvation media (Cell Applications, 209-250) with or without additional treatments, as specified in the results sections. Plates were placed in a hypoxia chamber (2% O2, C-Chamber and ProOx C21 from Biospherix) within a cell culture incubator at 37°C for six hours. Five images of each well were then taken on an Accu-Scope camera (Excelis). These images were of the center of the well and the areas immediately above and below, and to the right and left of the center. Images were then analyzed to quantify the number of branch points and boxes formed by tubules. Branch points were defined as points where at least two different cell/tubules intersected. Boxes were defined as areas surrounded completely by connected tubules. These values were collected for each image and averaged for each well and treatment.

Cellular proliferation

10,000 cells were plated per well of a 96-well plate in 100 µL of EC starvation media with or without additional treatment. Additional wells were filled with 100 µL of media without cells to use as a blank control. Cells were then cultured in a hypoxia chamber (2% O2, company info) within a cell culture incubator at 37°C for 24 hours. At 23 hours, 20 µL of MTS reagent (Promega) was added to each well and the plate placed back in the hypoxia chamber for one additional hour. Absorbance from each well was then read with a SpectraMAX 190 microplate

reader (Molecular Devices) at 490 nm and 665 nm. 665 nm values were subtracted from 490 nm to account for background. Blank control values were then subtracted from the absorbance values of each other well and these values were normalized to the vehicle control.

Cell activation

HUVECs were plated in a 24-well plate and allowed to grow in EC growth media until 90% confluent. Cells were then washed with PBS and cultured in EC starvation media for 30 minutes prior to the start of treatment. Cells were treated with specified treatments resuspended in EC starvation media for 2 hours. Cells were then harvested in Trizol for RNA extraction.

B cell culture and conditioned media preparation

B-1a, B-1b, and B-2 cells were sorted from peritoneal lavage samples (**Figure 2.3**) on the FACSAria Fusion or Influx cell sorters (BD). They were then resuspended in TLR9 agonist treatment media at 500,000 cells per 250 uL for 7 days or in EC starvation media at the same cell:media ratio for 6 hours. Cultures were then spun down and conditioned media supernatants transferred to fresh tubes and stored at -20°C. Cell pellets were resuspended in Trizol for RNA extraction.

Figure 2.3.

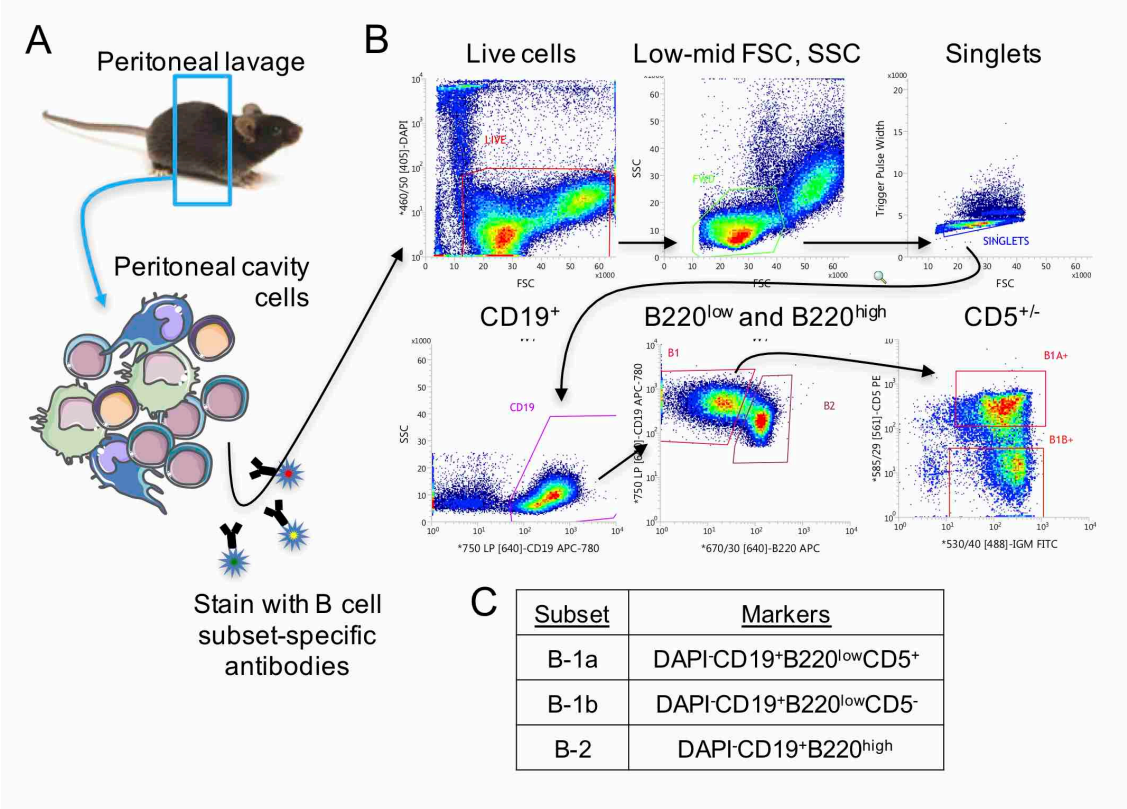

Subset	Markers
B-1a	DAPI^{-}CD19^{+}B220^{low}CD5^{+}
B-1b	DAPI^{-}CD19^{+}B220^{low}CD5^{-}
B-2	DAPI^{-}CD19^{+}B220^{high}

Figure 2.3. Live cell sorting strategy.
(A) Schematic of approach for preparing and staining samples that were then run on a flow cytometer to sort B-1a, B-1b, and B-2 cells. **(B)** Example gating strategy for the sorts. **(C)** Table clarifying markers used to identify each subset.

VI. Colorimetric assays

ELISA

Total IgM, total IgG, IgG1, IgG2a, IgG2b, IgG2c, and IgG3, HMGB1-specific IgM, and oxPAPC-IgM in mouse plasma was measured using colorimetric ELISA (**Tables 2.3,2.4**). EIA/RIA high-binding microplates were coated with IgX-specific antibody, HMGB1, or oxPAPC (**Table 2.4**). Mouse IgM, IgG, IgG1, IgG2b, IgG2c, and IgG3 standards (Southern Biotech), or plasma or serum samples were detected with alkaline phosphatase-conjugated goat anti-mouse IgM, IgG1, IgG2b, IgG2c or IgG3 secondary antibody (Southern Biotech) and pNPP substrate (Southern Biotech 0201-01). Absorbance measurements were analyzed with a SpectraMAX 190 microplate reader (Molecular Devices) at 405 nm. The standard curve was determined using a 4-parameter function and concentration measurements were extrapolated

using Softmax Pro 3.1.2 software. Only samples with CV<15% and within the standard curve were included in analysis.

Table 2.4. ELISA antibodies and dilutions

Assay	Coat/Capture		Standard		Sample dilution	Detection	
	Reagent	D/C	Reagent	D/C		Reagent	D/C
Total IgM	1020-01	1:1600	0101-01	200 ng/mL	Plasma, 1:2000; Muscle lysates, 1:100	1020-04	1:4000
HMGB1-specific IgM	HMGB1	1 µg/mL	12-week athero plasma	1:100	1:100	1020-04	1:4000
oxPAPC-specific IgM	oxPAPC	5 µg/mL	12-week athero plasma	1:200	1:100	1020-04	1:4000
Total IgG	1030-01	1:1600	0107-01	200 ng/mL	1:50000	1030-04	1:1000
IgG1	1070-1	1:1600	0102-01	200 ng/mL	1:5000	1070-04	1:8000
IgG2a	1080-01	1:400	Day 7 HLI plasma	1:100	1:5000	1080-04	1:1000
IgG2b	1090-01	1:800	0104-01	200 ng/mL	1:500	1090-04	1:2000
IgG2c	1079-01	1:400	0122-01	200 ng/mL	1:500	1079-04	1:500
IgG3	1100-01	1:1600	0105-01	200 ng/mL	1:50000	1100-04	1:8000

D/C = Dilution/Concentration

Total cholesterol levels

Plasma was subjected to colorimetric enzymatic assay to quantify total cholesterol using the Infinity Cholesterol kit (ThermoFisher, TR13421). Briefly, plasma was diluted in PBS and 2 uL were combined with 200 uL of reagent and incubated at 37 C for 5 minutes. Absorbance measurements were analyzed with a SpectraMAX 190 microplate reader (Molecular Devices) at 500 nm. Total cholesterol was calculated using the following equation: Total cholesterol (mg/dL) = $(Abs_{sample} – Abs_{blank}) / (Abs_{standard} – Abs_{blank})$ * 200 mg/dL * dilution factor, where the cholesterol concentration of the standard was 200 mg/dL.

VII. Gene expression

RNA extraction and cDNA synthesis

RNA was extracted from tissues and cells using Trizol extraction. 0.5 to 1 µg of RNA was then treated with DNase (Invitrogen) and used to reverse transcribe cDNA using an iScript cDNA synthesis kit (BioRad).

qRT-PCR

To quantify gene expression, cDNA was diluted in water as needed and combined with 0.5 mM forward and reverse primers (**Table 2.5**) and SYBR Green (SensiFast, BioLine). Semi-quantitative real-time PCR was performed on a CFX96 Real-Time System with an annealing temperature of 60°C for all reactions (BioRad). Data were calculated by the ΔΔCt method and expressed in arbitrary units that were normalized to 18s levels.

Table 2.5. qRT-PCR primers

Gene	Species	Forward sequence	Reverse sequence
Id3	Mouse	TGCTACGAGGCGGTGTGCTG	TGTCGTCCAAGAGGCTAAGAGGCT
18s	Mouse	CGGCTACCACATCCAAGGAA	AGCTGGAATTACCGCGGC

VIII. Histology

Preparing sections

Fixed hearts and skeletal muscle were incubated in 30% sucrose overnight at 4°C, rotating, until the tissues were saturated and sank to the bottom of the tube. Then, tissues were embedded in OCT and 10 µm sections were cut by Cryostat (Leica biosystems). Aortic roots were cut from the beginning of the three aortic leaflets to the aortic arch.

Immunofluorescence

Tissue sections were permeabilized with 0.25% Triton-100 in PBS, and then washed in PBS. Sections were blocked with 0.6% fish skin gelatin with 10% serum in PBS, then incubated with primary antibodies in 0.6% fish skin gelatin with 10% serum in PBS overnight at 4°C. Sections were washed as before and then incubated with secondary antibody for 1-2 hours at room temperature. Following one final wash, slides were counterstained with DAPI (1 µg/mL) and coverslipped using ProLong Gold (Life Technologies). Images were obtained using Zeiss

LSM700 confocal microscope, 20X objective. Figures shown are maximal intensity projection images.

Oil red O staining

Aortic root sections were stained with Oil Red O. Images were obtained with the Olympus BX51 Microscope (Olympus). Total root, total plaque, and Oil red O-positive plaque areas were quantified using Image-Pro Plus software (Media Cybernetics).

Movat

BCA sections were stained with Movat's pentachrome stain by Missy Bevard in the UVA CVRC Histology Core.

XI. En face analysis of aorta

Pinned aortas were stained using Sudan IV (Sigma) as previously described[129]. Aortas were imaged using a Nikon D70 DSLR camera and the percentage of the total aorta area that was Sudan IV+ plaque area was quantified using Image-Pro Plus software (Media Cybernetics).

X. Statistics

All statistical analysis was performed using Prism 7 or 8 (GraphPad Software, Inc.). Because sample n < 15 for all murine experiments, normal distribution could not be determined. Mann-Whitney tests were used to compare two experimental groups, Kruskal-Wallis tests were used to compare three experimental groups with one independent variable, and two-way ANOVAs were used to compare three or more experimental groups with two independent variables (such as both time and genotype, for example). Data are generally expressed as mean ± SD. P values and the specific statistical analyses use are specified in figure legends.

Chapter 3: Id3-mediated expansion of IgM-secreting B-1b cells augments ischemic angiogenesis in skeletal muscle

I. Abstract:

Background: Peripheral artery disease (PAD) is a prevalent vascular disease with many co-morbidities and few effective therapeutic options. There is a need to better understand the mechanisms mediating adaptive neovascularization and tissue perfusion in this patient population from a molecular and cellular level. In this study, we investigate the potential role(s) for helix-loop-helix transcription factor Inhibitor of differentiation 3 (Id3), B cells, and B-1 cell-derived IgM in regulating microvascular blood flow during murine hind limb ischemia, a model of PAD.

Methods: A murine model of hind limb ischemia (HLI) was employed to model PAD through ligation and resection of the femoral artery. Laser Doppler perfusion imaging and quantification of $CD31^+$ endothelial cells (ECs) in gastrocnemius muscles by immunofluorescence were employed to quantify microvascular blood flow and EC number during HLI in a series of Id3 KO lines. Flow cytometry and ELISA were utilized to quantify B cell subsets and IgM levels in skeletal muscle and in circulation during HLI. Cultured ECs were treated with conditioned media from B-1 subsets sorted from $sIgM^{+/+}$ and $sIgM^{-/-}$ mice followed by quantification of cell proliferation and tubule formation.

Results: B cell-specific loss of Id3, but neither EC- nor macrophage-specific loss, resulted in impaired perfusion recovery during HLI. B cell-specific Id3 KO mice ($Id3^{BKO}$) had reduced artery density in the tibialis anterior, but not the gastrocnemius muscle, compared to $Id3^{BWT}$ mice. Additionally $Id3^{BKO}$ mice had increased B-1b cell numbers in ischemic skeletal muscle, and increased local and circulating levels of total and DAMP-specific IgM. Treatment of ECs with conditioned media from $sIgM^{+/+}$ B-1b cells, but not $sIgM^{-/-}$ B-1b cells inhibited EC proliferation.

Conclusions: This study is the first to demonstrate that mice with loss of Id3 specifically in B cells results in impaired perfusion recovery during HLI. B cell-specific loss of Id3 promotes expansion of the IgM-secreting B-1b cell population raising the interesting hypothesis that IgM may impair perfusion recovery after HLI. Future studies are needed to investigate deeper mechanisms whereby Id3, B-1b cells, and IgM regulate ischemic vascular adaptation. These outcomes plus investigation of levels of IgM and B cell populations in human PAD subjects across a symptomatic spectrum may reveal potential novel therapeutic targets for this disease.

II. Introduction:

Peripheral artery disease (PAD) is a prevalent vascular disease with many co-morbidities and few effective therapeutic options[34, 134]. There is a need to identify novel molecular and cellular mechanisms regulating the capacity for individuals to maintain adequate tissue vascularization in response to reduced blood flow in major peripheral arteries. This can occur through multiple functions including arteriogenesis, angiogenesis, and vasodilation[135]. Studies demonstrate PAD is mediated by many different factors including genetics, inflammation, lifestyle, and lipid levels[57, 134, 136]. In this study, we investigated the potential role(s) for the helix-loop-helix transcription factor Inhibitor of differentiation 3 (Id3) and B cells in regulating vascularization during skeletal muscle ischemia.

Id3 is a broadly expressed member of the helix-loop-helix transcription factor family that regulates cell proliferation, differentiation, and responses to hyperlipidemia and mitogens including growth factors and inflammatory stimuli[121-126]. Id3 promotes angiogenesis during tumor growth and adipose tissue expansion[127, 128], but whether this is the case in the setting of ischemia remains unclear. Furthermore, the SNP rs11574 is located in the coding region of the human *ID3* gene and alters function of the protein[130]. Expression of the minor allele (Id3105T) significantly correlates with increased indices of coronary artery disease including intima-media thickness[130] and coronary artery calcium[131]. Given the established role of Id3 in mediating progression of cardiovascular disease, we hypothesized that Id3 also augments ischemic neovascularization during ischemia.

Id3 has an established role in regulating B-1 cell population size and function through direct and indirect mechanisms[30, 137]. Indeed, loss of Id3 globally and specifically in B cells results in expansion of B-1b cells[30, 137, 138]. B-1b cells are part of the B-1 subset of B cells, which are derived from the fetal liver and produce the majority of natural IgM found *in vivo*[24-26]. Additional results from global knockout studies suggest that Id3 likely has important roles in regulating other cell types including macrophages and endothelial cells (ECs) during cardiovascular disease progression[120, 129]. To date, however, the roles of global and cell-specific Id3 expression in hind limb ischemia (HLI) have not been investigated.

Prior cell-specific knockout studies have demonstrated essential roles for ECs[35, 68] and macrophages[69-71, 78, 139] in regulating ischemic neovascular adaptation in skeletal muscle. To date, however, very little is known about the role B cells might play in HLI or PAD. However, B

cells have been implicated in promoting angiogenesis in tumors, eye injury, and wounds[93, 94, 97-100, 103, 140] as well as in amplifying tissue damage during acute ischemia/reperfusion injuries in multiple tissues including skeletal muscle[107, 110, 141]. Thus, we investigated the EC-, macrophage-, and B cell-specific roles of Id3 in promoting microvascular blood flow during HLI.

III. Results:

Validation of EC-specific Id3 knockout

$Id3^{ECWT}$ and $Id3^{ECKO}$ were generated by breeding $Id3^{fl/+}Cdh5^{cre/ERT2+}$ mice. $Id3^{ECWT}$ had an $Id3^{+/+}$ genotype, while $Id3^{ECKO}$ mice had an $Id3^{fl/fl}$ genotype (**Figure 3.1A**). The cre/ERT2 required treatment for 10 days with tamoxifen to induce translocation of ERT2-cre from the plasma membrane to the nucleus. Of note, $Id3^{MKO}$ and $Id3^{BKO}$ mice were previously validated in the McNamara lab[30, 122]. Following two weeks of tamoxifen wash-out, lungs from $Id3^{ECWT}$ and $Id3^{ECKO}$ mice were extracted and digested to isolate a single-cell suspension (**Figure 3.1B**). Using live cell sorting, $CD45^{-}CD31^{+}$ ECs, $CD45^{-}CD31^{-}$ stromal cells, and $CD45^{+}$ immune cells were isolated and RNA was extracted to quantify Id3 mRNA expression. qRT-PCR results revealed that Id3 expression levels were reduced only in $Id3^{ECKO}$ EC populations, but not $Id3^{ECWT}$ EC populations, nor in non-EC populations of either genotype (**Figure 3.1C**). These results validate that our conditional knockout mouse effectively knocked out Id3 expression in an EC-specific manner.

Figure 3.1.

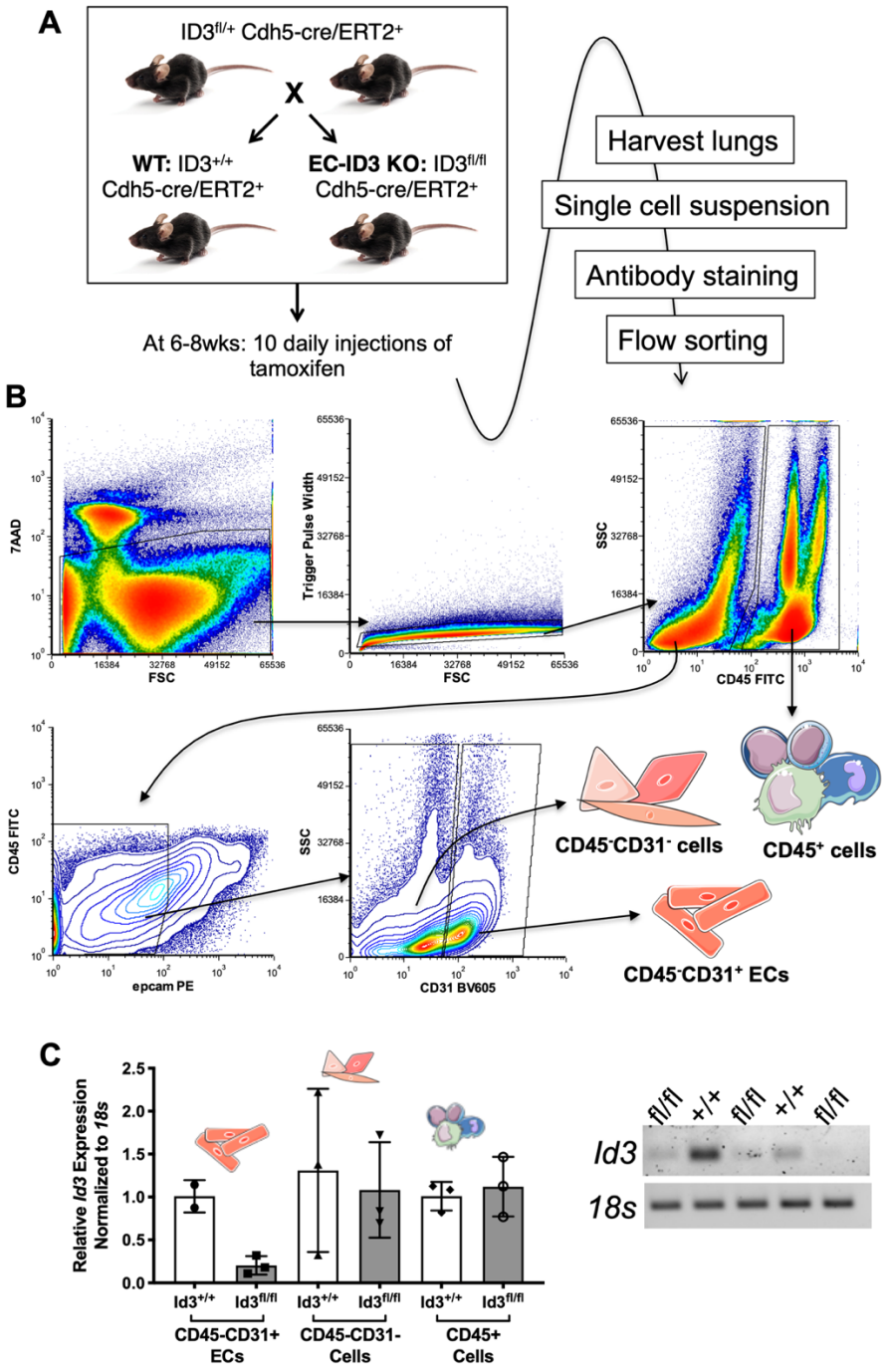

Figure 3.1. Validation of EC-specific Id3 knockout line.
(A) Schematic of the breeding to generate $Id3^{+/+}Cdh5^{cre+}$ ($Id3^{ECWT}$) and $Id3^{fl/fl}Cdh5^{cre+}$ ($Id3^{ECKO}$) mice. **(B)** Mice were treated with tamoxifen (1 mg/day). After that, lungs from each mouse were isolated and digested to isolate a single cell suspension. Using flow cytometry, $CD45^+$ immune cells, $CD45^-CD31^+$ endothelial cells, and $CD45^-CD31^-$ non-endothelial stromal cells were sorted for RNA extraction. **(C)** Following cDNA synthesis, Id3 mRNA levels were measured by qRT-PCR in all three cell subsets form $Id3^{ECWT}$ ($Id3^{+/+}$) and $Id3^{ECKO}$ ($Id3^{fl/fl}$) mice. Data shown is the mean ± standard deviation.

Id3 regulates microvascular blood flow in a B cell-specific manner

To investigate whether Id3 regulates microvascular blood flow in response to ischemia, HLI was surgically induced in Id3 knockout and wild type (WT) littermates (**Figure 3.2A**). At day 3 of HLI in wild type mice, *Id3* mRNA levels were significantly increased in ischemic gastrocnemius muscles compared to non-ischemic muscles (**Figure 3.2B**). Using laser Doppler perfusion imaging (LDPI), we found that $Id3^{GKO}$ mice had significantly reduced microvascular blood flow at days 14 and 21 of HLI compared to $Id3^{GWT}$ littermates (**Figure 3.2C**). Cell-specific Id3 knockout mice were employed to determine the role individual cell types played in the observed phenotype. Given the established role of both ECs and macrophages in ischemic angiogenesis, blood flow recovery during HLI in EC-specific Id3 knockout mice ($Id3^{ECKO}$) and wild type littermates ($Id3^{ECWT}$) as well as macrophage-specific Id3 knockout mice ($Id3^{MKO}$) and wild type littermates ($Id3^{MWT}$) was investigated. Interestingly, we found that the perfusion levels of $Id3^{ECKO}$ and $Id3^{MKO}$ were not significantly different from WT controls (**Figure 3.2D-E**).

While no literature exists to support a specific role for B cells in promoting blood flow recovery during HLI, prior studies in models of atherosclerosis and diet-induced obesity reveal that loss of Id3 has significant effects on B-1 cell populations and disease outcomes *in vivo*[30, 129, 137, 138]. Thus, we tested whether B cell-specific Id3 KO mice ($Id3^{BKO}$) had altered microvascular blood flow during HLI. Indeed, $Id3^{BKO}$ mice phenocopied $Id3^{GKO}$ mice with reduced microvascular blood flow relative to $Id3^{BWT}$ controls (**Figure 3.2F**).

Figure 3.2.

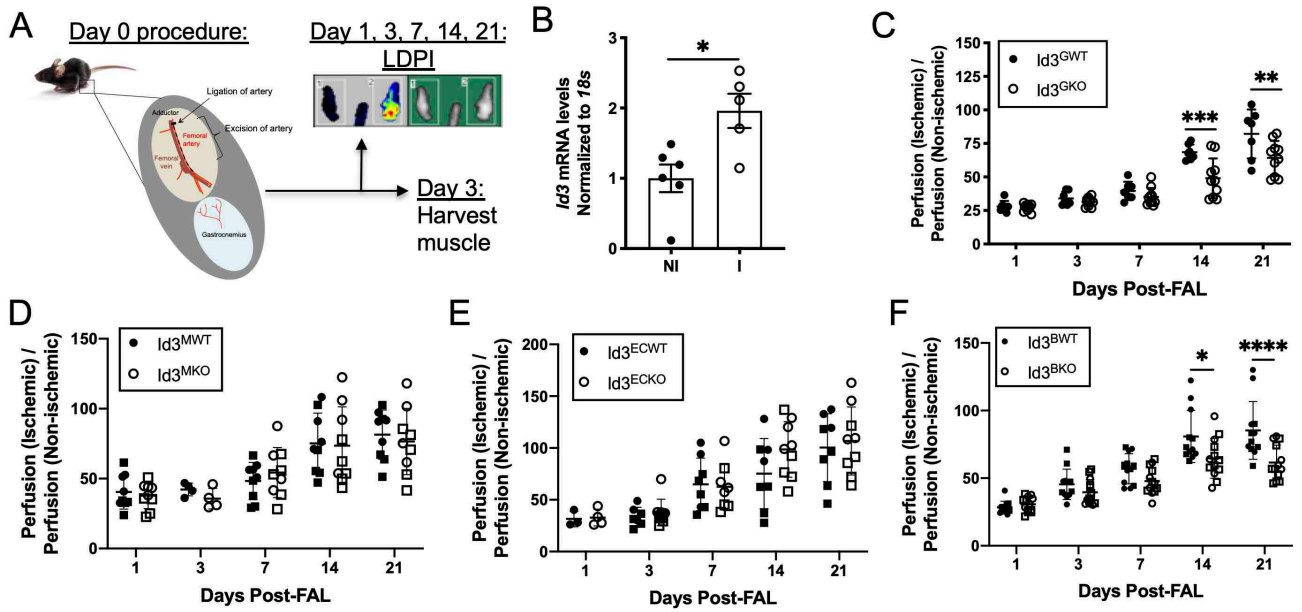

Figure 3.2. Id3 regulates blood flow in a B cell-specific manner.
(A) Schematic of the murine model of hind limb ischemia (HLI) and quantification of microvascular blood flow using laser Doppler perfusion imaging. **(B)** mRNA levels of *Id3* in ischemic (I) and non-ischemic (NI) gastrocnemius muscle lysates. **(C)** Results from laser Doppler perfusion imaging (LDPI) quantifying blood flow in the feet of $Id3^{GWT}$ and $Id3^{GKO}$ littermate males at days 1, 3, 7, 14, and 21 days post-femoral artery ligation. Blood flow is quantified as proportion of blood flow in ischemic foot over blood flow in the non-ischemic foot per mouse. **(D-F)** Blood flow results in $Id3^{MWT}$ and $Id3^{MKO}$ male littermates **(D)**, $Id3^{ECWT}$ and $Id3^{ECKO}$ male littermates **(E)**, and $Id3^{BWT}$ and $Id3^{BKO}$ male littermates **(F)**. Circles represent male mice, squares represent female mice, closed shapes represent WT littermates, and open shapes represent KO littermates. Data shown is the mean ± standard deviation. *$p < 0.05$, **$p < 0.01$, ***$p < 0.001$, ****$p < 0.0001$, as indicated. Statistical analyses were performed using Mann Whitney U test **(B)** and two-way ANOVA **(C-F)**.

$Id3^{BKO}$ mice demonstrate muscle-specific differences in artery density during HLI

To begin understanding how the vasculature changes in $Id3^{BKO}$ mice to account for differences in blood flow recovery, vascular density and artery size were quantified in gastrocnemius muscles at Day 28 of HLI. Vascular density in the gastrocnemius muscle was quantified by counting the number of $CD31^+$ structures per image (**Figure 3.3A**, arrowhead). Five images were captured per muscle section, one to three sections along different areas of the muscle were provided per mouse, and 6-8 mice were provided per experimental group. The number of $CD31^+$ structures per muscle section were quantified and averaged amongst all muscles in the same experimental group (i.e. NI $Id3^{BKO}$). Results demonstrate that vascular density was

greater in I muscles compared to NI muscles, but there were no differences between genotypes regardless of ischemia status (**Figure 3.3B**). The number of $CD31^+$ structures that co-localized with αSMA^+ staining were quantified to reflect the number of arteries in the gastrocnemius of each group (**Figure 3.3A**, arrow). Interestingly, the number of αSMA^+CD31^+ structures showed a statistically trending increase in I $Id3^{BKO}$ muscles compared to NI $Id3^{BKO}$ muscles. I $Id3^{BKO}$ muscles had more αSMA^+CD31^+ structures than NI $Id3^{BKO}$ muscles, but there was no difference between NI and I muscles in the $Id3^{BWT}$ groups (**Figure 3.3C**). However, when the number of αSMA^+CD31^+ structures was quantified as a proportion of total $CD31^+$ structures, there were no significant differences between experimental groups by genotype or ischemia status (**Figure 3.3D**). This suggests that the proportion of arteries to capillaries in each muscle group were generally the same, but increases in overall vascular density had a more profound effect on the number of arteries than capillaries in the tissue. Though $Id3^{BKO}$ mice have increased numbers of αSMA^+ arteries in gastrocnemius muscles, they have reduced blood flow recovery suggesting that these arteries may be smaller in size than arteries in $Id3^{BWT}$.

Thus, we then quantified the size of αSMA^+ arteries in gastrocnemius muscles to test whether the lumenal diameter of arteries were smaller in I $Id3^{BKO}$ muscles compared to I $Id3^{BWT}$ (**Figure 3.3E**). The maximal diameter ($diameter_{max}$) was measured in each artery as well as the diameter perpendicular to that of the $diameter_{max}$ to account for arteries that did not maintain a circular shape during tissue processing (**Figure 3.3E**). Diameters per artery were averaged and then averaged per image and muscle section to generate the overall average artery diameter per mouse. When compared amongst experimental groups, diameters were comparable regardless of ischemia status or genotype (**Figure 3.3F**). $Diameter_{max}$ measurements were also not different amongst all experimental groups (**Figure 3.3G**).

Figure 3.3.

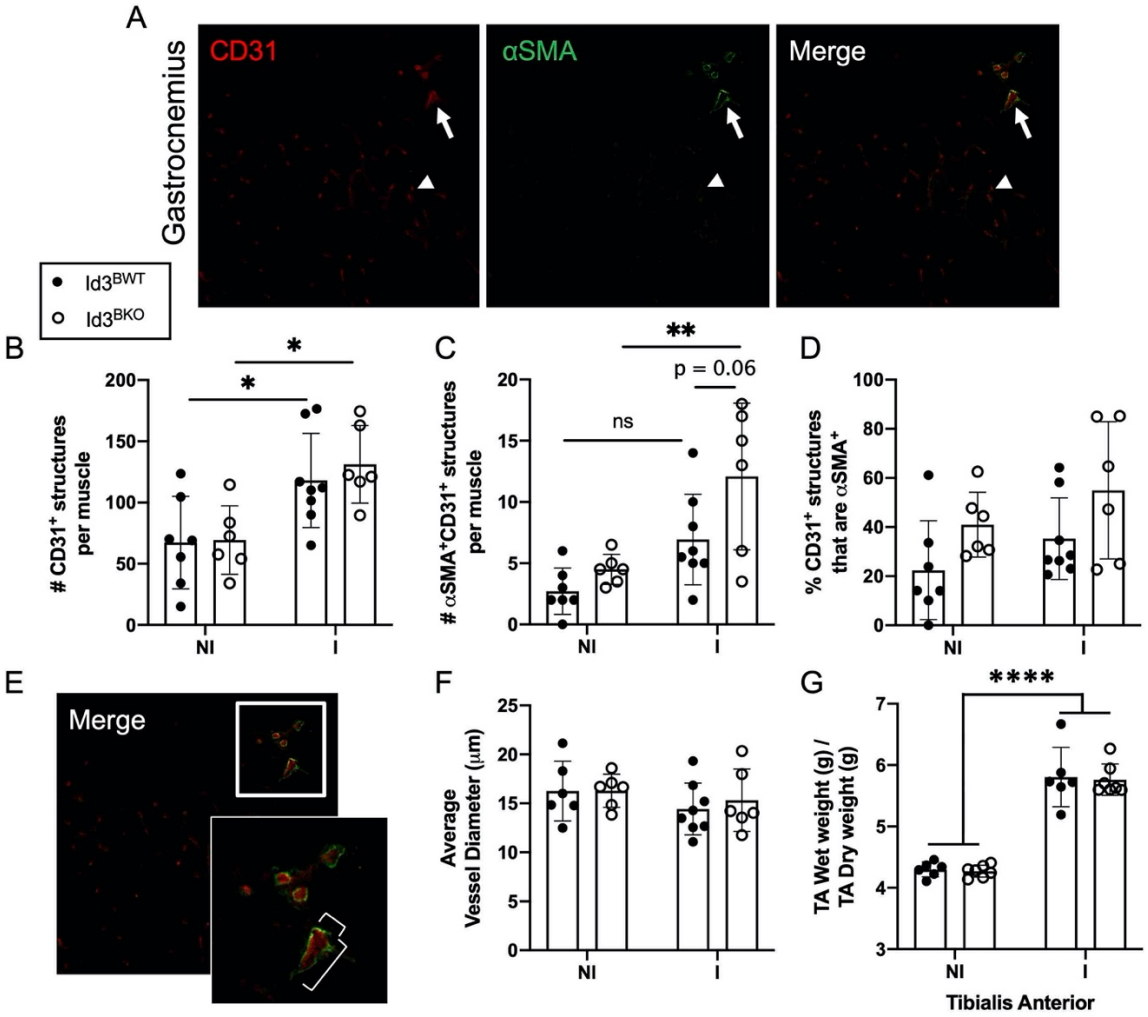

Figure 3.3. B cell-specific Id3 does not alter gastrocnemius vascular density or artery size during HLI.

(A-G) Gastrocnemius muscles from $Id3^{BWT}$ and $Id3^{BKO}$ mice were harvested at day 28 of HLI, then fixed, embedded, and sectioned. Sections were stained with antibodies against EC marker CD31 and contractile protein αSMA, which is typically expressed in perivascular cells such as pericytes and VSMCs. (A) A representative image of $CD31^+$ and $αSMA^+$ is provided. The white arrow points to a $αSMA^+CD31^+$ structure, while the arrowhead points to a $CD31^+$ structure. Scale bar delineates 50 μm. From each mouse, 1-3 sections at different locations along the muscle were stained. 5 images of each muscle were captured and quantified for $CD31^+$ and $αSMA^+$ structures. (A-C) The number of $CD31^+$ structures (B) and $αSMA^+CD31^+$ structures (C) per muscle section were quantified. (D) Additionally, the proportion of $CD31^+$ structures that were $αSMA^+$ was also quantified. (E-G) The maximal and perpendicular-to-the-maximal diameters of each $αSMA^+$ structure (E) were quantified and averaged to calculate average vessel diameter (F). Scale bar in (E) delineates 25 μm. (G) Maximal artery diameters were also calculated and plotted. Data shown is the mean ± standard deviation. *$p < 0.05$, **$p < 0.01$, ****$p < 0.0001$, as indicated. Statistical analyses were performed using two-way ANOVA. Vascular density and artery number and proportion **(A-D)** were quantified by Antony Haider.

Finally, blood flow recovery differences could be accounted for based on differences in vascular density or artery size in specific muscle groups. Thus, we applied the same quantification to tibialis anterior (TA) muscles from $Id3^{BWT}$ and $Id3^{BKO}$ mice as was used for gastrocnemius muscles (**Figure 3.4A**). Additionally, three sections 300 μm apart per muscle were stained to quantify vascular density and artery size across the muscle (**Figure 3.4B**). The average $CD31^{+}\alpha SMA^{-}$ capillary density per muscle was not different between genotypes (**Figure 3.4C**), nor was the area under the curve when capillary densities were plotted across each section (**Figure 3.4D-E**). However, when $\alpha SMA^{+}CD31^{+}$ artery density was averaged per muscle and plotted across sections, there was a trending reduction in the density of arteries both as an overall average per muscle and when densities were plotted across sections in the TA muscles of $Id3^{BKO}$ mice (**Figure 3.4F-H**). The size of these arteries were not different between genotypes (**Figure 3.4I-K**).

Additionally, increased vascular permeability suggests decreased vascular stability and thus lower perfusion. Early signs of edema and vascular permeability were assessed by quantifying the wet and dry weights of TA muscles after 7 days of HLI. While edema clearly increased with ischemia, there was no difference between genotypes (**Figure 3.4L**).

Figure 3.4

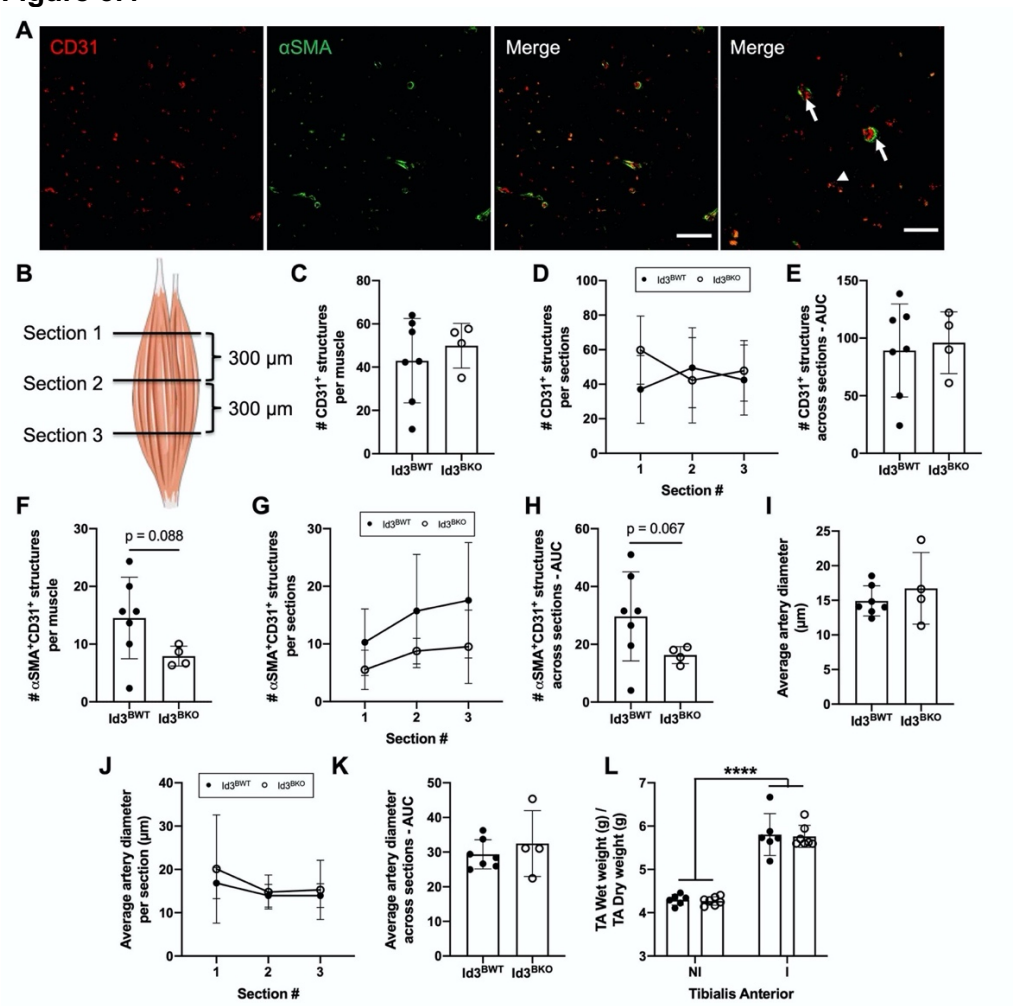

Figure 3.4. Id3^{BKO} mice have comparable capillary density, but lower artery density in ischemic tibialis anterior muscle.

(A-K) Ischemic tibialis anterior (TA) muscles from Id3^{BWT} and Id3^{BKO} mice were harvested at day 28 of HLI, then fixed, embedded, and sectioned. Sections were stained with antibodies against EC marker CD31 and contractile protein αSMA, which is typically expressed in perivascular cells such as pericytes and VSMCs. **(A)** A representative image of CD31$^+$ and αSMA$^+$ is provided. The white arrows point to αSMA$^+$CD31$^+$ structures, while the arrowhead points to a CD31$^+$ structure. Scale bar delineates 50 μm. **(B)** From each mouse, 3 sections 300 μm apart from one another along the TA muscle were stained. 5 images of each muscle were captured and quantified for CD31$^+$ and αSMA$^+$ structures. **(C)** The number of CD31$^+$αSMA$^-$ capillaries per muscle section were averaged across sections per mouse. **(D,E)** The number of CD31$^+$αSMA$^-$ capillaries were also plotted per section **(D)** and the area under the plotted curve quantified **(E)**. **(F-H)** The number of αSMA$^+$CD31$^+$ arteries per muscle section were averaged **(F)** and plotted across sections **(G)** and the area under the plotted curve also quantified **(H)**. **(I-K)** The average artery diameter per muscle section was also averaged **(I)**, plotted **(J)**, and AUC quantified **(K)**. **(L)** Finally, TA muscles from day 7 of HLI were harvested to measure wet and dry weights of the each muscle. The ratio of wet weight to dry weight were calculated and plotted. Data shown is the mean ± standard deviation. ****$p < 0.0001$, as indicated. Statistical analyses were performed using Mann Whitney tests **(C,E,F,H,I,K)** and two-way ANOVA **(L)**.

Id3^{BKO} mice have increased numbers of infiltrating B cells in ischemic skeletal muscle

To date, the presence of B cells in skeletal muscle during HLI has been investigated to a very limited extent[61]. Additionally, the extent to which other immune cell populations have been characterized in ischemic skeletal muscle compared to non-ischemic controls is also limited. Immune cell populations in ischemic and non-ischemic gastrocnemius muscles were characterized at HLI day 7 using flow cytometry to compare overall changes that occur to skeletal muscle immune populations in the presence of ischemia as well as in order to observe what changes occurred prior to the emergence of blood flow recovery differences between Id3^{BKO} and Id3^{BWT} mice (**Figure 3.5A, Figure 3.6**). We observed a significant increase in total CD45^{+} immune cells (**Figure 3.5B, Figure 3.7A**) as well as CD19^{+} B cells (**Figure 3.5C, Figure 3.7B**) in ischemic muscle compared to non-ischemic muscle. The overall increase in immune cells was in part due to increases in B cell numbers, however, there were also substantial increases in CD11b^{+}F4/80^{+} macrophages (**Figure 3.8E**), CD3^{+} T cells (**Figure 3.8F**), Ly6G^{+} neutrophils (**Figure 3.8J**) and other CD11b^{+} immune cells (**Figure 3.8K**). Furthermore, Id3^{BKO} mice had significantly higher numbers of total B cells in ischemic muscle compared to Id3^{BWT} mice (**Figure 3.5C**). These differences were due to increases in CD19^{+}B220^{low} B-1 cells (**Figure 3.5D**). B220^{high} B-2 cells (**Figure 3.5E**) were not different between genotypes, nor were CD5^{+} B-1a CD19^{+} cells (**Figure 3.5F**). However, the number of CD5^{-} B-1b cells (**Figure 3.5G**) were significantly higher in Id3^{BKO} mice compared to Id3^{BWT}. Total T cell, macrophage, neutrophil, and other immune cell numbers were not significantly changed in Id3^{BKO} mice (**Figure 3.8**). Additionally, B-1b cells numbers were significantly higher in the peritoneal cavity, spleen, and bone marrow of Id3^{BKO} mice compared to Id3^{BWT} mice (**Figure 3.9**).

Figure 3.5.

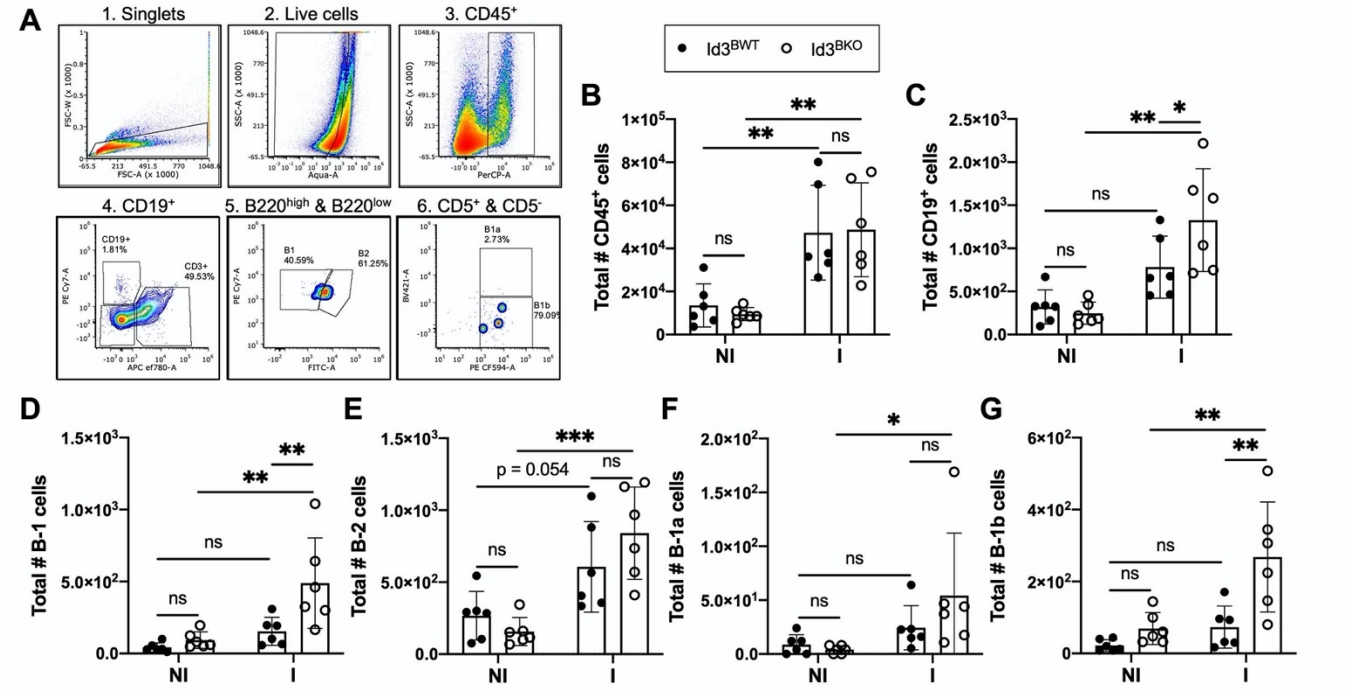

Figure 3.5. Loss of ID3 in B cells results in increased B-1b cell numbers in ischemic skeletal muscle.

(A) Flow cytometry gating strategy for identifying immune cell populations in digested gastrocnemius muscles. **(B)** Quantification of total $CD45^+$ cells per gastrocnemius muscle. **(C)** Quantification of total $CD19^+$ B cells per gastrocnemius muscle. **(D)** Quantification of total $CD19^+B220^{low}$ B1 cells per gastrocnemius muscle. **(E)** Quantification of total $CD5^-$ B-1b cells per gastrocnemius muscle. **(F)** Quantification of total $CD5^+$ B-1a cells per gastrocnemius muscle. **(G)** Quantification of total $CD19^+B220^{high}$ B-2 cells per gastrocnemius muscle. Data shown is the mean ± standard deviation. *$p < 0.05$, **$p < 0.01$, ***$p < 0.001$, as indicated. Statistical analyses were performed using two-way ANOVA.

Figure 3.6

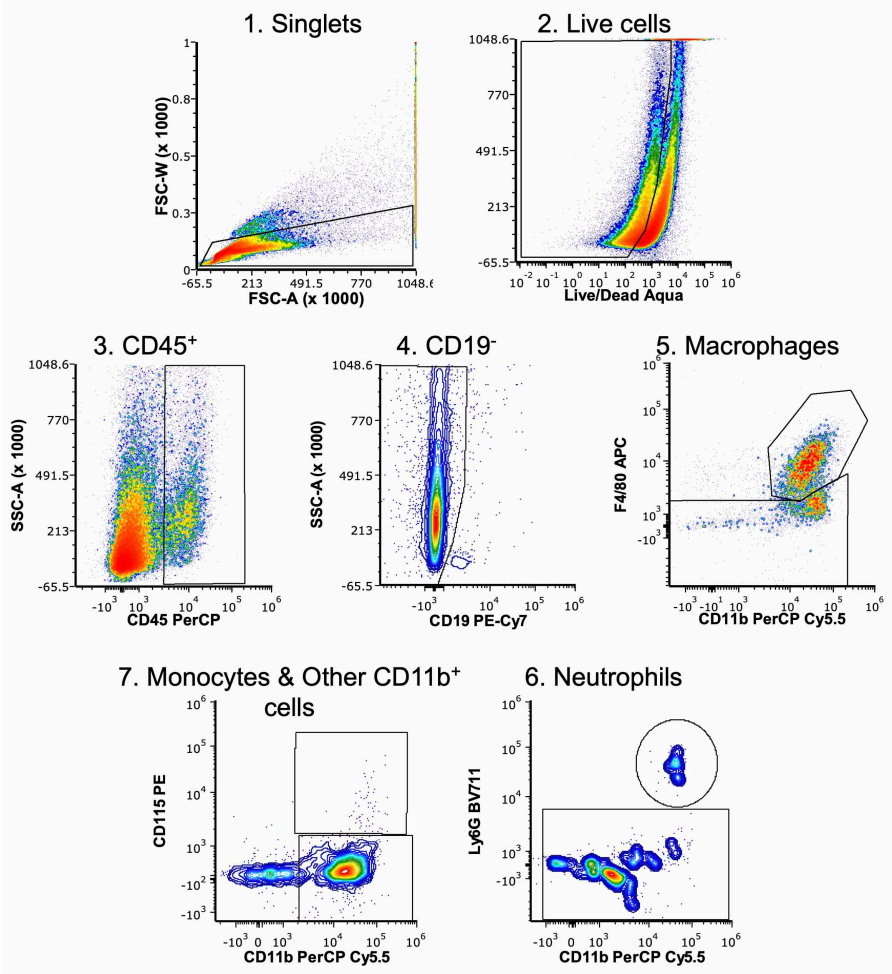

Figure 3.6. Gating strategy for non-B cells in ischemic gastrocnemius muscle.
To identify non-B cell immune subsets in gastrocnemius muscles at day 7 of HLI, singlets (1) that did not take up the Live/Dead stain (2) were analyzed. First, $CD45^+$ cells were gated (3), followed by $CD19^-$ cells (4). $CD11b^+F4/80^+$ macrophages were next identified (5) and the $F4/80^-$ remaining population was also gated. From that gate, $Ly6G^+$ neutrophils and $Ly6G^-$ cells were gated (6). And from the $Ly6G^-$ population, $CD115^+$ monocytes and other $CD11b^+$ cells were identified (7).

Figure 3.7.

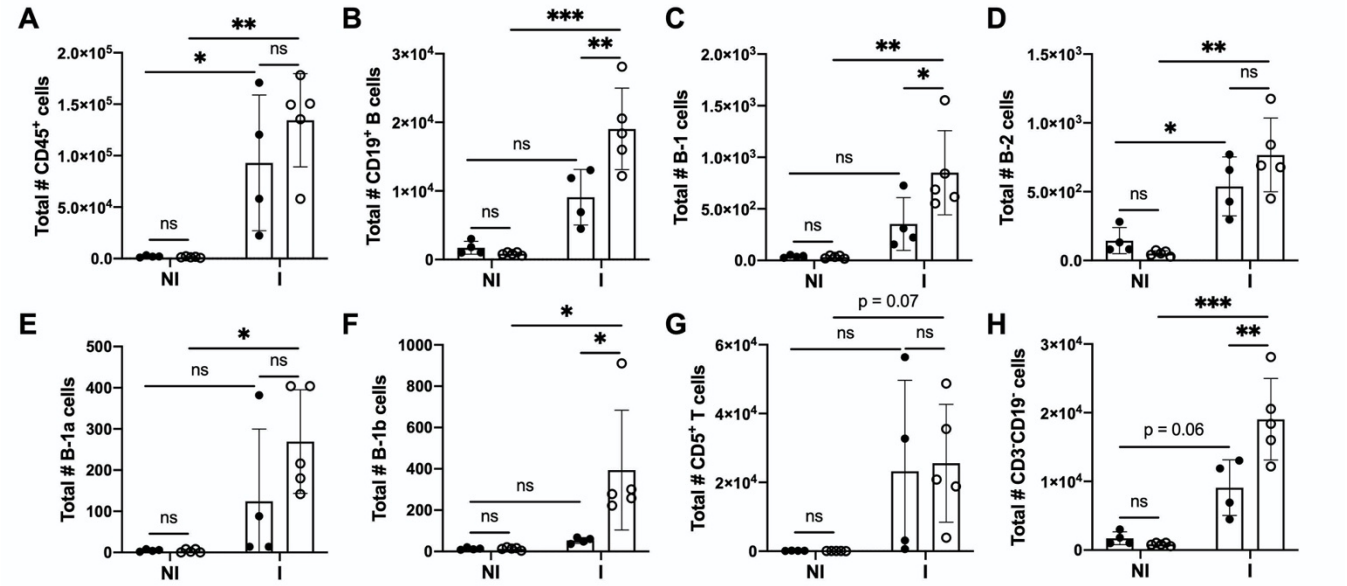

Figure 3.7. Id3^{BKO} female mice also demonstrated significant increases specifically in B-1b cell numbers in ischemic skeletal muscle.

(A-H) Gastrocnemius from non-ischemic (NI) and ischemic (I) legs were isolated from Id3^{BKO} and Id3^{BWT} mice at day 7 of HLI. **(A-H)** Flow cytometry was used to characterize cell populations of single-cell suspensions from NI and I gastrocnemius muscles. Total CD45^{+} cells **(A)**, total CD19^{+} B cells **(B)**, CD19^{+}B220^{low} B-1 cells **(C)**, CD19^{+}B220^{high} B-2 cells **(D)**, CD5^{+} B-1a cells **(E)**, CD5^{-} B-1b cells **(F)**, CD5^{+} T cells **(G)**, and CD19^{-}CD3^{-} cells **(H)** per muscle were quantified. Data shown is the mean ± standard deviation. *p < 0.05, **p < 0.01, as indicated. Statistical analyses were performed using two-way ANOVA.

Figure 3.8.

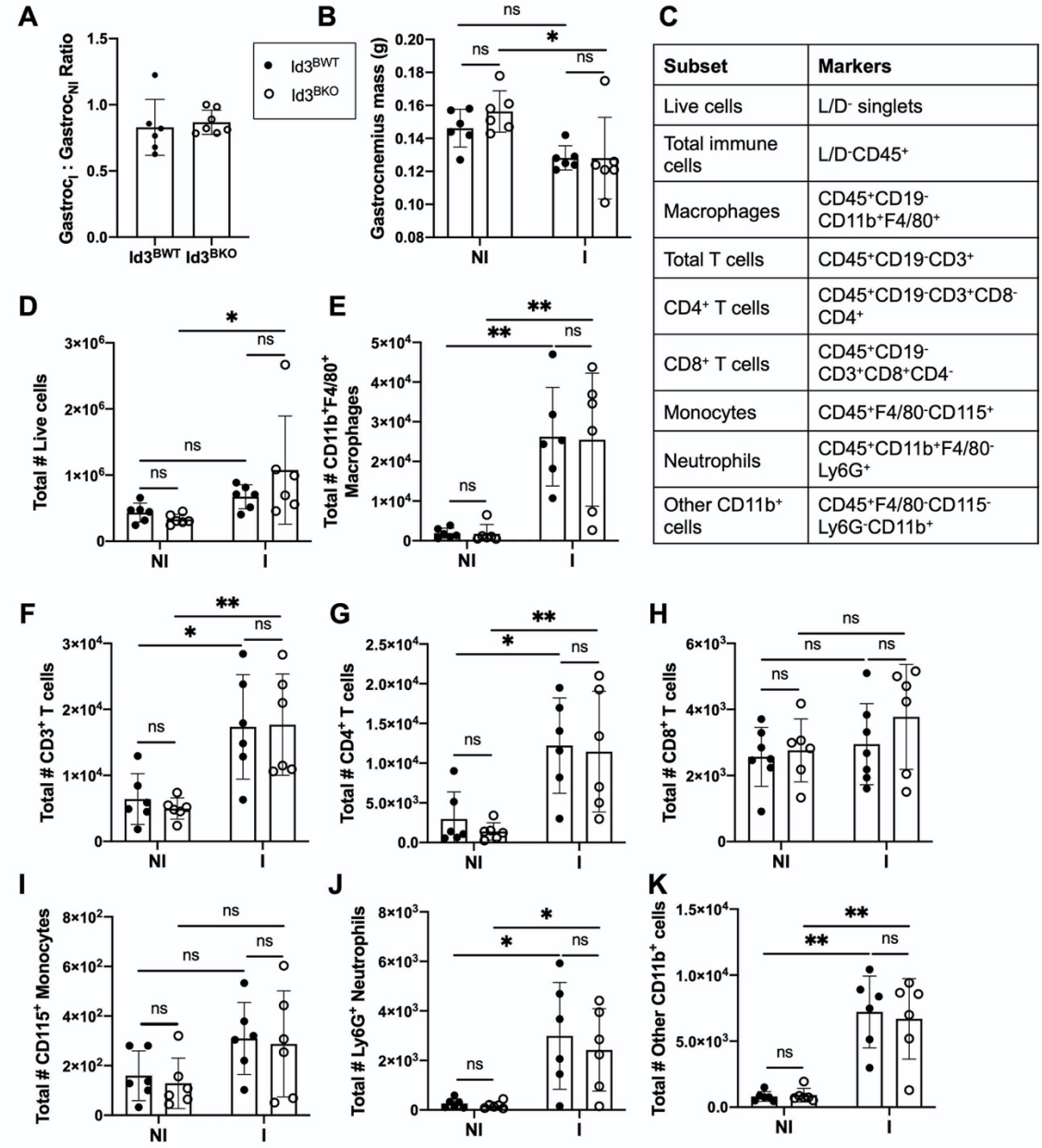

Subset	Markers
Live cells	L/D$^-$ singlets
Total immune cells	L/D$^-$CD45$^+$
Macrophages	CD45$^+$CD19$^-$ CD11b$^+$F4/80$^+$
Total T cells	CD45$^+$CD19$^-$CD3$^+$
CD4$^+$ T cells	CD45$^+$CD19$^-$CD3$^+$CD8$^-$ CD4$^+$
CD8$^+$ T cells	CD45$^+$CD19$^-$ CD3$^+$CD8$^+$CD4$^-$
Monocytes	CD45$^+$F4/80$^-$CD115$^+$
Neutrophils	CD45$^+$CD11b$^+$F4/80$^-$ Ly6G$^+$
Other CD11b$^+$ cells	CD45$^+$F4/80$^-$CD115$^-$ Ly6G$^-$CD11b$^+$

Figure 3.8. Id3^{BKO} mice did not have significant changes in non-B cell subsets in the ischemic skeletal muscle.

(A,B) Gastrocnemius from non-ischemic (NI) and ischemic (I) legs were weighed in Id3^{BKO} and Id3^{BWT} mice at day 7 of HLI. **(A)** The ratio of I gastrocnemius mass (GastrocI) to NI gastrocnemius mass (Gastroc$_{NI}$) demonstrate that GastrocI were generally smaller than GastrocNI. **(B)** All four experimental groups were also plotted to demonstrate similarities and differences in muscle masses. **(C-K)** Flow cytometry was used to characterize cell populations of single-cell suspensions from NI and I gastrocnemius muscles **(C)**. Total live cells **(D)**, CD11b$^+$F4/80$^+$ macrophages **(E)**, CD3$^+$ T cells **(F)**, CD4$^+$ T cells **(G)**, CD8$^+$ T cells **(H)**, CD115$^+$ monocytes **(I)**, and Ly6G$^+$ neutrophils **(J)**, and other CD11b$^+$ cells **(K)** per muscle were quantified. Data shown is the mean ± standard deviation. *$p < 0.05$, **$p < 0.01$, as indicated. Statistical analyses were performed using two-way ANOVA.

Figure 3.9

A

Tissue	Count* / p-value+	# Total immune cells	# Total B cells	# B-1 cells	# B-1a cells	# B-1b cells	# B-2 cells
Blood	$Id3^{BWT}$ count	5.236^4 (7.180^3)	2.129^4 (3.267^3)	2.275^3 (1.755^3)	1.894^4 (2.648^3)	6.536^2 (7.457^2)	9.886^2 (1.150^3)
	$Id3^{BKO}$ count	8.086^4 (2.706^4)	3.674^4 (1.280^4)	3.707^3 (1.967^3)	3.194^4 (1.038^4)	6.278^2 (4.349^2)	2.294^3 (1.504^3)
	p-value	0.0317	*0.0079*	0.0952	0.4206	0.0952	*0.0159*
Bone marrow	$Id3^{BWT}$ count	4.842^6 (5.210^5)	3.917^5 (1.098^5)	1.025^4 (3.474^3)	7.190^3 (2.542^3)	3.080^3 (9.712^2)	3.213^5 (7.806^4)
	$Id3^{BKO}$ count	4.551^6 (2.274^6)	4.568^5 (1.702^5)	1.419^4 (5.434^3)	7.250^3 (2.419^3)	6.970^3 (3.082^3)	3.791^5 (1.474^5)
	p-value	0.6905	0.3095	0.1508	0.8413	*0.0317*	0.3095
Peritoneal Cavity	$Id3^{BWT}$ count	1.585^6 (2.649^5)	6.960^5 (2.378^5)	2.887^5 (8.347^4)	1.764^5 (3.956^4)	1.010^5 (4.884^4)	4.205^5 (1.799^5)
	$Id3^{BKO}$ count	1.809^6 (2.139^5)	1.044^6 (2.145^5)	4.470^5 (8.493^4)	1.430^5 (4.382^4)	2.902^5 (4.336^4)	6.163^5 (1.419^5)
	p-value	0.4206	0.6905	0.3095	>0.9999	*0.0079*	0.0952
Spleen	$Id3^{BWT}$ count	1.483^7 (1.094^6)	8.179^6 (1.158^6)	1.213^5 (2.157^4)	3.110^4 (9.085^3)	2.648^4 (4.041^3)	7.831^6 (1.092^6)
	$Id3^{BKO}$ count	1.571^7 (1.678^6)	7.437^6 (6.171^5)	1.591^5 (1.731^4)	3.044^4 (3.634^3)	5.366^4 (8.896^3)	6.288^6 (5.740^5)
	p-value	0.3095	0.4206	0.0317	>0.9999	*0.0079*	*0.0159*

B **Blood & Peritoneal Cavity**

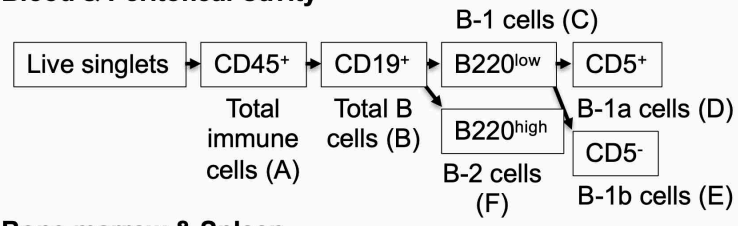

C **Bone marrow & Spleen**

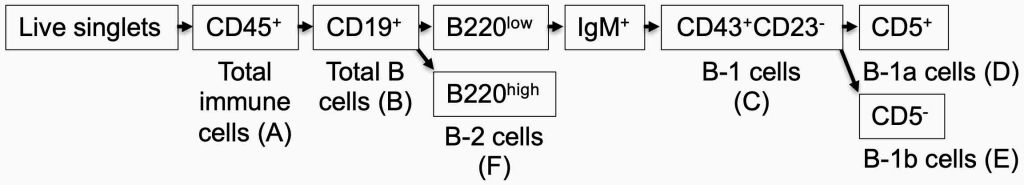

Figure 3.9. $Id3^{BKO}$ mice have increased B-1b cell numbers in the blood, bone marrow, peritoneal cavity, and spleen at day 7 of HLI.

(A-C) Blood, bone marrow, peritoneal cavity, and spleen cells were harvested and processed to a single-cell suspension. Cells were stained with antibodies to identify B cell subsets by flow cytometry. **(A)** Total $CD45^+$ immune cells, $CD19^+$ B cells, $B220^{low}$ B-1 cells, $CD5^+$ B-1a cells, $CD5^-$ B-1b cells, and $B220^{high}$ B-2 cells were quantified in each tissue of both $Id3^{BWT}$ and $Id3^{BKO}$ mice. 5 mice were quantified per genotype. **(B,C)** Gating strategy for B cell subsets in the blood and peritoneal cavity **(B)** and bone marrow and spleen **(C)**. *The cell count is number of cells per 50 µL of blood for blood cells, per tibia and fibula in one hind limb for the bone marrow, per whole lavage for the peritoneal cavity, and per whole tissue for the spleen. Counts are expressed as the mean with the standard deviation in parentheses. $^+$Statistical significance is defined as a *p*-value less than 0.05. Statistical analyses were performed using Mann Whitney tests.

Id3^{BKO} mice have higher levels of total and DAMP-specific IgM during HLI

B-1 cells are a major source of IgM[26] and prior studies suggest that expansion of the B-1b cell population *in vivo* will result in increased IgM levels[30, 129]. We found that Id3^{BKO} mice had significantly higher levels of total IgM in circulation with a particularly significant spike in IgM levels at day 7 of HLI (**Figure 3.10A**). IgM levels were also increased locally in skeletal muscle after 7 days of HLI and this appears to persist until day 28 of HLI (**Figure 3.10B**). IgM can be identified in ischemic skeletal muscle by immunofluorescence as well (**Figure 3.10C**). Additionally, total IgG, IgG1, IgG2a, IgG2b, IgG2c, and IgG3 levels were not different between genotypes after 7 days of HLI (**Figure 3.11**).

Figure 3.10.

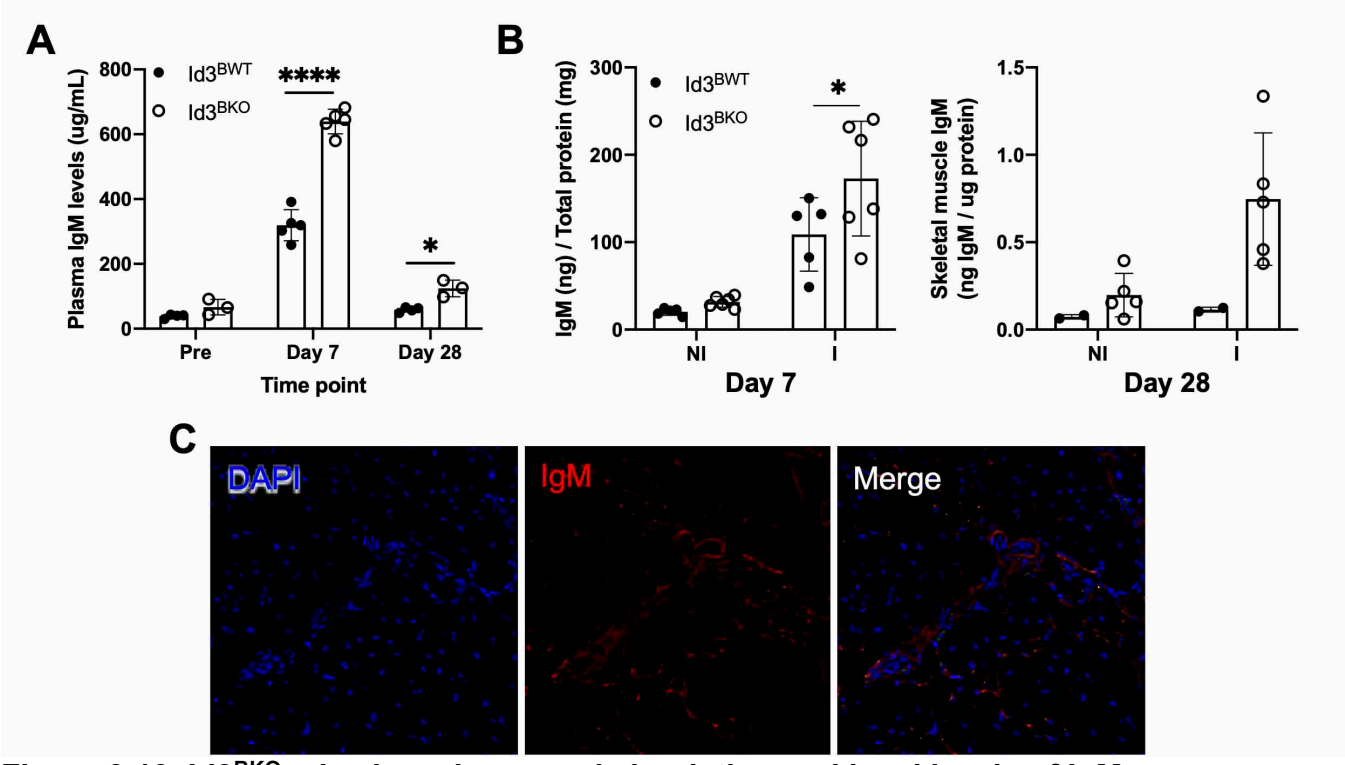

Figure 3.10. Id3^{BKO} mice have increased circulating and local levels of IgM.
A) Total IgM in plasma from Id3^{BWT} and Id3^{BKO} mice was measured by ELISA at pre-HLI, Day 7, and Day 28 of HLI. **(B)** Total IgM levels in non-ischemic (NI) and ischemic (I) skeletal muscle at days 7 and 28 of HLI. **(C)** IgM and DAPI staining in ischemic gastrocnemius muscle from day 21 of HLI. Data shown is the mean ± standard deviation. *$p < 0.05$, ****$p < 0.0001$, as indicated. Statistical analyses were performed using Two-way ANOVA.

Figure 3.11.

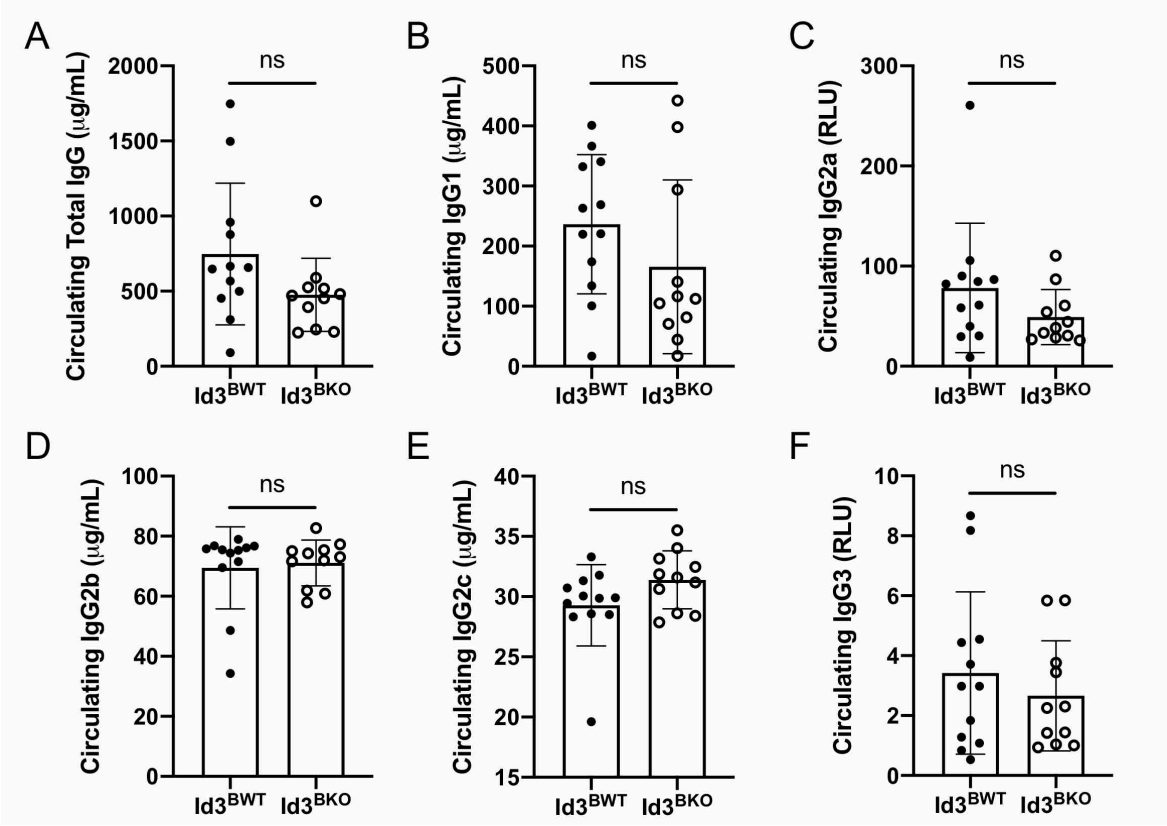

Figure 3.11. Levels of IgG isoforms in Id3^{BWT} and Id3^{BKO} mice.
(A-F) Plasma was collected from Id3^{BWT} and Id3^{BKO} mice at day 7 of HLI. (A-F) ELISA was used to measure circulating levels of total IgG **(A)**, IgG1 **(B)**, IgG2a **(C)**, IgG2b **(D)**, IgG2c **(E)**, and IgG3 **(F)**. Data shown is the mean ± standard deviation. Statistical analyses were performed using Mann Whitney U tests.

I was also interested in investigating whether IgM's specific to danger-associated molecular patterns (DAMPs) such as High mobility group box-1 (HMGB1) and oxidized phospholipid 1-palmitoyl-2-arachidonoyl-sn-glycero-3-phosphocholine (oxPAPC) (**Figure 3.12A**). Both of these molecules have been shown to have pro-angiogenic effects in ECs[46, 142-149]. IgM specific to HMGB1 and oxPAPC were significantly higher in the plasma of $Id3^{BKO}$ mice at day 7 of HLI (**Figure 3.12B,C**).

Figure 3.12

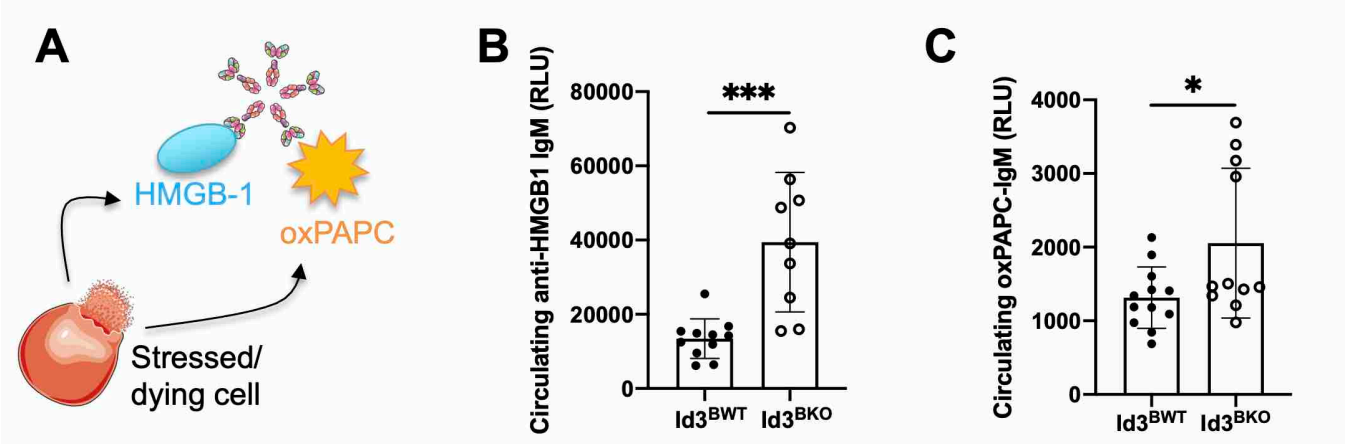

Figure 3.12. Circulating levels of DAMP-specific IgM levels are higher in $Id3^{BKO}$ mice. **(A)** IgM can bind to specific epitopes on danger-associated molecular patterns (DAMPs) known to be released in the setting of ischemia. **(B,C)** Plasma was collected from $Id3^{BWT}$ and $Id3^{BKO}$ mice at day 7 of HLI. ELISA was used to measure circulating levels of IgM specific to high-mobility group box-1 (HMGB1) **(B)** and oxidized 1-palmitoyl-2-arachidonoyl-sn-glycero-3-phosphocholine (oxPAPC) **(C).** Data shown is the mean ± standard deviation. *$p < 0.05$, ***$p < 0.001$, as indicated. Statistical analyses were performed using Mann Whitney U tests.

B cell and IgM deficiencies had limited effects HLI perfusion

Data thus far suggests a role for B cells and IgM in attenuating perfusion during HLI. To test whether reduction of B cells or IgM will increase blood flow during HLI, the capacity for B cell-deficient ($\mu MT^{-/-}$), B- and T cell-deficient ($Rag1^{-/-}$), and secreted IgM-deficient ($sIgM^{-/-}$) mice to recover blood flow during HLI was compared to WT controls. $\mu MT^{-/-}$ and $Rag1^{-/-}$ demonstrated reduced blood flow at day 7 of HLI, however, there were no differences between genotypes at later HLI time points (**Figure 3.13A**). Interestingly, $sIgM^{+/+}$ and $sIgM^{-/-}$ had comparable blood flow at all time points during HLI (**Figure 3.13B**).

Figure 3.13.

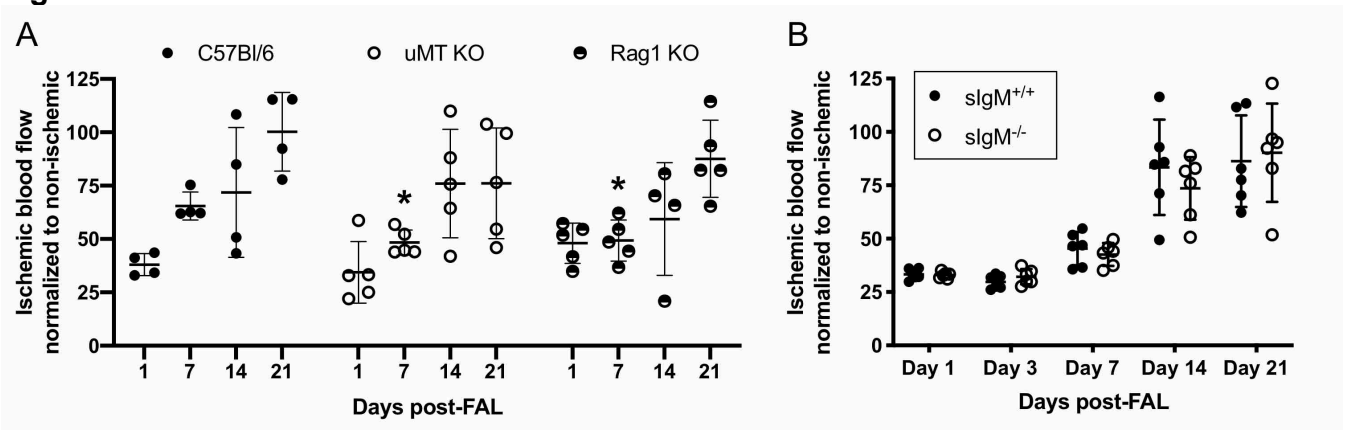

Figure 3.13. Blood flow during HLI in μMT, $Rag1^{-/-}$, and $sIgM^{-/-}$ mice.
(A) B cell-deficient ($\mu MT^{-/-}$), B- and T cell-deficient ($Rag1^{-/-}$), and B- and T cell sufficient control (C57Bl/6) mice were subjected to femoral artery ligation and resection to induce HLI. **(B)** Secreted IgM-deficient mice ($sIgM^{-/-}$) and wild type littermates ($sIgM^{+/+}$) were also subjected to femoral artery ligation and resection to induce HLI. **(A,B)** Blood flow was measured by LDPI at days 1, 7, 14, and 21 of HLI to determine if perfusion recovery was different between strains. Data shown is the mean ± standard deviation. *$p < 0.05$ compared to Day 7 C57Bl/6 values. Statistical analyses were performed using Two-way ANOVA.

IgM inhibits EC proliferation *in vitro*

To begin to investigate whether IgM has direct effects on the vasculature, ECs were cultured with conditioned media (CM) from sIgM$^{+/+}$ or sIgM$^{-/-}$ B-1b cells. Both EC proliferation and tubule formation were quantified (**Figure 3.14A**). ECs cultured with CM from sIgM$^{+/+}$ B-1b cells had reduced EC proliferation compared to vehicle and sIgM$^{-/-}$ CM-treated cells (**Figure 3.14B**). However, when tubule formation was quantified by the number of branch points and closed boxes formed in culture, there were no differences between treatment groups (**Figure 3.14C,D**).

Figure 3.14.

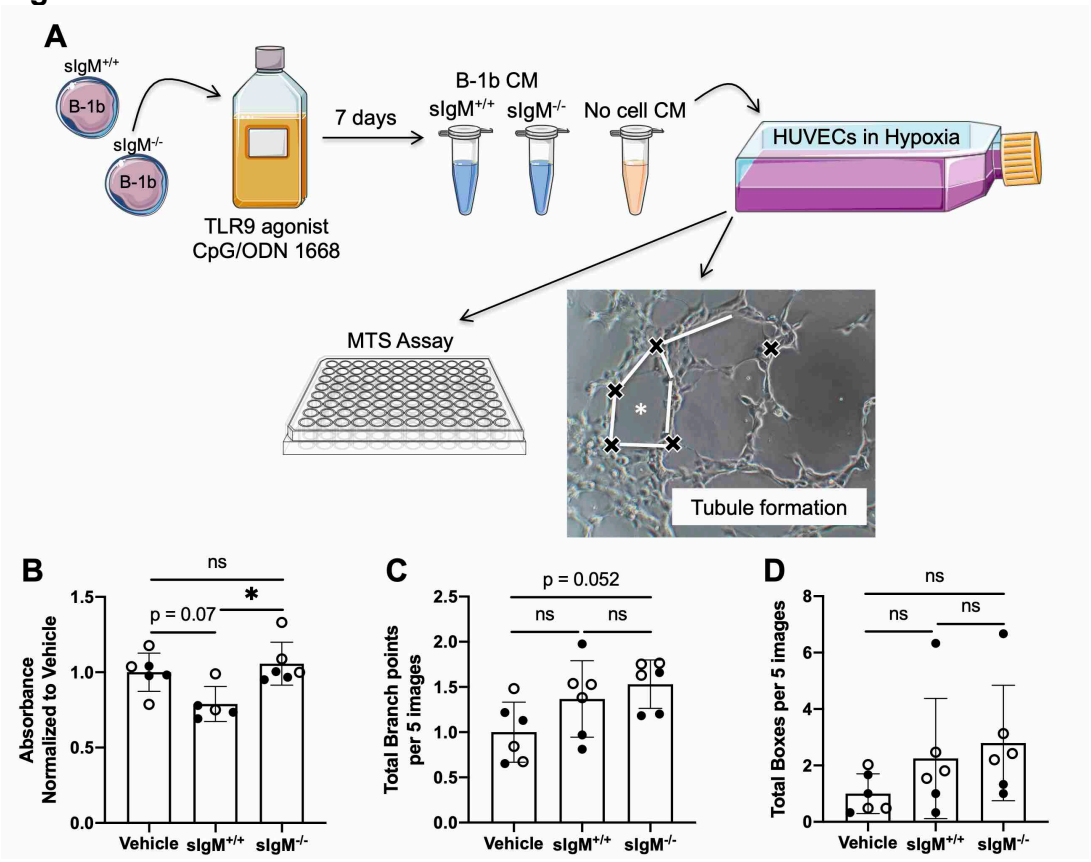

Figure 3.14. IgM inhibits EC proliferation, but not tubule formation *in vitro*.
(A) B-1b cells from sIgM$^{+/+}$ and sIgM$^{-/-}$ mice were sorted by flow and stimulated in vitro by a TLR9 agonist CpG/ODN 1668 for 7 days to induce IgM production. The conditioned media from each stimulation was then used to treat HUVECs in the setting of hypoxia. To account for affects induced by TLR9 agonist remaining in the conditioned media, this agonist was included in the vehicle control. **(B)** Proliferation was measured using an MTS assay. **(C,D)** And from a tubule formation assay, the number of branch points (black X's in A) **(C)** and closed boxes (white asterisk in A delineates the middle of a box) **(D)** formed by HUVECs were quantified. * $p < 0.05$, as specified. Statistical analyses were performed using one-way ANOVA.

IV. Discussion:

Conclusions and Discussion

These findings are the first to report that Id3 expression in B cells regulates blood flow recovery during HLI. To date, no other studies have specifically investigated whether B cells contribute to HLI perfusion recovery. In addition to pursuing deeper mechanisms by which B cell-specific Id3 promotes perfusion recovery, the potential impact that B cells have on skeletal muscle perfusion and symptoms in PAD patients remains unexplored.

These findings contribute to a broad and small body of work concerning the role of B cells in neovascularization. While studies have demonstrated roles for B cells and B cell-produced antibodies in regulating angiogenesis in the setting of cancer, eye injury, and wound healing, little is known about how B cells regulate neovascularization during HLI. Klotzsche-von Ameln *et al.* demonstrated that Del-1$^{-/-}$ mice have increased B and T cell recruitment to skeletal muscle and reduced blood flow recovery; however, the study did not demonstrate that B cell-intrinsic mechanisms were mediating neovascularization[61]. Two additional studies demonstrated that exogenous delivery of an anti-VEGFA antibody can inhibit capillary density and blood flow recovery during HLI via interactions with FcɣR on myeloid cells[100, 103]. It remains unclear, however, how much this signaling axis affects angiogenesis at homeostatic levels. B cells and IgM have also been implicated in promoting tissue injury during ischemia/reperfusion via complement deposition[107-112, 114, 150]. This injury model, however, is much more acute and lacks a chronic time point in which to observe and quantify a neovascular component. Furthermore, inflammation has generally been implicated in PAD and murine studies demonstrate roles for macrophages and T cells, but B cells are rarely considered. Results from this study are the first to implicate B cells in blood flow recovery during HLI.

<u>Identifying vascular changes mediating blood flow recovery</u>

Interestingly, we observed reduced blood flow in Id3^{BKO} mice at later time points, but there were no significant differences in total vascular density, αSMA^{+} artery density, or artery diameter in the gastrocnemius at day 28 of HLI. Fluid build-up in the TA muscle was also not different at day 7 of HLI. The question then remains, what is changing in the vasculature of these mice to manifest differences in blood flow? One potential mechanism could be adaptive

arteriogenesis in hind limb muscles other than the gastrocnemius. I hypothesize that arteriogenesis contributes to blood flow recovery more than angiogenesis because Arpino *et al*. demonstrated that new capillaries generated in response to ischemia in skeletal muscle are less functional than pre-ischemic vessels. With reduced perivascular cell investment and arterio-venule malformations, the neovessels demonstrated reduced red blood cell velocity in response to hypoxia persistently for months after induction of HLI[151]. These findings suggest that growth of new blood vessels during skeletal muscle ischemia may in fact contribute to persistent ischemia, rather than attenuate it. Instead, increased arteriogenesis in pre-existing arteries may be contributing to blood flow to a greater extent.

Furthermore, artery size was not different between $Id3^{BWT}$ and $Id3^{BKO}$ gastrocnemius muscles. Thus, it is possible that the gastrocnemius muscle is not the ideal muscle to quantify arteriogenesis differences in this HLI model. Indeed, J. Geoffrey Pickering's group presented an abstract at ATVB/PVD Vascular Discovery 2019 demonstrating that gastrocnemius muscles often do not fully infarct during HLI. In contrast, the TA muscle fully infarcts in the model of HLI used in these studies[152]. Thus, if the ischemia and neovascularization in the TA is more responsible for the reduced and then recovered blood flow observed in $Id3^{BKO}$ mice, then it would be most appropriate to quantify vascular changes such as artery diameter in the TA muscle.

In addition or alternative to reduced arteriogenesis, $Id3^{BKO}$ mice may also have attenuated vasodilatory functions during ischemia compared to $Id3^{BWT}$ mice. This would explain why vascular density and artery sizes were not different between genotypes, but blood flow recovery was. In order to test whether $Id3^{BKO}$ mice have reduced vasodilation responses in $Id3^{BKO}$ mice, the capacity for arteries to dilate in response to various stimuli *in vivo* and *ex vivo* must be tested. The specific arteries to test are higher order resistance arteries, which have an established role in regulating blood pressure, and thus the extend of blood flow to the periphery. Cardinal TR, *et al*. quantified *in vivo* vasodilation of the profunda femoris artery 14 days post-femoral artery ligation in the hind limb by using electrical stimulation of the gracilis muscle and additionally through bathing the artery in vasodilatory stimuli such as acetylcholine (Ach) and sodium nitroprusside (SNP)[153]. The profunda femoris was also removed, cannulated and pressurized to 80 mmHg, and treated with vasodilatory stimuli (Ach and SNP). Results demonstrated that vasodilation is attenuated in arteries exposed to chronic ischemia compared

to non-ischemic controls. I propose to conduct similar experiments with $Id3^{BWT}$ and $Id3^{BKO}$ mice after 21 days of HLI and hypothesize that $Id3^{BKO}$ ischemic arteries will demonstrate greater attenuation of vasodilation in response to stimuli compared to $Id3^{BWT}$ ischemic arteries.

Should our results demonstrate that $Id3^{BKO}$ arteries have attenuated vasodilatory responses, it is of interest to identify a signaling axis by which this is regulated. Endothelial production of nitric oxide (NO) induces vasodilation through diffusion of NO to SMCs, where cGMP-dependent protein kinase activity is induced to upregulate SMC relaxation[154]. Additionally, activation of TRPV4 channels in ECs causes an influx of calcium, which causes hyperpolarization of EC and SMC membranes co-localized at myoendothelial junctions. This results in SMC relaxation (reduced contractions) and vasodilation[155]. While these signaling axes promote a similar vasodilatory outcome at homeostasis, excess NOS activity can also inhibit vasodilation in diseased settings. A recent study from the Sonkusare Lab at UVA demonstrates that vasodilation is attenuated in the setting of obesity and inflammation due excess production of NO by NOS, leading to the production of peroxynitrate (PN). PN inhibits the vasodilatory effects of TRPV4 by inhibiting TRPV4 activation by AKAP150 (Ottolini M, in press). Whether a similar mechanism also occurs in ischemia is unknown.

To investigate the mechanism(s) whereby B cell-specific Id3 inhibits blood flow recovery via reduced vasodilation, I will measure expression of NO synthases (NOS's) such as endothelial-specific NOS (eNOS) and inducible NOS (iNOS) in ischemic arteries in the muscle. I hypothesize that $Id3^{BKO}$ arteries will have reduced NOS expression. However, should NOS expression be greater in $Id3^{BKO}$ arteries and vasodilation attenuated, we can investigate whether TRPV4 activation and signaling is attenuated. To do this, we will measure the levels of TRPV4 activity by quantifying calcium sparklet formation. Increased sparklet formation indicates increased TRPV4 activity and this correlated with increased vasodilation. I hypothesize that $Id3^{BKO}$ arteries will have reduced calcium sparklet and TRPV4 activity.

<u>Determine whether increased IgM levels inhibit blood flow recovery</u>

Loss of Id3 in B cells attenuated blood flow at later time points during HLI and this correlated with early increases in B-1b cell numbers in ischemic muscle and increases in local and circulating levels of IgM. In addition to total IgM, DAMP-specific IgM levels were also increased. These DAMPs, HMGB1 and oxPAPC, are pro-angiogenic and upregulated in the

setting of ischemia[46, 142-149]. More specifically, HMGB1 exogenously delivered during HLI was shown to promote blood flow recovery[156]. I hypothesize that increased levels of IgM specific to these molecules may result in increased IgM-DAMP binding, which could inhibit DAMP-induced mechanisms that promote blood flow recovery. DAMPs bind to pattern recognition receptors (PRRs), which are expressed on a multitude of different immune and vascular cells. The interactions between DAMPs and PRRs depends both on the ligand and receptor. HMGB1 can bind to TLR4 and RAGE to induce downstream signaling. TLR signaling has been shown to induce iNOS expression and NO levels, which may then induce vasodilation. Overall, this hypothesis introduces a potential novel role for IgM in ischemic neovascularization and one that opposes the disease-protective roles IgM is often associated with. For example, in the setting of atherosclerosis, IgM is atheroprotective by inhibiting oxLDL uptake by macrophages[22, 23, 30].

While results demonstrated that B cell and IgM-deficient mice do not augment blood flow recovery at late time points as initial results in $Id3^{BKO}$ mice might suggest, I do not believe this nullifies my aforementioned hypothesis regarding the potential role that excess IgM might play in inhibiting blood flow recovery. As I am hypothesizing that IgM inhibits blood flow, absence of IgM may promote greater blood flow or comparable blood flow to that of wild type controls. A multitude of studies have demonstrated that IgM is deposited in skeletal muscle during ischemia and this prompts deposition of complement[107, 108, 110, 112, 157, 158]. Complement plays a role in recruiting immune cells and promoting expression of pro-inflammatory cytokines[159]. Complement has also been shown to influence neovascular processes such as angiogenesis[160, 161]. One potential mechanism whereby excess IgM could inhibit blood flow recovery is via excess complement deposition and expression of pro-inflammatory cytokines. While some pro-inflammatory signaling can promote neovascularization, excess signals may instead induce cell death and dysfunction. This may interfere with normal blood flow recovery. Before determining the specific mechanism, however, experiments must be conducted to determine if excess IgM inhibits blood flow recovery.

To determine whether increased IgM levels inhibit blood flow recovery *in vivo*, $sIgM^{+/+}$ B-1b or $sIgM^{-/-}$ B-1b cells will be sorted (**Figure 2.3**) and transferred into $Rag1^{-/-}$ mice intravenously (**Figure 3.15A**). 250,000 to 300,000 cells will be transferred into each mouse and three weeks later, mice will be subjected to femoral artery ligation and resection to induce

HLI. Pilot data demonstrates that IgM levels are comparable to wild type (WT) mice at three weeks post-transfer (**Figure 3.15B**). Blood flow will then be measured at days 1, 7, 14, 21, and 28 of HLI (**Figure 3.15A**). I hypothesize that Rag1$^{-/-}$ that receive sIgM$^{+/+}$ B-1b cells will have reduced blood flow relative to sIgM$^{-/-}$ B-1b recipients due to the presence of IgM.

Figure 3.15.

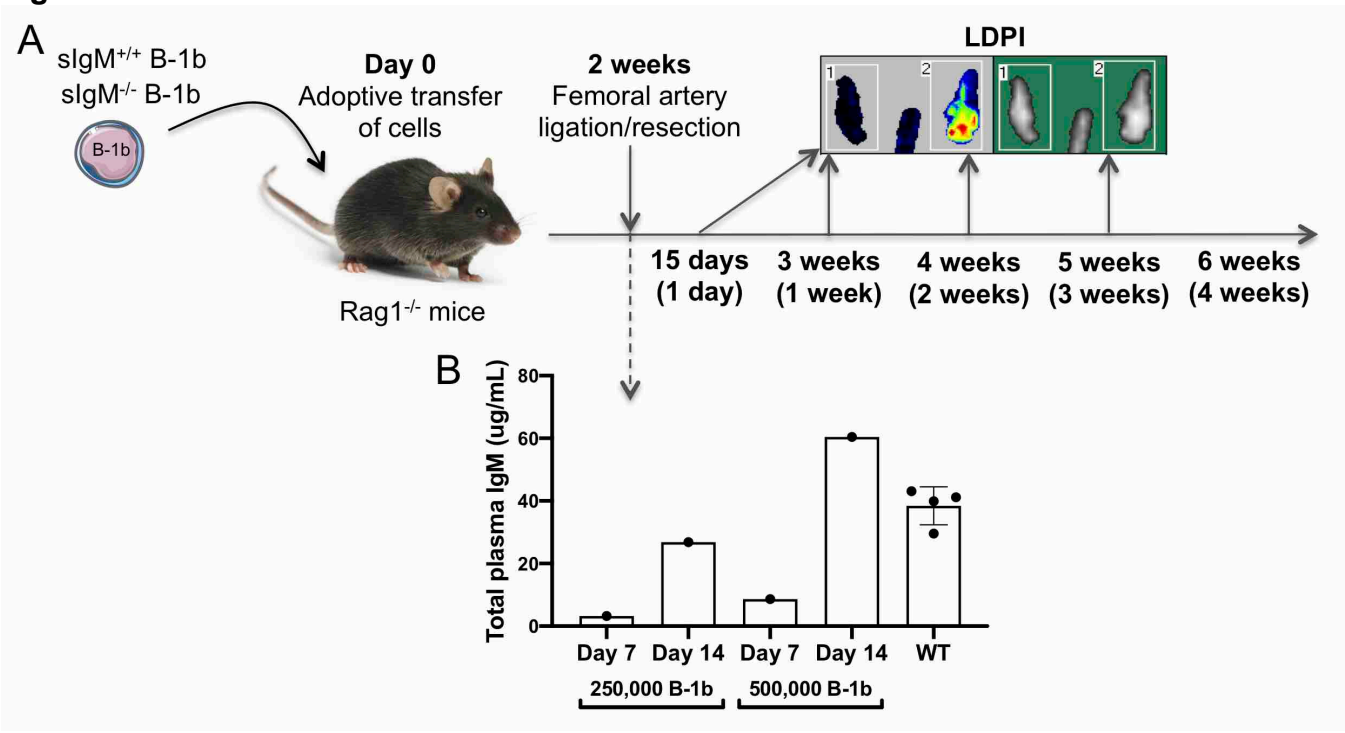

Figure 3.15. Experimental schematic for sIgM$^{+/+}$ and sIgM$^{-/-}$ B-1b adoptive transfers. **(A)** B-1b cells will be harvested from peritoneal cavity of sIgM$^{+/+}$ and sIgM$^{-/-}$ mice. 250,000 or 500,000 sIgM$^{+/+}$ or sIgM$^{-/-}$ B-1b cells will be adoptively transferred intravenously into Rag1$^{-/-}$ mice. Two weeks later, mice will be subjected to femoral artery ligation and resection to induce HLI. Laser Doppler perfusion imaging (LDPI) will then be used to quantify blood flow at 1 day, 1-, 2-, 3-, and 4 weeks of HLI (time spans specified in parentheses). **(B)** Total IgM was measured in plasma of a pilot group of Rag1$^{-/-}$ mice receiving WT B-1b cells at day 7 and 14 after transfer. Their circulating IgM values were compared to C57Bl/5 wild type mice (WT) pre-HLI surgery.

Summary

In summary, these studies are the first to demonstrate a role for B cells in regulating perfusion during HLI. The findings presented in this chapter implicate increased B-1b cell numbers and IgM levels as inhibitors of blood flow recovery during HLI. Further studies to precisely define the mechanisms whereby the vasculature changes to inhibit blood flow recovery are needed. Our current hypothesis is that loss of Id3 induces expansion of IgM-producing B-1b cells and this excess level of IgM has inhibitory effects on blood flow recovery (**Figure 3.16**). Finally, there is a strong interest in determining whether these findings translate into human patients. Future studies measuring IgM levels and describing B cell populations in PAD patients will be informative contributions to these studies.

Figure 3.16.

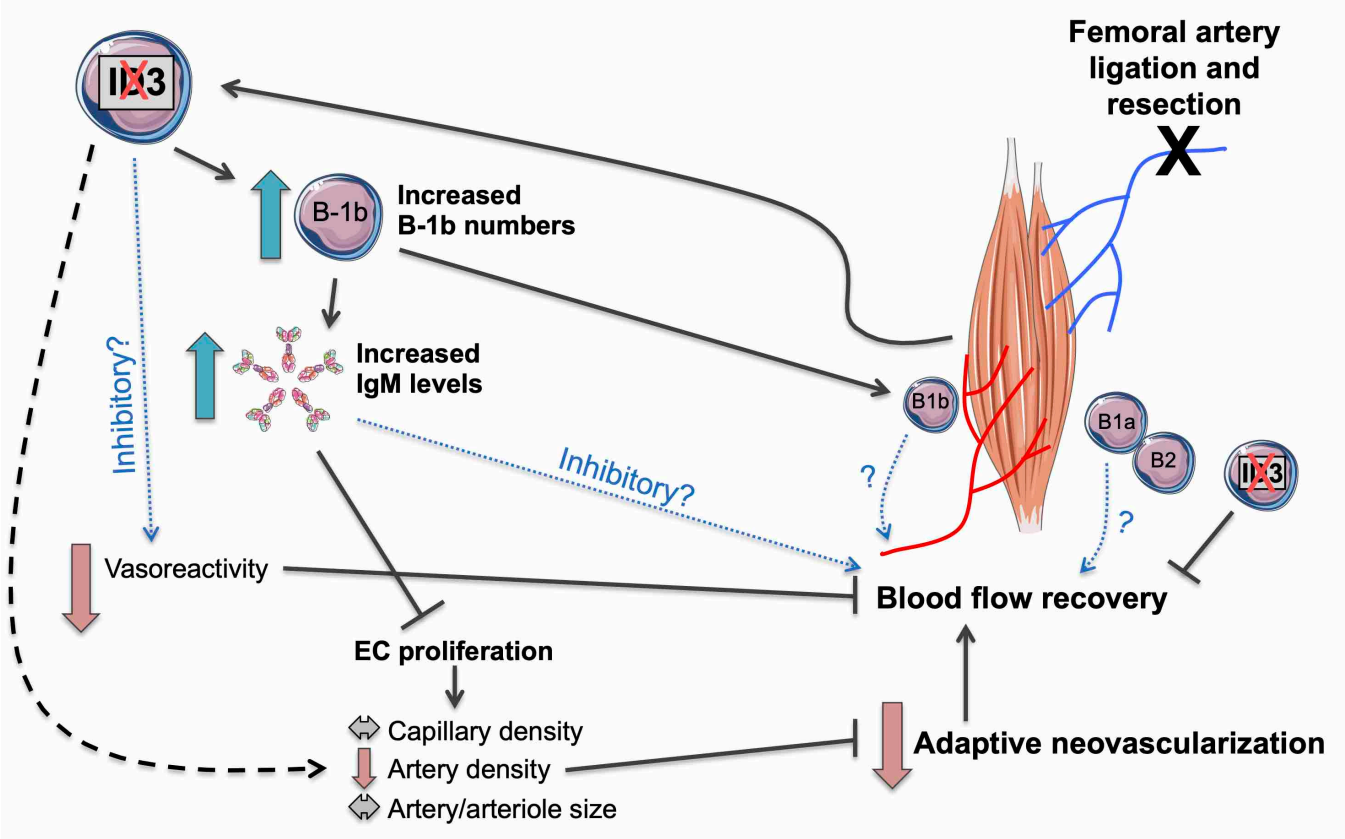

Figure 3.16. Schematic explaining working hypothesis.
B cell-specific Id3 KO mice have attenuated blood flow recovery and increased B-1b numbers and IgM levels. The working hypothesis is two-fold: 1.) B cell-specific Id3 KO attenuates blood flow recovery by inhibiting vasodilation in resistance arteries, and 2.) Increased B-1b cells produce IgM, which interacts with DAMPs produced during ischemia, such as oxPAPC and HMGB1, and attenuates their pro-angiogenic effects in ischemic skeletal muscle.

Chapter 4: Evaluating roles for endothelial- and macrophage-specific Id3 during atherosclerosis development

I. Abstract

Rationale: Previous studies from our lab demonstrated that Id3 attenuated atherosclerosis at least in part by inhibiting B cell recruitment to the aorta, macrophage numbers in the intima of plaques, and VCAM-1 expression in plaques. These studies, however, were conducted in global Id3 KO mice leaving to question what the cell-specific roles of Id3 are in this disease setting. Bone marrow transplant results demonstrate a role for both bone marrow-derived and non-bone marrow-derived cells in the mechanisms whereby Id3 controls atherogenesis. Many cell types play important roles in controlling atherosclerosis development. Two of the cell types central to this process are macrophages and endothelial cells (ECs). By employing cell type-specific Id3 knockout mouse lines, I investigated the potential role for Id3 in ECs and macrophages in controlling atherogenesis.

Approaches: Macrophage- and EC-specific Id3 KO mouse lines ($Id3^{MKO}$ and $Id3^{ECKO}$) were generated using LysM-cre and Cdh5-cre/ERT2 mice, respectively, crossed with Id3-floxed mice. Mice were administered AAV8 carrying an expression plasmid for mutated mPcsk9-D377Y to induce hyperlipidemia. Mice were fed Western diet (WD) for 12 weeks to induce atherosclerosis in $Id3^{MKO}$ and $Id3^{ECKO}$ mice and their respective littermates. Aortas, aortic roots, and brachiocephalic arteries (BCAs) were harvested to quantify lipid deposition and plaque size. Further immunofluorescence staining was used to quantify $CD68^{+}$ macrophage content and VCAM-1 expression. Finally, immune cell content and EC-specific VCAM-1 expression in PVAT from these mice were quantified using flow cytometry.

Results: $Id3^{MWT}$ and $Id3^{MKO}$ mice developed atherosclerosis similarly after 12 weeks of WD feeding. Early results, however, showed that $Id3^{ECKO}$ mice developed more atherosclerosis than $Id3^{ECWT}$ littermates after the same diet regimen. Plaque size was larger in $Id3^{ECKO}$ mice compared to $Id3^{ECWT}$ littermates, but VCAM-1 expression and CD68 content in the aortic root at this time point were no different between genotypes. Additionally, immune cell population sizes in the PVAT were not different between genotypes of either cell-specific strain.

Conclusions: Results from these studies demonstrate that Id3 expression in ECs, but not LysM-expressing macrophages may regulate development of atherosclerosis *in vivo*. More specifically, early results suggest that Id3 in ECs may inhibit atherogenesis in the aorta, the aortic root, and the BCA. Thus far, results demonstrate that EC-specific Id3 does not regulate VCAM-1 expression or recruitment of leukocytes after 12 weeks of WD feeding. Future studies

investigating VCAM-1 expression at earlier time points, the regional-specific recruitment of immune cells to plaques, and Id3's interaction with other signaling pathways in ECs may further elucidate the specific mechanisms whereby Id3 attenuates atherosclerosis *in vivo*.

II. Introduction

Atherosclerosis is a common cardiovascular disease (CVD) in the U.S. and worldwide that leads to severe complications such as heart failure and myocardial infarction[1]. Effective therapies that reduce risk factors such as lipid levels exist, but the prevalence of atherosclerosis remains. This suggests that additional therapeutic approaches based on new mechanisms are needed. While many cell types regulate atherosclerosis, dysfunction in ECs and macrophages are two notable processes by which atherogenesis occurs[15, 18]. Early pro-inflammatory signals and increased lipid levels begin to activate ECs in areas of disturbed flow in major arteries[14]. This results in breakdown of tight EC-EC junctions, upregulation of adhesion molecules such as VCAM-1 and ICAM1[11, 13], and the uptake of lipids into the vessel wall[14]. Monocytes and other immune cells are recruited to the site of inflammation and lipid deposition. While monocyte-derived macrophages play an important role in clearing excess lipid from the vessel wall, this often causes formation of foam cells[18]. These foam cells can secrete pro-inflammatory signals to recruit in further inflammatory cells[15], release ECM-degrading enzymes[162], and accumulate in the plaque where they can cause build-up of a necrotic, fatty core. This together leads to unstable, thrombosis-prone plaques[8]. While we generally understand the mechanisms whereby atherosclerosis develops, there is still a need for additional therapeutics to target novel mechanisms that may prevent or treat this disease. A better understanding of the molecular mechanisms mediating the dysfunction in ECs and macrophages may provide novel therapeutic targets.

Prior studies from the McNamara lab demonstrate that global loss of HLH-transcription factor Id3 results in increased atherosclerosis burden in Apoe$^{-/-}$ and Ldlr$^{-/-}$ mice fed a Western diet (WD)[120, 129]. Bone marrow transplant experiments demonstrate an athero-regulatory role for Id3 in both non-bone marrow-derived cells and bone marrow-derived cells[129]. Furthermore, the SNP rs11574 has been identified in the coding region of the human ID3 gene. Expression of the the minor allele, Id3105T, attenuates Id3's ability to interact with its binding partner

E12[130]. Id3105T is also associated with worsened indices of CAD including increased cIMT[130] and CAC[131]. These data demonstrate that Id3 plays an important role in regulating atherosclerosis in both mice and humans, however, the exact cell types in which Id3 is regulating these effects remains unclear.

Id3, ECs, and atherosclerosis

Given the important role endothelium plays in regulating atherogenesis[12, 18] and that Id3 is expressed in endothelial cells[133] (**Appendix 1, Figure A1.1**), it is possible that Id3 expression specifically in the endothelium plays a pivotal role in controlling plaque development. Accordingly, we hypothesized that loss of Id3 specifically in endothelial cells will result in increased atherosclerotic burden. One potential mechanism whereby Id3 in ECs might protect against atherogenesis is via immune cell recruitment. Global loss of Id3 results in increased macrophage content and VCAM-1 expression in the intima of aortic root lesions[120]. Thus, it can be further hypothesized that loss of Id3 in ECs will result in increased VCAM-1 expression on ECs and increased immune cell populations recruited to the plaque as well as the surrounding perivascular adipose tissue (PVAT).

Id3, macrophages, and atherosclerosis

Macrophages and other myeloid cells play an important role in promoting atherosclerosis through expression of pro-inflammatory cytokines and chemokines and ECM-degrading enzymes. I hypothesized that loss of Id3 specifically in macrophages would also result in increased atherosclerotic burden. This may be due to altered macrophage proliferation or differentiation. Indeed, prior studies demonstrated that $Id3^{GKO}$ mice have greater numbers of macrophages both in the aorta and in atherosclerotic plaques[120, 129]. Id3 has a well-established role in regulating proliferation and differentiation in a multitude of different cell types[122, 137, 163, 164]. Thus, I hypothesized that Id3 might protect against atherogenesis due to alterations in the number or types of macrophages found within plaques. An increase in pro-inflammatory (M1) macrophages may drive increased atherogenesis, thus if Id3 inhibits differentiation of macrophages toward an M1-phenotype, then $Id3^{MKO}$ mice may develop increased atherosclerosis.

Model of atherosclerosis

To address the questions posed in these studies, an emerging inducible approach for stimulating atherogenesis in mice was validated and utilized. AAV8-delivery of a plasmid expressing a mutated form of mPcsk9-D377Y induces hyperlipidemia and atherosclerosis in mice. Mutation D377Y in Pcsk9 causes an approximate ten-fold increase in PCKS9 protein expression levels in the liver. This overexpression of PCSK9 results in decreased expression of Low-density lipoprotein receptor (LDLR) on the surface of hepatocytes, which causes increased levels of lipid to remain in circulation. Multiple groups have successfully employed this method of inducing atherosclerosis in mice[165-167]. AAV8-mPcsk9-D377Y was administered to $Id3^{ECWT}$, $Id3^{ECKO}$, $Id3^{MWT}$, and $Id3^{MKO}$ mice, which were also fed a western diet (WD) to induce development of atherosclerosis.

III. Results

Validation of AAV8-mPcsk9-D377Y efficacy in inducing hyperlipidemia and weight gain in mice

To validate the effectiveness of our atherosclerosis induction and also determine whether all genotypes had comparable lipid levels and weight gain, weights and plasma samples were collected at the end of the 12-week study. Mice were weighed prior to or early on in the induction of atherosclerosis and at the end of 12 weeks of WD feeding. All mice were treated with one dose of AAV8-mPcsk9-D377Y one day prior to beginning WD feeding. Total body mass (**Figure 4.1A,C**) and weight gain (**Figure 4.1B,D**) were not different between genotypes in the EC- and macrophage-specific Id3 KO strains, but mice did gain a substantial amount of weight and adiposity. To quantify lipids, plasma was collected at the end of the WD feeding. Results reveal that $Id3^{MWT}$, $Id3^{MKO}$, $Id3^{ECWT}$, and $Id3^{ECKO}$ had comparable cholesterol and triglyceride levels and that mPcsk9-D377Y treatment did indeed induce hyperlipidemia (**Figure 4.1E-H**).

Figure 4.1.

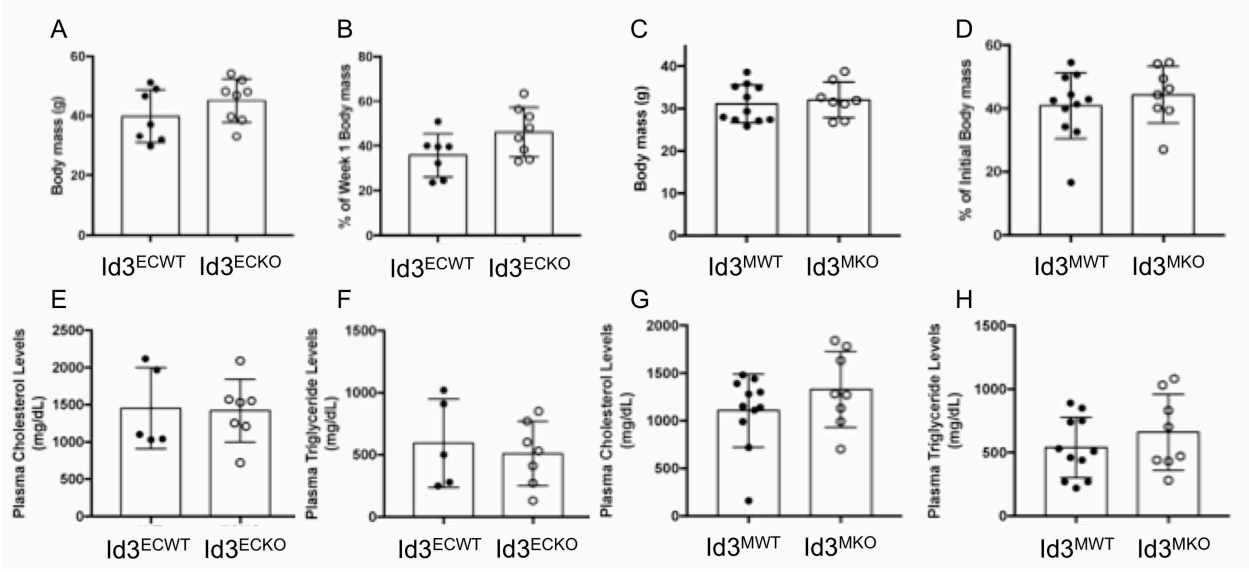

Figure 4.1. Body mass and lipid levels in EC- and macrophage-specific Id3 transgenic lines.

(A,C) Total body mass of $Id3^{ECWT}$ and $Id3^{ECKO}$ **(A)** and $Id3^{MWT}$ and $Id3^{MKO}$ **(C)** after 12 weeks of WD feeding. **(B)** The change in body mass as a percent of weights from one week of WD feeding were calculated in EC-specific Id3 WT and KO mice. **(D)** The change in body mass was calculated as a percent of pre-WD feeding for macrophage-specific Id3 WT and KO mice. **(E-H)** Lipids were quantified by the UVA Clinical labs to determine if cholesterol levels **(E,G)** and triglyceride levels (F,H) were different between $Id3^{ECWT}$ and $Id3^{ECKO}$ **(E,F)** and $Id3^{MWT}$ and $Id3^{MKO}$ **(G,H)** mice after 12 weeks of WD feeding.

Loss of Id3 in ECs, but not macrophages, augments atherosclerosis development

To determine if Id3 in macrophages or ECs regulates atherosclerosis development, mice were fed a WD for 12 weeks following induction of hyperlipidemia using AAV8-delivered mPsck9-D377Y. Atherosclerotic burden was quantified in the aortic root by Oil red O staining, the brachiocephalic artery (BCA) by Movat's staining, and the remainder of the aorta by en face staining. $Id3^{MKO}$ mice did not develop atherosclerosis to a different extent than $Id3^{MWT}$ littermates by en face staining (**Figure 4.2A**) in the whole aortic region (**Figure 4.2B**) or regionally in the arch (**Figure 4.2C**), thoracic (**Figure 4.2D**), or abdominal regions (**Figure 4.2E**). To quantify lesion size in the aortic root, 10 μm cross sections of the aortic root were collected and sets of 4 sections were selected at 200 μm increments along the root (**Figure 4.2F**). The total pixel area of lesion(s) per section was averaged amongst sets and all set averages were plotted along the root length (**Figure 4.2F,G**). The area under of the curve was then calculated to represent total area volume along the root (**Figure 4.2G**). No significant differences were seen between $Id3^{MWT}$ and $Id3^{MKO}$ mice. This same approach was used to calculate the proportion of the root that contained lesion and no differences were observed (**Figure 4.2H**). Furthermore, to assess lipid content in the lesion, the total lesional area of Oil red O^+ staining and the proportion of Oil red O^+ staining to total lesion area were calculated and plotted along the root (**Figure 4.2I,J**). Neither revealed significant differences in lipid content between genotypes (**Figure 4.2I,J**). Finally, lesion size (**Figure 4.2K**), the proportion of aortic root containing lesion (**Figure 4.2L**), total Oil Red O^+ area (**Figure 4.2M**), and proportion of lesion that was Oil Red O^+ (**Figure 4.2N**) were each calculated as a single average amongst all sections analyzed per mouse. No differences were observed between genotypes. While the AUC calculations better reflect the overall volume of lesion along the analyzed length of the vessel, the overall average will reveal if any mice have particularly large lesions along the vessel.

Figure 4.2.

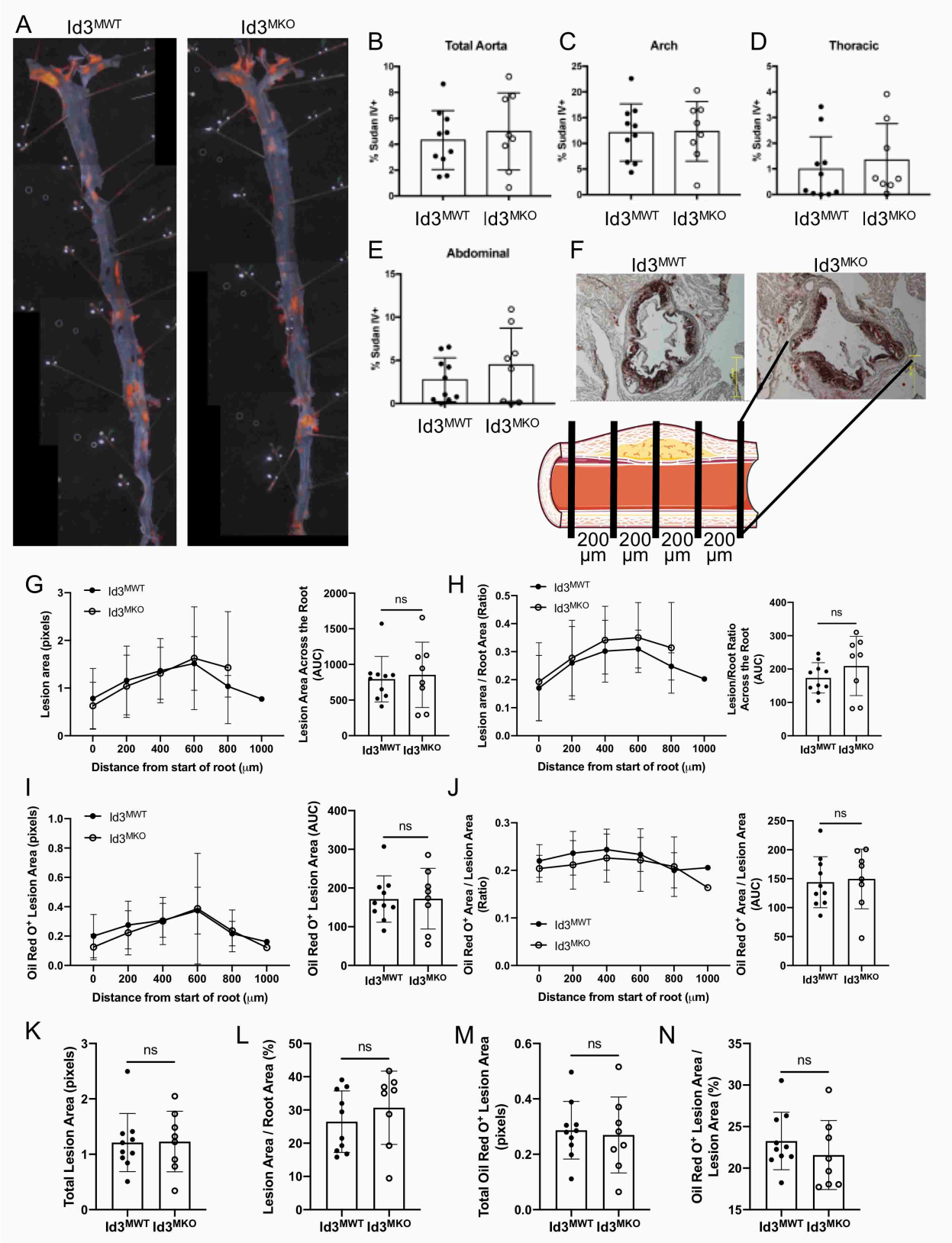
A
Id3MWT
Id3MKO
B
Total Aorta
C
Arch
D
Thoracic
% Sudan IV+
E
Abdominal
F
200 µm
200 µm
200 µm
200 µm
G
Lesion area (pixels)
Distance from start of root (µm)
Lesion Area Across the Root (AUC)
ns
H
Lesion area / Root Area (Ratio)
Lesion/Root Ratio Across the Root (AUC)
I
Oil Red O+ Lesion Area (pixels)
Oil Red O+ Lesion Area (AUC)
J
Oil Red O+ Area / Lesion Area (Ratio)
Oil Red O+ Area / Lesion Area (AUC)
K
Total Lesion Area (pixels)
L
Lesion Area / Root Area (%)
M
Total Oil Red O+ Lesion Area (pixels)
N
Oil Red O+ Lesion Area / Lesion Area (%)

Figure 4.2. Macrophage-specific loss of Id3 does not alter atherosclerosis development.
(A) En face staining of the lumen of $Id3^{MWT}$ and $Id3^{MKO}$ aortas was conducted to quantify total lipid content. **(B-E)** Lipid content in the total aorta **(B)**, arch region **(C)**, thoracic region **(D)**, and abdominal region **(E)** were quantified. **(F)** Aortic roots were also sectioned and stained with oil red o to quantify lipid-rich lesions. In order to quantify lesions throughout the entire root, sections were selected at 200 μm increments along the root. **(G)** Total lesion area at each 200 μm increment was calculated and plotted along the length of the root to calculate the area under the curve (AUC). This value serves to represent the overall volume of lesion in the root. The AUC for each mouse was averaged and quantified. **(H)** The ratio of lesion to total root area was also plotted to calculate the AUC. **(I,J)** The total area of Oil Red O^+ area in the lesions **(I)** and percent of total lesions that were Oil Red O^+ **(J)** were also calculated and plotted along the length of the root. **(K)** The average total pixel area of lesions across the entire root was also calculated for each mouse. (L-N) The same was done for lesion-to-root area ratio **(L)**, total Oil Red O^+ area **(M)**, and Oil Red O^+ area-to-lesion area **(N)**. Aortic roots were sectioned by Melissa Marshall and stained and quantified by Elias Ayoub.

To begin assessing whether EC-specific expression of Id3 regulates atherosclerosis development, a similar analysis was applied to a preliminary group of $Id3^{ECWT}$ and $Id3^{ECKO}$ mice. En face staining revealed a significant increase in total lipid content of the aorta in $Id3^{ECKO}$ mice compared to $Id3^{ECWT}$ littermates (**Figure 4.3A,B**), which appeared to be due to lesions within the aortic arch (**Figure 4.3C-E**). Lesion area when plotted along the length of the aortic root was trending towards being greater in $Id3^{ECKO}$ mice, but was not significant (**Figure 4.3F,G**). When plotted as the lesion-to-root area ratio, there was no significant difference between genotypes (**Figure 4.3H**). When assessing lipid content, however, the area of Oil red O^+ lesion was significantly greater in $Id3^{ECKO}$ mice (**Figure 4.3I**) and the Oil red O^+-to-total lesion area ratio was trending towards being significantly greater (**Figure 4.3J**). When averaged over the entire length of the root, total lesion area was significantly greater (**Figure 4.3K**), but the lesion-to-root area was not (**Figure 4.3L**). Both the total Oil Red O^+ area (**Figure 4.3M**) and the proportion of lipid staining within the lesions (**Figure 4.3N**) were trending towards being increased in $Id3^{ECKO}$ mice.

Finally, the BCA was also stained with Movat's stain to quantify total lesion size (**Figure 4.4A**). Sections were selected at 150 μm increments along the BCA. Total lesion area was calculated in each section and plotted along the length of the BCA. The area under the curve for each mouse was plotted and revealed that there was a trending increase in lesion volume in the $Id3^{ECKO}$ mice (**Figure 4.4B**). When an average of all sections per mouse was calculated,

there was a significant increase in total lesion area (**Figure 4.4C**), but not in the lesion-to-lumen area ratio (**Figure 4.4D**).

Figure 4.3.

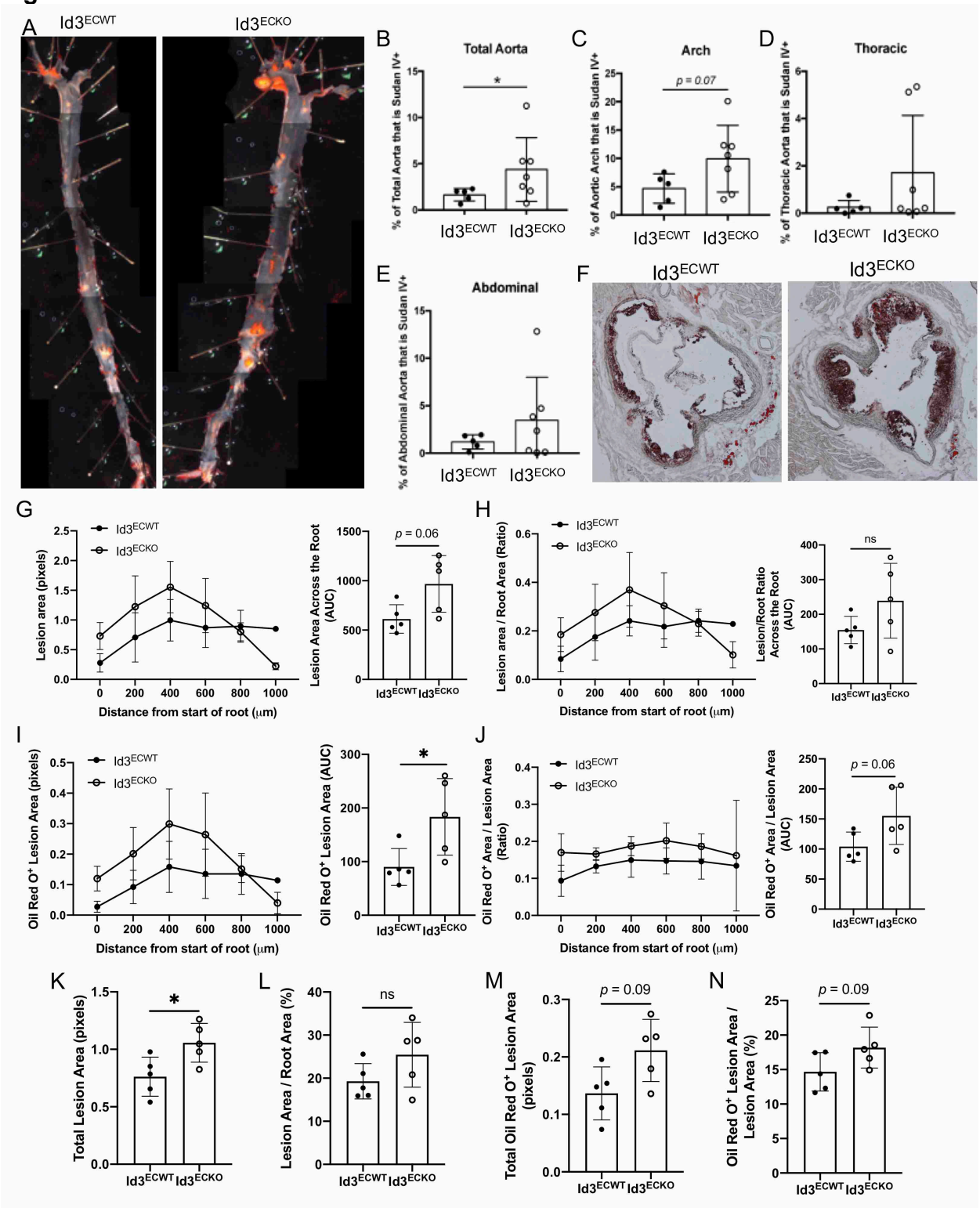

Figure 4.3. EC-specific loss of Id3 augments atherosclerosis development.
(A) En face staining of the lumen of $Id3^{ECWT}$ and $Id3^{ECKO}$ aortas was conducted to quantify total lipid content. **(B-E)** Lipid content in the total aorta **(B)**, arch region **(C)**, thoracic region **(D)**, and abdominal region **(E)** were quantified. **(F)** Aortic roots were also sectioned and stained with oil red o to quantify lipid-rich lesions. In order to quantify lesions throughout the entire root, sections were selected at 200 μm increments along the root. **(G)** Total lesion area at each 200 μm increment was calculated and plotted along the length of the root to calculate the area under the curve (AUC). This value serves to represent the overall volume of lesion in the root. The AUC for each mouse was averaged and quantified. **(H)** The ratio of lesion to total root area was also plotted to calculate the AUC. **(I,J)** The total area of Oil Red O^+ area in the lesions **(I)** and percent of total lesions that were Oil Red O^+ **(J)** were also calculated and plotted along the length of the root. **(K)** The average total pixel area of lesions across the entire root was also calculated for each mouse. **(L-N)** The same was done for lesion-to-root area ratio **(L)**, total Oil Red O^+ area **(M)**, and Oil Red O^+ area-to-lesion area **(N)**. Aortic roots were sectioned by Melissa Marshall and stained and quantified by Jason Li. * represents $p < 0.05$.

Figure 4.4.

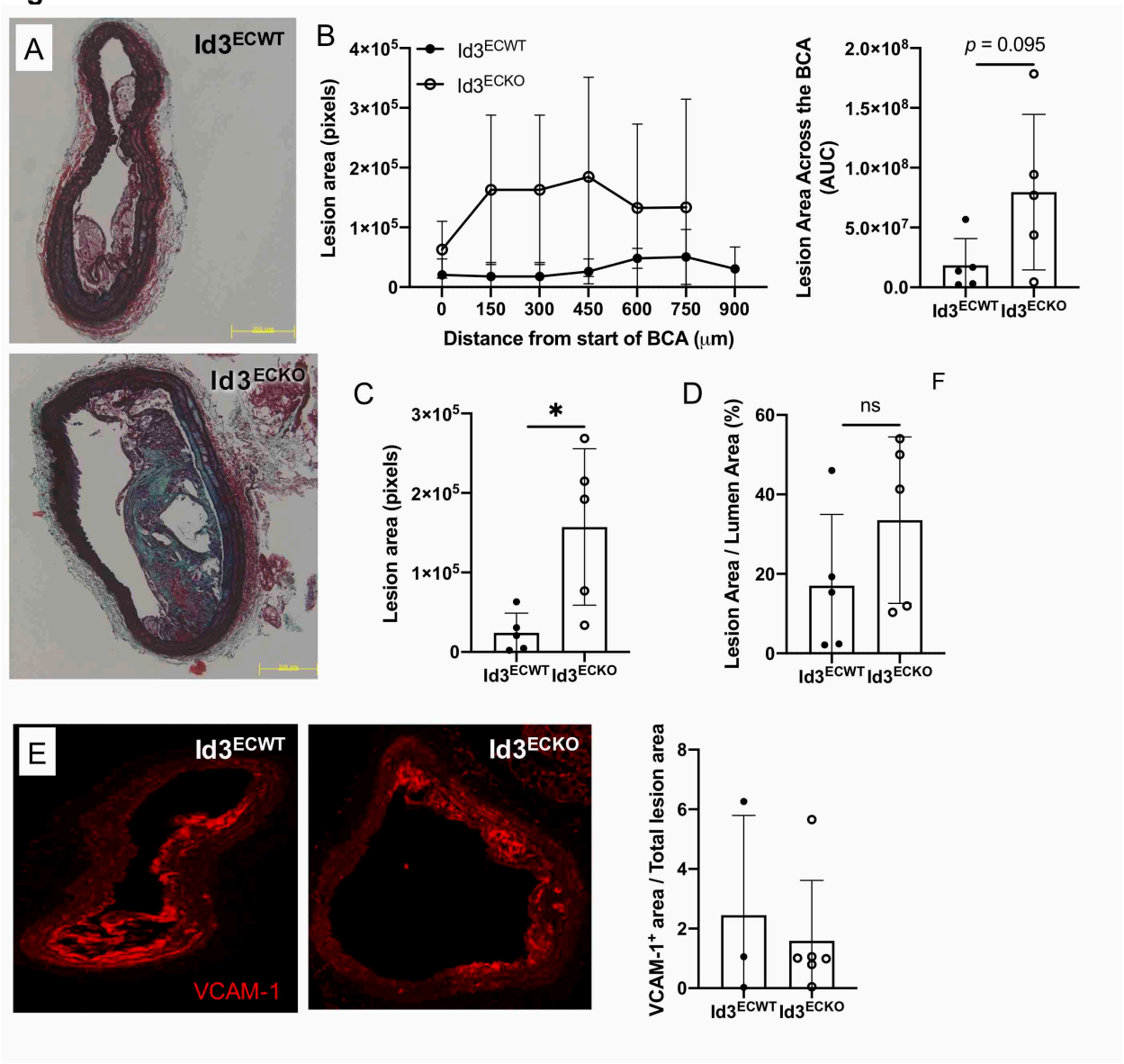

Figure 4.4. BCA lesion size and VCAM-1 expression quantification.
(A) BCAs were sectioned and stained with MOVAT to quantify total lesion area. **(B)** The lesion area in sections at 150 μm increments along the BCA were plotted and the area under the curves of each genotype were calculated. **(C)** The total pixel area of lesion per section was also averaged amongst all sections per mouse. **(D)** The proportion of BCA lumen area that contained lesion was also calculated. **(E)** BCAs were also stained for VCAM-1 expression using immunofluorescence. Total VCAM-1 pixel area as a percent of total lesion area was calculated. BCA embedding, sectioning, and MOVAT staining was performed by Missy Bevard in the CVRC Histology Core, VCAM-1 staining and quantification was performed by Jason Li.

Loss of Id3 does not alter VCAM-1 expression

To begin investigating the mechanism by which Id3 in ECs may inhibit atherosclerosis development, VCAM-1 expression was quantified in the aortic root and ECs from the PVAT. Total VCAM-1 expression by immunofluorescence was quantified in the BCA (**Figure 4.4E**). Initial results reveal no difference between $Id3^{ECWT}$ and $Id3^{ECKO}$ mice after 12 weeks of WD feeding (**Figure 4.4E**). To further assay VCAM-1 expression, the ECs in the PVAT were assessed for VCAM-1 expression levels and frequency after 12 weeks of WD (**Figure 4.5A**). Loss of Id3 in ECs did not alter the number of $CD31^+$ ECs nor other $CD45^-$ vascular or stromal cells (**Figure 4.5B**). $Id3^{ECKO}$ mice did not have different percent $VCAM\text{-}1^+$ ECs (**Figure 4.5C**) or VCAM-1 MFI on ECs (**Figure 4.5E**) compared to WT littermates. This was also the case for non-EC, $CD31^-$ stromal and vascular cells (**Figure 4.5D,F**). Overall, these data suggest that at a later time point of 12 week of WD feeding, EC-specific Id3 does not regulate VCAM-1 expression in PVAT-derived $CD45^-$ cells.

Figure 4.5.

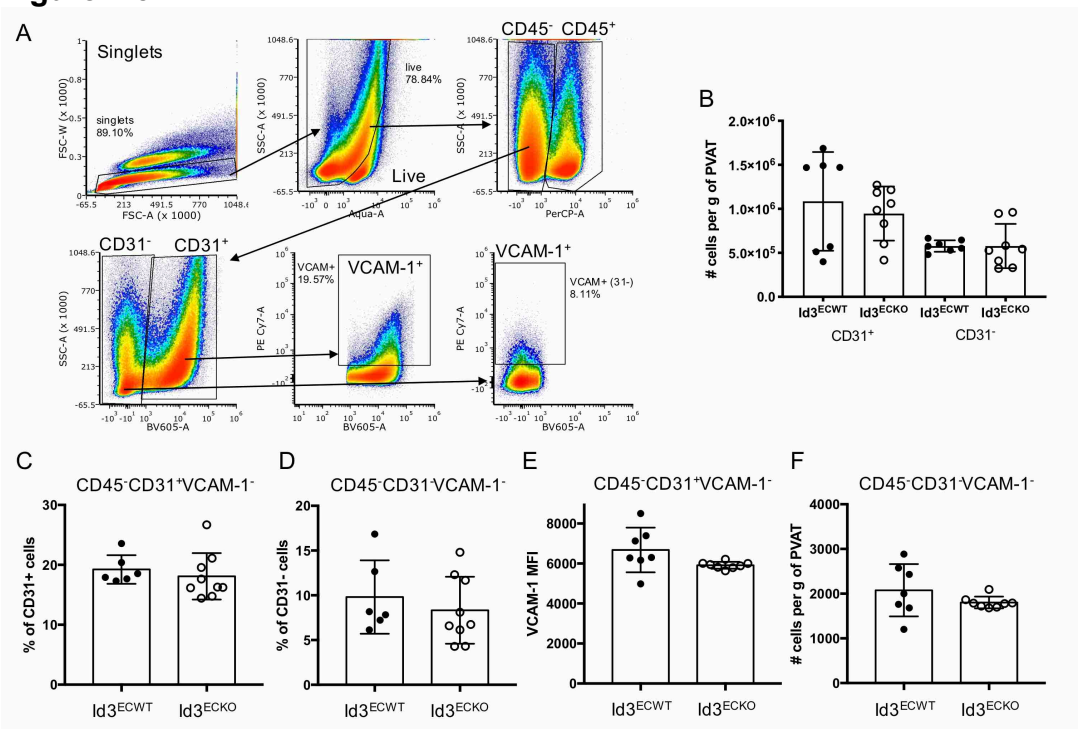

Figure 4.5. VCAM-1 expression on PVAT stromal and vascular cells.
(A) Flow cytometry was used to identify and quantify VCAM-1 populations from digested PVAT tissue. **(B)** Total $CD45^-CD31^+$ and $CD45^-CD31^-$ cell population sizes were compared between $Id3^{ECWT}$ and $Id3^{ECKO}$ mice. **(C,D)** The proportion of $CD31^+$ ECs **(C)** and $CD31^-$ non-EC stromal and vascular cells **(D)** that were VCAM-1 positive was calculated. **(E,F)** The MFI of VCAM-1 expression on $CD31^+$ **(E)** and $CD31^-$ **(F)** cells was also calculated.

Loss of Id3 in ECs does not alter immune cell population sizes in PVAT or the aortic root

Despite no apparent differences in VCAM-1 expression in assays performed thus far, it is still possible that immune cell populations may have been differentially recruited to the plaque and PVAT in $Id3^{ECKO}$ mice. Either VCAM-1 may be upregulated at earlier time points, or $Id3^{ECKO}$ mice could recruit cells to the plaque and PVAT in a VCAM-1-independent manner. Many other integrins and adhesion molecules participate in immune cell adherence and trans-endothelial migration. Further, past studies showed Id3 KO mice to differentially express other adhesion molecules[128]. To assess immune cell recruitment to the plaque and PVAT, immunofluorescence and flow cytometry were used, respectively (**Figure 4.6A** and **Figure 4.7A**). Aortic roots were stained with CD68, a marker of macrophages, and total CD68 pixel area per root was quantified (**Figure 4.6A**). By CD68 staining, there was no significant difference between $Id3^{ECWT}$ and $Id3^{ECKO}$ mice (**Figure 4.6B**), or $Id3^{MWT}$ and $Id3^{MKO}$ mice observed (**Figure 4.6C**). Additionally, PVAT was digested into single-cell suspensions and stained with antibodies against surface markers for a variety of immune cells (**Figure 4.7A**). Total numbers of each immune cell subset were no different between EC-specific genotypes (**Figure 4.7B**).

The same assay was applied to macrophage-specific Id3 KO mice. No difference in total numbers of different immune cell subsets was observed in $Id3^{MWT}$ and $Id3^{MKO}$ mice (**Figure 4.8A**). However, when calculated as a percentage of $CD45^+$ cells, $Id3^{MKO}$ mice had a significant increase in the proportion of B cells within the PVAT relative to $Id3^{MWT}$ mice (**Figure 4.8B**). This effect appeared to be due to increases in B-2 cells. Interestingly, while differences in B cell populations were observed, no changes in macrophage numbers were observed. This includes $CD11c^+$ M1 and $CD206^+$ M2 macrophages (**Figure 4.8C**).

Figure 4.6.

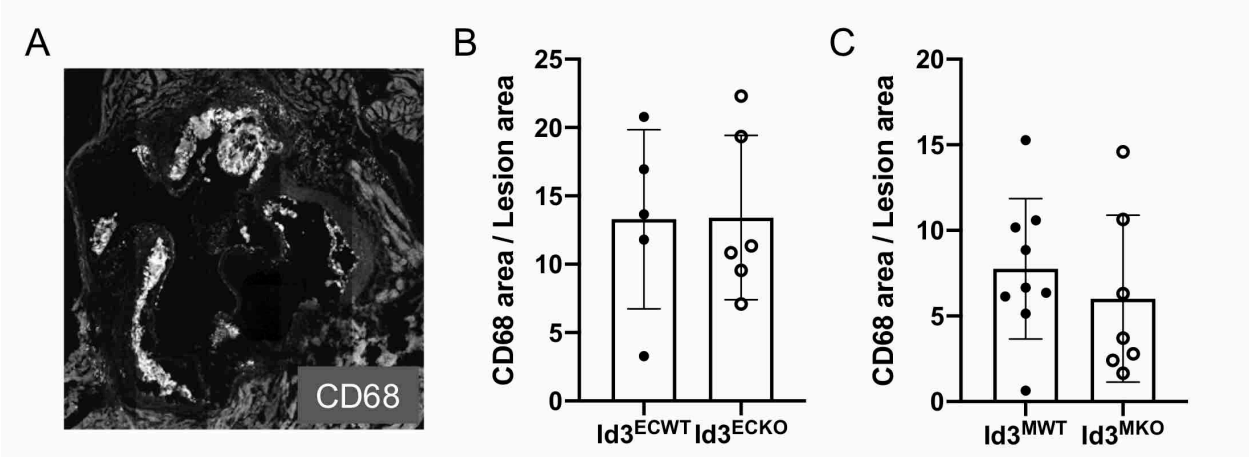

Figure 4.6. CD68 staining in the aortic root.
(A) Aortic roots from Id3^{ECWT}, Id3^{ECKO}, Id3^{MWT}, and Id3^{MKO} mice fed 12 weeks WD were isolated, sectioned, and stained with an antibody against CD68. **(B,C)** The total pixel area of CD68 in the lesions was calculated as a percent of total lesion area in Id3^{ECWT} and Id3^{ECKO} **(B)** and Id3^{MWT} and Id3^{MKO} mice **(C)**. Roots were sectioned by Melissa Marshall and stained and quantified by Jason Li (EC-Id3 line) and Elias Ayoub (Lysm-Id3 line).

Figure 4.7.

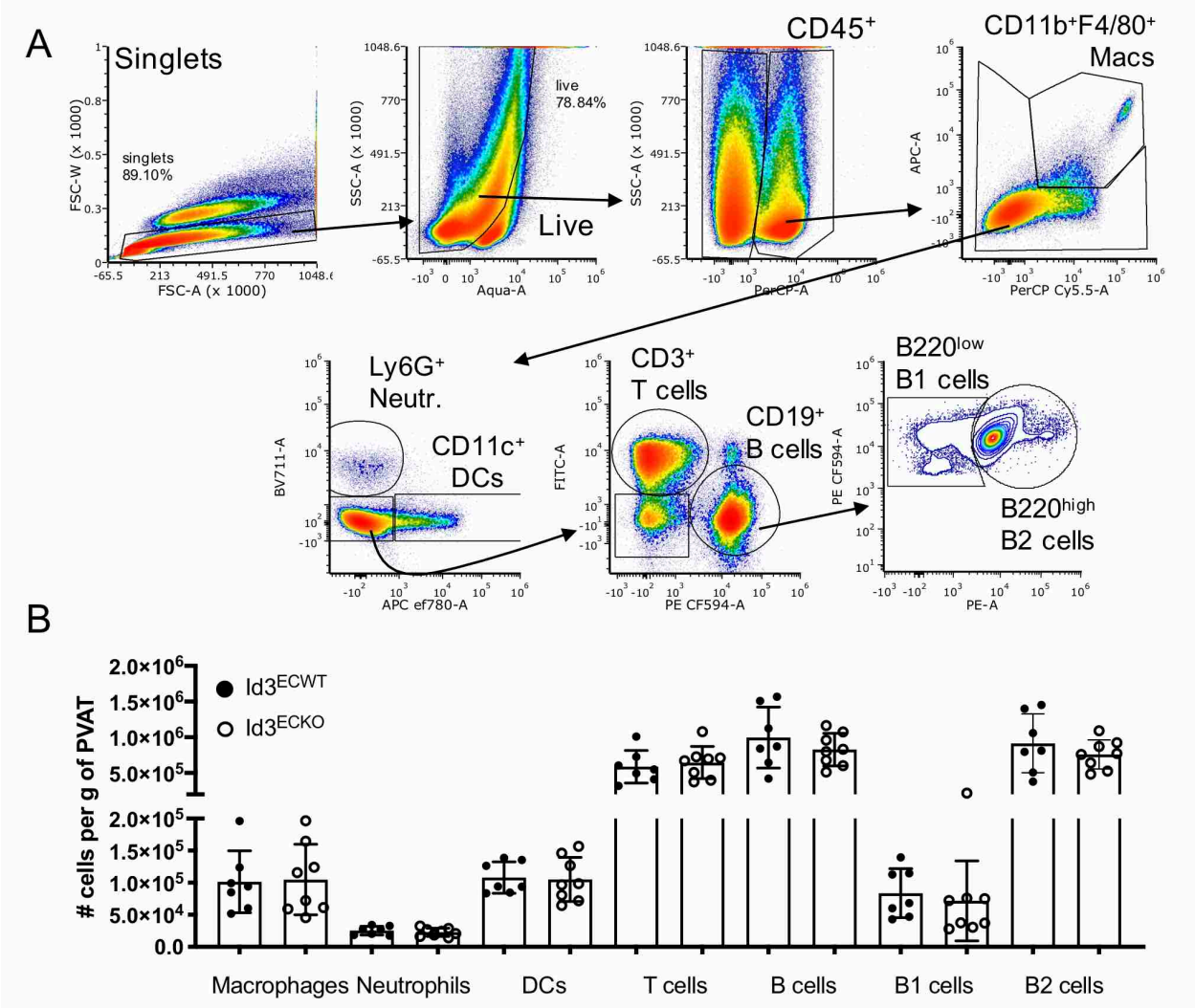

Figure 4.7. Immune cell populations in the PVAT of EC-specific transgenic lines. **(A)** Flow cytometry was used to identify and quantify immune cell populations from digested PVAT tissue. Immune cell populations analyzed included: $CD45^+CD11b^+F4/80^+$ macrophages (Macs), $Ly6G^+$ neutrophils (Neutr.), $CD11c^+$ dendritic cells (DCs), $CD3^+$ T cells, $CD19^+$ B cells, $B220^{low}$ B1 cells, $B220^{high}$ B2 cells, and $CD206^+$ M2 macrophages and $CD11c^+$ M1 macrophages. **(B)** Immune cell populations were quantified as the number of cells per g of PVAT in $Id3^{ECWT}$ and $Id3^{ECKO}$ mice after 12 weeks of WD.

Figure 4.8.

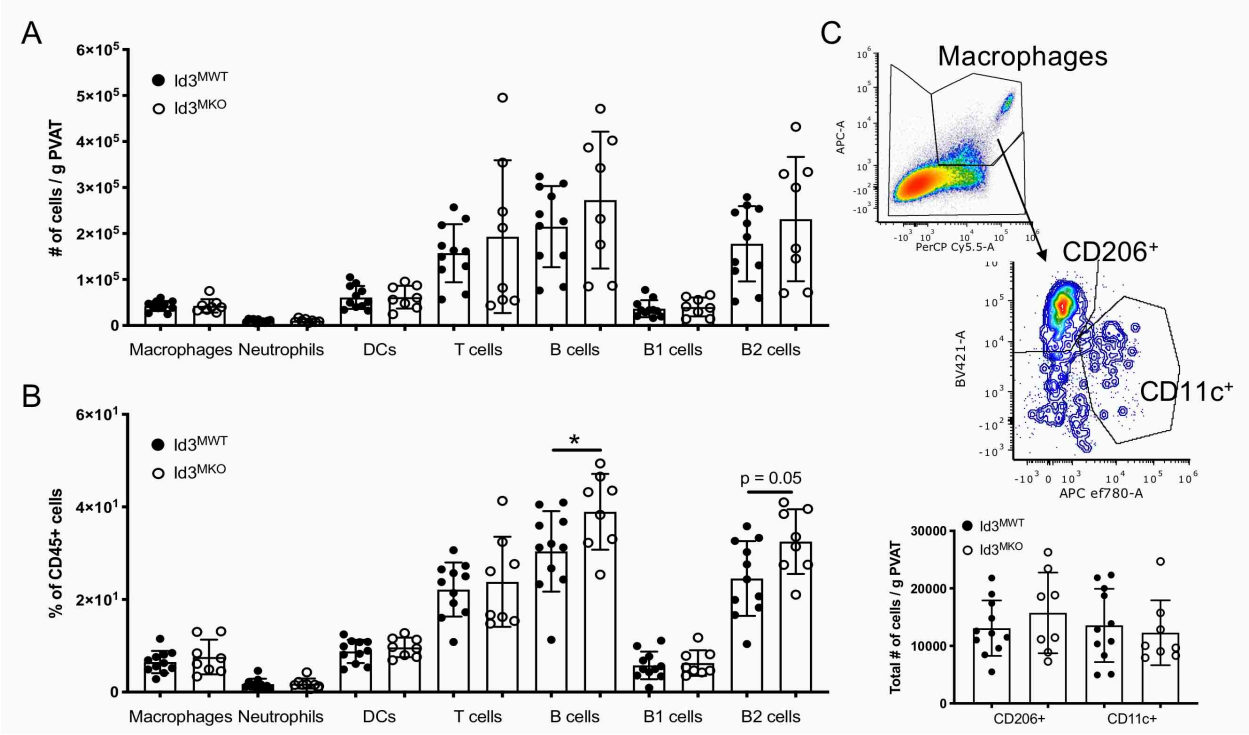

Figure 4.8. Immune cell populations in the PVAT of Id3^{MWT} and Id3^{MKO} mice. **(A)** Flow cytometry was used to identify and quantify immune cell populations from digested PVAT tissue as in Figure 4.7. Immune cell populations were quantified as the number of cells per g of PVAT in Id3^{MWT} and Id3^{MKO} mice after 12 weeks of WD. **(B)** The proportion of CD45^{+} immune cells that are comprised of each subset was also calculated in Id3^{MWT} and Id3^{MKO} mice. **(C)** The number of M1 and M2 macrophages was also quantified. * represents $p < 0.05$.

IV. Discussion

EC-specific Id3 KO Discussion and Conclusions

These findings are the first to suggest an EC-specific role for Id3 in regulating atherosclerosis development. In the presence of hyperlipidemia, preliminary results suggest that EC-specific Id3 prevents plaque development in the aortic arch, aortic root, and BCA. The exact mechanisms by which Id3 mediates these effects remains unclear, but findings thus far suggest it may be independent of late-time point VCAM-1 expression and recruitment of immune cells to the plaque and PVAT. Before definitively concluding this, however, a few considerations should be made regarding experimental approach. The first is simply that an additional cohort of mice should be assessed for atherosclerosis burden. While initial results

are promising, the cohort size is insufficient to confidently conclude that Id3 expression in ECs inhibits atherosclerosis development.

Second, ECs are one of the first cell types to respond to lipid and inflammatory signals that lead to development of atherosclerosis[18]. Thus, the 12-week time point utilized in these studies may be inappropriate for quantifying VCAM-1 expression, as a more chronic stage of atherosclerosis has been reached by then. Indeed, when comparing chow-fed $ApoE^{+/+}$ aortas to $ApoE^{-/-}$ aortas, VCAM-1 staining can be seen on $ApoE^{-/-}$ aortas at as early as 5 weeks of age[11] and preliminary work from the McNamara lab demonstrates that VCAM-1 is also expressed on endothelium after just a few weeks of WD feeding. Quantifying VCAM-1 expression at an earlier time point, such as after 2 or 4 weeks of WD, may demonstrate more significant differences. To date, aortas and aortic roots have been harvested from a cohort of $Id3^{ECWT}$ and $Id3^{ECKO}$ mice fed 4 weeks. The roots can be used to stain for VCAM-1 expression at an earlier time point. Should results from these studies demonstrate upregulation of VCAM-1 in Id3 KO ECs, a potential mechanism whereby this occurs is via Id3 inhibition of E12-promotion of VCAM-1 as previously shown in VSMCs by the McNamara lab[120]. Additional molecular mechanisms by which Id3 inhibits VCAM-1 should also be pursued. Aortas were also digested into a single-cell suspension and banked for future staining and analysis. These samples will be used for CyTOF staining and analysis in order to identify novel signaling proteins and surface markers in EC populations that may differ between $Id3^{ECWT}$ and $Id3^{ECKO}$ mice (see Chapter 5 for further details).

Second, recent findings from the McNamara lab and others demonstrate distinct differences in the cell populations in different regions of the PVAT along the aorta[23] (Srikakulapu P, in progress). The abdominal PVAT is more characteristic of white adipose, while adipocytes in the thoracic PVAT have characteristics of brown fat. More B cells are found in the PVAT localized around the arch than in the thoracic and abdominal regions. En face results demonstrated the greatest regional difference in the arch region of $Id3^{ECKO}$ compared to $Id3^{ECWT}$ aortas (**Figure 4.3A-E**). Thus, an informative next experiment would include a focused analysis to determine if immune cells are differentially recruited to PVAT specifically within the arch region.

Potential mechanisms whereby EC-specific Id3 inhibits atherosclerosis development

Beyond the specific mechanisms supported by previous studies from the McNamara lab, Id3 could also inhibit atherosclerosis development through other molecular mechanisms. Published literature demonstrates that factors such as CXCR4[168], TGFβ[169], Caveolin-1[170], $P2Y_2R$[171], and eNOS[172, 173] regulate atherogenesis in an EC-dependent manner. Id3 interacts with many of these factors either by regulating transcript levels of the protein or being upregulated or activated downstream of their signaling. Given this, it is possible that Id3 induces, inhibits, or responds to any or all of these factors to regulate atherosclerosis.

For example, the McNamara lab has shown that Id3 inhibits CXCR4 expression, but loss of *Cxcr4* in ECs results in increased atherosclerosis. Döring *et al*. demonstrated that CXCR4 inhibits atherosclerosis by activating AKT/WNT/β-catenin signaling to promote VE-Cadherin expression and maintain a stable endothelial barrier[168]. Thus, these data suggest conflicting phenotypic outcomes should Id3 indeed regulate CXCR4 in EC. An alternative mechanism may be that CXCR4 promotes Id3 expression. Id3 is also induced downstream of AKT[174], so it is also possible that CXCL12-CXCR4 signaling promotes Id3 expression to induce atheroprotection in ECs.

In other signaling contexts, however, Id3 inhibits AKT signaling[175, 176]. $P2Y_2R$ signaling induces AKT activation to induce eNOS expression and VCAM-1 expression, which promotes atherosclerosis development. Id3 may inhibit these signaling pathways by downregulating AKT. Additionally, TGFβ induces expression of Id3 in mammary carcinoma cells[177] and B lymphocyte progenitors[164] via Smad signaling. However, loss of *Tgfb* in ECs results in reduced atherosclerosis[169], while EC-specific *Id3* KO results in increased atherosclerosis. This suggests that Id3 may potentially serve as a negative regulator of TGFβ signaling in endothelial cells.

In summary, the signaling pathways regulating Id3 and other atherosclerosis mediators are complex and context-dependent. **Figure 4.9** summarizes potential pathways through which Id3 regulates atherosclerosis. Experiments centered on a focused question will be necessary to parse out the exact mechanism whereby EC-specific Id3 is atheroprotective. One approach to narrow down potential signaling pathways would be to identify those that are differentially regulated in Id3 KO ECs compared to Id3 WT ECs in the setting of atherosclerosis using a high-dimensional analysis approach such as CyTOF.

Figure 4.9.

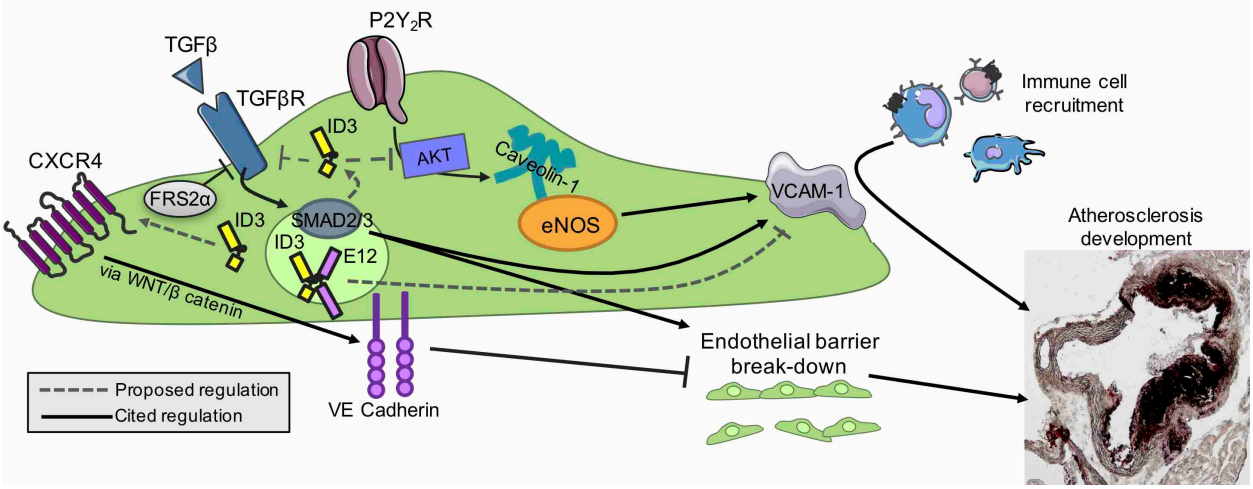

Figure 4.9. Potential mechanisms whereby Id3 regulates atherosclerosis development in ECs.
Atheroprotective CXCR4 may promote expression of Id3 to attenuate atherosclerosis development via maintenance of EC barrier. Id3 attenuation of E12-promoted VCAM-1 expression also has not been verified in ECs. Id3 may also attenuate AKT/eNOS- or TGFβ-induced atherogenesis.

LysM-specific Id3 KO Discussion and Conclusions

Additional results revealed no significant differences between atherosclerosis burden in $Id3^{MWT}$ and $Id3^{MKO}$ mice. This suggests that Id3 expression in a different bone marrow-derived population may be responsible for its atheroprotective effects. Prior work from the lab reveals that loss of Id3 in B cells was atheroprotective, contradicting the suggested results from prior bone marrow transplant experiments[30]. Loss of Id3 resulted in increased B-1b cell numbers and levels of IgM against oxidation-specific epitopes (OSEs). Adoptive transfer of B-1b cells into $Rag1^{-/-}$ resulted in increased OSE-specific IgM levels and attenuated atherosclerosis[30]. Furthermore, these OSE-specific IgMs have been shown to inhibit foam cell formation and atherosclerosis development *in vivo*[178-181]. Results from these studies thus far, however, do not rule out the possibility that loss of Id3 in B-2 cells may augment atherosclerosis development. Further studies are needed to better understand this potential mechanism. Additionally, while considered one of the optimal macrophage-specific genes to use, *LysM* is not expressed solely in macrophages, nor is it expressed in the entirety of macrophage populations *in vivo*[182, 183]. Thus, this simultaneous "leakiness" and "inefficiency" of the Id3 knockout may have influenced atherosclerosis outcomes. Unfortunately, a gene to drive macrophage-specific Cre expression has not yet been identified. Upon identifying one, it will be additionally informative to cross the

line with ROSA26$^{floxSTOP\text{-}YFP}$ line to simultaneously identify macrophages in case trans-differentiation or down-regulation of traditional macrophage markers occurs during disease progression.

Interestingly, Id3^{MKO} mice have increased proportions of PVAT-resident B cells. This brings to question how Id3 in macrophages may be affecting B cell behavior, recruitment, proliferation, or survival. The increase was predominantly due to B-2 cells, which preferentially recruit to the arch region of the aorta during atherosclerosis development[129]. This cell subset is also generally considered to be atherogenic[22]. As suggested in the discussion of EC-specific results, an additional study at the 12-week time point analyzing immune cell subsets in the arch, thoracic, and abdominal PVAT regions may reveal further differences between genotypes. In particular, I hypothesize that the increase in B cell numbers would be even more pronounced in the arch region of Id3^{MKO} mice.

There are a few possible mechanisms by which macrophages may influence B cell behavior to potentially regulate atherosclerosis development. First, macrophages secrete chemokines such as CXCL13 that recruit and retain B cells in tissues and sites of injury or disease[184, 185]. CXCL13 plays an important role in the formation of tertiary lymphoid organs (TLOs)[186], which form in the adventitial area surrounding arteries and adjacent to PVAT during atherosclerosis development[187]. B cells typically do not enter into atherosclerotic plaques, but rather remain in TLOs and the PVAT surrounding areas of plaque development[16]. Thus, it is feasible that monocyte-derived macrophages recruited to lesions in the intima may secrete CXCL13 and other chemokines that recruit B cells to the surrounding PVAT and adventitia to form TLOs.

Second, macrophages may stimulate B cells in TLOs and PVAT to affect B cell and macrophage behavior. CD40-CD40L interactions likely occur between B cells and macrophages and have been shown to be pro-inflammatory in the setting of atherosclerosis[188]. Additional findings from B cell lymphoma studies reveal that tumor-associated macrophages stimulate B cell activation and survival through STAT3, PI3K, and/or NFκB[189]. If Id3 promotes secretion or expression of signals or co-stimulatory molecules on macrophages, this may induce proliferation or activation of B cells in TLOs. In this case, these cells may produce additional atheroprotective or atherogenic Ig's, depending on the subsets activated.

With regard to experimental approach, it is possible that the selected 12-week time point may be too early. Should macrophages drive B cell recruitment, accumulation, and/or activation in an Id3-dependent manner, the effects on atherosclerosis development may not manifest until later, chronic time points. Indeed, B cells increasingly accumulate in artery tertiary lymphoid organs (ATLOs) with time[187]. Thus, additional studies quantifying atherosclerosis burden and immune cell accumulation after 18 or 24 weeks of WD may reveal differential effects between $Id3^{MWT}$ and $Id3^{MKO}$ mice.

Summary

In summary, these are the first studies to investigate the EC- and macrophage-specific roles for Id3 in atherosclerosis development. These studies also validate the effectiveness of utilizing AAV-delivery of mutated-Pcsk9-D377Y to induce hyperlipidemia in mice. 12-week WD studies reveal Id3 expression in ECs, but not macrophages, is atheroprotective. Lesions in the aortic root and BCA, and lipid content in the lumen of the aorta were greater in $Id3^{ECKO}$ mice than WT littermates. However, results thus far do not identify specific molecular and cellular mechanisms whereby Id3 protects against atherogenesis. Additional findings suggest Id3 expression in macrophages may inhibit B cell proliferation or recruitment to PVAT during atherosclerosis as $Id3^{MKO}$ mice have more B cells in aortic PVAT than WT littermates. Further studies investigating the molecular mechanism(s) whereby EC-specific Id3 attenuates atherosclerosis development and macrophage-specific Id3 controls PVAT-resident B cell numbers are needed.

Chapter 5: General Conclusions, Discussion, and Future Directions

These studies report findings centered on improving our understanding of the cell-specific roles that Id3 plays during vascular disease. One larger concept supported by my studies in conjunction with previously published McNamara Lab findings is that the disease-, tissue-, and cellular-context in which questions are asked and pursued is important. Further, recent advances in multi-dimensional approaches provide new opportunities to describe cellular populations at a deeper level. These approaches allow for discovery of novel cell populations and signaling pathways that are regulated by Id3. Finally, with my data and the prior two topics in mind, I will discuss the potential feasibility of Id3 as a therapeutic target and/or diagnostic biomarker in human disease and how these studies may inform some of these decisions.

I. Disease- and tissue-context is important

The role of the vasculature in disease pathogenesis varies depending on the tissue and disease in question. In some instances, augmentation of neovascularization or endothelium activation is beneficial, such as in the settings of ischemia or infection. In the absence of sufficient oxygen and nutrients, neovascularization is needed to adequately perfuse tissue to bring additional oxygen and nutrients. In the setting of infection, activation of endothelium to recruit in immune cells helps the individual clear the pathogen. However, in the setting of cancer, angiogenesis facilitates the growth of tumors and pro-angiogenic signals in the eye in people with diabetes can lead to retinopathy causing harm rather than healing. Results from our B cell- and EC-specific Id3 knockout studies contribute to this concept.

Id3 has distinct cell-specific roles in vascular disease

Prior studies demonstrate that loss of Id3 in B cells attenuates atherosclerosis, at least in part, by promoting the expansion of B-1b cells, which secrete IgM specific to oxidation-specific epitopes (OSEs) found on lipids both in the plaque and in circulation[30]. Increased levels of IgMs to OSEs protect against atherogenesis by binding to oxidized lipids and preventing formation of foam cells and induction of pro-inflammatory cytokines that further exacerbate atherogenesis[23]. Interestingly, my studies reveal that loss of Id3 in B cells attenuates protective neovascularization in ischemic skeletal muscle to promote perfusion. In this model, loss of Id3 promotes increased levels of IgM-secreting B-1b cells, but this correlates with worsened perfusion outcomes suggesting that these B-1b cells and IgM have detrimental effects in the

setting of HLI. Whether and how exactly IgM might be inhibiting neovascularization in response to ischemia still remains unclear. Early work suggests that it may at least in part be through direct effects of IgM on endothelial cells in the vasculature (**Chapter 3, Figure 3.14**).

Furthermore, our early atherosclerosis studies in the EC-specific Id3 KO mice suggest that Id3 in ECs is atheroprotective. However, loss of Id3 in ECs does not alter adipose tissue expansion (**Appendix 1, Figure A1.4**) nor tissue perfusion during HLI (Chapter 3). In the latter two disease models, angiogenesis plays a more central role in disease pathogenesis than in the setting of atherosclerosis. Id3 may promote EC signaling pathways more pivotal to large-artery diseases such as atherosclerosis but more precise experiments to test this are needed. There is also the consideration of tissue type in delineating the impact of Id3 in ECs on disease progression. EC characteristics are tissue-specific[190, 191], thus the regulatory signals that Id3 responds to in directing EC behavior may not be present or as prevalent in skeletal muscle or adipose tissue as they are in the aorta. Skeletal muscle and adipose tissue also depend on the microvascular for tissue perfusion and function and this could be another possible explanation for discrepancies between EC-specific Id3 effects.

II. Identifying novel mechanisms and cell populations in disease

Advances in cytometry and analytical techniques permit deeper characterization of cell populations

The use and advancement of techniques to collect and analyze large, multi-dimensional datasets is progressing rapidly. These approaches provide utility in identifying novel cellular subsets and biomarkers in disease, monitoring changes in cell populations over the course of disease progression, and understanding new signaling mechanisms in individual cells and cell populations. The basic research and clinical realms have identified progressive ways to use these approaches and they also demonstrate utility in advancing the studies presented in this document.

One such technology is mass cytometry or cytometry by time-of-flight (CyTOF). This approach uses heavy metal-conjugated antibodies and mass cytometry to characterize cell populations at a single-cell resolution using more parameters than currently permitted by traditional flow cytometry[192]. Studies can currently employ around 40 different metal-conjugated antibodies to characterize cell populations. Analytic techniques also exist to break

down, organize, and present this high-dimensional data in pragmatic and informative ways[193, 194]. CyTOF has been used to identify novel cellular subsets and biomarkers in disease, monitor changes in cell populations over the course of disease progression, and also determine the effects of treatments on cellular populations[195-197].

The technologies employed for RNA sequencing at the bulk- and single cell-level are also rapidly expanding and improving. Advancement of techniques to amplify small amounts of RNA transcripts have made single-cell sequencing more feasible. As a result, single-cell sequencing is a more appealing technique for many given the ability to assess cells at a single cell level rather than from a bulk, heterogeneous population. Analysis of these datasets have permitted deeper characterization of heterogeneous cell populations and mapping of cell fate trajectories[198-201].

Since there can be a disparity between the level of transcript and protein measured in a cell at any given time, there is one additional technique that incorporates sequencing with proteomics to quantify transcript and protein levels at the same time. BD's platform is known as Rhapsody and this technology employs oligonucleotide-conjugated antibodies and single-cell sequencing to both quantify the full transcriptome of a cell as well as the levels of proteins targeted by each oligo-conjugated antibody[202]. Early results using these approaches indeed confirm that RNA levels do not always track linearly with their corresponding protein in a cell demonstrating a unique utility for this approach for scientific discovery and also validation of how effectively sequencing approaches translate to proteomics. Overall, these approaches are rapidly improving and provide promise for both discovery and hypothesis-directed investigations related to the work presented in this dissertation.

Identifying novel cell populations in human disease

Results from our HLI studies implicate a role for B cells in regulating neovascularization during ischemia in skeletal muscle. To date, it is unclear if and which B cell populations may contribute to adaptive neovascularization in PAD patients. CyTOF can be used to begin understanding how B cells might be involved in human PAD and adaptive neovascularization during ischemia (ANDI). While obtaining muscle biopsies to look at muscle-resident B cell populations may be difficult, analysis of circulating B cells for differences in number and expression of proteins that may regulate their trafficking to skeletal muscle during ischemia

(such as chemokine receptors) may provide important insights. It is also possible that B cells may influence neovascular outcomes via secreted factors or Ig's or by stimulating other cell populations, such as monocytes, T cells, and macrophages that are also found in ischemic skeletal muscle. I propose that analysis of circulating B cells is a useful starting point for identifying novel B cell sub-populations in PAD and individuals with insufficient ANDI.

Identification of PAD-associated B cell populations can be achieved by comparing the B cell populations of PAD patients to age-, sex-, smoking status-, and type 2 diabetes-matched controls. Blood samples from these patients can be stained with the panel proposed in **Figure 5.1** and clustered based on B cell and progenitor markers. Following that, control and PAD samples can be compared to determine if the expression of activation markers, or the frequency of any B cell sub-populations change in the setting of PAD (**Figure 5.1**).

Figure 5.1.

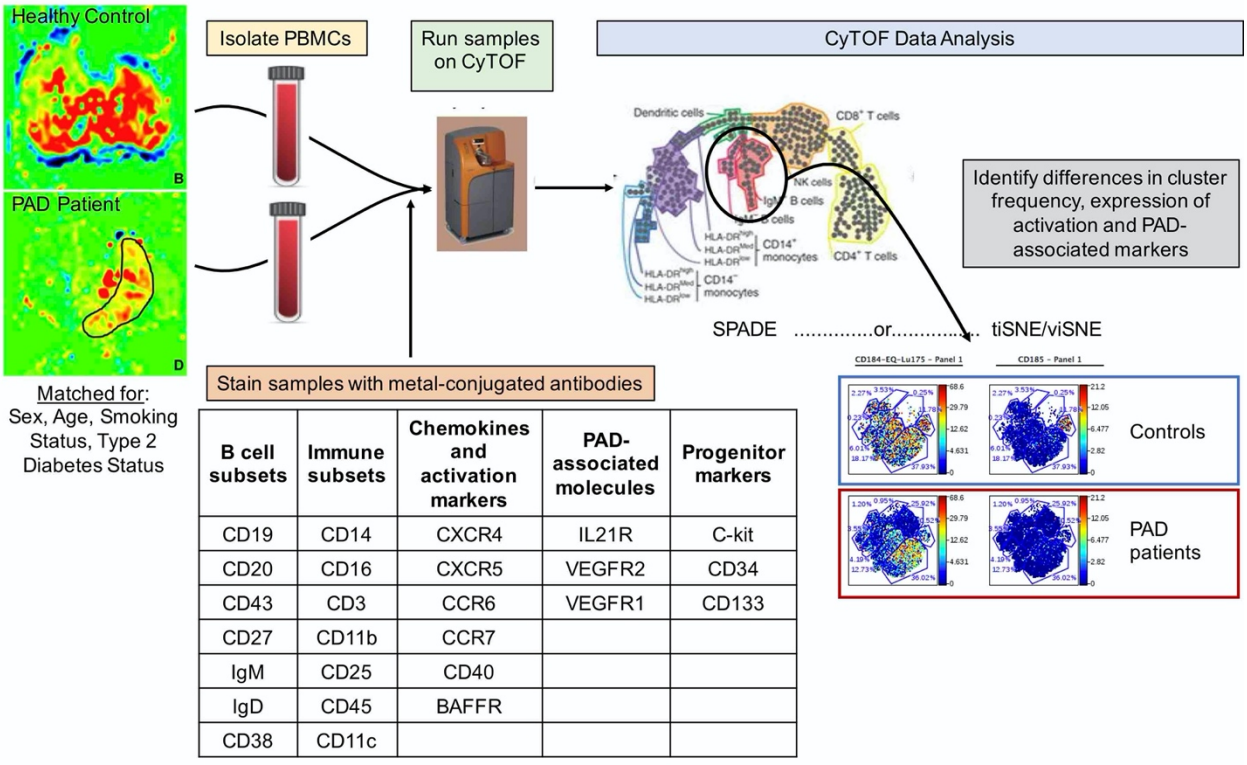

B cell subsets	Immune subsets	Chemokines and activation markers	PAD-associated molecules	Progenitor markers
CD19	CD14	CXCR4	IL21R	C-kit
CD20	CD16	CXCR5	VEGFR2	CD34
CD43	CD3	CCR6	VEGFR1	CD133
CD27	CD11b	CCR7		
IgM	CD25	CD40		
IgD	CD45	BAFFR		
CD38	CD11c			

Figure 5.1. Schematic of CyTOF staining and analysis of PAD and control PBMCs. ASL images in upper left-hand corner were adopted from Lopez *et al*[203]. CyTOF analysis images are from previous analysis conducted by Chantel McSkimming and Hema Kothari.

An additional approach would be to compare cell populations amongst PAD patients with varying disease severity. For example, PAD patients with intermittent claudication (IC)

may be compared to critical limb ischemia (CLI) patients, who arguably have reduced ANDI, to identify populations that may change in the presence of more severe disease (CLI). We have an ongoing collaboration with Dr. Christopher Kramer in Cardiovascular Medicine at UVA to collect blood samples from PAD patients whose reperfusion capacity is quantified by arterial spin labeling (ASL)[203]. ASL is a cardiovascular magnetic resonance imaging technique that enhances the ability to detect arterial blood flow without utilizing a contrast agent. This technique also allows both spatial and temporal resolution of perfusion. Dr. Kramer uses ASL to quantify perfusion in response to an ischemic event by applying a cuff to the leg of the participant temporarily. Upon release of the cuff, agent is administered and perfusion in the skeletal muscle of the lower limb is imaged and later quantified. This allows Dr. Kramer to quantify the magnitude and speed with which patients' muscles perfuse following an ischemic event. Reduced perfusion reflects the extent of vascularization in the tissue and potential vascular dysfunction that may prevent blood flow through existing vessels. The upper left panels of **Figure 5.1** are the resultant images reflecting the extent of perfusion in healthy and PAD patients. The goal with this study is to identify novel populations of B cells or markers on a subset of B cells that correlate with ANDI that can be determined by perfusion capacity following an acute ischemic episode.

One potential population to investigate is B cells expressing progenitor markers such as CD34 or c-Kit or angiogenic markers such as VEGFR2 or CXCR4. CD34, c-Kit, VEGFR2, and CXCR4 have all been identified on putative circulating "endothelial progenitor cells" (EPCs) or "circulating angiogenic progenitor cells" (CACs)[204-206]. Due to limited use of other cell subsetting markers, the true identity of these populations remains unclear. However, a published study from 1991 demonstrated that human B cell populations from bone marrow and the blood express CD34[207] suggesting that at least some of these EPC/CACs may be B cells. Furthermore, a recently published study from Steffen *et al.* demonstrates that many Sca-1^{+}VEGFR2^{+} "EPCs" found in circulation in mice during vascular injury are $CD45^{+}CD19^{+}$[208] demonstrating that what was previously considered an EPC could in fact be circulating leukocytes such as a B cell. In a study from Hayek *et al*., reduced numbers of circulating $CD34^{+}$VEGFR2^{+} cells correlated with increased risk of PAD diagnosis or -associated events in a cohort[209] demonstrating a potential role for these circulating "pro-angiogenic" cells in PAD and ANDI.

These studies would provide useful data for generating new hypotheses and identifying potential new biomarkers for PAD and reduced ANDI. However, follow-up studies using larger cohorts of patients and pursuing potential mechanisms whereby the identified populations or proteins change with disease will also be necessary to determine their utility as biomarker or therapeutic targets.

Identifying novel signals and cellular characteristics regulated by Id3

CyTOF and RNA sequencing approaches can also be applied to our cell-specific Id3 KO mice of interest to identify cell populations and signaling pathways that may be regulated by Id3 in the setting of atherosclerosis or ischemia. In the context of atherosclerosis, Id3 WT and Id3 KO ECs can be sequenced or stained for CyTOF analysis following an atherogenic stimulus such as a short-term WD feeding or *ex vivo* treatment with pro-inflammatory cytokines and oxidized lipids (**Figure 5.2**). Because the populations isolated from mouse aortas will be very heterogeneous, CyTOF or a single-cell sequencing approach will be optimal to ensure accurate identification of ECs. Some potential pathways that Id3 may be interacting with in ECs were proposed in Chapter 4 (**Chapter 4, Figure 4.9**). These and others will guide development of a CyTOF panel that can be used to assess EC characteristics in $Id3^{ECWT}$ and $Id3^{ECKO}$ mice (**Figure 5.2**).

Graduate student Chris Henderson in the McNamara lab is also optimizing induced pluripotent stem cell (iPSC) cultures and CRISPR-Cas9 constructs to generate Id3 WT and Id3 KO stem cells as well as those expressing the major and minor alleles of ID3 SNP rs11574. We have successfully differentiated these cells into ECs and thus, this may serve as a useful tool in testing changes in EC characteristics and signaling pathways in the absence of Id3. Bulk RNA sequencing may be applied to this setting as the cells are less heterogeneous than the primary cell experiments previously proposed. Overall, these approaches will permit unbiased and/or directed investigation into changes in protein expression and signaling pathway activation in response to changes in Id3 expression.

Figure 5.2.

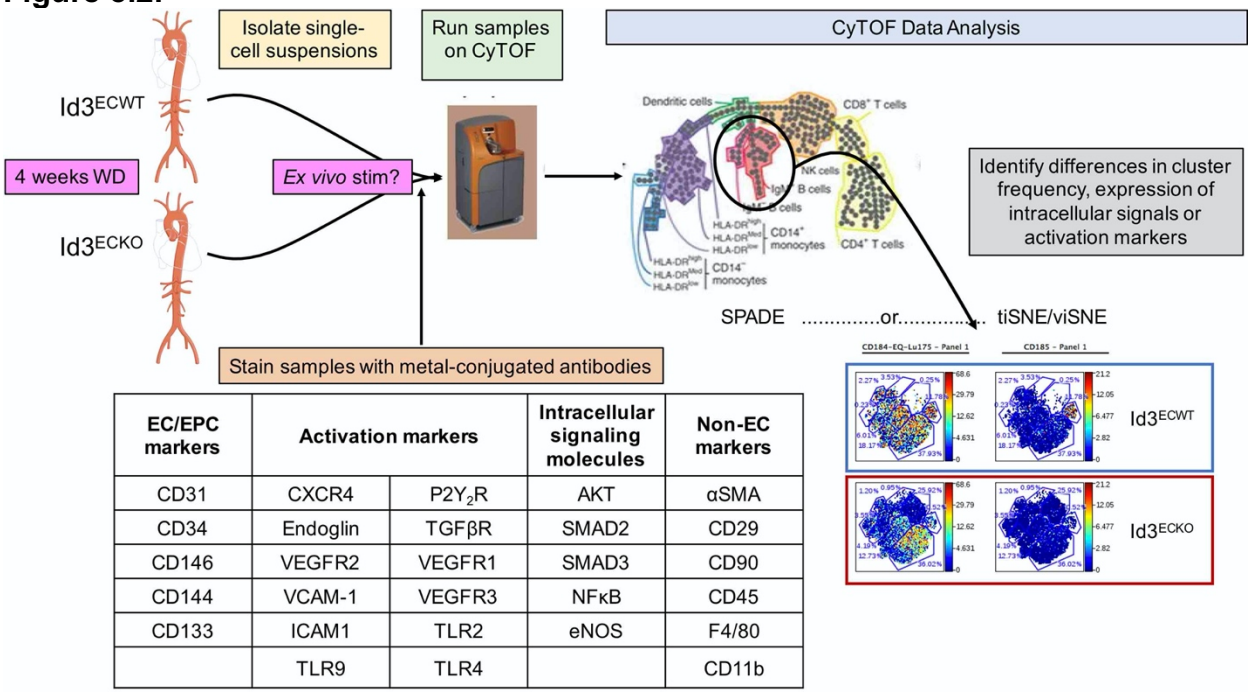

EC/EPC markers	Activation markers		Intracellular signaling molecules	Non-EC markers
CD31	CXCR4	$P2Y_2R$	AKT	αSMA
CD34	Endoglin	TGFβR	SMAD2	CD29
CD146	VEGFR2	VEGFR1	SMAD3	CD90
CD144	VCAM-1	VEGFR3	NFκB	CD45
CD133	ICAM1	TLR2	eNOS	F4/80
	TLR9	TLR4		CD11b

Figure 5.2. Schematic EC Id3 KO CyTOF staining and analysis.
CyTOF analysis images are from previous analysis conducted by Chantel McSkimming and Hema Kothari.

III. Id3: A good therapeutic target or diagnostic marker?

Finally, it is worthwhile to consider whether Id3 may serve as an effective therapeutic target and/or diagnostic biomarker based on my findings and our general knowledge of Id3. Id3 has emerged as an important regulator in multiple diseases including atherosclerosis[30, 120, 129-131], cancer[123, 125, 128, 174, 175], and obesity[122, 127, 138, 210]. Generally, it is induced by many stimuli relevant in disease progression and is also expressed broadly amongst cell and tissue types. Cell-specific knockout studies suggest that it may have contradicting roles in the same disease, such as atherosclerosis, depending on the cell type in which it is knocked out. Thus, targeted delivery would be needed to effectively use Id3 as a therapeutic target.

There are many questions to consider on this matter. Would blocking or inducing Id3 expression effectively attenuate CVD symptoms? How does one target Id3 to treat CVD symptoms? Is there are a way to specifically target Id3 expression in certain cell types? What about using Id3 as a biomarker for disease onset or severity? Id3 expression in the setting of cancer serves as a good example of how it might be used as a biomarker[211, 212]. Id1 and Id3

have been shown to promote cancer cell proliferation and increased expression of these proteins correlates with worsened prognosis[211, 212]. Thus, in certain cases, patient samples can be analyzed for the extent of Id3 expression to assess the risk-level of the patient. Additionally, it is important to consider the challenges to targeting or interpreting Id3 as a biomarker. Initial studies to determine feasibility in human cohorts may also need to be conducted.

Approaches and Challenges to Targeting Id3

One way to target Id3 activity is by controlling expression levels of the gene. This can be done by delivering a short hairpin RNA (shRNA) to inhibit Id3 expression or a small expression plasmid to promote expression of Id3. Techniques to load nucleotides in liposomes has advanced and can effectively deliver gene-modifying compounds to cells *in vivo*[213]. Furthermore, results from our collaborative project with the Boucher, Kelly, and Klibanov labs reveal that most cell types are capable to taking up liposomes to different extents (Appendix 2). Because of this, a more targeted approach should be employed. The use of phage display to identify peptides that bind specifically to a certain cell type or protein has been successful and may prove effective for this objective[214, 215]. Additionally, contradicting outcomes from cell-specific knockouts of Id3 suggest that the directionality in which Id3 will regulate CVD pathogenesis is cell type-dependent. Broad non-specific delivery may not be effective or may cause untoward effects further supporting development of cell-specific targeting approaches.

There are a few additional challenges and caveats to consider. First, our data as well as what has already been in the literature suggests that phagocytes and the reticulendothelial system (especially the spleen and liver) most efficiently take up liposomes[216-218]. A liposome will need to be designed in a way to potentially reduce some of this uptake to make more particles available for uptake by our cell(s) of interest. Adding polyethylene glycol (PEG) is an effective way of slowing down phagocytosis of liposomes, but our data demonstrates that uptake will inevitably occur. Second, thorough evaluation of liposome biodistribution over time will be needed to confidently determine where liposomes are taken up and when. Data from our studies shows that immediate uptake of liposomes is distinct from later uptake. Liposome localization and side effects after chronic dosing will be needed to ensure that targeting is effective and untoward effects are minimized. These types of studies are costly and time-

consuming, so thorough planning to ensure testing is executed in the proper sequence and at adequate time points will be needed.

Oligonucleotides can also be targeted without liposome-encapsulation. Won *et al*. demonstrated effective delivery of an shRNA to *Fabp4* using an adipose-specific peptide conjugated to a D-form 9-arginine construct, which serves as a carrier for shRNA oligonucleotides[219]. Treatment attenuated *Fabp4* expression in adipose tissue and improved metabolic outcomes in a model of obesity-associated dysmetabolism. Using an approach such as this may be a promising alternative to liposomal delivery. Additional studies utilizing the ATS-9R construct to target other transcriptional regulatory elements have also been conducted successfully. Chung *et al*. delivered a CRISPR interference (CRISPRi) construct consisting of a catalytically inactive Cas9 and a single guide RNA to the *Fabp4* gene to inhibit *Fabp4* expression in adipose tissue[220]. This too attenuated dysmetabolism associated with obesity. Targeting delivery of nucleotide constructs with a peptide-9-arginine system may be an even more effective means of targeting Id3 expression *in vivo*.

Small molecule inhibitors are another possible approach for inhibiting Id3 activity. To date, no Id3-specific inhibitors have been developed, however. AGX51 is a pan-Id inhibitor that attenuates ocular neovascularization[221]. Unfortunately, this molecule is not specific to Id3 and thus could induce untoward effects due to inhibition of other Id's. A study from the McNamara lab in 2004 did, however, demonstrate that phosphorylation of Id3 at a serine residue (Ser5) promotes Id3 activity[121]. Phosphorylation of Id3 at Ser5 results in increased proliferation of vascular smooth muscle cells (VSMCs) and attenuation of $p21^{Cip1}$ expression due to inhibitory interactions between Id3 and E-protein binding partners. Thus, development of a small molecule that can inhibit the phosphorylation of Id3 at Ser5 is one potential way to block Id3 activity.

Finally, it is important to consider that Id3 is a transcription factor that interacts with multiple transcriptional binding partners that each regulates a different set of genes. Thus, it is upstream of many cellular processes and this can make it challenging to target Id3 and perhaps some of its downstream effects without also inducing unwanted side effects. From this perspective, it may be difficult to consider Id3 as a promising therapeutic target. Rather, it may be useful as a tool in basic, mechanistic research to identify altered downstream pathways that are protective or pathogenic in the setting of CVD. Approaches such as RNA sequencing and

CyTOF that generate large datasets and allow unbiased inquiries into signaling pathways and cell characteristics during disease perturbations will serve useful in tools in this endeavor.

Id3 as a Potential Diagnostic Marker

While it is yet untested whether Id3 can serve as an effective therapeutic target, findings from the McNamara lab and other suggest it can serve as a useful biomarker for disease severity. For example, ID3 expression is upregulated in multiple forms of cancer and leads to increased cell proliferation and tumor growth[211, 212]. It is thus used as a biomarker to indicate a higher risk cancer. Inhibition of Id3 family member Id1 in experimental settings has proven to be effective at attenuating tumor growth and severity[211]. The Id3 SNP rs11574 is associated with altered indices of CVD severity. Expression of the minor allele of this SNP (Id3105T) results in attenuated interactions specifically with its binding partner E12. Id3105T also correlates with worsened indices of CVD: increased carotid intima-media thickness (cIMT)[130] and increased coronary artery calcium (CAC)[131].

Many risk scores exist for predicting cardiovascular morbidity and mortality associated with atherosclerosis including the Framingham Risk Score[222], the Systemic Coronary Risk Evaluation (SCORE)[223], and the SYNTAX score[224]. Each score is tailored to a slightly different population of atherosclerosis patients whether that is a specific age group, presence or absence of previous myocardial infarctions, or other factors. Further, none of these incorporate gene or SNP expression, though there is an established genetic component to this disease[225, 226]. Findings from our lab suggest that genotyping for the Id3 SNP may provide an additional useful variable to improve the capacity for predicting atherosclerosis risk.

Id3105T may also serve as a useful marker for PAD risk. Indeed, our murine studies demonstrate that global knockout of Id3 attenuates skeletal muscle perfusion during HLI (Chapter 3). To begin addressing this question, initial association analyses were run to determine if expression of Id3105T correlated with a lower average ankle-brachial index (ABI). This was done with in collaboration with Josyf Mychaleckyj from the Center for Public Health Genomics at UVA. Values from the Multi-Ethnic Study of Atherosclerosis (MESA) were used in the analysis. An individual is determined to have PAD if they have an ABI of less than 0.9. MESA is a longitudinal study collecting blood samples and clinical information from participants at multiple exams occurring over time. ABI's were measured during the first and fifth exams of

MESA. We found that there was no association between expression of Id3105T and ABI levels either at the initial exam or when the change in ABI was measured from exam 1 to exam 5 (**Table 5.1**).

Table 5.1. Early investigation into ID3 SNP rs11574 expression and ABI measurements. Data from MESA was used to quantify the association between expression of the minor allele of ID3 SNP rs11574 and ABI values. ∆ABI is defined as the change in ABI per subject from exam 1 to exam 5. ABI = ankle-brachial index, CAU = Caucasian, AFA = African American, N = number of subjects Beta = effect size estimate, SE = standard error.

Phenotype	Race Group	N	Beta	SE	*P*-value
ABI (exam1 = baseline)	CAU	2400	0.0026	0.004	0.53
	AFA	2458	-0.001	0.001	0.90
ΔABI (exam 5 – exam 1)	CAU	1678	0.0033	0.0062	0.59
	AFA	981	-0.022	0.017	0.20

However, these findings highlight some important factors to consider when conducting analyses like this. First, Criqui and Aboyans point out that while ABI measurements have a high specificity for diagnosing PAD, the sensitivity of this approach is lower[227]. This means the rate of false-negative diagnoses is higher than it should be. Thus, we may not be accounting for all subjects with PAD in this cohort and the population with high ABI's may not be completely free of PAD. Additionally, ABI does not correlate with time to claudication or maximal claudication[228]. Unfortunately, this was the only clinical readout for PAD collected in MESA. Angiography is considered the gold standard for diagnosing PAD, thus, finding a large database with this readout for PAD diagnosis would be ideal for conducting a study. However, further assays to quantify distal tissue perfusion (such as ASL) and severity of disease (IC and CLI diagnoses) are also needed to discern between patients with and without adequate ANDI. While there are a few studies suggesting a genetic component to PAD development, the strongest risk factor for PAD is smoking. Kullo and Leeper suggest that it is difficult to identify genes associated with PAD development because of the strong environmental influence on this disease[229]. While two patients may have been exposed to similar environmental factors and developed comparable macrovascular blockages, they will not necessarily have comparable ANDI and resultant symptoms. By utilizing disease severity diagnostics and ASL,

we may better resolve the influence of genetics on the severity and progression of PAD. A powered study with initial angiography diagnoses, disease severity diagnostics, and ASL would be ideal to determine if Id3105T is more frequently expressed in patients with PAD and or PAD patients with maladaptive neovascularization.

Finally, findings from cell-specific Id3 KO studies raise the question of the effectiveness of studies correlating Id3105T expression with disease burden in humans. Since the SNP is in the germline, it is present in all cells, making it difficult to determine how Id3105T may be influencing behaviors in individual cell types in the body. Cell-specific studies in mice demonstrate loss of Id3 in certain cell types (non-bone marrow-derived cells, ECs) augments atherosclerosis development, while it attenuates atherosclerosis in other settings (B cells, other bone marrow-derived cells)[30, 129]. If findings from my studies (Chapter 3) translate to human disease, expression of the Id3105T in B cells attenuates ANDI during PAD, while Id3105T expression in macrophages and ECs do not affect the ANDI. Thus, expression of the Id3105T in PAD patients may then only demonstrate an association with greater disease severity and inadequate ANDI if the frequency of B cells in that patient is higher, or the capacity for their B cells to localize to skeletal muscle are greater. In order to parse out these complex mechanism, more thorough characterization of each patient is required. Coupling the genotype of the ID3 SNP rs11574 with characterization of circulating immune cells using CyTOF in a population of PAD and control patients may better inform us on the potential for Id3105T to be used as a biomarker in conjunction with other biomarkers. These studies raise interesting questions concerning whether ID3 can be used to predict CVD burden and risk, but it is clear that further investigation is needed before they can be implemented.

IV. Summary

In total, these studies have demonstrated novel cell-specific roles for Id3 in the development of vascular disease. The McNamara lab has previously established a strong rationale for continued study into the roles Id3 plays in regulating cardiovascular disease development. Results from these studies provide new directions along which to investigate how Id3 regulates vascular disease. We have implicated B cells as a new cell type that regulates adaptive neovascularization during skeletal muscle ischemia and an important molecular mediator of their effects: Id3. Early studies suggest a role for EC-specific Id3 in attenuating atherosclerosis development as well. Continued investigation into the mechanisms behind these observed

effects could provide us with novel therapeutic targets or biomarkers for PAD and/or atherosclerosis. However, it is clear that further inquiries into the expression of Id3 and the presence and characterization of B cell populations during human CVD are needed as well. Continued advancements in our understanding of basic cellular and molecular mechanisms coupled with the progression of research techniques such as CyTOF and single-cell sequencing make these inquiries possible and further spark a sense of excitement as the ever-present drive to understand, treat, and prevent human disease continues.

Chapter 6: Literature Cited

1. Benjamin EJ, Muntner P, Alonso A, Bittencourt MS, Callaway CW, Carson AP, Chamberlain AM, Chang AR, Cheng S, Das SR, Delling FN, Djousse L, Elkind MSV, Ferguson JF, Fornage M, Jordan LC, Khan SS, Kissela BM, Knutson KL, Kwan TW, Lackland DT, Lewis TT, Lichtman JH, Longenecker CT, Loop MS, Lutsey PL, Martin SS, Matsushita K, Moran AE, Mussolino ME, O'Flaherty M, Pandey A, Perak AM, Rosamond WD, Roth GA, Sampson UKA, Satou GM, Schroeder EB, Shah SH, Spartano NL, Stokes A, Tirschwell DL, Tsao CW, Turakhia MP, VanWagner LB, Wilkins JT, Wong SS, Virani SS, American Heart Association Council on E, Prevention Statistics C and Stroke Statistics S. Heart Disease and Stroke Statistics-2019 Update: A Report From the American Heart Association. *Circulation*. 2019;139:e56-e528.
2. Heron M. Deaths: Leading Causes for 2017. *National Vital Statistics Reports*. 2019;68:76.
3. Stoekenbroek RM, Hartgers ML, Rutte R, de Wijer DD, Stroes ESG and Hovingh GK. PCSK9 inhibitors in clinical practice: Delivering on the promise? *Atherosclerosis*. 2018;270:205-210.
4. Wang Y and Liu ZP. PCSK9 Inhibitors: Novel Therapeutic Strategies for Lowering LDLCholesterol. *Mini Rev Med Chem*. 2019;19:165-176.
5. Ridker PM, Everett BM, Thuren T, MacFadyen JG, Chang WH, Ballantyne C, Fonseca F, Nicolau J, Koenig W, Anker SD, Kastelein JJP, Cornel JH, Pais P, Pella D, Genest J, Cifkova R, Lorenzatti A, Forster T, Kobalava Z, Vida-Simiti L, Flather M, Shimokawa H, Ogawa H, Dellborg M, Rossi PRF, Troquay RPT, Libby P, Glynn RJ and Group CT. Antiinflammatory Therapy with Canakinumab for Atherosclerotic Disease. *N Engl J Med*. 2017;377:1119-1131.
6. Viana-Huete V and Fuster JJ. Potential Therapeutic Value of Interleukin 1b-targeted Strategies in Atherosclerotic Cardiovascular Disease. *Rev Esp Cardiol (Engl Ed)*. 2019;72:760-766.
7. Hiatt WR, Goldstone J, Smith SC, Jr., McDermott M, Moneta G, Oka R, Newman AB, Pearce WH and American Heart Association Writing G. Atherosclerotic Peripheral Vascular Disease Symposium II: nomenclature for vascular diseases. *Circulation*. 2008;118:2826-9.
8. Hansson GK, Libby P and Tabas I. Inflammation and plaque vulnerability. *J Intern Med*. 2015;278:483-93.
9. Shah PK, Falk E, Badimon JJ, Fernandez-Ortiz A, Mailhac A, Villareal-Levy G, Fallon JT, Regnstrom J and Fuster V. Human monocyte-derived macrophages induce collagen breakdown in fibrous caps of atherosclerotic plaques. Potential role of matrix-degrading metalloproteinases and implications for plaque rupture. *Circulation*. 1995;92:1565-9.
10. Fryar CD, Chen TC and Li X. Prevalence of uncontrolled risk factors for cardiovascular disease: United States, 1999-2010. *NCHS Data Brief*. 2012:1-8.
11. Nakashima Y, Raines EW, Plump AS, Breslow JL and Ross R. Upregulation of VCAM-1 and ICAM-1 at atherosclerosis-prone sites on the endothelium in the ApoE-deficient mouse. *Arterioscler Thromb Vasc Biol*. 1998;18:842-51.
12. Gimbrone MA, Jr. and Garcia-Cardena G. Endothelial Cell Dysfunction and the Pathobiology of Atherosclerosis. *Circ Res*. 2016;118:620-36.
13. Galkina E and Ley K. Vascular adhesion molecules in atherosclerosis. *Arterioscler Thromb Vasc Biol*. 2007;27:2292-301.
14. Hansson GK and Hermansson A. The immune system in atherosclerosis. *Nat Immunol*. 2011;12:204-12.
15. Ilhan F and Kalkanli ST. Atherosclerosis and the role of immune cells. *World J Clin Cases*. 2015;3:345-52.

16. Winkels H, Ehinger E, Vassallo M, Buscher K, Dinh HQ, Kobiyama K, Hamers AAJ, Cochain C, Vafadarnejad E, Saliba AE, Zernecke A, Pramod AB, Ghosh AK, Anto Michel N, Hoppe N, Hilgendorf I, Zirlik A, Hedrick CC, Ley K and Wolf D. Atlas of the Immune Cell Repertoire in Mouse Atherosclerosis Defined by Single-Cell RNA-Sequencing and Mass Cytometry. *Circ Res*. 2018;122:1675-1688.
17. Sedding DG, Boyle EC, Demandt JAF, Sluimer JC, Dutzmann J, Haverich A and Bauersachs J. Vasa Vasorum Angiogenesis: Key Player in the Initiation and Progression of Atherosclerosis and Potential Target for the Treatment of Cardiovascular Disease. *Front Immunol*. 2018;9:706.
18. Tabas I, Garcia-Cardena G and Owens GK. Recent insights into the cellular biology of atherosclerosis. *J Cell Biol*. 2015;209:13-22.
19. Shankman LS, Gomez D, Cherepanova OA, Salmon M, Alencar GF, Haskins RM, Swiatlowska P, Newman AA, Greene ES, Straub AC, Isakson B, Randolph GJ and Owens GK. KLF4-dependent phenotypic modulation of smooth muscle cells has a key role in atherosclerotic plaque pathogenesis. *Nat Med*. 2015;21:628-37.
20. Chen PY and Simons M. Fibroblast growth factor-transforming growth factor beta dialogues, endothelial cell to mesenchymal transition, and atherosclerosis. *Curr Opin Lipidol*. 2018;29:397-403.
21. Chistiakov DA, Melnichenko AA, Myasoedova VA, Grechko AV and Orekhov AN. Mechanisms of foam cell formation in atherosclerosis. *J Mol Med (Berl)*. 2017;95:1153-1165.
22. Srikakulapu P and McNamara CA. B cells and atherosclerosis. *Am J Physiol Heart Circ Physiol*. 2017;312:H1060-H1067.
23. Srikakulapu P, Upadhye A, Rosenfeld SM, Marshall MA, McSkimming C, Hickman AW, Mauldin IS, Ailawadi G, Lopes MBS, Taylor AM and McNamara CA. Perivascular Adipose Tissue Harbors Atheroprotective IgM-Producing B Cells. *Front Physiol*. 2017;8:719.
24. Baumgarth N. The double life of a B-1 cell: self-reactivity selects for protective effector functions. *Nat Rev Immunol*. 2011;11:34-46.
25. Hardy RR and Hayakawa K. B cell development pathways. *Annu Rev Immunol*. 2001;19:595-621.
26. Baumgarth N, Herman OC, Jager GC, Brown L, Herzenberg LA and Herzenberg LA. Innate and acquired humoral immunities to influenza virus are mediated by distinct arms of the immune system. *Proc Natl Acad Sci U S A*. 1999;96:2250-5.
27. Griffin DO, Holodick NE and Rothstein TL. Human B1 cells in umbilical cord and adult peripheral blood express the novel phenotype CD20+ CD27+ CD43+ CD70. *J Exp Med*. 2011;208:67-80.
28. Rothstein TL, Griffin DO, Holodick NE, Quach TD and Kaku H. Human B-1 cells take the stage. *Ann N Y Acad Sci*. 2013;1285:97-114.
29. Rothstein TL and Quach TD. The human counterpart of mouse B-1 cells. *Ann N Y Acad Sci*. 2015;1362:143-52.
30. Rosenfeld SM, Perry HM, Gonen A, Prohaska TA, Srikakulapu P, Grewal S, Das D, McSkimming C, Taylor AM, Tsimikas S, Bender TP, Witztum JL and McNamara CA. B-1b Cells Secrete Atheroprotective IgM and Attenuate Atherosclerosis. *Circ Res*. 2015;117:e28-39.
31. Hardman RL, Jazaeri O, Yi J, Smith M and Gupta R. Overview of classification systems in peripheral artery disease. *Semin Intervent Radiol*. 2014;31:378-88.
32. Gerhard-Herman MD, Gornik HL, Barrett C, Barshes NR, Corriere MA, Drachman DE, Fleisher LA, Fowkes FG, Hamburg NM, Kinlay S, Lookstein R, Misra S, Mureebe L, Olin JW, Patel RA, Regensteiner JG, Schanzer A, Shishehbor MH, Stewart KJ, Treat-Jacobson D and

Walsh ME. 2016 AHA/ACC Guideline on the Management of Patients With Lower Extremity Peripheral Artery Disease: Executive Summary: A Report of the American College of Cardiology/American Heart Association Task Force on Clinical Practice Guidelines. *Circulation*. 2017;135:e686-e725.
33. Annex BH. Therapeutic angiogenesis for critical limb ischaemia. *Nat Rev Cardiol*. 2013;10:387-96.
34. Annex BH and Beller GA. Towards the Development of Novel Therapeutics for Peripheral Artery Disease. *Trans Am Clin Climatol Assoc*. 2016;127:224-234.
35. Cohen RA, Murdoch CE, Watanabe Y, Bolotina VM, Evangelista AM, Haeussler DJ, Smith MD, Mei Y, Tong X, Han J, Behring JB, Bachschmid MM and Matsui R. Endothelial Cell Redox Regulation of Ischemic Angiogenesis. *J Cardiovasc Pharmacol*. 2016;67:458-64.
36. Lee JW, Ko J, Ju C and Eltzschig HK. Hypoxia signaling in human diseases and therapeutic targets. *Exp Mol Med*. 2019;51:68.
37. Schioppa T, Uranchimeg B, Saccani A, Biswas SK, Doni A, Rapisarda A, Bernasconi S, Saccani S, Nebuloni M, Vago L, Mantovani A, Melillo G and Sica A. Regulation of the chemokine receptor CXCR4 by hypoxia. *J Exp Med*. 2003;198:1391-402.
38. Schutyser E, Su Y, Yu Y, Gouwy M, Zaja-Milatovic S, Van Damme J and Richmond A. Hypoxia enhances CXCR4 expression in human microvascular endothelial cells and human melanoma cells. *Eur Cytokine Netw*. 2007;18:59-70.
39. Yeo EJ. Special issue on hypoxia. *Exp Mol Med*. 2019;51:69.
40. Semenza GL. Hypoxia-inducible factor 1 and cardiovascular disease. *Annu Rev Physiol*. 2014;76:39-56.
41. Zimna A and Kurpisz M. Hypoxia-Inducible Factor-1 in Physiological and Pathophysiological Angiogenesis: Applications and Therapies. *Biomed Res Int*. 2015;2015:549412.
42. Boone BA and Lotze MT. Targeting damage-associated molecular pattern molecules (DAMPs) and DAMP receptors in melanoma. *Methods Mol Biol*. 2014;1102:537-52.
43. Rosin DL and Okusa MD. Dangers within: DAMP responses to damage and cell death in kidney disease. *J Am Soc Nephrol*. 2011;22:416-25.
44. Murad S. Toll-like receptor 4 in inflammation and angiogenesis: a double-edged sword. *Front Immunol*. 2014;5:313.
45. Wu J, Cui H, Dick AD and Liu L. TLR9 agonist regulates angiogenesis and inhibits corneal neovascularization. *Am J Pathol*. 2014;184:1900-10.
46. Jeong J, Lee J, Lim J, Cho S, An S, Lee M, Yoon N, Seo M, Lim S and Park S. Soluble RAGE attenuates AngII-induced endothelial hyperpermeability by disrupting HMGB1-mediated crosstalk between AT1R and RAGE. *Exp Mol Med*. 2019;51:113.
47. Ferrara N. VEGF-A: a critical regulator of blood vessel growth. *Eur Cytokine Netw*. 2009;20:158-63.
48. Hoeben A, Landuyt B, Highley MS, Wildiers H, Van Oosterom AT and De Bruijn EA. Vascular endothelial growth factor and angiogenesis. *Pharmacol Rev*. 2004;56:549-80.
49. Adams RH and Alitalo K. Molecular regulation of angiogenesis and lymphangiogenesis. *Nat Rev Mol Cell Biol*. 2007;8:464-78.
50. Edgar LT, Hoying JB, Utzinger U, Underwood CJ, Krishnan L, Baggett BK, Maas SA, Guilkey JE and Weiss JA. Mechanical interaction of angiogenic microvessels with the extracellular matrix. *J Biomech Eng*. 2014;136:021001.
51. Petit I, Jin D and Rafii S. The SDF-1-CXCR4 signaling pathway: a molecular hub modulating neo-angiogenesis. *Trends Immunol*. 2007;28:299-307.

52. Pitulescu ME, Schmidt I, Giaimo BD, Antoine T, Berkenfeld F, Ferrante F, Park H, Ehling M, Biljes D, Rocha SF, Langen UH, Stehling M, Nagasawa T, Ferrara N, Borggrefe T and Adams RH. Dll4 and Notch signalling couples sprouting angiogenesis and artery formation. *Nat Cell Biol*. 2017;19:915-927.
53. Nunez-Gomez E, Pericacho M, Ollauri-Ibanez C, Bernabeu C and Lopez-Novoa JM. The role of endoglin in post-ischemic revascularization. *Angiogenesis*. 2017;20:1-24.
54. Limbourg FP, Takeshita K, Radtke F, Bronson RT, Chin MT and Liao JK. Essential role of endothelial Notch1 in angiogenesis. *Circulation*. 2005;111:1826-32.
55. Moya IM, Umans L, Maas E, Pereira PN, Beets K, Francis A, Sents W, Robertson EJ, Mummery CL, Huylebroeck D and Zwijsen A. Stalk cell phenotype depends on integration of Notch and Smad1/5 signaling cascades. *Dev Cell*. 2012;22:501-14.
56. Jazwa A, Florczyk U, Grochot-Przeczek A, Krist B, Loboda A, Jozkowicz A and Dulak J. Limb ischemia and vessel regeneration: Is there a role for VEGF? *Vascul Pharmacol*. 2016;86:18-30.
57. Brevetti G, Giugliano G, Brevetti L and Hiatt WR. Inflammation in peripheral artery disease. *Circulation*. 2010;122:1862-75.
58. Ridker PM, Cushman M, Stampfer MJ, Tracy RP and Hennekens CH. Plasma concentration of C-reactive protein and risk of developing peripheral vascular disease. *Circulation*. 1998;97:425-8.
59. Liang KP, Liang KV, Matteson EL, McClelland RL, Christianson TJ and Turesson C. Incidence of noncardiac vascular disease in rheumatoid arthritis and relationship to extraarticular disease manifestations. *Arthritis Rheum*. 2006;54:642-8.
60. Shireman PK. The chemokine system in arteriogenesis and hind limb ischemia. *J Vasc Surg*. 2007;45 Suppl A:A48-56.
61. Klotzsche-von Ameln A, Cremer S, Hoffmann J, Schuster P, Khedr S, Korovina I, Troullinaki M, Neuwirth A, Sprott D, Chatzigeorgiou A, Economopoulou M, Orlandi A, Hain A, Zeiher AM, Deussen A, Hajishengallis G, Dimmeler S, Chavakis T and Chavakis E. Endogenous developmental endothelial locus-1 limits ischaemia-related angiogenesis by blocking inflammation. *Thromb Haemost*. 2017;117:1150-1163.
62. Ridiandries A, Tan JT and Bursill CA. The Role of CC-Chemokines in the Regulation of Angiogenesis. *Int J Mol Sci*. 2016;17.
63. Chen Y, Zheng Y, Liu L, Lin C, Liao C, Xin L, Zhong S, Cheng Q and Zhang L. Adiponectin Inhibits TNF-alpha-Activated PAI-1 Expression Via the cAMP-PKA-AMPK-NF-kappaB Axis in Human Umbilical Vein Endothelial Cells. *Cell Physiol Biochem*. 2017;42:2342-2352.
64. Hu L, Zang MD, Wang HX, Li JF, Su LP, Yan M, Li C, Yang QM, Liu BY and Zhu ZG. Biglycan stimulates VEGF expression in endothelial cells by activating the TLR signaling pathway. *Mol Oncol*. 2016;10:1473-1484.
65. Xu J, Benabou K, Cui X, Madia M, Tzeng E, Billiar T, Watkins S and Sachdev U. TLR4 Deters Perfusion Recovery and Upregulates Toll-like Receptor 2 (TLR2) in Ischemic Skeletal Muscle and Endothelial Cells. *Mol Med*. 2015;21:605-15.
66. Nishimoto S, Aini K, Fukuda D, Higashikuni Y, Tanaka K, Hirata Y, Yagi S, Kusunose K, Yamada H, Soeki T, Shimabukuro M and Sata M. Activation of Toll-Like Receptor 9 Impairs Blood Flow Recovery After Hind-Limb Ischemia. *Front Cardiovasc Med*. 2018;5:144.
67. Iwata A, Morgan-Stevenson V, Schwartz B, Liu L, Tupper J, Zhu X, Harlan J and Winn R. Extracellular BCL2 proteins are danger-associated molecular patterns that reduce tissue damage in murine models of ischemia-reperfusion injury. *PLoS One*. 2010;5:e9103.

68. Lopez-Pastrana J, Ferrer LM, Li YF, Xiong X, Xi H, Cueto R, Nelson J, Sha X, Li X, Cannella AL, Imoukhuede PI, Qin X, Choi ET, Wang H and Yang XF. Inhibition of Caspase-1 Activation in Endothelial Cells Improves Angiogenesis: A NOVEL THERAPEUTIC POTENTIAL FOR ISCHEMIA. *J Biol Chem*. 2015;290:17485-94.
69. Capoccia BJ, Gregory AD and Link DC. Recruitment of the inflammatory subset of monocytes to sites of ischemia induces angiogenesis in a monocyte chemoattractant protein-1-dependent fashion. *J Leukoc Biol*. 2008;84:760-8.
70. Krishnasamy K, Limbourg A, Kapanadze T, Gamrekelashvili J, Beger C, Hager C, Lozanovski VJ, Falk CS, Napp LC, Bauersachs J, Mack M, Haller H, Weber C, Adams RH and Limbourg FP. Blood vessel control of macrophage maturation promotes arteriogenesis in ischemia. *Nat Commun*. 2017;8:952.
71. Hellingman AA, Zwaginga JJ, van Beem RT, Te RMSMC, Hamming JF, Fibbe WE, Quax PH and Geutskens SB. T-cell-pre-stimulated monocytes promote neovascularisation in a murine hind limb ischaemia model. *Eur J Vasc Endovasc Surg*. 2011;41:418-28.
72. Kwee BJ, Budina E, Najibi AJ and Mooney DJ. CD4 T-cells regulate angiogenesis and myogenesis. *Biomaterials*. 2018;178:109-121.
73. Stabile E, Kinnaird T, la Sala A, Hanson SK, Watkins C, Campia U, Shou M, Zbinden S, Fuchs S, Kornfeld H, Epstein SE and Burnett MS. CD8+ T lymphocytes regulate the arteriogenic response to ischemia by infiltrating the site of collateral vessel development and recruiting CD4+ mononuclear cells through the expression of interleukin-16. *Circulation*. 2006;113:118-24.
74. Hellingman AA, van der Vlugt LE, Lijkwan MA, Bastiaansen AJ, Sparwasser T, Smits HH, Hamming JF and Quax PH. A limited role for regulatory T cells in post-ischemic neovascularization. *J Cell Mol Med*. 2012;16:328-36.
75. Zouggari Y, Ait-Oufella H, Waeckel L, Vilar J, Loinard C, Cochain C, Recalde A, Duriez M, Levy BI, Lutgens E, Mallat Z and Silvestre JS. Regulatory T cells modulate postischemic neovascularization. *Circulation*. 2009;120:1415-25.
76. Kwee BJ, Seo BR, Najibi AJ, Li AW, Shih TY, White D and Mooney DJ. Treating ischemia via recruitment of antigen-specific T cells. *Sci Adv*. 2019;5:eaav6313.
77. Albini A, Bruno A, Noonan DM and Mortara L. Contribution to Tumor Angiogenesis From Innate Immune Cells Within the Tumor Microenvironment: Implications for Immunotherapy. *Front Immunol*. 2018;9:527.
78. Brechot N, Gomez E, Bignon M, Khallou-Laschet J, Dussiot M, Cazes A, Alanio-Brechot C, Durand M, Philippe J, Silvestre JS, Van Rooijen N, Corvol P, Nicoletti A, Chazaud B and Germain S. Modulation of macrophage activation state protects tissue from necrosis during critical limb ischemia in thrombospondin-1-deficient mice. *PLoS One*. 2008;3:e3950.
79. Krzyszczyk P, Schloss R, Palmer A and Berthiaume F. The Role of Macrophages in Acute and Chronic Wound Healing and Interventions to Promote Pro-wound Healing Phenotypes. *Front Physiol*. 2018;9:419.
80. Mor F, Quintana FJ and Cohen IR. Angiogenesis-inflammation cross-talk: vascular endothelial growth factor is secreted by activated T cells and induces Th1 polarization. *J Immunol*. 2004;172:4618-23.
81. Leung OM, Li J, Li X, Chan VW, Yang KY, Ku M, Ji L, Sun H, Waldmann H, Tian XY, Huang Y, Lau J, Zhou B and Lui KO. Regulatory T Cells Promote Apelin-Mediated Sprouting Angiogenesis in Type 2 Diabetes. *Cell Rep*. 2018;24:1610-1626.

82. Zhong Q, Jenkins J, Moldobaeva A, D'Alessio F and Wagner EM. Effector T Cells and Ischemia-Induced Systemic Angiogenesis in the Lung. *Am J Respir Cell Mol Biol*. 2016;54:394-401.
83. D'Alessio FR, Zhong Q, Jenkins J, Moldobaeva A and Wagner EM. Lung Angiogenesis Requires CD4(+) Forkhead Homeobox Protein-3(+) Regulatory T Cells. *Am J Respir Cell Mol Biol*. 2015;52:603-10.
84. Deng W, Xu M, Meng Q, Li Z, Qiu X, Yin S, Sun D, Dai C and Liu Y. CD8+CD103+ iTregs inhibit the progression of lupus nephritis by attenuating glomerular endothelial cell injury. *Rheumatology (Oxford)*. 2019;58:2039-2050.
85. Ahmed A and Koma MK. Interleukin-33 Triggers B1 Cell Expansion and Its Release of Monocyte/Macrophage Chemoattractants and Growth Factors. *Scand J Immunol*. 2015;82:118-24.
86. Dubey LK, Karempudi P, Luther SA, Ludewig B and Harris NL. Interactions between fibroblastic reticular cells and B cells promote mesenteric lymph node lymphangiogenesis. *Nat Commun*. 2017;8:367.
87. Wenger RH, Marti HH, Schuerer-Maly CC, Kvietikova I, Bauer C, Gassmann M and Maly FE. Hypoxic induction of gene expression in chronic granulomatous disease-derived B-cell lines: oxygen sensing is independent of the cytochrome b558-containing nicotinamide adenine dinucleotide phosphate oxidase. *Blood*. 1996;87:756-61.
88. Healy ME, Bergin R, Mahon BP and English K. Mesenchymal stromal cells protect against caspase 3-mediated apoptosis of CD19(+) peripheral B cells through contact-dependent upregulation of VEGF. *Stem Cells Dev*. 2015;24:2391-402.
89. Mezquita P, Parghi SS, Brandvold KA and Ruddell A. Myc regulates VEGF production in B cells by stimulating initiation of VEGF mRNA translation. *Oncogene*. 2005;24:889-901.
90. Ali MF, Dasari H, Van Keulen VP, Cornec D, Vasmatzis G, Peikert T and Carmona EM. Microbial Antigens Stimulate Metalloprotease-7 Secretion in Human B-Lymphocytes Using mTOR-Dependent and Independent Pathways. *Sci Rep*. 2017;7:3869.
91. Aung LL, Mouradian MM, Dhib-Jalbut S and Balashov KE. MMP-9 expression is increased in B lymphocytes during multiple sclerosis exacerbation and is regulated by microRNA-320a. *J Neuroimmunol*. 2015;278:185-9.
92. Trocme C, Gaudin P, Berthier S, Barro C, Zaoui P and Morel F. Human B lymphocytes synthesize the 92-kDa gelatinase, matrix metalloproteinase-9. *J Biol Chem*. 1998;273:20677-84.
93. Yang C, Lee H, Pal S, Jove V, Deng J, Zhang W, Hoon DS, Wakabayashi M, Forman S and Yu H. B cells promote tumor progression via STAT3 regulated-angiogenesis. *PLoS One*. 2013;8:e64159.
94. Andreu P, Johansson M, Affara NI, Pucci F, Tan T, Junankar S, Korets L, Lam J, Tawfik D, DeNardo DG, Naldini L, de Visser KE, De Palma M and Coussens LM. FcRgamma activation regulates inflammation-associated squamous carcinogenesis. *Cancer Cell*. 2010;17:121-34.
95. Chen J, Trounstine M, Alt FW, Young F, Kurahara C, Loring JF and Huszar D. Immunoglobulin gene rearrangement in B cell deficient mice generated by targeted deletion of the JH locus. *Int Immunol*. 1993;5:647-56.
96. Nishio N, Ito S, Suzuki H and Isobe K. Antibodies to wounded tissue enhance cutaneous wound healing. *Immunology*. 2009;128:369-80.
97. Sirbulescu RF, Boehm CK, Soon E, Wilks MQ, Ilies I, Yuan H, Maxner B, Chronos N, Kaittanis C, Normandin MD, El Fakhri G, Orgill DP, Sluder AE and Poznansky MC. Mature B

cells accelerate wound healing after acute and chronic diabetic skin lesions. *Wound Repair Regen*. 2017;25:774-791.
98. Iwata Y, Yoshizaki A, Komura K, Shimizu K, Ogawa F, Hara T, Muroi E, Bae S, Takenaka M, Yukami T, Hasegawa M, Fujimoto M, Tomita Y, Tedder TF and Sato S. CD19, a response regulator of B lymphocytes, regulates wound healing through hyaluronan-induced TLR4 signaling. *Am J Pathol*. 2009;175:649-60.
99. Fagiani E, Bill R, Pisarsky L, Ivanek R, Ruegg C and Christofori G. An immature B cell population from peripheral blood serves as surrogate marker for monitoring tumor angiogenesis and anti-angiogenic therapy in mouse models. *Angiogenesis*. 2015;18:327-45.
100. Yasuma R, Cicatiello V, Mizutani T, Tudisco L, Kim Y, Tarallo V, Bogdanovich S, Hirano Y, Kerur N, Li S, Yasuma T, Fowler BJ, Wright CB, Apicella I, Greco A, Brunetti A, Ambati BK, Helmers SB, Lundberg IE, Viklicky O, Leusen JH, Verbeek JS, Gelfand BD, Bastos-Carvalho A, De Falco S and Ambati J. Intravenous immune globulin suppresses angiogenesis in mice and humans. *Signal Transduct Target Ther*. 2016;1.
101. Sumiyoshi K, Mokuno H, Iesaki T, Shimada K, Miyazaki T, Kume A, Kiyanagi T, Kuremoto K, Watanabe Y, Tada N and Daida H. Deletion of the Fc receptors gamma chain preserves endothelial function affected by hypercholesterolaemia in mice fed on a high-fat diet. *Cardiovasc Res*. 2008;80:463-70.
102. Li F, Ulrich M, Jonas M, Stone IJ, Linares G, Zhang X, Westendorf L, Benjamin DR and Law CL. Tumor-Associated Macrophages Can Contribute to Antitumor Activity through FcγR-Mediated Processing of Antibody-Drug Conjugates. *Mol Cancer Ther*. 2017;16:1347-1354.
103. Bogdanovich S, Kim Y, Mizutani T, Yasuma R, Tudisco L, Cicatiello V, Bastos-Carvalho A, Kerur N, Hirano Y, Baffi JZ, Tarallo V, Li S, Yasuma T, Arpitha P, Fowler BJ, Wright CB, Apicella I, Greco A, Brunetti A, Ruvo M, Sandomenico A, Nozaki M, Ijima R, Kaneko H, Ogura Y, Terasaki H, Ambati BK, Leusen JH, Langdon WY, Clark MR, Armour KL, Bruhns P, Verbeek JS, Gelfand BD, De Falco S and Ambati J. Human IgG1 antibodies suppress angiogenesis in a target-independent manner. *Signal Transduct Target Ther*. 2016;1.
104. Justiniano SE, Elavazhagan S, Fatehchand K, Shah P, Mehta P, Roda JM, Mo X, Cheney C, Hertlein E, Eubank TD, Marsh C, Muthusamy N, Butchar JP, Byrd JC and Tridandapani S. Fcγ receptor-induced soluble vascular endothelial growth factor receptor-1 (VEGFR-1) production inhibits angiogenesis and enhances efficacy of anti-tumor antibodies. *J Biol Chem*. 2013;288:26800-9.
105. Fridman WH. Fc receptors and immunoglobulin binding factors. *FASEB J*. 1991;5:2684-90.
106. Bournazos S, Wang TT, Dahan R, Maamary J and Ravetch JV. Signaling by Antibodies: Recent Progress. *Annu Rev Immunol*. 2017;35:285-311.
107. Austen WG, Jr., Zhang M, Chan R, Friend D, Hechtman HB, Carroll MC and Moore FD, Jr. Murine hindlimb reperfusion injury can be initiated by a self-reactive monoclonal IgM. *Surgery*. 2004;136:401-6.
108. Chan RK, Ding G, Verna N, Ibrahim S, Oakes S, Austen WG, Jr., Hechtman HB and Moore FD, Jr. IgM binding to injured tissue precedes complement activation during skeletal muscle ischemia-reperfusion. *J Surg Res*. 2004;122:29-35.
109. Zhang M, Austen WG, Jr., Chiu I, Alicot EM, Hung R, Ma M, Verna N, Xu M, Hechtman HB, Moore FD, Jr. and Carroll MC. Identification of a specific self-reactive IgM antibody that initiates intestinal ischemia/reperfusion injury. *Proc Natl Acad Sci U S A*. 2004;101:3886-91.

110. Weiser MR, Williams JP, Moore FD, Jr., Kobzik L, Ma M, Hechtman HB and Carroll MC. Reperfusion injury of ischemic skeletal muscle is mediated by natural antibody and complement. *J Exp Med*. 1996;183:2343-8.
111. Williams JP, Pechet TT, Weiser MR, Reid R, Kobzik L, Moore FD, Jr., Carroll MC and Hechtman HB. Intestinal reperfusion injury is mediated by IgM and complement. *J Appl Physiol (1985)*. 1999;86:938-42.
112. Sheu EG, Oakes SM, Ahmadi-Yazdi C, Afnan J, Carroll MC and Moore FD, Jr. Restoration of skeletal muscle ischemia-reperfusion injury in humanized immunodeficient mice. *Surgery*. 2009;146:340-6.
113. Arumugam TV, Magnus T, Woodruff TM, Proctor LM, Shiels IA and Taylor SM. Complement mediators in ischemia-reperfusion injury. *Clin Chim Acta*. 2006;374:33-45.
114. Zhang M, Michael LH, Grosjean SA, Kelly RA, Carroll MC and Entman ML. The role of natural IgM in myocardial ischemia-reperfusion injury. *J Mol Cell Cardiol*. 2006;41:62-7.
115. Kubli SP, Vornholz L, Duncan G, Zhou W, Ramachandran P, Fortin J, Cox M, Han S, Nechanitzky R, Nechanitzky D, Snow BE, Jones L, Li WY, Haight J, Wakeham A, Bray MR and Mak TW. Fcmr regulates mononuclear phagocyte control of anti-tumor immunity. *Nat Commun*. 2019;10:2678.
116. Zhu Y, Xian X, Wang Z, Bi Y, Chen Q, Han X, Tang D and Chen R. Research Progress on the Relationship between Atherosclerosis and Inflammation. *Biomolecules*. 2018;8.
117. Price DT and Loscalzo J. Cellular adhesion molecules and atherogenesis. *Am J Med*. 1999;107:85-97.
118. Kawakami A, Aikawa M, Alcaide P, Luscinskas FW, Libby P and Sacks FM. Apolipoprotein CIII induces expression of vascular cell adhesion molecule-1 in vascular endothelial cells and increases adhesion of monocytic cells. *Circulation*. 2006;114:681-7.
119. O'Brien KD, McDonald TO, Chait A, Allen MD and Alpers CE. Neovascular expression of E-selectin, intercellular adhesion molecule-1, and vascular cell adhesion molecule-1 in human atherosclerosis and their relation to intimal leukocyte content. *Circulation*. 1996;93:672-82.
120. Lipinski MJ, Campbell KA, Duong SQ, Welch TJ, Garmey JC, Doran AC, Skaflen MD, Oldham SN, Kelly KA and McNamara CA. Loss of Id3 increases VCAM-1 expression, macrophage accumulation, and atherogenesis in Ldlr-/- mice. *Arterioscler Thromb Vasc Biol*. 2012;32:2855-61.
121. Forrest ST, Taylor AM, Sarembock IJ, Perlegas D and McNamara CA. Phosphorylation regulates Id3 function in vascular smooth muscle cells. *Circ Res*. 2004;95:557-9.
122. Kaplan JL, Marshall MA, C CM, Harmon DB, Garmey JC, Oldham SN, Hallowell P and McNamara CA. Adipocyte progenitor cells initiate monocyte chemoattractant protein-1-mediated macrophage accumulation in visceral adipose tissue. *Mol Metab*. 2015;4:779-94.
123. Ling F, Kang B and Sun XH. Id proteins: small molecules, mighty regulators. *Curr Top Dev Biol*. 2014;110:189-216.
124. Nickenig G, Baudler S, Muller C, Werner C, Werner N, Welzel H, Strehlow K and Bohm M. Redox-sensitive vascular smooth muscle cell proliferation is mediated by GKLF and Id3 in vitro and in vivo. *FASEB J*. 2002;16:1077-86.
125. Zhang X, Ai F, Li X, She X, Li N, Tang A, Qin Z, Ye Q, Tian L, Li G, Shen S and Ma J. Inflammation-induced S100A8 activates Id3 and promotes colorectal tumorigenesis. *Int J Cancer*. 2015;137:2803-14.

126. Taylor AM, Li F, Thimmalapura P, Gerrity RG, Sarembock IJ, Forrest S, Rutherford S and McNamara CA. Hyperlipemia and oxidation of LDL induce vascular smooth muscle cell growth: an effect mediated by the HLH factor Id3. *J Vasc Res*. 2006;43:123-30.
127. Cutchins A, Harmon DB, Kirby JL, Doran AC, Oldham SN, Skaflen M, Klibanov AL, Meller N, Keller SR, Garmey J and McNamara CA. Inhibitor of differentiation-3 mediates high fat diet-induced visceral fat expansion. *Arterioscler Thromb Vasc Biol*. 2012;32:317-24.
128. Lyden D, Young AZ, Zagzag D, Yan W, Gerald W, O'Reilly R, Bader BL, Hynes RO, Zhuang Y, Manova K and Benezra R. Id1 and Id3 are required for neurogenesis, angiogenesis and vascularization of tumour xenografts. *Nature*. 1999;401:670-7.
129. Doran AC, Lipinski MJ, Oldham SN, Garmey JC, Campbell KA, Skaflen MD, Cutchins A, Lee DJ, Glover DK, Kelly KA, Galkina EV, Ley K, Witztum JL, Tsimikas S, Bender TP and McNamara CA. B-cell aortic homing and atheroprotection depend on Id3. *Circ Res*. 2012;110:e1-12.
130. Doran AC, Lehtinen AB, Meller N, Lipinski MJ, Slayton RP, Oldham SN, Skaflen MD, Yeboah J, Rich SS, Bowden DW and McNamara CA. Id3 is a novel atheroprotective factor containing a functionally significant single-nucleotide polymorphism associated with intima-media thickness in humans. *Circ Res*. 2010;106:1303-11.
131. Manichaikul A, Rich SS, Perry H, Yeboah J, Law M, Davis M, Parker M, Ragosta M, Connelly JJ, McNamara CA and Taylor AM. A functionally significant polymorphism in ID3 is associated with human coronary pathology. *PLoS One*. 2014;9:e90222.
132. Lyden D, Hattori K, Dias S, Costa C, Blaikie P, Butros L, Chadburn A, Heissig B, Marks W, Witte L, Wu Y, Hicklin D, Zhu Z, Hackett NR, Crystal RG, Moore MA, Hajjar KA, Manova K, Benezra R and Rafii S. Impaired recruitment of bone-marrow-derived endothelial and hematopoietic precursor cells blocks tumor angiogenesis and growth. *Nat Med*. 2001;7:1194-201.
133. Sakurai D, Tsuchiya N, Yamaguchi A, Okaji Y, Tsuno NH, Kobata T, Takahashi K and Tokunaga K. Crucial role of inhibitor of DNA binding/differentiation in the vascular endothelial growth factor-induced activation and angiogenic processes of human endothelial cells. *J Immunol*. 2004;173:5801-9.
134. Fowkes FG, Aboyans V, Fowkes FJ, McDermott MM, Sampson UK and Criqui MH. Peripheral artery disease: epidemiology and global perspectives. *Nat Rev Cardiol*. 2017;14:156-170.
135. Castro PR, Barbosa AS, Pereira JM, Ranfley H, Felipetto M, Goncalves CAX, Paiva IR, Berg BB and Barcelos LS. Cellular and Molecular Heterogeneity Associated with Vessel Formation Processes. *Biomed Res Int*. 2018;2018:6740408.
136. Carmelli D, Fabsitz RR, Swan GE, Reed T, Miller B and Wolf PA. Contribution of genetic and environmental influences to ankle-brachial blood pressure index in the NHLBI Twin Study. National Heart, Lung, and Blood Institute. *Am J Epidemiol*. 2000;151:452-8.
137. Perry HM, Oldham SN, Fahl SP, Que X, Gonen A, Harmon DB, Tsimikas S, Witztum JL, Bender TP and McNamara CA. Helix-loop-helix factor inhibitor of differentiation 3 regulates interleukin-5 expression and B-1a B cell proliferation. *Arterioscler Thromb Vasc Biol*. 2013;33:2771-9.
138. Harmon DB, Srikakulapu P, Kaplan JL, Oldham SN, McSkimming C, Garmey JC, Perry HM, Kirby JL, Prohaska TA, Gonen A, Hallowell P, Schirmer B, Tsimikas S, Taylor AM, Witztum JL and McNamara CA. Protective Role for B-1b B Cells and IgM in Obesity-Associated Inflammation, Glucose Intolerance, and Insulin Resistance. *Arterioscler Thromb Vasc Biol*. 2016;36:682-91.

139. Hsieh PL, Rybalko V, Baker AB, Suggs LJ and Farrar RP. Recruitment and therapeutic application of macrophages in skeletal muscles after hind limb ischemia. *J Vasc Surg*. 2018;67:1908-1920 e1.
140. Bruno A, Pagani A, Pulze L, Albini A, Dallaglio K, Noonan DM and Mortara L. Orchestration of angiogenesis by immune cells. *Front Oncol*. 2014;4:131.
141. Enyindah-Asonye G, Li Y, Xin W, Singer NG, Gupta N, Fung J and Lin F. CD6 Receptor Regulates Intestinal Ischemia/Reperfusion-induced Injury by Modulating Natural IgM-producing B1a Cell Self-renewal. *J Biol Chem*. 2017;292:661-671.
142. De Mori R, Straino S, Di Carlo A, Mangoni A, Pompilio G, Palumbo R, Bianchi ME, Capogrossi MC and Germani A. Multiple effects of high mobility group box protein 1 in skeletal muscle regeneration. *Arterioscler Thromb Vasc Biol*. 2007;27:2377-83.
143. Fiuza C, Bustin M, Talwar S, Tropea M, Gerstenberger E, Shelhamer JH and Suffredini AF. Inflammation-promoting activity of HMGB1 on human microvascular endothelial cells. *Blood*. 2003;101:2652-60.
144. Jiang R, Cai J, Zhu Z, Chen D, Wang J, Wang Q, Teng Y, Huang Y, Tao M, Xia A, Xue M, Zhou S and Chen AF. Hypoxic trophoblast HMGB1 induces endothelial cell hyperpermeability via the TRL-4/caveolin-1 pathway. *J Immunol*. 2014;193:5000-12.
145. Luo Y, Li SJ, Yang J, Qiu YZ and Chen FP. HMGB1 induces an inflammatory response in endothelial cells via the RAGE-dependent endoplasmic reticulum stress pathway. *Biochem Biophys Res Commun*. 2013;438:732-8.
146. Lv B, Wang H, Tang Y, Fan Z, Xiao X and Chen F. High-mobility group box 1 protein induces tissue factor expression in vascular endothelial cells via activation of NF-kappaB and Egr-1. *Thromb Haemost*. 2009;102:352-9.
147. Singh B, Biswas I, Bhagat S, Surya Kumari S and Khan GA. HMGB1 facilitates hypoxia-induced vWF upregulation through TLR2-MYD88-SP1 pathway. *Eur J Immunol*. 2016;46:2388-2400.
148. Yang S, Xu L, Yang T and Wang F. High-mobility group box-1 and its role in angiogenesis. *J Leukoc Biol*. 2014;95:563-74.
149. Bochkov VN, Philippova M, Oskolkova O, Kadl A, Furnkranz A, Karabeg E, Afonyushkin T, Gruber F, Breuss J, Minchenko A, Mechtcheriakova D, Hohensinner P, Rychli K, Wojta J, Resink T, Erne P, Binder BR and Leitinger N. Oxidized phospholipids stimulate angiogenesis via autocrine mechanisms, implicating a novel role for lipid oxidation in the evolution of atherosclerotic lesions. *Circ Res*. 2006;99:900-8.
150. van der Pol P, Roos A, Berger SP, Daha MR and van Kooten C. Natural IgM antibodies are involved in the activation of complement by hypoxic human tubular cells. *Am J Physiol Renal Physiol*. 2011;300:F932-40.
151. Arpino JM, Nong Z, Li F, Yin H, Ghonaim N, Milkovich S, Balint B, O'Neil C, Fraser GM, Goldman D, Ellis CG and Pickering JG. Four-Dimensional Microvascular Analysis Reveals That Regenerative Angiogenesis in Ischemic Muscle Produces a Flawed Microcirculation. *Circ Res*. 2017;120:1453-1465.
152. Lee JJAJMN, Z.; Yin, H.; Hashi, A.A.; Chevalier, J.; O'Neil, C.; Pickering, J.G. Abstract 634: Hindlimb Mapping and Systematic Review of Angiogenesis Following Mouse Hindlimb Ischemia: New Insights Into Quality Assurance Imperatives. *Arteriosclerosis, Thrombosis, and Vascular Biology*. 2019;2019:A634.
153. Cardinal TR, Struthers KR, Kesler TJ, Yocum MD, Kurjiaka DT and Hoying JB. Chronic hindlimb ischemia impairs functional vasodilation and vascular reactivity in mouse feed arteries. *Front Physiol*. 2011;2:91.

154. Simmonds MJ, Detterich JA and Connes P. Nitric oxide, vasodilation and the red blood cell. *Biorheology*. 2014;51:121-34.
155. Hill-Eubanks DC, Gonzales AL, Sonkusare SK and Nelson MT. Vascular TRP channels: performing under pressure and going with the flow. *Physiology (Bethesda)*. 2014;29:343-60.
156. Sachdev U, Cui X, Hong G, Namkoong S, Karlsson JM, Baty CJ and Tzeng E. High mobility group box 1 promotes endothelial cell angiogenic behavior in vitro and improves muscle perfusion in vivo in response to ischemic injury. *J Vasc Surg*. 2012;55:180-91.
157. Banz Y and Rieben R. Role of complement and perspectives for intervention in ischemia-reperfusion damage. *Ann Med*. 2012;44:205-17.
158. Gorsuch WB, Chrysanthou E, Schwaeble WJ and Stahl GL. The complement system in ischemia-reperfusion injuries. *Immunobiology*. 2012;217:1026-33.
159. Ricklin D and Lambris JD. Complement in immune and inflammatory disorders: pathophysiological mechanisms. *J Immunol*. 2013;190:3831-8.
160. Langer HF, Chung KJ, Orlova VV, Choi EY, Kaul S, Kruhlak MJ, Alatsatianos M, DeAngelis RA, Roche PA, Magotti P, Li X, Economopoulou M, Rafail S, Lambris JD and Chavakis T. Complement-mediated inhibition of neovascularization reveals a point of convergence between innate immunity and angiogenesis. *Blood*. 2010;116:4395-403.
161. Bossi F, Tripodo C, Rizzi L, Bulla R, Agostinis C, Guarnotta C, Munaut C, Baldassarre G, Papa G, Zorzet S, Ghebrehiwet B, Ling GS, Botto M and Tedesco F. C1q as a unique player in angiogenesis with therapeutic implication in wound healing. *Proc Natl Acad Sci U S A*. 2014;111:4209-14.
162. Newby AC. Metalloproteinase production from macrophages - a perfect storm leading to atherosclerotic plaque rupture and myocardial infarction. *Exp Physiol*. 2016;101:1327-1337.
163. Forrest ST, Barringhaus KG, Perlegas D, Hammarskjold ML and McNamara CA. Intron retention generates a novel Id3 isoform that inhibits vascular lesion formation. *J Biol Chem*. 2004;279:32897-903.
164. Kee BL, Rivera RR and Murre C. Id3 inhibits B lymphocyte progenitor growth and survival in response to TGF-beta. *Nat Immunol*. 2001;2:242-7.
165. Goettsch C, Hutcheson JD, Hagita S, Rogers MA, Creager MD, Pham T, Choi J, Mlynarchik AK, Pieper B, Kjolby M, Aikawa M and Aikawa E. A single injection of gain-of-function mutant PCSK9 adeno-associated virus vector induces cardiovascular calcification in mice with no genetic modification. *Atherosclerosis*. 2016;251:109-118.
166. Kumar S, Kang DW, Rezvan A and Jo H. Accelerated atherosclerosis development in C57Bl6 mice by overexpressing AAV-mediated PCSK9 and partial carotid ligation. *Lab Invest*. 2017;97:935-945.
167. Lu H, Howatt DA, Balakrishnan A, Graham MJ, Mullick AE and Daugherty A. Hypercholesterolemia Induced by a PCSK9 Gain-of-Function Mutation Augments Angiotensin II-Induced Abdominal Aortic Aneurysms in C57BL/6 Mice-Brief Report. *Arterioscler Thromb Vasc Biol*. 2016;36:1753-7.
168. Doring Y, Noels H, van der Vorst EPC, Neideck C, Egea V, Drechsler M, Mandl M, Pawig L, Jansen Y, Schroder K, Bidzhekov K, Megens RTA, Theelen W, Klinkhammer BM, Boor P, Schurgers L, van Gorp R, Ries C, Kusters PJH, van der Wal A, Hackeng TM, Gabel G, Brandes RP, Soehnlein O, Lutgens E, Vestweber D, Teupser D, Holdt LM, Rader DJ, Saleheen D and Weber C. Vascular CXCR4 Limits Atherosclerosis by Maintaining Arterial Integrity: Evidence From Mouse and Human Studies. *Circulation*. 2017;136:388-403.
169. Chen PY, Qin L, Li G, Wang Z, Dahlman JE, Malagon-Lopez J, Gujja S, Kauffman KJ, Sun L, Sun H, Zhang X, Aryal B, Canfran-Duque A, Liu R, Kusters P, Sehgal A, Jiao Y,

Anderson DG, Gulcher J, Fernandez-Hernando C, Lutgens E, Schwartz MA, Pober JS, Chittenden TW, Tellides G and Simons M. Endothelial TGF-beta signalling drives vascular inflammation and atherosclerosis. *Nat Metab*. 2019;1:912-926.
170. Ramirez CM, Zhang X, Bandyopadhyay C, Rotllan N, Sugiyama MG, Aryal B, Liu X, He S, Kraehling JR, Ulrich V, Lin CS, Velazquez H, Lasuncion MA, Li G, Suarez Y, Tellides G, Swirski FK, Lee WL, Schwartz MA, Sessa WC and Fernandez-Hernando C. Caveolin-1 Regulates Atherogenesis by Attenuating Low-Density Lipoprotein Transcytosis and Vascular Inflammation Independently of Endothelial Nitric Oxide Synthase Activation. *Circulation*. 2019;140:225-239.
171. Chen X, Qian S, Hoggatt A, Tang H, Hacker TA, Obukhov AG, Herring PB and Seye CI. Endothelial Cell-Specific Deletion of P2Y2 Receptor Promotes Plaque Stability in Atherosclerosis-Susceptible ApoE-Null Mice. *Arterioscler Thromb Vasc Biol*. 2017;37:75-83.
172. Ponnuswamy P, Schrottle A, Ostermeier E, Gruner S, Huang PL, Ertl G, Hoffmann U, Nieswandt B and Kuhlencordt PJ. eNOS protects from atherosclerosis despite relevant superoxide production by the enzyme in apoE mice. *PLoS One*. 2012;7:e30193.
173. Sharma A, Sellers S, Stefanovic N, Leung C, Tan SM, Huet O, Granville DJ, Cooper ME, de Haan JB and Bernatchez P. Direct Endothelial Nitric Oxide Synthase Activation Provides Atheroprotection in Diabetes-Accelerated Atherosclerosis. *Diabetes*. 2015;64:3937-50.
174. Jin X, Yin J, Kim SH, Sohn YW, Beck S, Lim YC, Nam DH, Choi YJ and Kim H. EGFR-AKT-Smad signaling promotes formation of glioma stem-like cells and tumor angiogenesis by ID3-driven cytokine induction. *Cancer Res*. 2011;71:7125-34.
175. Chen FF, Lv X, Zhao QF, Xu YZ, Song SS, Yu W and Li XJ. Inhibitor of DNA binding 3 reverses cisplatin resistance in human lung adenocarcinoma cells by regulating the PI3K/Akt pathway. *Oncol Lett*. 2018;16:1634-1640.
176. Miyazaki M, Miyazaki K, Chen S, Chandra V, Wagatsuma K, Agata Y, Rodewald HR, Saito R, Chang AN, Varki N, Kawamoto H and Murre C. The E-Id protein axis modulates the activities of the PI3K-AKT-mTORC1-Hif1a and c-myc/p19Arf pathways to suppress innate variant TFH cell development, thymocyte expansion, and lymphomagenesis. *Genes Dev*. 2015;29:409-25.
177. Kowanetz M, Valcourt U, Bergstrom R, Heldin CH and Moustakas A. Id2 and Id3 define the potency of cell proliferation and differentiation responses to transforming growth factor beta and bone morphogenetic protein. *Mol Cell Biol*. 2004;24:4241-54.
178. Chang MK, Binder CJ, Miller YI, Subbanagounder G, Silverman GJ, Berliner JA and Witztum JL. Apoptotic cells with oxidation-specific epitopes are immunogenic and proinflammatory. *J Exp Med*. 2004;200:1359-70.
179. Binder CJ, Horkko S, Dewan A, Chang MK, Kieu EP, Goodyear CS, Shaw PX, Palinski W, Witztum JL and Silverman GJ. Pneumococcal vaccination decreases atherosclerotic lesion formation: molecular mimicry between Streptococcus pneumoniae and oxidized LDL. *Nat Med*. 2003;9:736-43.
180. Horkko S, Bird DA, Miller E, Itabe H, Leitinger N, Subbanagounder G, Berliner JA, Friedman P, Dennis EA, Curtiss LK, Palinski W and Witztum JL. Monoclonal autoantibodies specific for oxidized phospholipids or oxidized phospholipid-protein adducts inhibit macrophage uptake of oxidized low-density lipoproteins. *J Clin Invest*. 1999;103:117-28.
181. Tsimikas S, Miyanohara A, Hartvigsen K, Merki E, Shaw PX, Chou MY, Pattison J, Torzewski M, Sollors J, Friedmann T, Lai NC, Hammond HK, Getz GS, Reardon CA, Li AC,

Banka CL and Witztum JL. Human oxidation-specific antibodies reduce foam cell formation and atherosclerosis progression. *J Am Coll Cardiol*. 2011;58:1715-27.
182. Abram CL, Roberge GL, Hu Y and Lowell CA. Comparative analysis of the efficiency and specificity of myeloid-Cre deleting strains using ROSA-EYFP reporter mice. *J Immunol Methods*. 2014;408:89-100.
183. Shi J, Hua L, Harmer D, Li P and Ren G. Cre Driver Mice Targeting Macrophages. *Methods Mol Biol*. 2018;1784:263-275.
184. Smedbakken LM, Halvorsen B, Daissormont I, Ranheim T, Michelsen AE, Skjelland M, Sagen EL, Folkersen L, Krohg-Sorensen K, Russell D, Holm S, Ueland T, Fevang B, Hedin U, Yndestad A, Gullestad L, Hansson GK, Biessen EA and Aukrust P. Increased levels of the homeostatic chemokine CXCL13 in human atherosclerosis - Potential role in plaque stabilization. *Atherosclerosis*. 2012;224:266-73.
185. Kim K, Shim D, Lee JS, Zaitsev K, Williams JW, Kim KW, Jang MY, Seok Jang H, Yun TJ, Lee SH, Yoon WK, Prat A, Seidah NG, Choi J, Lee SP, Yoon SH, Nam JW, Seong JK, Oh GT, Randolph GJ, Artyomov MN, Cheong C and Choi JH. Transcriptome Analysis Reveals Nonfoamy Rather Than Foamy Plaque Macrophages Are Proinflammatory in Atherosclerotic Murine Models. *Circ Res*. 2018;123:1127-1142.
186. Luo S, Zhu R, Yu T, Fan H, Hu Y, Mohanta SK and Hu D. Chronic Inflammation: A Common Promoter in Tertiary Lymphoid Organ Neogenesis. *Front Immunol*. 2019;10:2938.
187. Srikakulapu P, Hu D, Yin C, Mohanta SK, Bontha SV, Peng L, Beer M, Weber C, McNamara CA, Grassia G, Maffia P, Manz RA and Habenicht AJ. Artery Tertiary Lymphoid Organs Control Multilayered Territorialized Atherosclerosis B-Cell Responses in Aged ApoE-/- Mice. *Arterioscler Thromb Vasc Biol*. 2016;36:1174-85.
188. Lutgens E and Daemen MJ. CD40-CD40L interactions in atherosclerosis. *Trends Cardiovasc Med*. 2002;12:27-32.
189. Pham LV, Pogue E and Ford RJ. The Role of Macrophage/B-Cell Interactions in the Pathophysiology of B-Cell Lymphomas. *Front Oncol*. 2018;8:147.
190. Aird WC. Phenotypic heterogeneity of the endothelium: II. Representative vascular beds. *Circ Res*. 2007;100:174-90.
191. Aird WC. Phenotypic heterogeneity of the endothelium: I. Structure, function, and mechanisms. *Circ Res*. 2007;100:158-73.
192. Kimball AK, Oko LM, Bullock BL, Nemenoff RA, van Dyk LF and Clambey ET. A Beginner's Guide to Analyzing and Visualizing Mass Cytometry Data. *J Immunol*. 2018;200:3-22.
193. Palit S, Heuser C, de Almeida GP, Theis FJ and Zielinski CE. Meeting the Challenges of High-Dimensional Single-Cell Data Analysis in Immunology. *Front Immunol*. 2019;10:1515.
194. Olsen LR, Leipold MD, Pedersen CB and Maecker HT. The anatomy of single cell mass cytometry data. *Cytometry A*. 2019;95:156-172.
195. Orecchioni M, Bedognetti D, Newman L, Fuoco C, Spada F, Hendrickx W, Marincola FM, Sgarrella F, Rodrigues AF, Menard-Moyon C, Cesareni G, Kostarelos K, Bianco A and Delogu LG. Single-cell mass cytometry and transcriptome profiling reveal the impact of graphene on human immune cells. *Nat Commun*. 2017;8:1109.
196. Hartmann FJ and Bendall SC. Immune monitoring using mass cytometry and related high-dimensional imaging approaches. *Nat Rev Rheumatol*. 2020;16:87-99.
197. Hartmann FJ, Babdor J, Gherardini PF, Amir ED, Jones K, Sahaf B, Marquez DM, Krutzik P, O'Donnell E, Sigal N, Maecker HT, Meyer E, Spitzer MH and Bendall SC.

Comprehensive Immune Monitoring of Clinical Trials to Advance Human Immunotherapy. *Cell Rep*. 2019;28:819-831 e4.
198. Papalexi E and Satija R. Single-cell RNA sequencing to explore immune cell heterogeneity. *Nat Rev Immunol*. 2018;18:35-45.
199. Hwang B, Lee JH and Bang D. Single-cell RNA sequencing technologies and bioinformatics pipelines. *Exp Mol Med*. 2018;50:96.
200. Hedlund E and Deng Q. Single-cell RNA sequencing: Technical advancements and biological applications. *Mol Aspects Med*. 2018;59:36-46.
201. Winkels H, Ehinger E, Ghosheh Y, Wolf D and Ley K. Atherosclerosis in the single-cell era. *Curr Opin Lipidol*. 2018;29:389-396.
202. Shum EY, Walczak EM, Chang C and Christina Fan H. Quantitation of mRNA Transcripts and Proteins Using the BD Rhapsody Single-Cell Analysis System. *Adv Exp Med Biol*. 2019;1129:63-79.
203. Lopez D, Pollak AW, Meyer CH, Epstein FH, Zhao L, Pesch AJ, Jiji R, Kay JR, DiMaria JM, Christopher JM and Kramer CM. Arterial spin labeling perfusion cardiovascular magnetic resonance of the calf in peripheral arterial disease: cuff occlusion hyperemia vs exercise. *J Cardiovasc Magn Reson*. 2015;17:23.
204. Steinmetz M, Nickenig G and Werner N. Endothelial-regenerating cells: an expanding universe. *Hypertension*. 2010;55:593-9.
205. Medina RJ, Barber CL, Sabatier F, Dignat-George F, Melero-Martin JM, Khosrotehrani K, Ohneda O, Randi AM, Chan JKY, Yamaguchi T, Van Hinsbergh VWM, Yoder MC and Stitt AW. Endothelial Progenitors: A Consensus Statement on Nomenclature. *Stem Cells Transl Med*. 2017;6:1316-1320.
206. Madonna R and De Caterina R. Circulating endothelial progenitor cells: Do they live up to their name? *Vascul Pharmacol*. 2015;67-69:2-5.
207. Schmitt C, Eaves CJ and Lansdorp PM. Expression of CD34 on human B cell precursors. *Clin Exp Immunol*. 1991;85:168-73.
208. Steffen E, Mayer von Wittgenstein WBE, Hennig M, Niepmann ST, Zietzer A, Werner N, Rassaf T, Nickenig G, Wassmann S, Zimmer S and Steinmetz M. Murine sca1/flk1-positive cells are not endothelial progenitor cells, but B2 lymphocytes. *Basic Res Cardiol*. 2020;115:18.
209. Hayek SS, MacNamara J, Tahhan AS, Awad M, Yadalam A, Ko YA, Healy S, Hesaroieh I, Ahmed H, Gray B, Sher SS, Ghasemzadeh N, Patel R, Kim J, Waller EK and Quyyumi AA. Circulating Progenitor Cells Identify Peripheral Arterial Disease in Patients With Coronary Artery Disease. *Circ Res*. 2016;119:564-71.
210. Timmons JA, Knudsen S, Rankinen T, Koch LG, Sarzynski M, Jensen T, Keller P, Scheele C, Vollaard NB, Nielsen S, Akerstrom T, MacDougald OA, Jansson E, Greenhaff PL, Tarnopolsky MA, van Loon LJ, Pedersen BK, Sundberg CJ, Wahlestedt C, Britton SL and Bouchard C. Using molecular classification to predict gains in maximal aerobic capacity following endurance exercise training in humans. *J Appl Physiol (1985)*. 2010;108:1487-96.
211. Roschger C and Cabrele C. The Id-protein family in developmental and cancer-associated pathways. *Cell Commun Signal*. 2017;15:7.
212. Sharma P, Patel D and Chaudhary J. Id1 and Id3 expression is associated with increasing grade of prostate cancer: Id3 preferentially regulates CDKN1B. *Cancer Med*. 2012;1:187-97.
213. Aboul-Fadl T. Antisense oligonucleotide technologies in drug discovery. *Expert Opin Drug Discov*. 2006;1:285-8.

214. Chen Y, Molnar M, Li L, Friberg P, Gan LM, Brismar H and Fu Y. Characterization of VCAM-1-binding peptide-functionalized quantum dots for molecular imaging of inflamed endothelium. *PLoS One*. 2013;8:e83805.
215. Kelly KA, Allport JR, Tsourkas A, Shinde-Patil VR, Josephson L and Weissleder R. Detection of vascular adhesion molecule-1 expression using a novel multimodal nanoparticle. *Circ Res*. 2005;96:327-36.
216. Kelly C, Jefferies C and Cryan SA. Targeted liposomal drug delivery to monocytes and macrophages. *J Drug Deliv*. 2011;2011:1-11.
217. Allen TM and Cullis PR. Liposomal drug delivery systems: from concept to clinical applications. *Adv Drug Deliv Rev*. 2013;65:36-48.
218. Sercombe L, Veerati T, Moheimani F, Wu SY, Sood AK and Hua S. Advances and Challenges of Liposome Assisted Drug Delivery. *Front Pharmacol*. 2015;6:286.
219. Won YW, Adhikary PP, Lim KS, Kim HJ, Kim JK and Kim YH. Oligopeptide complex for targeted non-viral gene delivery to adipocytes. *Nat Mater*. 2014;13:1157-64.
220. Chung JY, Ain QU, Song Y, Yong SB and Kim YH. Targeted delivery of CRISPR interference system against Fabp4 to white adipocytes ameliorates obesity, inflammation, hepatic steatosis, and insulin resistance. *Genome Res*. 2019;29:1442-1452.
221. Wojnarowicz PM, Lima ESR, Ohnaka M, Lee SB, Chin Y, Kulukian A, Chang SH, Desai B, Garcia Escolano M, Shah R, Garcia-Cao M, Xu S, Kadam R, Goldgur Y, Miller MA, Ouerfelli O, Yang G, Arakawa T, Albanese SK, Garland WA, Stoller G, Chaudhary J, Norton L, Soni RK, Philip J, Hendrickson RC, Iavarone A, Dannenberg AJ, Chodera JD, Pavletich N, Lasorella A, Campochiaro PA and Benezra R. A Small-Molecule Pan-Id Antagonist Inhibits Pathologic Ocular Neovascularization. *Cell Rep*. 2019;29:62-75 e7.
222. Wilson PW, D'Agostino RB, Levy D, Belanger AM, Silbershatz H and Kannel WB. Prediction of coronary heart disease using risk factor categories. *Circulation*. 1998;97:1837-47.
223. Conroy RM, Pyorala K, Fitzgerald AP, Sans S, Menotti A, De Backer G, De Bacquer D, Ducimetiere P, Jousilahti P, Keil U, Njolstad I, Oganov RG, Thomsen T, Tunstall-Pedoe H, Tverdal A, Wedel H, Whincup P, Wilhelmsen L, Graham IM and group Sp. Estimation of ten-year risk of fatal cardiovascular disease in Europe: the SCORE project. *Eur Heart J*. 2003;24:987-1003.
224. Tolunay H and Kurmus O. Comparison of coronary risk scoring systems to predict the severity of coronary artery disease using the SYNTAX score. *Cardiol J*. 2016;23:51-6.
225. Lusis AJ. Genetics of atherosclerosis. *Trends Genet*. 2012;28:267-75.
226. Rader DJ. Human genetics of atherothrombotic disease and its risk factors. *Arterioscler Thromb Vasc Biol*. 2015;35:741-7.
227. Criqui MH and Aboyans V. Epidemiology of peripheral artery disease. *Circ Res*. 2015;116:1509-26.
228. Gardner AW, Skinner JS, Cantwell BW and Smith LK. Prediction of claudication pain from clinical measurements obtained at rest. *Med Sci Sports Exerc*. 1992;24:163-70.
229. Kullo IJ and Leeper NJ. The genetic basis of peripheral arterial disease: current knowledge, challenges, and future directions. *Circ Res*. 2015;116:1551-60.
230. Elias I, Franckhauser S and Bosch F. New insights into adipose tissue VEGF-A actions in the control of obesity and insulin resistance. *Adipocyte*. 2013;2:109-12.
231. Honek J, Seki T, Iwamoto H, Fischer C, Li J, Lim S, Samani NJ, Zang J and Cao Y. Modulation of age-related insulin sensitivity by VEGF-dependent vascular plasticity in adipose tissues. *Proc Natl Acad Sci U S A*. 2014;111:14906-11.

232. Sun K, Wernstedt Asterholm I, Kusminski CM, Bueno AC, Wang ZV, Pollard JW, Brekken RA and Scherer PE. Dichotomous effects of VEGF-A on adipose tissue dysfunction. *Proc Natl Acad Sci U S A*. 2012;109:5874-9.
233. Sung HK, Doh KO, Son JE, Park JG, Bae Y, Choi S, Nelson SM, Cowling R, Nagy K, Michael IP, Koh GY, Adamson SL, Pawson T and Nagy A. Adipose vascular endothelial growth factor regulates metabolic homeostasis through angiogenesis. *Cell Metab*. 2013;17:61-72.
234. Tam J, Duda DG, Perentes JY, Quadri RS, Fukumura D and Jain RK. Blockade of VEGFR2 and not VEGFR1 can limit diet-induced fat tissue expansion: role of local versus bone marrow-derived endothelial cells. *PLoS One*. 2009;4:e4974.
235. Tang W, Zeve D, Suh JM, Bosnakovski D, Kyba M, Hammer RE, Tallquist MD and Graff JM. White fat progenitor cells reside in the adipose vasculature. *Science*. 2008;322:583-6.
236. Schlich R, Willems M, Greulich S, Ruppe F, Knoefel WT, Ouwens DM, Maxhera B, Lichtenberg A, Eckel J and Sell H. VEGF in the crosstalk between human adipocytes and smooth muscle cells: depot-specific release from visceral and perivascular adipose tissue. *Mediators Inflamm*. 2013;2013:982458.
237. Park J, Kim M, Sun K, An YA, Gu X and Scherer PE. VEGF-A-Expressing Adipose Tissue Shows Rapid Beiging and Enhanced Survival After Transplantation and Confers IL-4-Independent Metabolic Improvements. *Diabetes*. 2017;66:1479-1490.
238. Pang C, Gao Z, Yin J, Zhang J, Jia W and Ye J. Macrophage infiltration into adipose tissue may promote angiogenesis for adipose tissue remodeling in obesity. *Am J Physiol Endocrinol Metab*. 2008;295:E313-22.
239. Bourlier V, Zakaroff-Girard A, Miranville A, De Barros S, Maumus M, Sengenes C, Galitzky J, Lafontan M, Karpe F, Frayn KN and Bouloumie A. Remodeling phenotype of human subcutaneous adipose tissue macrophages. *Circulation*. 2008;117:806-15.
240. Russo L and Lumeng CN. Properties and functions of adipose tissue macrophages in obesity. *Immunology*. 2018;155:407-417.
241. Xu F, Burk D, Gao Z, Yin J, Zhang X, Weng J and Ye J. Angiogenic deficiency and adipose tissue dysfunction are associated with macrophage malfunction in SIRT1-/- mice. *Endocrinology*. 2012;153:1706-16.
242. Tran KV, Gealekman O, Frontini A, Zingaretti MC, Morroni M, Giordano A, Smorlesi A, Perugini J, De Matteis R, Sbarbati A, Corvera S and Cinti S. The vascular endothelium of the adipose tissue gives rise to both white and brown fat cells. *Cell Metab*. 2012;15:222-9.
243. Doran AC, Meller N, Cutchins A, Deliri H, Slayton RP, Oldham SN, Kim JB, Keller SR and McNamara CA. The helix-loop-helix factors Id3 and E47 are novel regulators of adiponectin. *Circ Res*. 2008;103:624-34.
244. Loveys DA, Streiff MB and Kato GJ. E2A basic-helix-loop-helix transcription factors are negatively regulated by serum growth factors and by the Id3 protein. *Nucleic Acids Res*. 1996;24:2813-20.
245. Lusis AJ, Seldin MM, Allayee H, Bennett BJ, Civelek M, Davis RC, Eskin E, Farber CR, Hui S, Mehrabian M, Norheim F, Pan C, Parks B, Rau CD, Smith DJ, Vallim T, Wang Y and Wang J. The Hybrid Mouse Diversity Panel: a resource for systems genetics analyses of metabolic and cardiovascular traits. *J Lipid Res*. 2016;57:925-42.
246. Seaman ME, Peirce SM and Kelly K. Rapid analysis of vessel elements (RAVE): a tool for studying physiologic, pathologic and tumor angiogenesis. *PLoS One*. 2011;6:e20807.
247. Osinski V, Bauknight DK, Dasa SSK, Harms MJ, Kroon T, Marshall MA, Garmey JC, Nguyen AT, Hartman J, Upadhye A, Srikakulapu P, Zhou A, O'Mahony G, Klibanov AL, Kelly

KA, Boucher J and McNamara CA. In vivo liposomal delivery of PPARalpha/gamma dual agonist tesaglitazar in a model of obesity enriches macrophage targeting and limits liver and kidney drug effects. *Theranostics*. 2020;10:585-601.
248. Bauknight DK, Osinski V, Dasa SSK, Nguyen AT, Marshall MA, Hartman J, Harms M, O'Mahony G, Boucher J, Klibanov AL, McNamara CA and Kelly KA. Importance of thorough tissue and cellular level characterization of targeted drugs in the evaluation of pharmacodynamic effects. *PLoS One*. 2019;14:e0224917.
249. Song G, Petschauer JS, Madden AJ and Zamboni WC. Nanoparticles and the mononuclear phagocyte system: pharmacokinetics and applications for inflammatory diseases. *Curr Rheumatol Rev*. 2014;10:22-34.
250. He H, Ghosh S and Yang H. Nanomedicines for dysfunctional macrophage-associated diseases. *J Control Release*. 2017;247:106-126.
251. Deshpande PP, Biswas S and Torchilin VP. Current trends in the use of liposomes for tumor targeting. *Nanomedicine (Lond)*. 2013;8:1509-28.
252. Xue Y, Xu X, Zhang XQ, Farokhzad OC and Langer R. Preventing diet-induced obesity in mice by adipose tissue transformation and angiogenesis using targeted nanoparticles. *Proc Natl Acad Sci U S A*. 2016;113:5552-7.
253. Chatzigeorgiou A, Karalis KP, Bornstein SR and Chavakis T. Lymphocytes in obesity-related adipose tissue inflammation. *Diabetologia*. 2012;55:2583-2592.
254. Szoka F, Jr. and Papahadjopoulos D. Procedure for preparation of liposomes with large internal aqueous space and high capture by reverse-phase evaporation. *Proc Natl Acad Sci U S A*. 1978;75:4194-8.
255. Kulkarni JA, Witzigmann D, Leung J, van der Meel R, Zaifman J, Darjuan MM, Grisch-Chan HM, Thony B, Tam YYC and Cullis PR. Fusion-dependent formation of lipid nanoparticles containing macromolecular payloads. *Nanoscale*. 2019;11:9023-9031.
256. Ergen C, Heymann F, Al Rawashdeh W, Gremse F, Bartneck M, Panzer U, Pola R, Pechar M, Storm G, Mohr N, Barz M, Zentel R, Kiessling F, Trautwein C, Lammers T and Tacke F. Targeting distinct myeloid cell populations in vivo using polymers, liposomes and microbubbles. *Biomaterials*. 2017;114:106-120.
257. Choi JY, Ryu J, Kim HJ, Song JW, Jeon JH, Lee DH, Oh DJ, Gweon DG, Oh WY, Yoo H, Park K and Kim JW. Therapeutic Effects of Targeted PPAR Activation on Inflamed High-Risk Plaques Assessed by Serial Optical Imaging In Vivo. *Theranostics*. 2018;8:45-60.
258. Kang H, Jung HJ, Kim SK, Wong DSH, Lin S, Li G, Dravid VP and Bian L. Magnetic Manipulation of Reversible Nanocaging Controls In Vivo Adhesion and Polarization of Macrophages. *ACS Nano*. 2018;12:5978-5994.
259. Kang H, Kim S, Wong DSH, Jung HJ, Lin S, Zou K, Li R, Li G, Dravid VP and Bian L. Remote Manipulation of Ligand Nano-Oscillations Regulates Adhesion and Polarization of Macrophages in Vivo. *Nano Lett*. 2017;17:6415-6427.

Appendix 1: Investigating the role of Id3 during adipose tissue expansion and angiogenesis

I. Introduction

Obesity is a prevalent disease affecting around one third of the U.S. population. Characterized by excess adiposity, it can lead to many co-morbidities include diabetes and dyslipidemia. The mechanisms driving development of obesity and excess adiposity are still being characterized as are additional effective treatments for the disease. In addition to the data presented in Chapters 3 and 4, I addressed questions concerning cell-specific expression of Id3 and the role of Id3 in the vasculature during adipose tissue expansion during my studies. These questions were prompted by findings published by Cutchins *et al*. in 2012 demonstrating that global loss of Id3 attenuates high-fat diet (HFD)-induced adipose tissue expansion as well as microvascular blood volume (MBV)[127]. How this change in blood volume is regulated and whether the reduction in MBV in part drove reduced adipose tissue expansion remains unclear.

Adipose tissue and the vasculature intersect in many ways beyond simply co-localizing. Adipose tissue expansion depends on neovascularization and changes in pro-angionic signals such as VEGFA result in altered adipose tissue size and characteristics[230-234]. Indeed, adipocyte progenitor cells (AdPCs) establish a niche along the vasculature of adipose tissue[235]. Additionally, adipocytes[233, 236, 237] and other adipose-resident cells such as macrophages[238-241] secrete pro-angiogenic factors to support vascular growth in adipose tissue. Finally, ECs have been shown to differentiate into adipocytes[242] further solidifying the close relationship between adipose tissue and the vasculature.

Id3 regulates adipose tissue differentiation[122, 243] and angiogenesis[128, 132, 221], but whether Id3 in part regulates adipose tissue expansion due to its role in the vasculature remains unclear. Utilizing global and endothelial cell (EC) Id3 KO lines as well as a novel Id3-GFP reporter mouse, we investigated the three larger questions: 1.) In what cell types is Id3 expression promoted during HFD feeding? 2.) Does Id3 promote the angiogenic potential of adipose tissue? and 3.) Is adipose tissue expansion dependent on Id3 activity in ECs?

II. Id3 promoter activation in cell subsets

A. Rationale

Id3 is a broadly expressed transcription factor that regulates homeostatic functions and disease pathogenesis in a multitude of cells and tissues. Prior studies demonstrate its expression in vascular smooth muscle cells (VSMCs)[121, 163], B cells[30], macrophages[122], myocytes[244], and endothelial cells[133]. These studies are all conducted under different disease settings and the cells originate from a variety of tissue beds. I was interested in beginning to understand the breadth and extent to which Id3 is expressed in various cell types within a single tissue. To do this, I utilized an Id3-reporter mouse in the setting of a brief high-fat diet (HFD) feeding to 1.) identify the cell types expressing Id3, and 2.) determine if Id3 expression changed at all in the setting of early hyperlipidemia – a condition observed in many patients with PAD or atherosclerosis.

B. Results

To begin to understand the cell types that express Id3, we utilized a transgenic Id3-reporter mouse. In this mouse, the GFP gene is inserted downstream of the Id3 promoter in one allele (**Figure A1.1A**). The mice are generated as heterozygotes for the GFP-insertion to avoid generating Id3 KO mice and potentially altering normal tissue function due to a lack of Id3 expression. Id3-GFP mice were fed one week of chow or HFD and then epididymal adipose depots were harvested from each mouse. The stromal vascular fraction was isolated from each fat sample and stained for flow cytometry (**Figure A1.1B**). A variety of cell subsets were quantified during analysis (**Figure A1.1C**). Please note, a GFP^- littermate was used in this experiment to generate a GFP fluorescence-minus-one (FMO) control. The percent of each cell subset that was GFP^+ was calculated and T cells and B cells demonstrated some of the highest percentages of GFP expression (**Figure A1.1D**). Additionally, one week of HFD induced increased percent of GFP^+ cells in T cells, B cells, macrophage and monocytes, endothelial progenitor cells (EPCs), and AdPCs (**Figure A1.1D**). Finally, the amount of GFP expressed per cell was analyzed using the mean fluorescence intensity values for each subset. In general, the $CD45^-$ populations expressed a higher GFP MFI than $CD45^+$ cells. More specifically, ECs and mesenchymal stem cells (MSCs) had some of the highest MFIs of all populations (**Figure A1.1E**).

Figure A1.1.

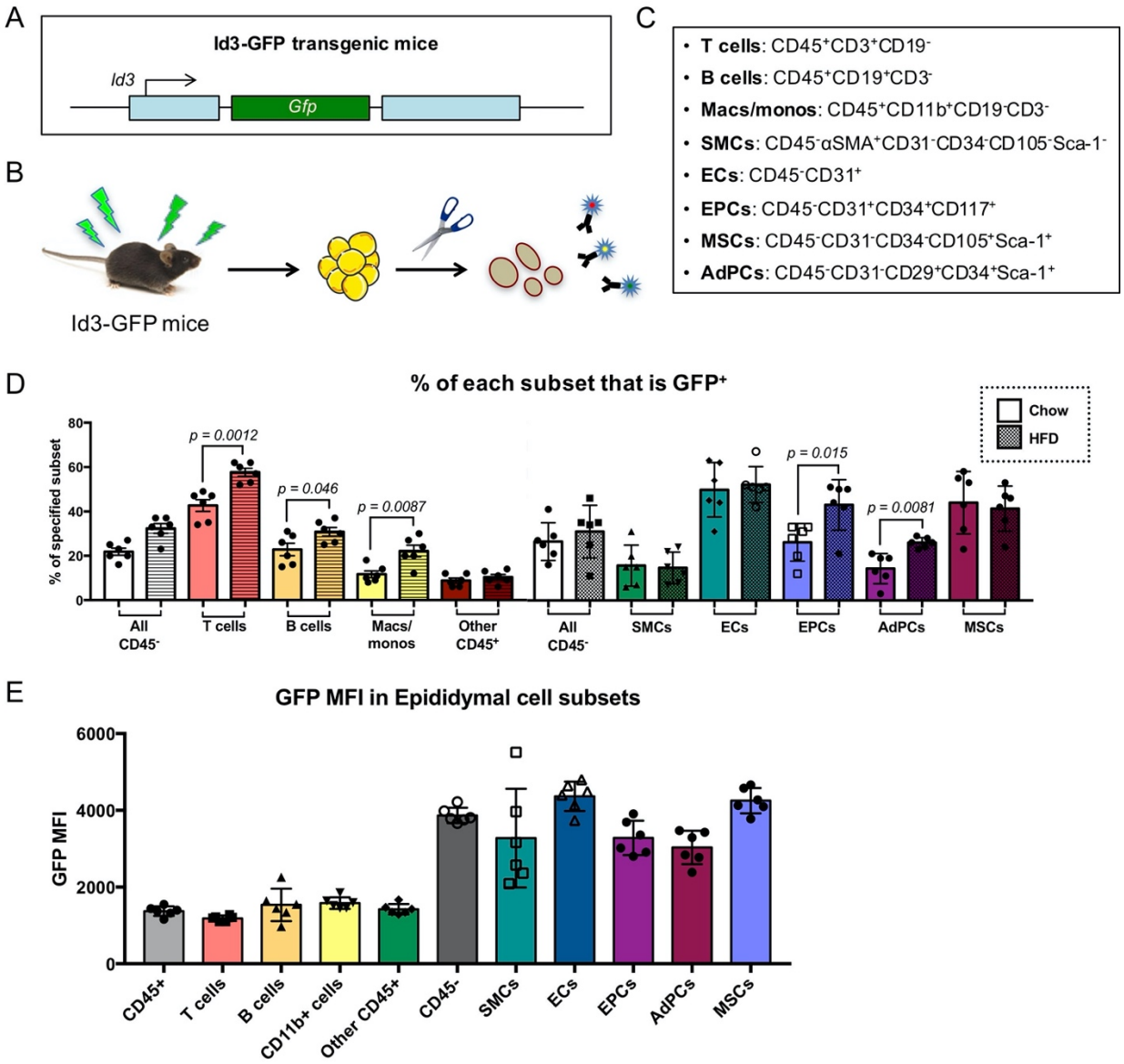

Figure A1.1. Id3 promoter activation in cell types within the epididymal adipose stromal vascular fraction.

(A) Schematic explaining the Id3-GFP transgenic line. The GFP gene was knocked in immediately downstream of the Id3 gene. The genotype of GFP+ mice was $Id3^{Gfp/+}$ to avoid producing full Id3 knockouts. **(B)** Experimental schematic: mice were fed either one week of obesity diet (60% kcal from fat) or chow and then epididymal adipose depots were harvested, digested, and stained for flow cytometry analysis. **(C)** Markers used to identify each subset. Subset abbreviation definitions are as follows: Macrophages and monocytes (Macs/monos), smooth muscle cells (SMCs), endothelial cells (ECs), endothelial progenitor cells (EPCs), mesenchymal stem cells (MSCs), and one week of chow or obesity diet (HFD). **(D,E)** The proportion of **(D)** and magnitude **(**MFI, **E)** of Id3 promoter activation in $CD45^+$ immune and $CD45^-$ stromal and vascular cell subsets. Data collected with the help of Anh Nguyen.

C. Conclusions and Discussion

These results revealed the proportion and extent to which Id3 expression was promoted in a multitude of cells from epididymal adipose SVF after one week of chow or HFD feeding. Generally, ECs and MSCs had the highest GFP signal per cell and T cells and ECs had the greatest proportion of GFP^+ cells. An important caveat to bear in mind when reviewing these results is that this is an Id3-reporter mouse and thus GFP expression does not necessarily reflect Id3 protein levels in each of these cell subsets. Gene promoter activation is not congruent with mRNA transcription, which is not congruent with protein translation or stabilization, thus it would be inaccurate to project these results to protein levels of Id3. These data did, however, direct our attention towards ECs as being a potential cell type of interest in which to study the effects of Id3 expression.

III. Id3's role in adipose tissue angiogenesis and expansion

A. Rationale

Previous studies from the McNamara lab showed that Id3 global KO ($Id3^{GKO}$) mice have attenuated adipose tissue expansion, microvascular blood volume, and VEGFA expression during HFD-feeding[127]. The literature shows there is a clear connection between adipose tissue expansion and vascular growth[230, 232-234] and results from Cutchins *et al*. suggest there may be a vascular component to the inhibited adipose tissue expansion observed. Whether this change in vascular blood volume is due to attenuated angiogenesis remains unclear. Thus, in these studies I aimed to quantify the angiogenic potential of $Id3^{GWT}$ and $Id3^{GKO}$ adipose tissue depots to begin to better understand the role the vasculature might play in $Id3^{GKO}$ mice during adipose tissue expansion.

B. Results

To begin to address the possibility that Id3 may be regulating angiogenesis in adipose tissue, we analyzed mouse adipose tissue gene expression data from the Hybrid Mouse Diversity Panel database[245]. The strength of correlations between each gene in the database and Id3 was calculated. The top 100 most highly-correlated genes were then subjected to Gene Ontology (GO) enrichment analysis where the top five pathways that emerged were related to angiogenesis and neovascularization (**Table A1.1**). This suggested to us that Id3 could be playing a role in angiogenesis in adipose tissue.

Table A1.1. Id3 gene expression correlates with angiogenic and blood vessel regulatory genes.
Top five hits from Gene oncology enrichment analysis. 100 genes with the highest expression correlation with Id3 were clustered according to their functional role. *P*-values reflect significance of correlation. Analysis was performed by Mete Civelek.

Cluster	P-value
Vasculature development	4.45E-08
Blood vessel development	3.22E-07
Angiogenesis	1.66E-06
Blood vessel morphogenesis	3.83E-06
Vasculogenesis	1.53E-04

Next, to determine the angiogenic potential of adipose tissue in $Id3^{GWT}$ and $Id3^{GKO}$ mice, adipose was extracted from both genotypes and cultured in Matrigel to quantify vascular sprouting over time. Images taken each day revealed that sprouting in these conditions was maximal by the fourth day of culture (**Figure A1.2A-C**). Furthermore, the proportion of subcutaneous and omental adipose tissue that sprouted was much higher than epididymal adipose. Finally, there were no differences in sprouting potential of any adipose depots between $Id3^{GWT}$ and $Id3^{GKO}$ mice (**Figure A1.2A-C**). In addition to quantifying the potential for sprouts in each aliquot, the extent of sprouting in each sprouted explant was quantified. To do this, the area of the explant and the area of the explant plus its sprouts were quantified. Explant plus its sprouts area was greater than that of the explant along (**Figure A1.2D,E**). To quantify the extent of sprouting, the explant plus sprouts area was divided by the area of the explant only and multiplied by 100 to generate a percentage. Note that epididymal explants were not quantified due to the limited number of explants that sprouted. Neither subcutaneous (**Figure A1.2D**) nor omental adipose explants (**Figure A1.2E**) demonstrated differences between genotypes.

Figure A1.2.

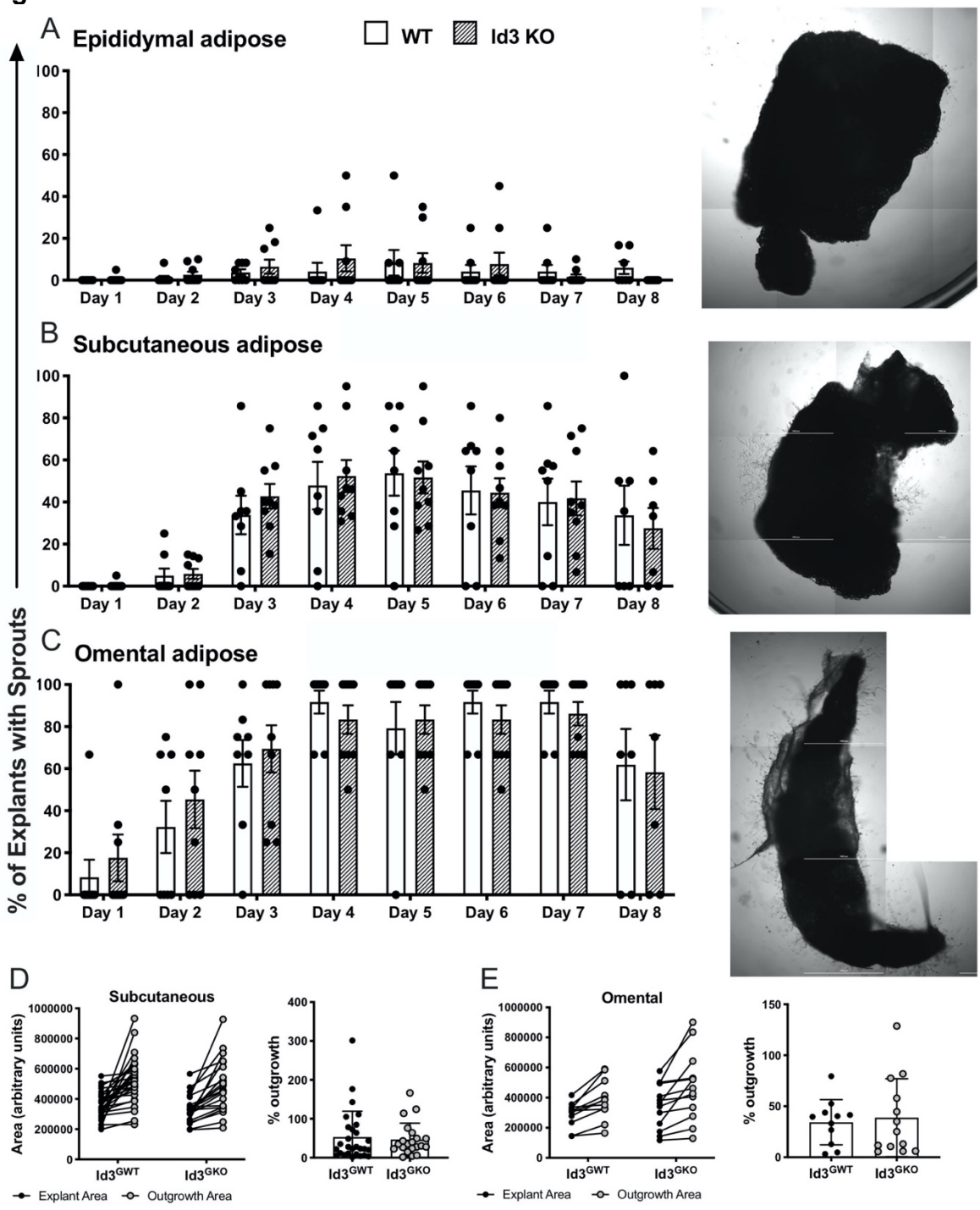

Figure A1.2. Adipose explant sprouting is not regulated by Id3.
(A-C) The number of epididymal **(A)**, subcutaneous **(B)**, and omental **(C)** explants that generated sprouts was quantified as a percentage of total explants cultured. **(D,E)** The area of explant plus sprouts and explant alone were quantified and plotted to demonstrate that the area of explant plus sprouts was greater than explant alone in most cases. The extent of sprouting was calculated as the percent of explant plus sprouts area that was taken up by explant area alone in the subcutaneous explants **(D)** and omental explants **(E)**.

Finally, vascular density in the adipose tissue of Id3^{GWT} and Id3^{GKO} littermates was also quantified to determine if vascular density was altered after a short-term HFD feeding. Adipose tissue aliquots were stained with BODIPY and lectin and whole mounted for imaging (**Figure A1.3A**). Rapid analysis of vessel elements (RAVE) analysis (see methods) was used to quantify the total area of lectin staining (**Figure A1.3B**), total length of vascular structures (**Figure A1.3C**), the tortuosity of the vessels (**Figure A1.3D**), and the number of branch points (**Figure A1.3E**) in each adipose image. By all of these metrics, there was no difference between Id3^{GWT} and Id3^{GKO} mice after 4-6 weeks of HFD feeding.

Figure A1.3.

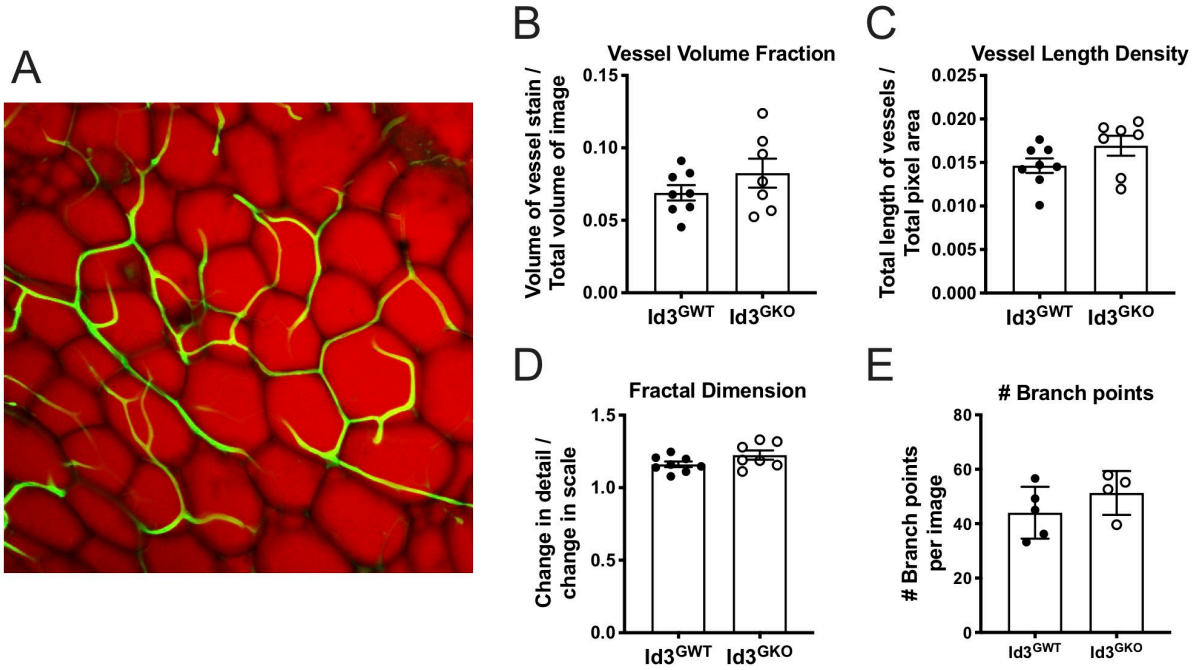

Figure A1.3. Adipose vascular density after 4-6 weeks of HFD feeding is not regulated by Id3.
(A) Adipose tissue was stained with BODIPY and lectin and whole mounted. **(B)** The total volume of lectin^{+} staining relative to the total volume of each image was calculated as the Vessel Volume Fraction. **(C)** The total length of vessels per image was calculated as the Vessel Length Density. **(D)** The change in detail over the change in the scale, or tortuosity, of the vessels was calculated as the Fractal Dimension. **(E)** The number of points where at least two vessels met was quantified as the number of Branch points.

C. Conclusion and Discussion

GO enrichment analysis of transcripts from mouse epididymal adipose tissue collected in the Hybrid Mouse Diversity Panel revealed that Id3 significantly correlated with many genes involved in angiogenesis and neovascularization. Assays, however, revealed that angiogenic potential and the extent of vascular content were not different in adipose of $Id3^{GWT}$ and $Id3^{GKO}$ littermates during HFD-feeding. One additional assay that could be conducted to determine whether Id3 regulates angiogenesis in adipose tissue would be to quantify $CD31^{+}$ capillary structures in cross sections of adipose tissue. Simultaneously, the diameter of larger arteries in the adipose tissue can be quantified to determine if arteriogenic processes may be contributing to the reduced MVB observed in $Id3^{GKO}$ mice.

Results from adipose explant experiments also revealed that mouse omental and subcutaneous adipose tissue have a greater angiogenic potential than epididymal adipose tissue. Why this is remains unclear, but raises interesting questions regarding the differences between adipocytes and other adipose-resident cells in each of these depots. Is there an intrinsic difference in the vasculature within each depot that results in differential angiogenic potential? Or perhaps the populations of non-vascular cells in the stromal-vascular fraction (SVF) of each depot secrete different angio-regulatory factors.

IV. EC-specific Id3 does not regulate weight gain or late-term adipose mass *in vivo*

A. Rationale

While results thus far suggest that Id3 does not regulate angiogenic sprouting in adipose tissue, it is still possible that Id3 activities in the vasculature regulate adipose tissue expansion. Indeed, we observed that ECs had the largest proportion of cells with Id3 promoter activity and there are mechanisms independent of sprouting angiogenesis that may regulate MBV. Further, Tang *et al*. showed that AdPCs occupy a perivascular niche in adipose tissue[235] and Tran *et al*. demonstrated that ECs are capable of differentiating to adipose tissue[242]. These results suggest that ECs can play a role in adipose tissue homeostasis that may not stem from neovascularization processes. In these studies, we utilized the EC-specific Id3 WT ($Id3^{ECWT}$) and KO ($Id3^{ECKO}$) littermates validated in Chapter 3 (**Figure 3.1**) to address whether Id3 expression in ECs would regulate adipose tissue expansion during HFD feeding. I

hypothesized that Id3^{ECKO} mice would demonstrate attenuated adipose tissue expansion and overall weight gain.

B. Results

Id3^{ECWT} and Id3^{ECKO} mice were fed a HFD for 20 weeks. Over the course of the diet, mice were weighed to track weight gain and no difference was observed in total weights (**Figure A1.4A**) or weight gain (**Figure A1.4B**) between genotypes. Though there was no difference in weight gain, it is possible that glucose handling may have been affected by changes in the adipose tissue. However, no difference in glucose tolerance was observed after conducting a glucose tolerance test (**Figure A1.4C**). Finally, at the end of the diet, adipose tissue and the liver were harvested and weights compared. There were no differences in the mass of the liver (**Figure A1.4D**), epididymal adipose tissue (**Figure A1.4E**), or subcutaneous adipose tissue (**Figure A1.4F)** of Id3^{ECWT} and Id3^{ECKO} mice. However, the mass of omental fat was significantly reduced in Id3^{ECKO} mice (**Figure A1.4G**).

Figure A1.4.

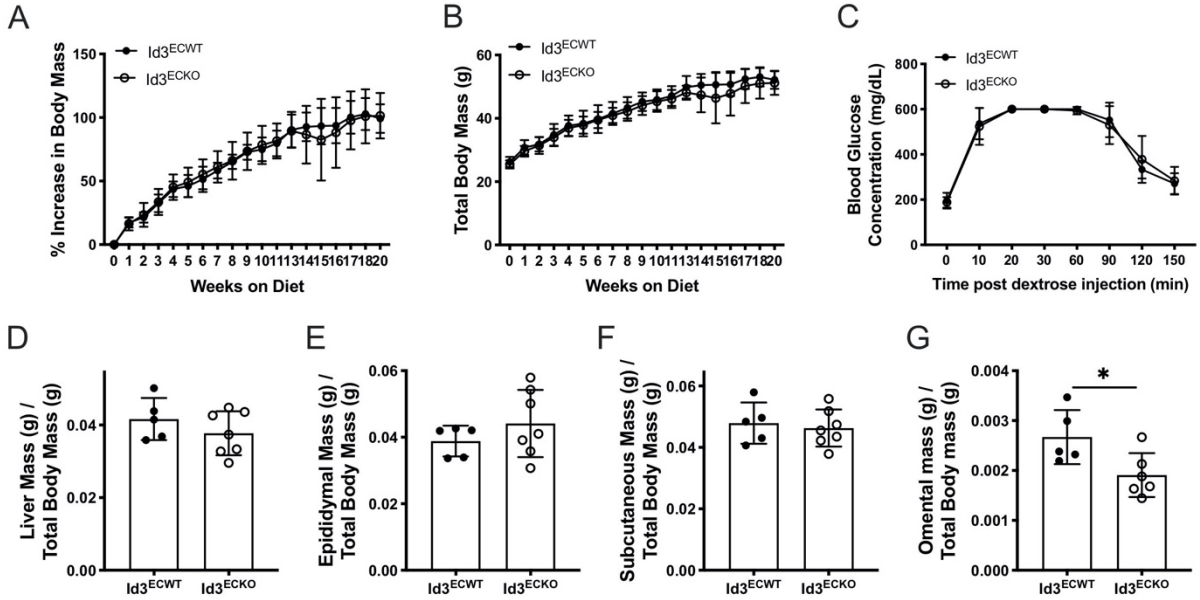

Figure A1.4. Results from obesity study in Id3^{ECWT} and Id3^{ECKO} mice.
(A,B) Id3^{ECWT} and Id3^{ECKO} mice were fed HFD for approximately 20 weeks and weighed everyone 1-2 weeks. **(C)** Towards the end of the diet regimen, a glucose tolerance was conducted on the mice. **(D-G)** At the end of feed, livers **(D)**, epididymal adipose **(E)**, subcutaneous adipose **(F)**, and omental adipose **(G)** were weighed and normalized to the total body weight of each mouse to account for variations in overall weight gain.

C. Conclusions and Discussion

While no significant differences were observed in total weight gain or glucose tolerance between $Id3^{ECWT}$ and $Id3^{ECKO}$ mice, there was an observed difference in omental mass between genotypes. This demonstrates that Id3 in ECs regulates omental fat mass, but the mechanism whereby this occurs remains unclear. It is possible that Id3 could promote angiogenesis in omental fat, which in turn would support further expansion of adipose tissue mass. Given the greater angiogenic potential of omental fat compared to epididymal and subcutaneous fat (**Figure A1.2**), it is possible that $Id3^{ECKO}$ omental fat explants may demonstrate attenuated EC sprouting relative to $Id3^{ECWT}$ controls. It is also important to note that adipose tissue weights were not measured at earlier time points, thus we cannot yet conclude if Id3 has an effect on early adipose tissue expansion that is later overcome by compensatory mechanisms or chronic conditions. While many findings from this experiment revealed no phenotypic differences between genotypes, these results contribute to a fuller understanding of the EC-specific role that Id3 plays during disease.

V. Methods

Animals and Feeding

Id3-reporter mice, $Id3^{GWT}$ and $Id3^{GKO}$ littermates, and $Id3^{ECWT}$ and $Id3^{ECKO}$ littermates were generated and housed at the University of Virginia. All animal experiments performed in this study were approved by the Institutional Animal Care and Use Committee of the University of Virginia. Mice were fed a high-fat diet (HFD) composed to 60% kcal from fat for varying amounts of time as specified in Results sections. When needed, chow controls were fed normal chow diet instead of HFD.

Prepared Buffers and Media

AKC lysis buffer: 0.15 M NH4Cl + 0.01 M KHCO3 + 0.1 mM EDTA in ddH_2O

FACS buffer: 0.05% NaN3 + 1% BSA in PBS

Digestion buffer: 1 mg/mL collagenase type I in FACS buffer or DMEM

Tissue processing

In general, mice were euthanized by CO_2 overdose. Mice were perfused through the left ventricle (after cutting the right atrium) with 10 mL PBS supplemented with 0.5 mM EDTA followed by 5–10 mL of PBS before harvesting tissues. Tissues were store in PBS during processing to keep them hydrated. Epididymal adipose depots were placed in digestion buffer, minced, and incubated at 37°C, shaking, for ~45 minutes. Digested tissue was then pipetted up and down to create a single-cell suspension, passed through a 70 μm filter, washed with FACS buffer, and pelleted. Cells were treated with AKC lysis buffer to lyse remaining red blood cells as needed. Cells were then stained for flow cytometry.

Flow cytometry

All cells were stained with fluorophore-conjugated antibodies against cell surface proteins (**Table A1.2**) in Brilliant Violet Stain Buffer (BD) for 25 minutes at 4°C then washed with FACS buffer. Cells were then stained with Live/Dead (Fisher) in PBS for 30 minutes at 4°C then washed with FACS buffer. Cells were then fixed with 2% PFA for 7–10 minutes at room temperature and washed with FACS buffer. Finally, cells were resuspended in FACS buffer and stored at 4°C until analyzed. Cells were run on the LSR Fortessa (Beckton Dickison) by Anh Nguyen and compensated and analyzed in FlowJo (FlowJo).

Table A1.2. Flow cytometry antibodies

Antigen	Clone	Vendor
Alpha-SMA	1A4	Sigma-Aldrich
CD3	145-2C11	eBioscience
CD11b	M1/70	BD Biosciences
CD19	Id3	eBioscience
CD29	HMB1-1	eBioscience
CD31	390	eBioscience
CD34	MEC14.7	Biolegend
CD45	30-F11	BD Biosciences
CD105	MJ7/18	Biolegend
CD117	2B8	Biolegend
GFP	FM264G	Biolegend
Sca-1	D7	Invitrogen

Tissue harvesting

In general, mice were euthanized by CO_2 overdose. Mice were perfused through the left ventricle (after cutting the right atrium) with 10 mL PBS supplemented with 0.5 mM EDTA followed by 5–10 mL of PBS before harvesting tissues. Epididymal, omental, and subcutaneous adipose depots were then harvested. Inguinal lymph nodes were removed prior to harvesting subcutaneous adipose depots.

Adipose tissue explants

Epididymal, subcutaneous, and omental fat were aliquoted into small pieces approximately 1-2 mm by 1-2 mm. Matrigel was placed into wells of a 96-well plate and stored on ice to keep the Matrigel in liquid-phase. One adipose aliquot was then added into each well and EC Growth Media was added on top (Lonza). The plates were then placed in a 37ºC incubator for up to 8 days. Plates were removed each day and imaged on a Cytation 3 (BioTek). Images were processed and analyzed using Image J software.

Adipose tissue whole mounts

Aliquots of epididymal adipose were fixed in 4% PFA then washed in PBS. Adipose was blocked and permeabilized in 5% BSA, 0.3% Triton in PBS before incubating overnight with BODIPY 558/568 (Life technologies, D-3835) and Isolectin GS-IB_4 AF488 conjugate (Thermofisher) at 4°C. After a final wash, samples were mounted in a 1:1 solution of PBS: Glycerol and digital images were acquired using confocal microscopy (Nikon Instruments Incorporated, Model TE200-E2; 20X objective). Images were processed using ImageJ software. Once processed, images were analyzed using Rapid analysis of vessel elements (RAVE) algorithm to quantify aspects of vessel density and complexity[246]. This analysis tool was developed by a former graduate student, Marc Seaman, while he studied in the laboratory of Shayn Peirce-Cottler to streamline analysis of various aspects of blood vessels identified in tissue.

Gene expression analysis

RNA transcript levels were obtained from the Hybrid Mouse Diversity Panel database, which is a database of genetic, metabolic, and cardiovascular traits from approximately 100 inbred

strains of mice. Transcripts were analyzed to determine the top 100 genes that correlated most significantly with Id3 RNA expression levels. Those 100 genes were then applied to Gene Ontology (GO) enrichment analysis (http://geneontology.org/docs/go-enrichment-analysis/) to identify the signaling pathways most significantly associated with the identified genes. These analyses were performed by Mete Civelek in the Center for Public Health Genomics and UVa.

Appendix 2: Characterizing cellular uptake of liposomes *in vivo*

Adapted from Osinski V, et al. In vivo *Liposomal Delivery of PPARα/γ Dual Agonist Tesaglitazar in a Model of Obesity Enriches Macrophage Targeting and Limits Liver and Kidney Drug Effects. Theranostics, 2020: 10(2)*[247]

I. Rationale

In collaboration with the Boucher, Kelly, and Klibanov labs at AstraZeneca and UVA, we conducted studies to identify novel peptides to target liposomes to adipocytes. The overall goal was to identify novel targeting approaches to delivery PPARα/γ tesaglitazar. More specifically, we hoped to target tesaglitazar to adipocytes to avoid unwanted side effects including markers of kidney dysfunction that were previously observed in tesaglitazar clinical trials. During these studies, we came across interesting findings regarding non-targeted liposomal distribution *in vivo*. These and other results have been reported in full in Theranostics[247] and PLoS One[248], but findings summarized in this document will center around our findings regarding *in vivo* uptake of liposomes.

Liposomal drug delivery has emerged as a promising strategy to limit the side effects of otherwise effective therapeutics by directing the active compound to the cells and tissue of interest while avoiding others, such as the liver and kidney, which often contribute to undesired side effects[217, 218]. With the addition of polyethylene glycol (PEG) to liposome formulations, half-life of circulating liposomes increases and uptake by the reticuloendothelial system (RES, comprised of the liver, kidneys, spleen, bone marrow, lungs, and lymph nodes) and free drug in circulation are reduced. Even with such advancements in liposome formulations, uptake of liposomes by the liver and other RES tissues and phagocytes is still prevalent[218]. Liposomes enrich drug delivery to phagocytic cells such as tissue-resident macrophages including liver-resident macrophages known as Kupffer cells [249]. Liposome delivery has been identified as a promising approach for diseases associated with macrophage dysfunction[216, 250]. There is current interest in using targeted nanoparticle approaches to deliver compounds to both macrophages and a variety of non-macrophage cell types including cancer cells[251] and endothelial cells [252], but a thorough characterization of the cell types that take up liposomes *in vivo* has not been reported. In the context of obesity-associated dysmetabolism, a disease characterized and driven by macrophage dysfunction, the capacity to target drugs to macrophages or other non-phagocytic immune cell types including B cells and T cells in the adipose may prove useful as both cell types play important roles in regulating inflammation and macrophage recruitment to the adipose tissue during obesity[253]. To address this, we used fluorescent labeling of liposomes coupled with fluorescently activated cell sorting (FACS) and

fluorescence molecular tomography (FMT) imaging to thoroughly describe these tissues and cell types *in vivo* in an unbiased manner.

Abbreviations:

AT: adipose tissue; ATM: adipose tissue macrophages; DSPC: 1,2-distearoyl-sn-glycero-3-phosphocholine; DSPE: 1,2-distearoyl-sn-glycero-3-phosphoethanolamine; Ehhadh: enol-CoA hydratase and 3-hydroxyacyl CoA dehydrogenase; EC: endothelial cell; Epid: epididymal; Fabp: fatty acid binding protein; FACS: fluorescently activated cell sorting; FMT: fluorescence molecular tomography; GR: gluococorticoid receptor; Lpl: lipoprotein lipase; MCP-1: monocyte chemoattractant protein-1; MFI: mean fluorescent intensity; Pdk4: Pyruvate dehydrogenase kinase 4; PEG: polyethylene glycol; PerC: peritoneal cavity; PPAR: peroxisome proliferator-activated receptor; RES: reticuloendothelial system; SC: subcutaneous; SD: standard deviation; SVF: stromal vascular fraction; Tbp: tata box binding protein; VSMCs: vascular smooth muscle cells

II. Methods

Non-liposomal drug preparation

Tesaglitazar was dissolved in 0.5% carboxymethyl cellulose to a concentration of 0.35 mM. Volumes administered to mice were calculated based on body weights in order to delivery 1 µmol per kg of body weight each day. The vehicle used for non-liposomal drug treatments was 0.5% carboxymethyl cellulose administered at equal volumes to that of tesaglitazar.

Liposome preparation and characterization

Liposome preparation

Liposomes were initially prepared with the remote loading attractant calcium acetate using the reverse-phase evaporation technique [254] with DSPC (phosphocholine), cholesterol and PEG-2000 DSPE at a mass ratio of 2:1:1 (phospholipids were from Avanti or Lipoid; cholesterol from Sigma). Additionally, during this step liposomes were fluorescently labeled by adding DiD lipid dye at a concentration of 1 mg DiD per 1 ml of liposomes (molar ratio of 46:1 of DSPC:DiD). DiD is an accepted abbreviation for 1,1'-dioctadecyl-3,3,3',3'tetramethylindocarbocyanine dye.

As this material has two octadecyl "fatty tails", exactly as DSPC, the main component of the liposomes, we do not expect a significant amount to be outside of the lipid membrane. Long-chain phospholipids normally possess critical micelle concentrations in the picomolar range, so we expect a negligible amount of free dye present. Lipid dyes like DiO, DiD and DiI are routunely used for liposome research and they are considered non-exchangeable [255].

Briefly, an ether-chloroform solution of lipids was mixed with aqueous calcium acetate (Ca-acetate, 1 M, pH 7.4). The ratio between organic and aqueous phase was 4:1. A mixture was subjected to emulsification by sonication (XL2020, Misonix, 50% power, 30 sec) and then organic solvents were removed under vacuum using a rotary evaporator (Re111, Buchi) connected to a vacuum line. Resulting liposomes were subjected to repeated Nuclepore filtration to achieve homogeneous size distribution, as determined by dynamic laser light scattering (DLS, Nicomp 370). External Ca-acetate was removed using a Zeba spin-column and to half of the batch, aqueous tesaglitazar in HEPES buffer (pH 7.4) was added and incubated with mixing at 37°C for 1 hour. External unentrapped tesaglitazar was removed from liposomes with a Zeba spin-column. The vehicle used for liposomal treatments was liposomes containing aqueous calcium acetate. These were administered at volumes calculated to deliver comparable numbers of vehicle-loaded liposomes to the number of tesaglitazar-loaded liposomes.

Quantifying drug loading, liposome size, shape, and zeta potential

Drug loading was determined by measuring 270 nm using ultraviolet-visible spectroscopy (UV-vis). Particles per volume were quantified by Nanoparticle Tracking Analysis (Nanosight NS300, Malvern Instruments Ltd., Worcestershire, UK) in order to calculate µg of tesaglitazar per mg of DPSC lipid. Dynamic light scattering (Particle Sizing System, Inc, Santa Barbara, CA) was utilized to quantify particle size. Liposomes were also imaged using cryoTEM to assess particle structure. Additionally, zeta potential was measured using a Malvern ZetaSizer, in 10 mM HEPES buffer pH 7.4 and 25°C.

Liposome release kinetics

Release kinetics were determined by ultrafiltration in an Amicon 10 KDa 0.5 ml ultrafilter cartridge, where an aliquot of liposomes was added to buffer and spun to separate liposomes

from the released free drug in the buffer. Concentration of tesaglitazar outside of liposomes was quantified by UV-vis following ultrafiltration.

Animals

Male C57Bl/6 leptin-deficient (*ob/ob*) and high-fat diet-fed C57Bl/6 (DIO) mice were purchased from Jackson Labs (Stock # 000632 and # 380050, respectively). Experiments were performed using 9- to 14-week old male *ob/ob* mice and 16-week old male DIO mice that were fed an obesity diet (60% cholesterol, Research Diets D12492) for 10 weeks. All animal experiments were performed in accordance with the Institutional Animal Care and Use Committee of the University of Virginia.

***Ex vivo* biodistributions and blood pharmacokinetics**

Blood pharmacokinetics

To quantify pharmacokinetics of tesaglitazar-loaded liposomes, a dose of approximately 2.5 μmol tesaglitazar/kg was administered via tail vein. Blood draws were collected at 1 min, 3 min, 5 min, 10 min, 15 min, 30 min, 1 h, 2 h, 6 h, and 24 h post-injection. Fluorescence molecular tomography (FMT) imaging was used to measure the amount of liposomes in circulation at each time point. Samples were imaged using the 680nm laser of the FMT 4000 system (PerkinElmer, Waltham, MA). Pharmacokinetics of orally administered tesaglitazar and liposomal tesaglitazar were determined using non-compartmental analysis (NCA) was performed using Phoenix WinNonlin 8.1, Certara, NJ USA).

Ex vivo biodistribution

Tissues were harvested four and 24 hours post-injection. Liposome tissue biodistribution was measured using *ex vivo* FMT imaging of organs to determine the amount of DiD present in tissues. It was represented as percentage of injected dose per gram of tissue (%ID / g) and calculated by %ID / g = (Tissue Value * 100) / (Total injected dose) where the total injected dose was the sum of injected doses in instances in which treatments involved multiple injections.

Processing tissues for flow cytometry

Peritoneal cells

Peritoneal cells were collected by peritoneal lavage. Lavages were spun down and treated with AKC lysis buffer (0.15 M NH_4Cl, 0.01 M $KHCO_3$, 0.1 mM EDTA) to lyse remaining red blood cells. Cells were then washed with FACS buffer (PBS, 0.05% NaN_3, 1% BSA) to be stained for flow cytometry.

Adipose stromal vascular fraction (SVF) cells

Whole adipose tissue was placed in digestion buffer (0.12 M NaCl, 4.7 mM KCl, 1.3 mM $CaCl_2 2H_2O$, 1.2 mM KH_2PO_4, 1.2 mM $MgSO_4 7H_2O$, 40 mM HEPES (pH 7.5), 2.5% BSA, 200 nM adenosine, 1 mg/mL Collagenase Type 1), minced, and incubated at 37°C with shaking for 45 minutes. Digested tissue was then washed with FACS buffer, and pelleted separating floating adipocytes from the remaining stromal vascular fraction (SVF) in the pellet. Cells were treated with AKC lysis buffer to lyse remaining red blood cells and then filtered through a 70 μm filter to remove undigested tissue and/or matrix proteins. Cells were then stained for flow cytometry.

Bone marrow cells

Following perfusion, rear femurs and tibias were harvested and excess muscle and tissue removed. The ends of each bone were cut away to access the marrow. Using 5mL of PBS per bone, each bone was flushed using a syringe. Cell suspensions were spun and treated with AKC lysis buffer to lyse remaining red blood cells. Cells were then washed with FACS buffer to be stained for flow cytometry.

Spleen

Spleens were mashed through a 70 μm filter and washed with 10 mL of FACS buffer, then spun down. Cell pellets were resuspended in 5 mL of AKC lysis buffer and incubated for 5 minutes before being quenched with 5 mL of FACS buffer. Cells were then spun down and aliquoted to use $1/50^{th}$ of each sample for flow cytometry.

Blood cells

100 µL of blood was treated with AKC lysis buffer for 5 minutes. Lysis was quenched with FACS buffer and cells were spun down to be stained for flow cytometry.

Flow cytometry

All cells were stained with Live/Dead in PBS for 30 minutes at 4°C then washed with FACS buffer. Next, the cells were stained with fluorescently-labeled antibodies against cell surface proteins (**Table A2.1**) in FACS buffer for 25 minutes at 4°C then washed with FACS buffer. Cells were then fixed with 2% PFA for 7-10 minutes at room temperature and washed with FACS buffer. If cells were sorted, they were not fixed. Finally, cells were re-suspended in FACS buffer and stored at 4°C until analyzed. Fixed samples were run on the Attune NxT (Thermofisher; one-week liposome uptake experiments) or CyAN ADP LX (Beckman Coulter; four hour and 24 hour liposome uptake and one-week macrophage subset experiments) and live cells were sorted on the INFLUX (BD).

Table A2.1: Flow cytometry antibodies

Marker	Fluorochrome(s)	Company	Clone
CD3	FITC	Pharmingen, BD Biosciences	145-2C11
CD11b	BV421, FITC	BioLegend	M1/70
CD11b	PerCP Cy5.5	BD Biosciences	M1/70
CD11c	APC ef780	eBioscience	N418
CD19	PE	eBiosciences	eBio1D3
CD19	PE CF594	BD Biosciences	1D3
CD31	FITC	eBioscience	390
CD31	BV605	Biolegend	390
CD45	PE-CF495, PerCP	BD Biosciences	30-F11
CD115	PE	eBioscience	AFS98
B220	BV421	Biolegend	RA3-6B2
F4/80	PE-Cy7	BioLegend	BM8

III. Results

Synthesis, circulation kinetics, and tissue biodistribution of tesaglitazar-loaded liposomes

PEGylated liposomes labeled with fluorescent DiD and loaded with tesaglitazar were synthesized for these studies with an average size of approximately 160 nm (**Figure A2.1A-C**). Following months of refrigerated storage, particle size and size distribution did not change significantly (**Figure A2.1A**). Repeats of the ultrafiltration tests showed that tesaglitazar was not presented at a significant quantity outside the ultrafilters, with over 90% retained. This drug retention is similar to what is observed for Doxil/Lipodox, which is also prepared by remote loading (**Figure A2.1A**). The zeta potential of the liposomes was -19.2 mV ± 13 mV and drug loading was 245 µg/mg of DSPC (**Figure A2.1A**). Pharmacokinetic and biodistribution studies were performed using LC-MS and fluorescence molecular tomography (FMT) and the amount of DiD in each tissue was quantifed from reconstructed images. The half-life of the liposomes in circulation was estimated to be 22.4 ± 10.4 h by non-compartmental analysis. It is hence in the same order of magnitude as the half-life of orally delivered tesaglitazar (35.4 ± 23.4 h, **Figure A2.1D**). Estimations of the C-max reveal a value of 0.62 ± 0.20 µmol tesaglitazar/L for orally-delivered tesaglitazar, while liposomal delivery demonstrated a C-max value of 4.38 ± 0.68 (**Figure A2.1D**). Calculated as percent injected dose per gram of tissue, DiD content in the liver, spleen, kidney, heart, epididymal (Epid) and subcutaneous (SC) adipose tissues were quantified at four hours, 24 hours and 7 days post-liposome treatment (**Figure A2.1E**).

Figure A2.1.

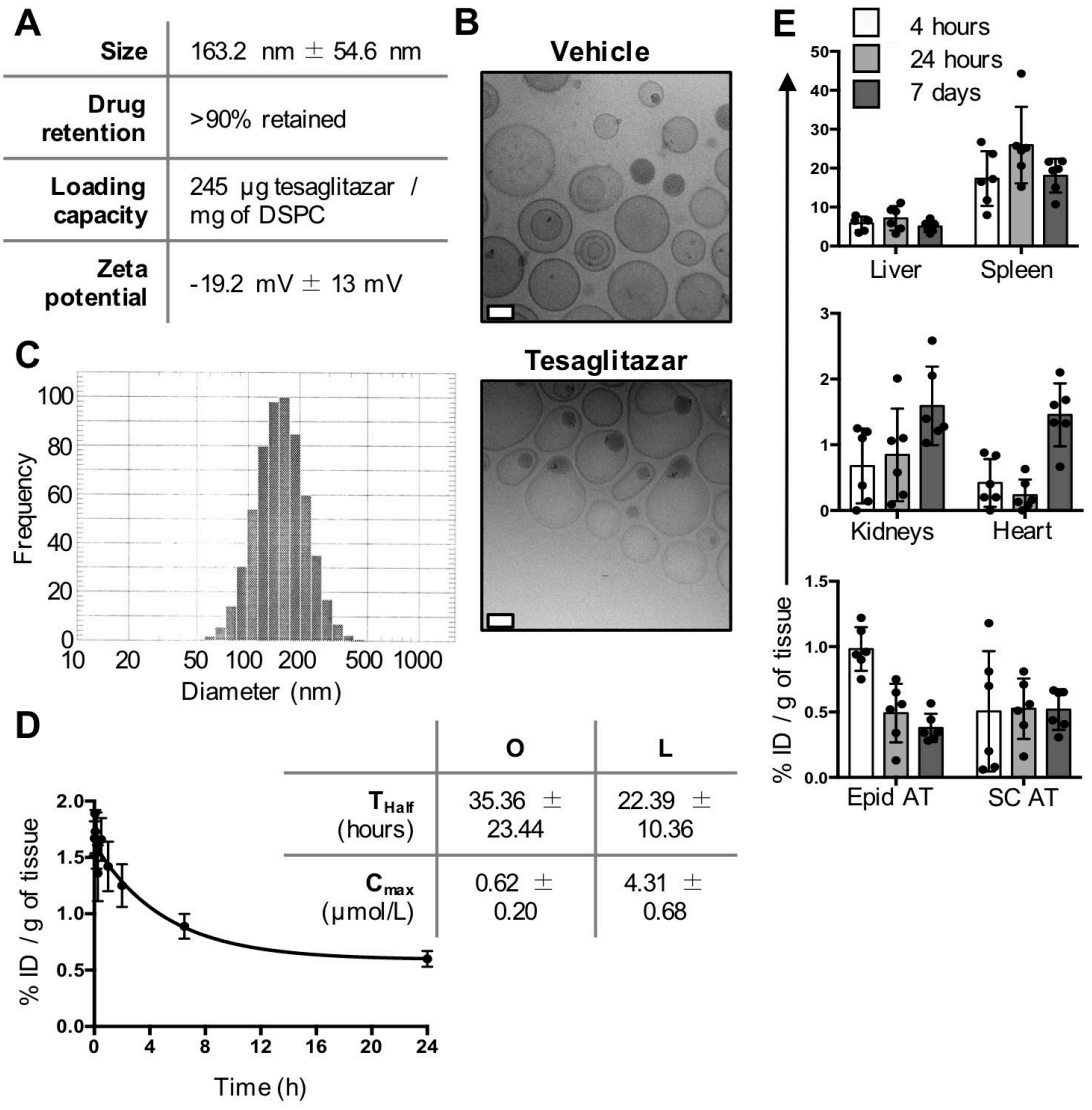

Figure A2.1. Liposome synthesis and blood and tissue PK and biodistribution. **(A)** Liposomes were synthesized, labeled with DiD, and loaded with tesaglitazar. Data reporting liposome characteristics are listed. **(B)** CryoTEM images of vehicle- and tesaglitazar-loaded liposomes are displayed to provide examples of liposome shape. White scale bars represent 50 nm. **(C)** DLS was utilized to quantify liposome size. **(D)** Tesaglitazar was administered orally (Oral) and in DiD-labeled liposomes (Liposomes) and blood was harvested at multiple time points to calculate the half-life (T_{half}) and C-max (C_{max}) of drug in circulation using non-compartmental analysis. **(E)** FMT was used to quantify liposome uptake in liver, spleen, kidneys, heart, Epid and SC adipose tissues four and 24 hours following administration as well as after seven days with three administrations of liposomes. **(F,G)** LC-MS was utilized to quantify tesaglitazar levels in circulation **(F)** and in liver tissue **(G)** at 24-hour and 7-day time points post-treatment. Standard oral formulation (oral) and liposomal delivery methods were compared to verify comparable drug exposure levels. Data represents the mean ± SD.

Macrophages were the predominant cell type that took up liposomes in visceral white adipose tissue

To characterize the cell types that take up drug-loaded liposomes in our system, DiD-labeled liposomes were administered intravenously to *ob/ob* mice three times over the course of one week (**Figure A2.2A**). Immunofluorescence staining of livers from these mice revealed co-localization of DiD and Kupffer cell marker CLECSF13 (**Figure A2.2B, Figure A2.3**). Flow cytometry was performed to identify the cell types that take up tesaglitazar-loaded liposomes in adipose tissue and the peritoneal cavity (**Figure A2.4A, Figure A2.5A**). We found that nearly all $CD45^+F4/80^+$ macrophages in the adipose stromal vascular fraction (SVF) and the peritoneal cavity (PerC) were DiD^+ (**Figure A2.2C**). Consistent with flow cytometry findings, immunofluorescent staining with the macrophage marker CD68 demonstrated that DiD-labeled liposomes co-localized with macrophages within whole mounted white adipose tissue samples (**Figure A2.2D, Figure A2.6**). Of the total DiD^+ population, macrophages made up approximately 67% and 40% of DiD^+ cells in epididymal (**Figure A2.2E**) and subcutaneous (**Figure A2.2F**) SVFs, respectively. Other $CD45^+$ cells as well as $CD45^-$ vascular and stromal cells, particularly endothelial cells (ECs), were DiD^+ demonstrating that cells other than professional phagocytes are capable of liposomal uptake (**Figure A2.2E-F, Figure A2.4B,C**). Various cell types including macrophages and other immune cells such as B and T cells in the peritoneal cavity (**Figure A2.5B**), bone marrow (**Figure A2.7B**), and blood (**Figure A2.8B**) also took up liposomes.

Figure A2.2.

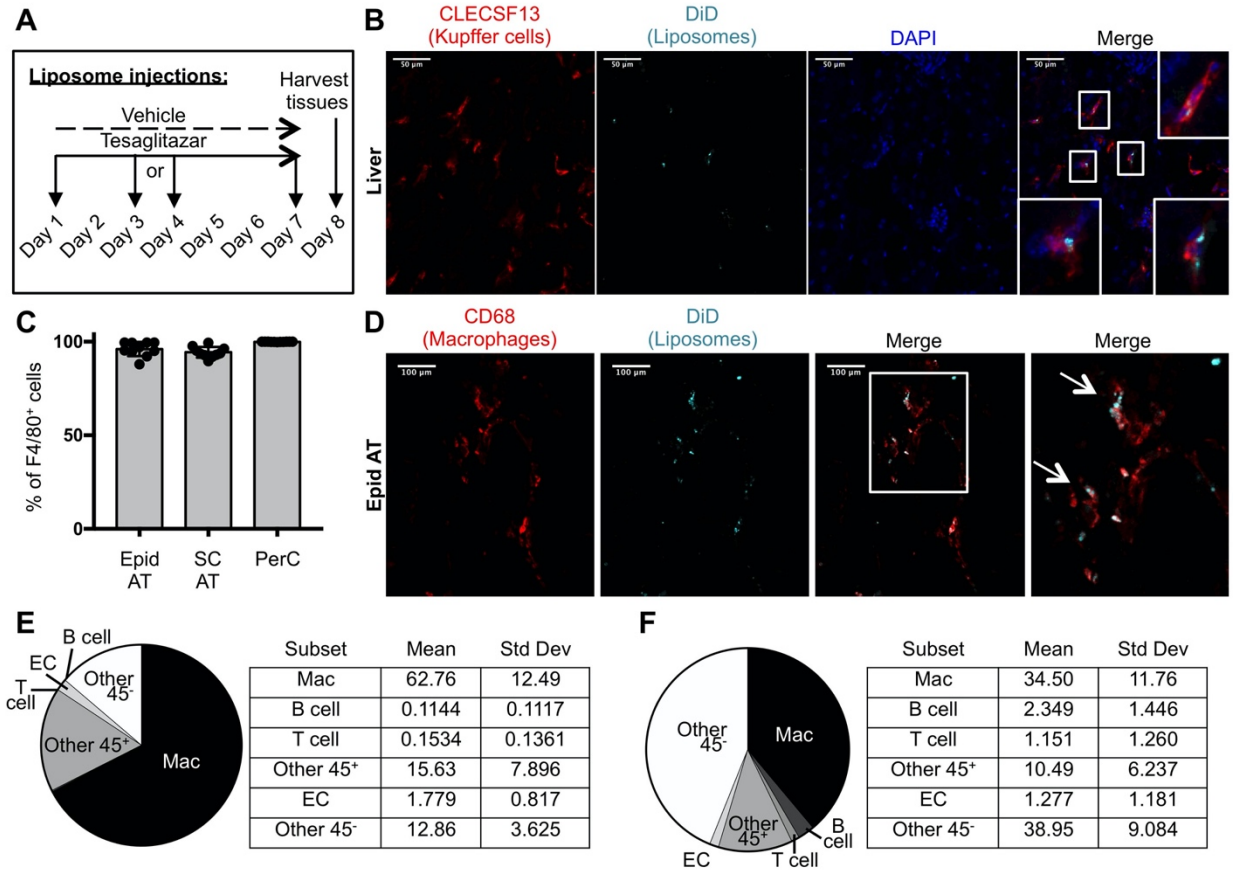

Subset	Mean	Std Dev
Mac	62.76	12.49
B cell	0.1144	0.1117
T cell	0.1534	0.1361
Other 45+	15.63	7.896
EC	1.779	0.817
Other 45-	12.86	3.625

Subset	Mean	Std Dev
Mac	34.50	11.76
B cell	2.349	1.446
T cell	1.151	1.260
Other 45+	10.49	6.237
EC	1.277	1.181
Other 45-	38.95	9.084

Figure A2.2. Cellular characterization of liposome uptake after one week of treatment. **(A)** DiD-labeled liposomes were injected intravenously into male *ob/ob* mice three times over the course of seven days. **(B)** Z-stack images of liver sections from *ob/ob* mice treated with tesaglitazar-loaded liposomes were stained with CLECS13F to identify Kupffer cells and assessed for co-localization with DiD-labeled liposomes. Co-localization of $CLECS13F^+$ cells and DiD are marked by white arrows. **(C)** Peritoneal lavages and Epid and SC AT were harvested to stain peritoneal cavity (PerC) cells and SVF cells, respectively, for analysis by flow cytometry. The percentage of $CD45^+F4/80^+$ macrophages that were DiD^+ was quantified. **(D)** Z-stack images of whole mounted Epid AT from an *ob/ob* mouse treated with tesaglitazar-loaded liposomes was stained with CD68 to identify macrophages and assessed for co-localization with DiD-labeled liposomes. Co-localization of interstitial $CD68^+$ cells and DiD are marked by white arrows. The white box delineates the area of the merged image that is enlarged (right-most panel). **(E,F)** DiD^+ macrophages and other cell subsets were also quantified as a percent of total DiD^+ cells in the Epid AT **(E)** and SC AT **(F)**, n = 5 in each group. The cell subsets analyzed were macrophages ($CD45^+F4/80^+$), B cells ($CD45^+CD19^+$), T cells ($CD45^+CD3^+$), other $CD45^+$ Cells ($CD45^+CD19^-CD3^-F4/80^-$), endothelial cells ($CD45^-CD31^+$), and other $CD45^-$ cells ($CD45^-CD31^-$). Data represents the mean ± SD.

Figure A2.3.

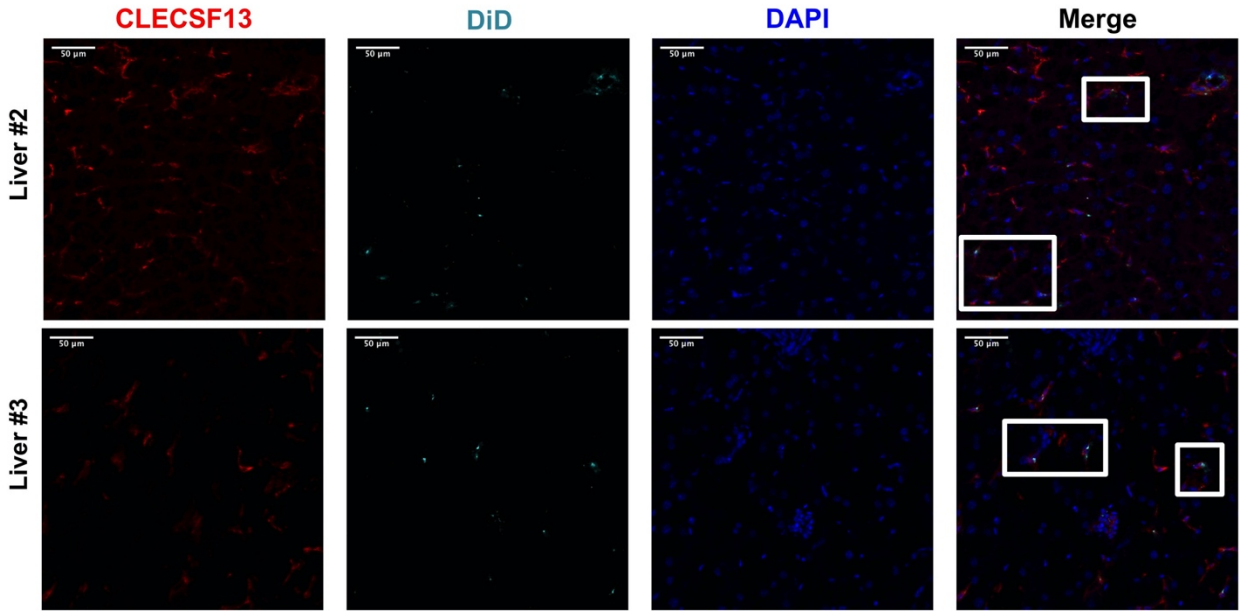

Figure A2.3. DiD$^+$ liposomes co-localized with CLECSF13 in liver.
Z-stack images of liver sections from an additional two *ob/ob* mice treated with tesaglitazar-loaded liposomes were stained with CLECS13F to identify Kupffer cells and assessed for co-localization with DiD-labeled liposomes. Co-localization of CLECS13F$^+$ cells and DiD are marked by white boxes.

Figure A2.4.

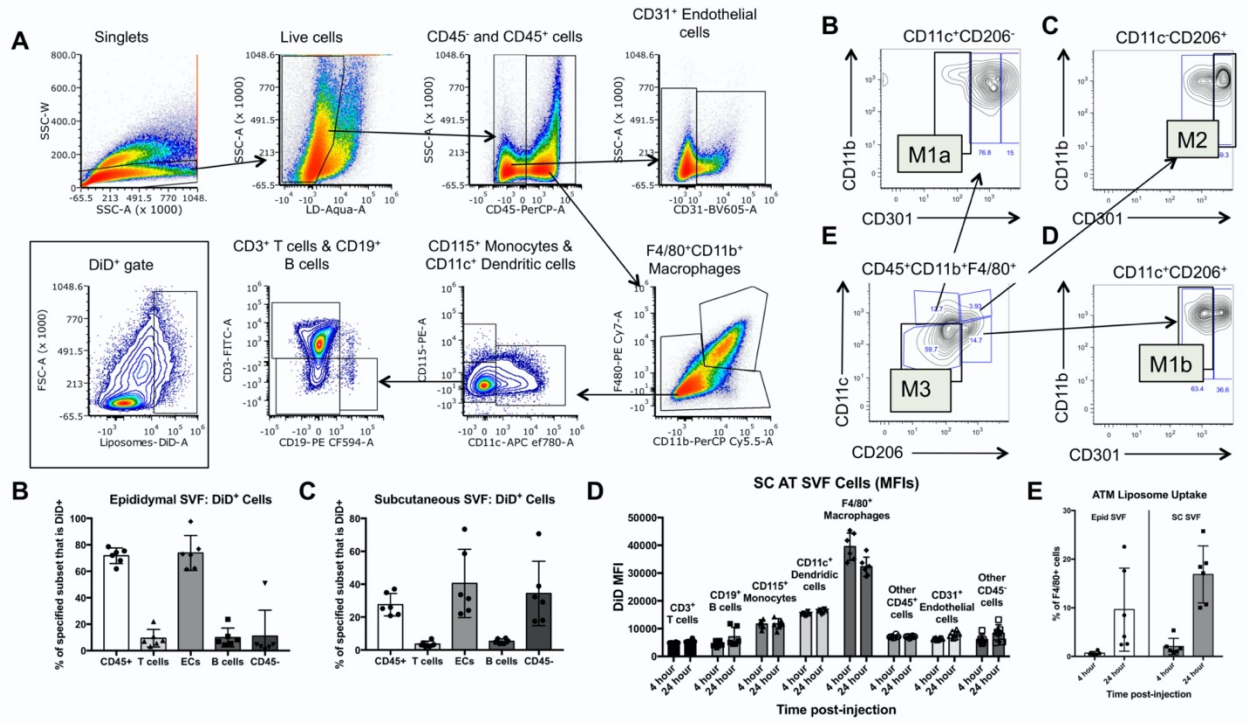

Figure A2.4. Cell subsets that took up liposomes in the Epid and SC adipose SVF and ATM subset flow cytometry gating strategy.
(A-E) Epid and SC ATs from treated *ob/ob* mice were harvested and processed. Representative flow plots demonstrate flow cytometry gating to identify $CD45^+F4/80^+$ macrophages, $CD45^-CD31^+$ endothelial cells, $CD45^+CD115^+$ monocytes, $CD45^+CD11c^+$ dendritic cells, $CD45^+CD3^+$ T cells, $CD45^+CD19^+$ B cells, and the DiD^+ population within each of these subsets **(A)** as well as $CD45^+CD11b^+F4/80^+$ macrophage subsets: $CD11c^+CD206^-CD301^-$ M1a **(B)**, $CD11c^+CD206^+CD301^{low}$ M1b **(E)**, $CD11c^-CD206^+CD301^{high}$ M2 **(C)**, and $CD11c^-CD206^-$ M3 **(D)**. **(B,C)** Quantification of the percentage of specified non-macrophage subsets that are DiD^+ in the Epid SVF **(B)** and SC SVF **(C)** after 7 days of liposome treatments. **(D)** The DiD MFI in all cell subsets of the SC SVF at four- and 24-hour time points were also quantified. **(E)** Finally, the percent of $F4/80^+$ macrophages that are DiD^+ was also quantified in Epid and SC AT at four- and 24-hour time points. Mice were treated with tesaglitazar-loaded liposomes. Data represents the mean ± SD

Figure A2.5.

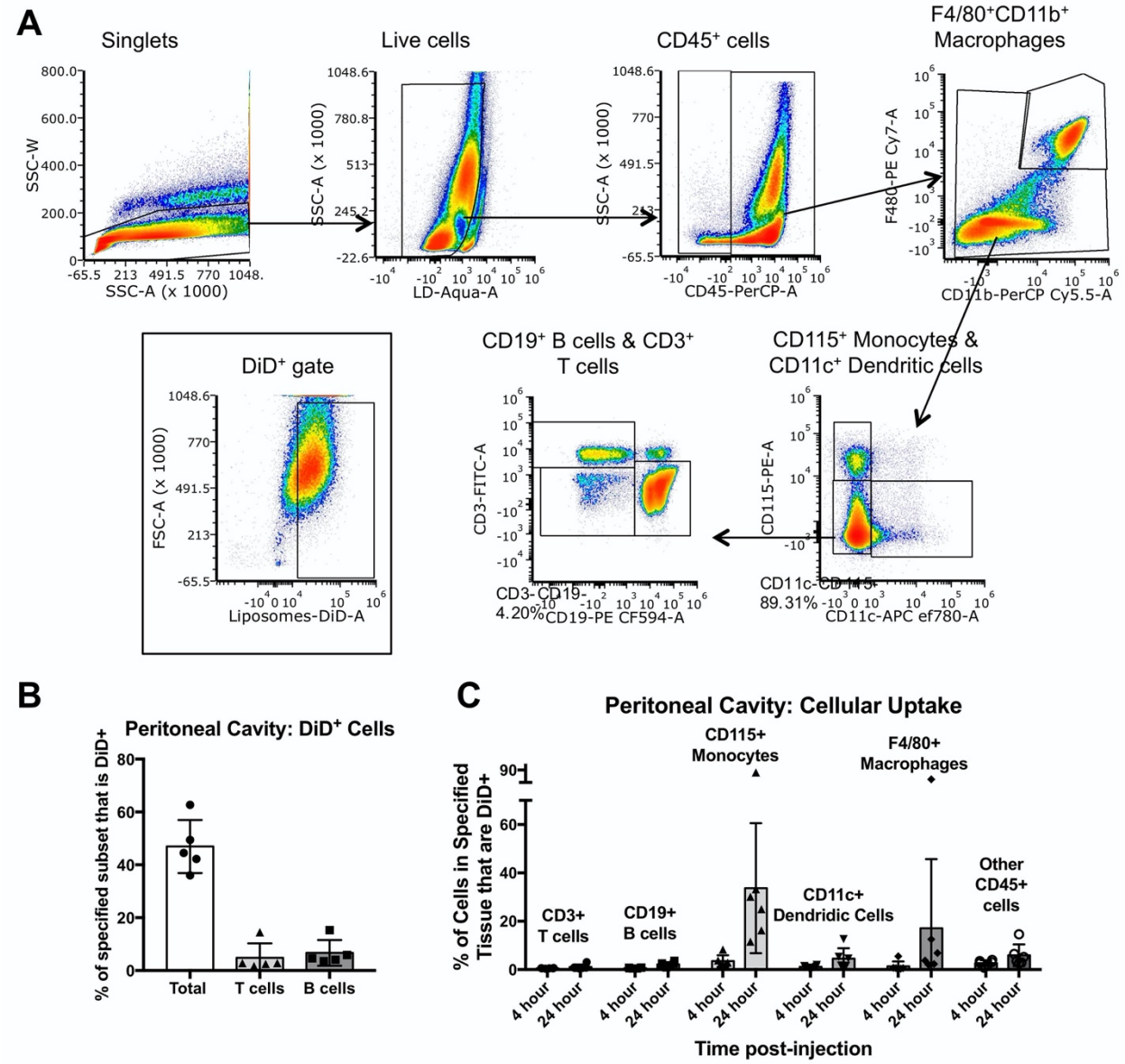

Figure A2.5. Cell subsets that took up liposomes in the peritoneal cavity and flow cytometry gating strategy.

(A) Peritoneal lavages from treated *ob/ob* mice were harvested and processed. Representative flow plots demonstrate flow cytometry gating to identify $CD45^+F4/80^+$ macrophages, $CD45^+CD115^+$ monocytes, $CD45^+CD11c^+$ dendritic cells, $CD45^+CD3^+$ T cells, $CD45^+CD19^+$ B cells, and the DiD^+ population within each of these subsets. **(B)** Quantification of the percentage of non-macrophage cell subsets that are DiD^+ in the peritoneal cavity after seven days of treatment was performed. **(C)** The percent of all subsets that are DiD^+ was also quantified at four- and 24-hour time points. Mice were treated with tesaglitazar-loaded liposomes. Data represents the mean ± SD.

Figure A2.6.

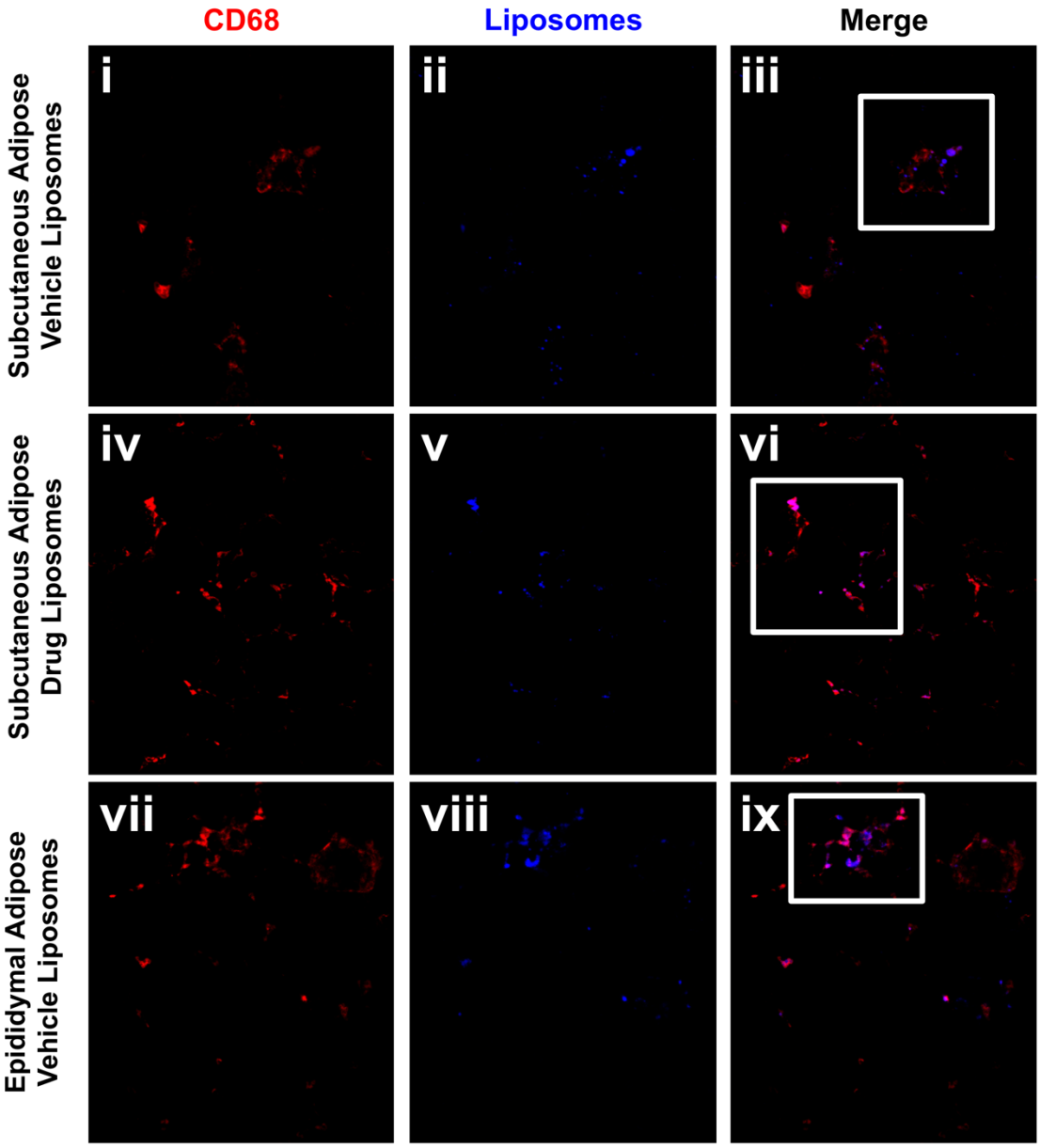

Figure A2.6. DiD$^+$ liposomes co-localized with CD68$^+$ macrophages in white adipose tissue and CLECSF13 in liver.
(Ai-ix) 40-μm Z stack images of whole mounted SC AT **(Ai-vi)** or Epid AT **(Avii-ix)** from *ob/ob* mice treated with vehicle- **(Ai-iii, Avii-ix)** or drug-loaded **(Aiv-vi)** liposomes were stained with CD68 to mark macrophages and assessed for co-localization with DiD-labeled liposomes. Co-localization of interstitial CD68$^+$ cells and DiD are marked by white boxes.

Figure A2.7.

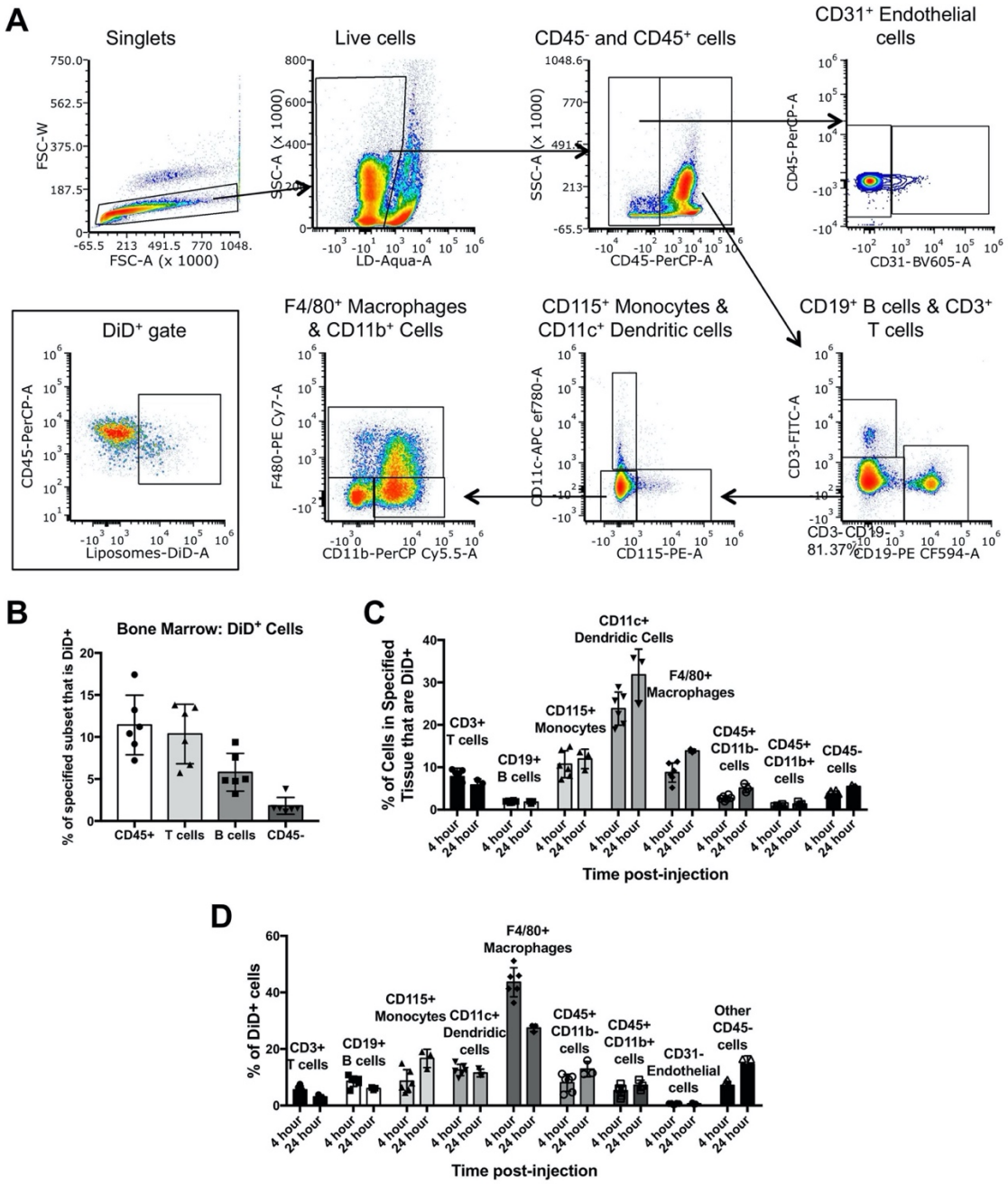

Figure A2.7. Cell subsets that took up liposomes in the bone marrow and flow cytometry gating strategy.

(A) Representative flow plots demonstrate flow cytometry gating to identify $CD45^+F4/80^+$ macrophages, $CD45^-CD31^+$ endothelial cells, $CD45^+CD115^+$ monocytes, $CD45^+CD11c^+$ dendritic cells, $CD45^+CD3^+$ T cells, $CD45^+CD19^+$ B cells, other $CD45^+CD11b^+$ cells that include cells such as NK cells and neutrophils, and the DiD^+ population within each of these subsets. **(B,C)** Quantification of the percentage of cells subsets that are DiD^+ in the peritoneal cavity after seven days **(B)** or four- and 24-hour time points **(C)** was performed. **(D)** The proportion of DiD^+ cells that are represented by each cell subset was also calculated. Mice were treated with tesaglitazar-loaded liposomes. Data represents the mean ± SD.

Figure A2.8.

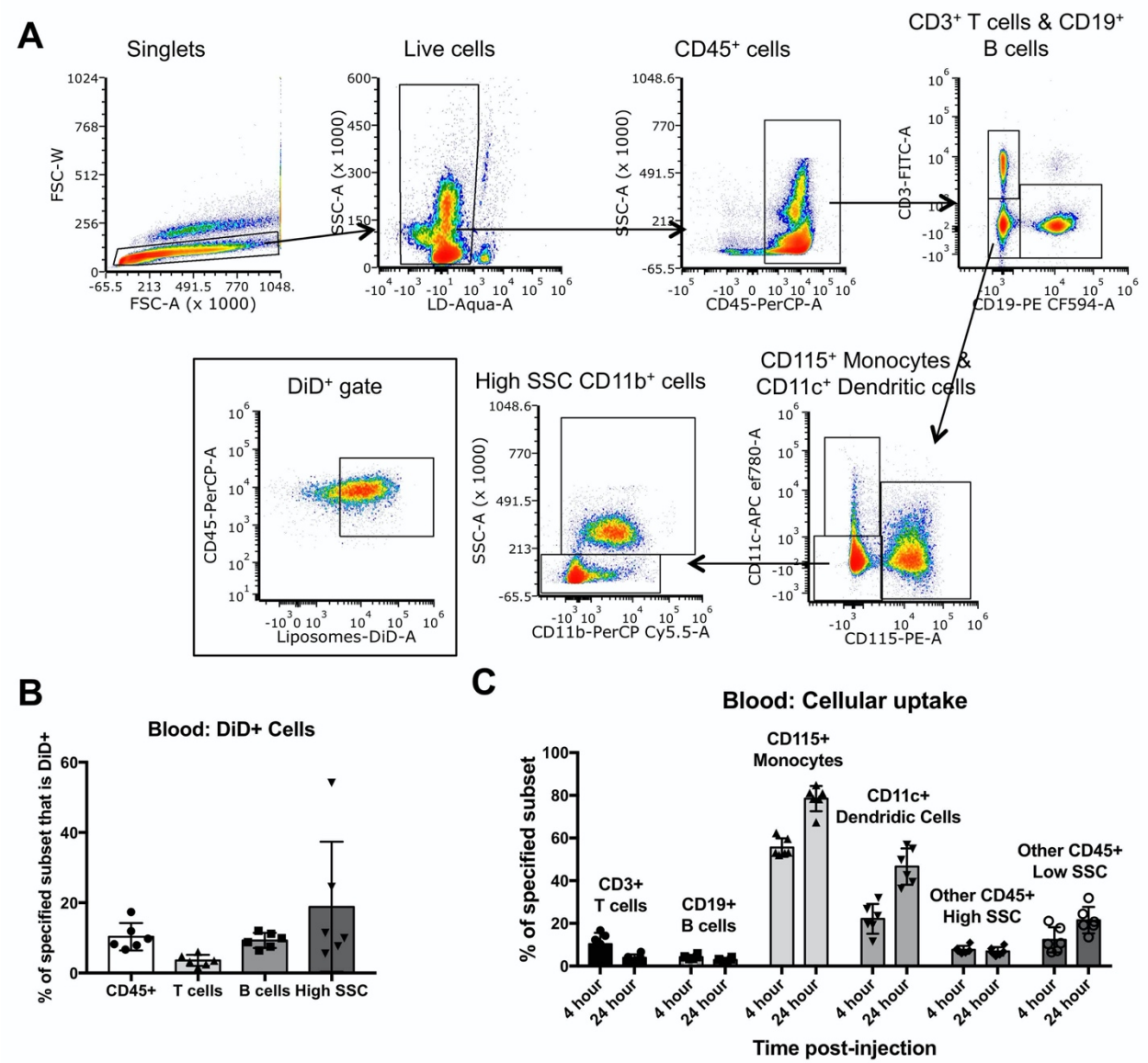

Figure A2.8. Cell subsets that took up liposomes in the blood and flow cytometry gating strategy.

(A) Representative flow plots demonstrate flow cytometry gating to identify $CD45^+CD115^+$ monocytes, $CD45^+CD11c^+$ dendritic cells, $CD45^+CD3^+$ T cells, $CD45^+CD19^+$ B cells, other $CD45^+CD11b^+SSC^{high}$ cells that include neutrophils, $CD45^+$ $CD115^-CD11c^-CD3^-CD19^-SSC^{low}$ that include NK cells, and the DiD^+ population within each of these subsets. **(B,C)** Quantification of the percentage of specified subsets that are DiD^+ in the blood after seven days **(B)** or four- and 24-hour time points **(C)** was performed. Mice were treated with tesaglitazar-loaded liposomes. Data represents the mean ± SD.

To better understand the initial kinetics by which liposomes are taken up by macrophages and other cell types, male *ob/ob* mice were administered a single dose of tesaglitazar-loaded DiD-labelled liposomes and the circulation time and cellular uptake of liposomes at four and 24 hours post-injection was assessed. A significant proportion of monocytes, which can differentiate into macrophages, in the blood were DiD^+ at four and 24 hours post-injection (**Figure A2.8C**). Additionally, nearly all macrophages found in the spleen were also DiD^+ at early time points (**Figure A2.9**) and within the bone marrow, macrophages make up the highest proportion of DiD^+ cells (**Figure A2.7D**). Within the adipose, a smaller proportion of macrophages were DiD^+ and, notably, $CD31^+$ ECs and other CD45- stromal and vascular cells made up a greater proportion of DiD^+ cells after four and 24 hours (**Figure A2.10A-D**). However, when quantifying the DiD mean fluorescent intensity (MFI), which is the level of fluorescence per cell, DiD MFI was highest in the macrophage population suggesting that macrophages took up a larger portion of liposomes per cell than other subsets (**Figure A2.10E**). When comparing uptake at four hours post-injection to 24 hours post-injection, an increase in the proportion of macrophages that were DiD^+ can already be observed (**Figure A2.11).** This accumulation of liposomes in the adipose tissue as well as the peritoneal cavity continues over the course of a seven-day treatment (**Figure A2.10F**).

Figure A2.9.

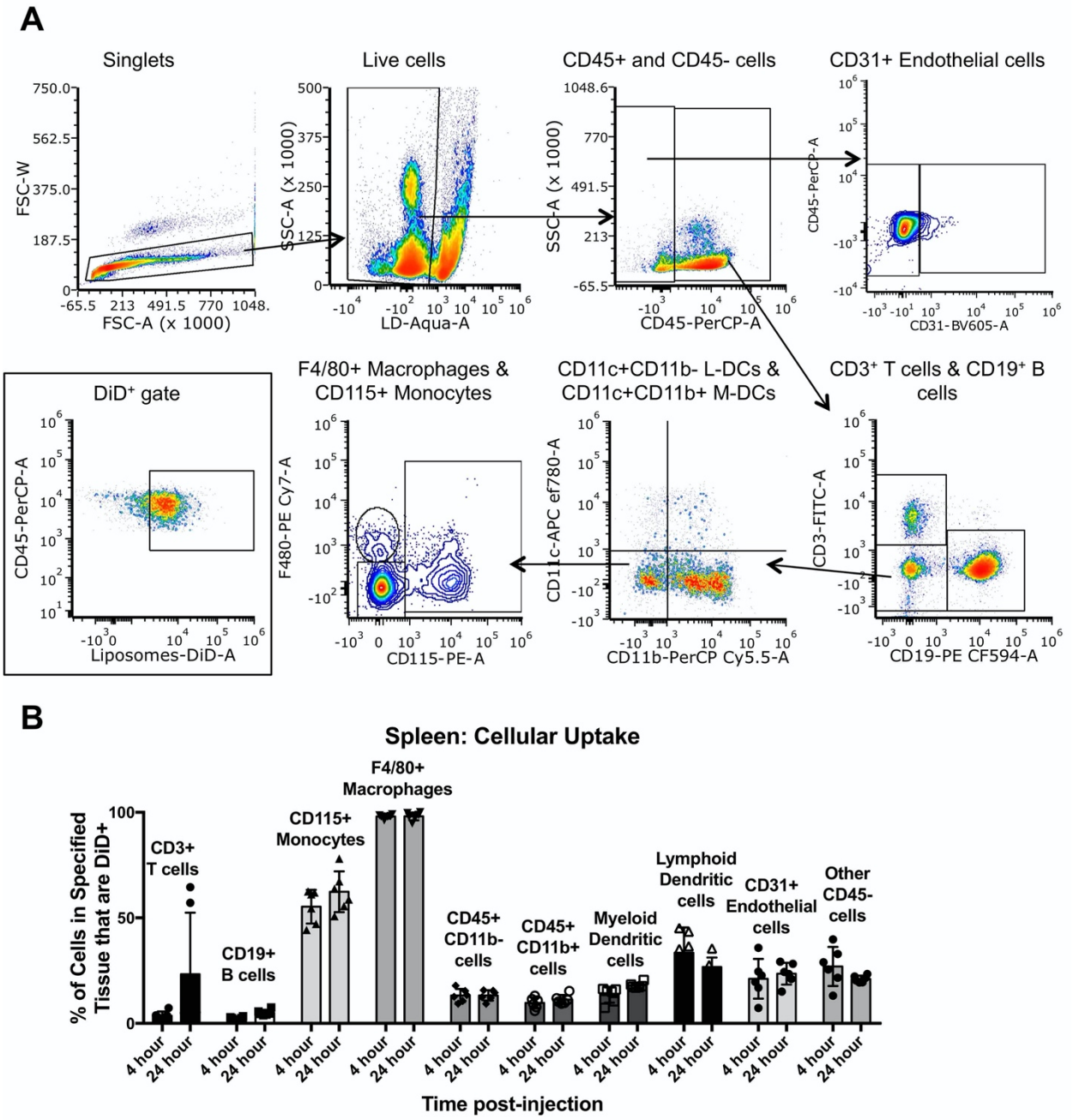

Figure A2.9. Cell subsets that took up liposomes in the spleen and flow gating strategy. **(A)** Representative flow plots demonstrate flow cytometry gating to identify $CD45^+F4/80^+$ macrophages, $CD45^-CD31^+$ endothelial cells, $CD45^+CD115^+$ monocytes, $CD45^+CD11c^+CD11b^-$ lymphoid dendritic cells, $CD45^+CD11c^+CD11b^+$ myeloid dendritic cells, $CD45^+CD3^+$ T cells, $CD45^+CD19^+$ B cells, and the DiD^+ population within each of these subsets. **(B)** Quantification of the percentage of specified subsets that are DiD^+ in the blood at four- and 24-hour time points was performed. Mice were treated with tesaglitazar-loaded liposomes. Data represents the mean ± SD.

Figure A2.10.

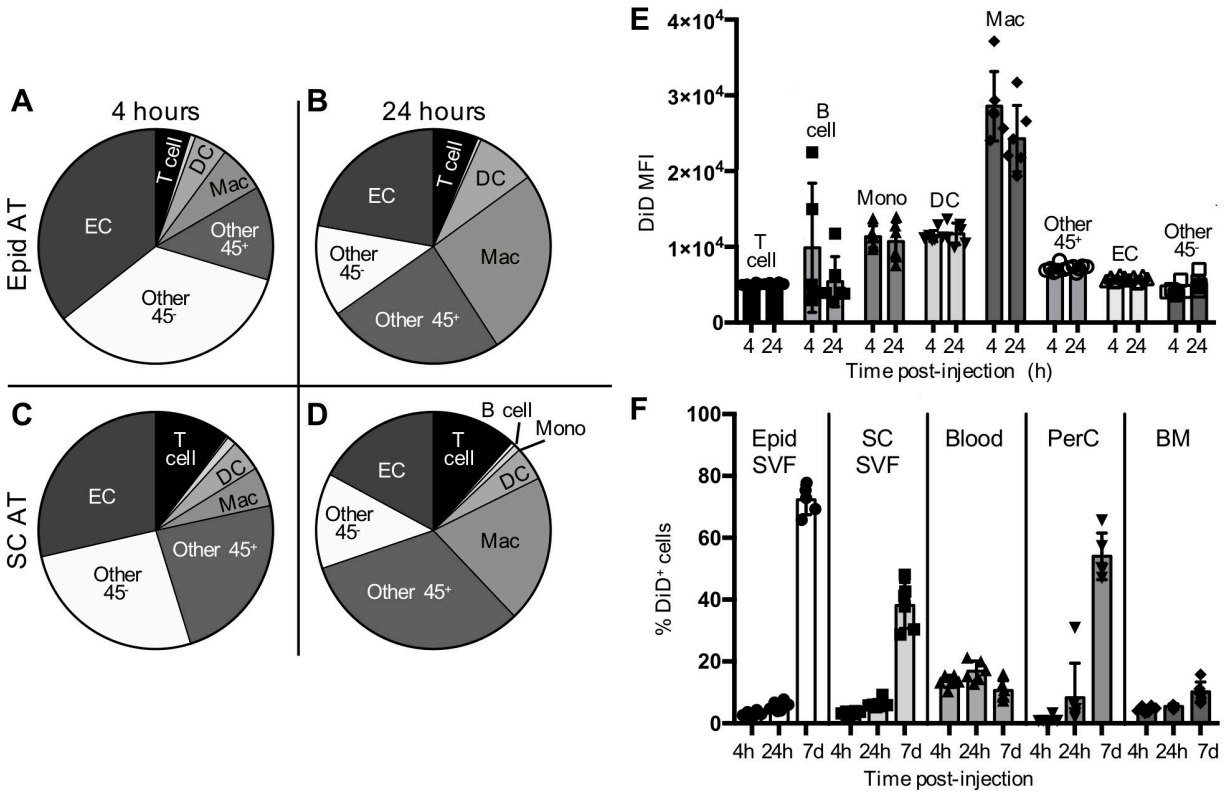

Figure A2.10. Cellular biodistribution of liposomes at four- and 24-hour time points. **(A-D)** DiD-labeled liposomes were injected intravenously into male *ob/ob* mice and tissues were harvested four or 24 hours later. Peritoneal lavages, bone marrow, blood and Epid and SC AT were harvested to stain peritoneal cavity (PerC), bone marrow (BM), blood, and SVF cells, respectively, for analysis by flow cytometry. DiD^+ macrophages and other cell subsets were also quantified as a percent of total DiD^+ cells at four and 24 hours post-injection in the Epid AT **(A,C)** and SC AT **(B, D)**, n = 6 in each group. The cell subsets analyzed were macrophages ($CD45^+F4/80^+$), B cells ($CD45^+CD19^+$), T cells ($CD45^+CD3^+$), monocytes ($CD45^+CD115^+$), dendritic cells ($CD45^+CD11c^+$), other $CD45^+$ Cells ($CD45^+CD19^-CD3^-F4/80^-CD11c^-$ $CD115^-$), endothelial cells ($CD45^-CD31^+$), and other $CD45^-$ cells ($CD45^-CD31^-$). **(E)** The mean fluorescence intensity (MFI) of DiD within each of these subsets was also quantified in Epid AT. **(F)** The percent of total cells in all aforementioned tissues that were DiD^+ was also quantified. Data represents the mean ± SD.

Figure A2.11.

	Marker	$CD45^+$ $CD3^+$	$CD45^+$ $CD19^+$	$CD45^+$ $CD115^+$	$CD45^+$ $CD11c^+$	$CD45^+$ $F4/80^+$	$CD45^+$ $CD3^-$ $CD19^-$	$CD45^-$ $CD31^-$	$CD45^-$ $CD31^+$
	Cell type	T Cells	B Cells	Monocytes	Dendritic Cells	Macrophages	Other $CD45^+$ Cells	Other $CD45^-$ Cells	Endothelial Cells
Time post-injection		**Epididymal Adipose SVF**							
4h	Average	4.74	0.04	0.75	4.55	6.54	13.00	34.75	35.62
	Standard Dev	0.65	0.03	0.23	0.67	2.00	0.80	6.37	5.59
24h	Average	6.17	0.03	0.50	8.24	25.91	24.39	12.60	22.15
	Standard Dev	0.78	0.02	0.17	2.54	9.70	4.93	2.41	5.48
		Subcutaneous Adipose SVF							
4h	Average	10.33	0.26	1.25	4.37	5.38	23.58	26.23	28.58
	Standard Dev	0.68	0.53	0.15	1.64	4.06	1.15	5.55	3.89
24h	Average	11.69	0.49	0.90	4.65	20.13	31.95	13.02	17.17
	Standard Dev	1.02	0.99	0.22	1.40	6.15	3.91	3.57	3.79

Figure A2.11. Proportion of cell subsets that were DiD^+ in adipose SVF at early time points.

Table reporting the percent of DiD^+ cells in the Epid and SC SVF that are $CD45^+F4/80^+$ macrophages, $CD45^-CD31^+$ endothelial cells, $CD45^+CD115^+$ monocytes, $CD45^+CD11c^+$ dendritic cells, $CD45^+CD3^+$ T cells, $CD45^+CD19^+$ B cells, and other $CD45^+$ or $CD45^-$ cells. Uptake percentages are reported at four- and 24 hours post-injection. These data provide quantification for the pie charts reported in Figure A2.10A-D, n = 6 per time point.

IV. Conclusions and Discussion

In this study, a murine model of obesity-associated dysmetabolism was treated with PPARα/γ dual agonist tesaglitazar as a standard oral formulation or intravenously in liposomes in order to (1) further characterize the cell types that take up liposomes *in vivo*, (2) investigate whether liposomes could effectively attenuate drug action in the liver and kidney, and (3) determine if tesaglitazar delivered either as a standard oral formulation or in liposomes had anti-inflammatory effects on macrophage populations.

Ergen *et al*. recently found that myeloid subsets including macrophages take up liposomes in a number of tissues including liver, kidney, and lung, but uptake in the adipose tissue and by non-myeloid cells was not determined [256]. Our results represent a fuller characterization of *in vivo* liposomal uptake in myeloid and non-myeloid cell types and include analysis of adipose tissue at multiple time points. After one week of treatment, liposomes were taken up by nearly 100% of macrophages in adipose tissue and peritoneal cavity, so with regard to potentially treating macrophage-induced effects in adipose tissue, our data would suggest that excellent delivery could be achieved. But many other cell types including $CD19^+$ B cells, $CD3^+$ T cells, and $CD31^+$ ECs, and other $CD45^-$ cells, which could be fibroblasts, vascular smooth muscle cells (VSMCs), or progenitor cells, also took up these liposomes in adipose tissue of obese mice. This finding introduces an important caveat of our study as well as many other studies employing the use of liposomes that may affect our understanding of the mechanisms driving observed biological outcomes.

Additionally, assessment of liposomal uptake at different time points revealed that monocytes in circulation and vascular cells in adipose tissue initially take up liposomes. However, within the first 24 hours, the percentage of adipose SVF cells that contain liposomes significantly increases even as the MFI, or amount of DiD in the cell, does not. This suggests that it may be the cells rather than the liposomes alone that are entering from the circulation with time. These data suggest that penetration of the vessel wall by liposomes to effect drug delivery of immune cells in inflamed tissues may be facilitated by disease-associated increases in tissue immune cell accumulation. These findings prompt additional questions regarding liposome biodistribution over time and the specificity of liposome targeting that could be pursued in future studies. Overall, our fulsome approach for evaluating liposome uptake *in vivo* with flow cytometry is a useful tool to understand the cellular mechanisms by which liposomal

delivery of compounds may influence biological outcomes and the residual potential risks of off target effects.

Beyond simply using liposomes to deliver drug to a specific cell type, using cell-specific targeting moieties may improve delivery outcomes. Recently, a study utilizing a mannose receptor-targeted nanoparticle to target delivery of PPARα/γ agonist, lobeglitazone, to macrophages in advanced atherosclerotic plaques effectively reduced plaque burden and inflammation[257]. Future studies evaluating the capacity of this targeted particle to target ATMs and improve symptoms in an obese, diabetic model may prove successful. Additionally, studies have demonstrated that delivery of magnetic nanoparticles to macrophages followed by induction of varying mechanical forces can alter macrophage phenotype[258, 259]. Applying such a technique *in vivo* to induce an anti-inflammatory phenotype may effectively treat symptoms of obesity-associated dysmetabolism. With regard to non-macrophage cells, further investigation into effective targeting moieties and delivery vessels is necessary before full development of a targeted therapy. Given how many macrophages and other phagocytes within the RES take up liposomes passively, this intrinsic pathway will need to be substantially overcome in order to ensure adequate delivery to other non-phagocytic cells, such as B cell.

Overall, these studies provided novel insights into the specific cell types take up untargeted liposomes *in vivo* at short and longer time points. I hope these findings will be of use to researchers developing novel targeted therapies and also serve as strong rationale for utilizing unbiased approaches to evaluate distribution of new delivery systems.